

THE OPTICAL POLARIZATION OF
BL LACERTAE OBJECTS

by

Buell Tomasson Jannuzi

A Dissertation Submitted to the Faculty of the
DEPARTMENT OF ASTRONOMY
In Partial Fulfillment of the Requirements
For the Degree of
DOCTOR OF PHILOSOPHY
In the Graduate College
THE UNIVERSITY OF ARIZONA

1 9 9 0

INFORMATION TO USERS

The most advanced technology has been used to photograph and reproduce this manuscript from the microfilm master. UMI films the text directly from the original or copy submitted. Thus, some thesis and dissertation copies are in typewriter face, while others may be from any type of computer printer.

The quality of this reproduction is dependent upon the quality of the copy submitted. Broken or indistinct print, colored or poor quality illustrations and photographs, print bleedthrough, substandard margins, and improper alignment can adversely affect reproduction.

In the unlikely event that the author did not send UMI a complete manuscript and there are missing pages, these will be noted. Also, if unauthorized copyright material had to be removed, a note will indicate the deletion.

Oversize materials (e.g., maps, drawings, charts) are reproduced by sectioning the original, beginning at the upper left-hand corner and continuing from left to right in equal sections with small overlaps. Each original is also photographed in one exposure and is included in reduced form at the back of the book.

Photographs included in the original manuscript have been reproduced xerographically in this copy. Higher quality 6" x 9" black and white photographic prints are available for any photographs or illustrations appearing in this copy for an additional charge. Contact UMI directly to order.

U·M·I

University Microfilms International
A Bell & Howell Information Company
300 North Zeeb Road, Ann Arbor, MI 48106-1346 USA
313/761-4700 800/521-0600

Order Number 9111942

The optical polarization of BL Lacertae objects

Jannuzi, Buell Tomasson, Ph.D.

The University of Arizona, 1990

U·M·I

**300 N. Zeeb Rd.
Ann Arbor, MI 48106**

NOTE TO USERS

**THE ORIGINAL DOCUMENT RECEIVED BY U.M.I. CONTAINED PAGES
WITH SLANTED PRINT. PAGES WERE FILMED AS RECEIVED.**

THIS REPRODUCTION IS THE BEST AVAILABLE COPY.

THE OPTICAL POLARIZATION OF
BL LACERTAE OBJECTS

by

Buell Tomasson Jannuzi

A Dissertation Submitted to the Faculty of the
DEPARTMENT OF ASTRONOMY
In Partial Fulfillment of the Requirements
For the Degree of
DOCTOR OF PHILOSOPHY
In the Graduate College
THE UNIVERSITY OF ARIZONA

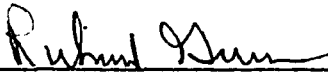
1 9 9 0

THE UNIVERSITY OF ARIZONA
GRADUATE COLLEGE

2

As members of the Final Examination Committee, we certify that we have read
the dissertation prepared by Buell Tomasson Jannuzi
entitled The Optical Polarization of BL Lacertae Objects

and recommend that it be accepted as fulfilling the dissertation requirement
for the Degree of Doctor of Philosophy.



Richard Green

9/19/90

Date



Christopher Impey

9/19/90

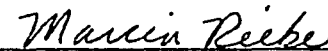
Date



Bill Bechtold

9/19/90

Date



Marcia Rieke

9/19/90

Date

Date

Final approval and acceptance of this dissertation is contingent upon the
candidate's submission of the final copy of the dissertation to the Graduate
College.

I hereby certify that I have read this dissertation prepared under my
direction and recommend that it be accepted as fulfilling the dissertation
requirement.



Dissertation Director Richard Green

9/19/90

Date

STATEMENT BY AUTHOR

This dissertation has been submitted in partial fulfillment of requirements for an advanced degree at The University of Arizona and is deposited in the University Library to be made available to borrowers under rules of the Library.

Brief quotations from this dissertation are allowable without special permission, provided that accurate acknowledgment of source is made. Requests for permission for extended quotation from or reproduction of this manuscript in whole or in part may be granted by the head of the major department or the Dean of the Graduate College when in his or her judgment the proposed use of the material is in the interests of scholarship. In all other instances, however, permission must be obtained from the author.

SIGNED: Buell Z. Janney

ACKNOWLEDGEMENTS

As I wait, early in the morning, for the laser printer to finish the library and graduate school's copy of my dissertation I have finally had that "new insight" that we all hope to gain from working on a dissertation...I have discovered two deep fundamental truths about a dissertation: One can never catch all of the typos and bad grammar in a dissertation and one page is not enough for the acknowledgements. There is not enough room to thank everyone who helped me reach my goal of beginning a career in astronomy. I have therefore decided that the copies of this dissertation which go to everyone else (including the Steward Observatory Library) but the graduate college will have a longer, and obviously more complete list of "thanked" people. You will be able to read the list there, or write to the author for a copy. However, I am sure that I will leave people off of that list who also deserve my thanks and appreciation, and I must ask your forgiveness in advance. This dissertation depended on observing the EMSS x-ray selected BL Lacs before their positions and redshifts had been published. I thank John Stocke and the EMSS team for kindly making the list of objects available to me. Thanks Dave Monet and Sidney Wolff for respectively making the Monet Machine and providing access to the computing facilities of NOAO. Thank you Gary Schmidt and the University of Minnesota for allowing me to spend numerous nights with your child, "Two-Holer". Without that reliable instrument this dissertation would not have been possible. I also thank Peter Strittmatter and five years of Steward Observatory TACs for giving me the necessary telescope time. Thank you Richard Elston and Paul "A.G." S. Smith for helping to teach me how to do polarimetry. Paul spent too many nights with me and the Wagner Box on Mount Bigelow patiently counting photons and listening for squirrels over the Bartok. Thank you Richard for your friendship, guidance, and advice since we first shared an office at the VLA in 1983. Most of what little I know about observing I have learned from you. Thanks go to everyone on my thesis committee for reading and helping me improve a work that grew much longer than intended and certainly was too heavy to carry home at night; Marcia Rieke, Jill Bechtold, and Chris Impey.

It is hard to adequately express my thanks to Richard Green for his guidance and assistance during my graduate career. Not only was his optimistic but careful approach to every problem we dealt with essential to this work being completed, but his past success with large surveys was an example that helped me generate the necessary energy to complete the optical polarization survey.

Thanks to my extended family for their love and support. Thank you Tom, Barbara, and Frank. Naturally I saved the biggest thanks for last. My wife Alison foolishly decided to marry me before I started writing my dissertation, not knowing there was no escape clause. Her love and friendship has helped sustain me throughout graduate. Thank you Alison for leaving Austin for Tucson.

TABLE OF CONTENTS

	Page
LIST OF FIGURES	9
LIST OF TABLES	13
ABSTRACT	14
PART I: GENERAL INTRODUCTION	16
CHAPTER 1 INTRODUCTION: WHAT IS A BL LACERTAE?	17
1.1 Still Enigmatic, After All These Years	17
1.2 What Kind of Monster is a BL Lac?	18
1.3 The Observational Definition of a BL Lac	20
1.4 How Polarized Light is Produced	21
1.5 Superluminal Motion in BL Lacs	24
1.6 BL Lacs, HPQs, OVV's, Blazars, and Radio Galaxies:	
Organizing the Active Galaxy Union	25
1.7 Are All BL Lacs the Same?	29
PART II: THE OPTICAL POLARIZATION PROPERTIES OF X-RAY	
SELECTED BL LACS	32
CHAPTER 2 INTRODUCTION: WHAT IS AN X-RAY SELECTED	
BL LAC?	33
CHAPTER 3 EXISTING SAMPLES OF BL LACS AND HPQs	39
3.1 X-ray Selected Samples of BL Lacs	40
a. The <i>HEAO 1</i> A-2 High-Latitude Sample	41
b. BL Lacs from the <i>HEAO 1</i> MC-LASS Catalog	
of Identified X-Ray Sources	41
c. The Einstein Observatory	
Medium Sensitivity Survey	43
d. The Einstein Observatory Extended Medium	
Sensitivity Survey	45
e. EXOSAT High Galactic Latitude Survey	48
f. Future Samples of XSBLs	48
3.2 Radio Selected BL Lac Samples	49
a. The 1 Jy 5 GHz Radio Selected BL Lac Sample	49

1. The Stickel 1 Jy Sample	50
2. The Kühr and Schmidt 1 Jy Sample	51
b. The S5 5 GHz Radio Sample	53
3.3 Samples of Quasars	53
a. The Impey and Tapia Complete Quasar Samples ...	54
1. The 2 Jy Sample	55
2. The 1.5 Jy Sample	56
b. The Ledden and O'Dell HPQ and BL Lac Samples	56
c. Polarization Studies of Incomplete Samples	57
1. Sitko, Schmidt, and Stein 1985	57
2. P.S. Smith 1986	58
d. The Palomar-Green Bright Quasar Sample	59
3.4 Radio Loud X-ray Selected Active Galactic Nuclei	59
3.5 Objects Included in Our Study	60
CHAPTER 4 101 ARIZONA NIGHTS: OBSERVING TECHNIQUES AND DATA REDUCTION	62
4.1 Polarimetry and Photometry with "Two-Holer"	63
a. The "Two-Holer" Polarimeter/Photometer	63
b. Polarimetry	63
c. Photometry	71
4.2 Polarimetry with a CCD	78
CHAPTER 5 ARE XSBLs BL LAC OBJECTS? POLARIMETRY AND PHOTOMETRY OF XSBLs	81
5.1 Polarimetry of XSBLs	83
a. Are XSBLs Polarized?	83
b. Maximum Observed Polarization	84
c. The Duty Cycle of Polarization	92
d. Variability of Polarization	95
e. Frequency Dependence of Polarization	96
f. Preferred Polarization Position Angles	98
5.2 Are XSBLs Photometric Variables? Photometry of XSBLs	103
5.3 Are XSBLs Really BL Lacs?	106

5.4 Polarimetry of RLXSAGN: The Search for X-ray Selected HPQs	109
5.5 Summary of Results	112
CHAPTER 6 COMPARISON OF THE POLARIZATION PROPERTIES OF XSBLs AND RSBLs	
6.1 The Spectral Energy Distribution of BL Lacs	115
6.2 The P_m of XSBLs and RSBLs	133
6.3 The Relation of P_m to Other Observed Properties	140
6.4 The Frequency Dependence of The Polarized Emission and Dilution by the Host Galaxy	162
6.5 The Duty Cycle of Polarization for BL Lacs.....	163
6.6 BL Lac Objects with Preferred Polarization Position Angles .	164
6.7 The Total Flux Variations of BL Lacs	172
6.8 Models of the Polarization of BL Lacs	173
6.9 The Range of Polarization Properties Explained as the Effect of a Distribution of Viewing Angles	176
6.10 Why aren't BL Lacs more like QSOs?.....	178
6.11 Summary	181
PART III: THE HUNTING OF THE OPTICALLY SELECTED BL LAC- AN OPTICAL POLARIZATION SURVEY	
CHAPTER 7 AN OPTICAL POLARIZATION SURVEY FOR BL LACS	
7.1 Introduction	183
7.2 The Palomar 48" Schmidt Telescope Polarization Survey	188
a. The Schmidt Plates	189
b. Scanning of Plates	195
c. Photometric Calibration of Survey	197
d. Measuring the Photographically Determined Polarization	209
1. Matching Up the Images	209
2. The Observed Modulation for a Given Incident Polarization	210
3. Determining the Error in the Measured Modulation	218
7.3 Selection and Followup of Candidate Polarized Objects	223

a. Selecting Candidates	223
b. The Followup Observations	225
c. Results of the Followup	226
d. A Candidate HPQ, OP 0229+06	228
e. A Candidate BL Lac, OP 1106+36	231
7.4 Setting a Useful Limit	234
a. Using Monte Carlo Simulations to Determine our Survey Limits	234
b. What Should We Have Found?	241
c. What Have Others Predicted We Should Find? ...	243
d. Can We Rule out the Existence of Radio Quiet BL Lacs?	246
CHAPTER 8 THE EIGHTH FIT: SUMMATION	247
8.1 Summary of Our Observational Programs	248
8.2 Constraining The Emission Mechanism of BL Lacs	249
8.3 Determining The Source Geometry	251
8.4 Identifying the Parent Population	253
8.5 Future Work	255
APPENDIX I. POLARIMETRY AND PHOTOMETRY OF XSBLs	257
APPENDIX II. NOTES ON INDIVIDUAL OBJECTS	312
APPENDIX III. POLARIMETRY OF RADIO LOUD X-RAY SELECTED AGN	343
APPENDIX IV. FINDING CHARTS	347
LIST OF REFERENCES	357

LIST OF FIGURES

5.1	Q/I vs. U/I plot for MS 2143.4+0704	101
6.1	α_{ro} vs. α_{ox} for XSBLs, RSBLs, and Quasars	120
6.2	α_{ro} vs. α_{ox} for XSBLs and RSBLs	121
6.3	α_{ro} vs. α_{ox} for Complete Samples of XSBLs and RSBLs ..	122
6.4	Radio Luminosity vs. α_{ro} for XSBLs, RSBLs, and HPQs .	127
6.5	Optical Luminosity vs. α_{ro} for XSBLs, RSBLs, and HPQ .	128
6.6	X-ray Luminosity vs. α_{ro} for XSBLs	129
6.7	X-ray Luminosity vs. α_{ox} for XSBLs	130
6.8	X-ray Luminosity vs. α_{rx} for XSBLs.....	131
6.9	P_{m} vs. α_{ro} for XSBLs, RSBLs, and Quasars	142
6.10	P_{m} vs. α_{ro} for XSBLs and RSBLs	143
6.11	P_{m} vs. α_{ro} for Complete Samples of XSBLs and RSBLs ..	144
6.12	P_{m} vs. α_{ox} for XSBLs, RSBLs, and HPQs	145
6.13	P_{m} vs. α_{ox} for XSBLs and RSBLs	146
6.14	P_{m} vs. α_{ox} for Complete Samples of XSBLs and RSBLs ...	147
6.15	Results of KS Tests	148
6.16	Polarized Luminosity vs. α_{ro} for XSBLs, RSBLs, and HPQs	151

LIST OF FIGURES (Continued)

6.17	Polarized Luminosity vs. α_{ox} for XSBLs and RSBLs	152
6.18	Polarized Luminosity vs. α_{rx} for XSBLs, RSBLs, and HPQs	153
6.19	Unpolarized Nonthermal Luminosity vs. α_{ro}	156
6.20	Total Nonthermal Luminosity vs. α_{ro}	157
6.21	Unpolarized Nonthermal Luminosity vs. α_{ox}	158
6.22	Total Nonthermal Luminosity vs. α_{ox}	159
6.23	Unpolarized Nonthermal Luminosity vs. α_{rx}	160
6.24	Total Nonthermal Luminosity vs. α_{rx}	161
6.25	Q/I vs. U/I for 0735+178	165
6.26	Q/I vs. U/I for OI 090.4	166
6.27	Q/I vs. U/I for MS 1221.8+2452	169
6.28	Q/I vs. U/I for 1E 1415.6+2557	170
6.29	P_{m} vs. Δ mv for BL Lacs	174
7.1	Roundness of Images on Plates	202
7.2	Callibration of Magnitudes for PS28264	206
7.3	Callibration of Magnitudes for PS27033, PS27037, PS28263, PS28264	207

7.4	Relationship Between Measured Modulation and Percent Polarization	216
7.5	Mean Modulation vs. Percent Polarization.....	217
7.6	Distribution of Magnitude Differences	220
7.7	Determining the RMS of the Magnitude Difference	221
7.8	Spectrum of OP 0229+06	230
7.9	Spectrum of OP 1106+36	233
II.1	Frequency Dependence of Polarization, H 0323+022	323
II.2	Frequency Dependence of Polarization, 1E 1415.6+2557.....	324
II.3	Frequency Dependence of Polarization, H 1652+398	325
II.4	Frequency Dependence of Polarization, H 2154–304	326
II.5	Q/I vs. U/I Plot, MS 0257.9+3429	327
II.6	Q/I vs. U/I Plot, MS 0317.0+1834	328
II.7	Q/I vs. U/I Plot, H 0323+022	329
II.8	Q/I vs. U/I Plot, 1E 0514+064	330
II.9	Q/I vs. U/I Plot, H 0548–322	331
II.10	Q/I vs. U/I Plot, MS 0737.9+7441	332
II.11	Q/I vs. U/I Plot, H 1219+305	333

II.12	Q/I vs. U/I Plot, MS 1221.8+2452	334
II.13	Q/I vs. U/I Plot, MS 1402.3+0416	335
II.14	Q/I vs. U/I Plot, 1E 1415.6+2557	336
II.15	Q/I vs. U/I Plot, MS 1458.8+2249	337
II.16	Q/I vs. U/I Plot, MS 1552.1+2020	338
II.17	Q/I vs. U/I Plot, H 1652+398	339
II.18	Q/I vs. U/I Plot, H 1722+119	340
II.19	Q/I vs. U/I Plot, MS 2143.4+0704	341
II.20	Q/I vs. U/I Plot, H 2154-304.....	342

LIST OF TABLES

4.1 Apertures for “Two-Holer” and “Octopol”	66
4.2 Filters Available with “Two-Holer”	67
4.3 Polarimetry Efficiency Corrections	69
4.4 <i>UBVRI</i> Comparison Stars in the fields of XSBLs	73
5.1 Summary of Polarimetry and Photometry of XSBLs	90
5.2 Frequency Dependence of the Polarization of XSBLs	97
5.3 The Long Term Variability of XSBLs Polarization Position Angles ...	100
5.4 Relationship between P_m , Polarized Flux, and $m_{v,Br}$	107
5.5 The Properties of RLXSAGN	111
6.1 Results of KS Tests Between X-Ray and Radio Selected Samples	136
6.2 Results of Further KS Tests Between Samples	139
6.3 RSBLs with Preferred Polarization Position Angles	167
7.1 Optical Polarization Survey Fields	192
7.2 Limits on the Surface Density of Polarized Objects	240
7.3 Limits on the Surface Density of RSBLs and XSBLs	244

ABSTRACT

We have used the optical polarization properties of BL Lacertae objects to gain insights into the range and physical causes of their extreme and spectacular observed properties. This dissertation consists of three parts. In Part I we provide an introduction to BL Lacs and other active galactic nuclei. In Part II we present the result of an extensive monitoring program of the optical polarization of x-ray selected BL Lacs (XSBLs). In Part III we present the results of the most extensive optical polarization survey so far undertaken.

Our study of the optical polarization properties of XSBLs confirms that the BL Lac candidates found in x-ray surveys like the Einstein Extended Medium Sensitivity Survey meet the requirements for membership in the class of BL Lacs. In addition to having featureless optical spectra, the majority of the XSBLs are also variable in their flux output and have intrinsic and variable polarized emission. Although x-ray selected BL Lac candidates have proven to be BL Lacs, the characteristics of their optical polarized emission are different from those of the classical radio selected BL Lacs. The XSBLs have lower maximum percent polarizations, a lower duty cycle, smaller variations in flux, and a greater tendency to have preferred angles of polarization than radio selected BL Lacs (RSBLs). We discuss the consequences of these differences and their consistency with the “beaming” model first proposed by Blandford and Rees (1978).

Our optical polarization survey is the most extensive survey of its kind ever undertaken. The survey is complete to a B magnitude of 20 and covers 560 square degrees. Our sensitivity to polarized objects is a function of survey field. We did not find any confirmed BL Lacs or highly polarized quasars, but we are able to constrain the surface density of the various populations of polarized objects. For example we are able to rule out at the 90.0% confidence level the presence of a population of radio quiet BL Lacs or highly polarized quasars (with optical flux and polarization properties similar to radio selected BL Lacs) that would have a cumulative surface density of 0.03 per square degree down to a B magnitude of 20.

PART I

GENERAL INTRODUCTION

CHAPTER 1

INTRODUCTION:

WHAT IS A BL LACERTAE?

1.1 Still Enigmatic, After All These Years

BL Lacertae objects are among the most spectacular, rare, and interesting objects in the universe. Classical BL Lac objects are capable of large outputs of energy from a very small region. It was partially the aperiodic changes in brightness of the “irregular star” BL Lacertae which led to their discovery. When it was discovered that this “star” was coincident with a strong radio source, it was declared “outstandingly interesting” (Schmitt 1968). After the discovery of linearly polarized radiation at radio (Olsen 1969) and optical (Visvanathan 1969) wavelengths, it was “unusual”. Similar objects were quickly identified (e.g. OJ 287). When astronomers gathered in Pittsburgh after a decade of frustrating attempts to understand these objects with featureless spectra and unpredictable fluxes and polarizations, they had become “some of the most enigmatic objects in the Universe” (Wolfe 1978). Twenty years after the identification of BL Lac as

the radio source VRO 42.2201 and after the continued efforts of many researchers, BL Lacs are “still enigmatic sources” (Maraschi *et al.* 1989).

1.2 What Kind of Monster is a BL Lac?

*“There’s a monster lurking in the heart of these galaxies,
and food is being fed to the monster.” — Richard Green¹*

In addition to understanding an “enigma”, astronomers hope that by studying BL Lacs they will gain an understanding of the physical processes that produce all active galactic nuclei (AGN). It is generally (although not universally) believed that both BL Lacs and quasars have similar active nuclei inside a host galaxy.

Although both BL Lacs and quasars might have “monsters” in their cores, they present different faces to the spectroscopist. Unlike most quasars, BL Lacs have featureless spectra. The lack of strong spectral features removes the possibility of using spectral line diagnostics to study the physical conditions in BL Lacs and makes the determination of these objects’ distance (from an emission line redshift) difficult to impossible. In fact, it is not possible to prove

¹ From page 143 of *Thursday’s Universe* by Marcia Bartusiak.

that every BL Lac is an extragalactic object. However, there are three pieces of evidence that support the contention that these objects are extragalactic and unusually luminous. For many BL Lacs, including the prototype, we observe faint nebulosities believed to be the “host” galaxy. We have only been able to identify the type of the host galaxy for fifteen BL Lacs. In all but one of these cases, the host appears to be an elliptical galaxy (Ulrich 1989; the only exception is 1E 1415+2557 and recent observations suggest that this object is also in a host elliptical galaxy; Stickel 1990). Even if a nebula can not be identified, absorption lines produced by intervening intergalactic material (e.g. foreground galaxies) can sometimes be detected in the spectrum of BL Lacs. This provides a lower limit on the objects distance. Finally, for several well studied objects the constraints of the Compton catastrophe require that these unresolved objects be at extragalactic distances.

Without the usual variety of spectroscopic tools to study BL Lacs, we are fortunate that other properties of BL Lacs allow the use of powerful diagnostic techniques of the energetics and structure of BL Lacs. The continuum emission of BL Lacs is variable (at all wavelengths) and strongly polarized (confirmed from the near UV to radio wavelengths). By monitoring the brightness and polarization of BL Lacs, we can gather data that constrains theoretical models of the physical structure and evolution of these objects.

1.3 The Observational Definition of a BL Lac

It is the properties of the first known BL Lacs that have provided us with our observational definition of the class of BL Lacertae Objects. Throughout this dissertation we use the term BL Lac to describe objects which possesses the following properties:

1. They are intrinsically luminous with strong and “rapid” variability.
2. They have “featureless” optical spectra.
3. Unlike most quasars, the electromagnetic radiation from BL Lacs is observed to be linearly polarized.

All known BL Lacs are also detected radio sources (Stocke *et al.* 1990). The vast majority are also believed to be strong x-ray sources (e.g. Schwartz *et al.* 1978; Maraschi *et al.* 1986). We have not included a requirement that a BL Lac be a radio source (or an x-ray source) to allow for the possibility of there existing a BL Lac analogue to the radio quiet quasar. We will see in later chapters, however, that only by studying the complete spectral energy distribution of BL Lacs can we begin to understand the observed optical polarization properties.

1.4 How Polarized Light is Produced

We will now briefly discuss the basic mechanisms that could cause the light from an astronomical object to be linearly polarized. We also discuss how the characteristics of the polarized light are related to the geometry and other properties of the region that produced the polarized emission. We know from direct observation that the emitted radiation from BL Lac objects is linearly polarized. How did the light become polarized? There are basically two classes of polarizing mechanisms that can affect the light from astronomical sources. The polarization is either intrinsic or extrinsic to the production of the radiated light.

Examples of extrinsic processes are scattering by electrons, atoms, molecules, or dust. While the light is originally produced by another source (a star or active galactic nucleus for example), it becomes polarized after being scattered. Scattering by molecules is responsible for the polarization of the blue light of daytime sky. There are numerous interstellar examples of polarization due to scattering of starlight by dust (reflection nebulae; polarization of starlight by interstellar dust). An example of electron scattering is the linear polarization of Be stars. Extragalactic examples of polarized light produced by scattering range from the polarization of Seyfert galaxies and low redshift radio galax-

ies (e.g. Rudy, Schmidt, Stockman, and Moore 1983; Antonucci 1984; Miller and Antonucci 1983; Berriman 1989) to (perhaps) high redshift radio galaxies (di Serego Alighieri *et al.* 1990; Jannuzi and Elston 1991).

There are also mechanisms that intrinsically produce polarized light. Virtually all of these mechanisms require the presence of a significant and ordered magnetic field and charged particles or atoms and molecules. Synchrotron radiation, produced by relativistic electrons in the presence of a magnetic field, is intrinsically polarized (e.g. Jackson 1962; Pacholczyk 1970; Pacholczyk 1977). Examples of sources which produce synchrotron radiation range from the Crab Nebulae to BL Lac objects. Other intrinsically polarized emission mechanisms exist. An example is the production of circularly polarized light by some molecules when they are emitting radiation in the presence of a strong and ordered magnetic field. An example is the circularly polarized emission of the G band of CH observed in the magnetic white dwarf G99-37 (Angel 1974).

The common feature of all of the polarizing mechanisms mentioned above is the requirement of order or structure in the region producing the observed radiation. Consider the following example. When we measure the polarization of a synchrotron emitting source from a great distance (the only option available if we are observing an astronomical source) we are measuring the “net” polarization. In other words, each subcomponent of the source will contribute light with its own electric field vector, \mathbf{E} , at a particular position angle.

Our polarization measurement is of the vector addition of the contributions from the entire unresolved region. If the magnetic field in a region producing synchrotron radiation was completely disorganized and random (and the source was optically thin), then observed linear polarization would be zero. If the observed polarization is not zero, it is a direct consequence of the projected magnetic field and the geometry, size, and other characteristics of the source.

The requirements mentioned above also apply to scattering mechanisms. Consider a light source embedded in a sphere of scattering particles. If the sphere is resolved, the light from each region will be polarized with the position angle of the electric field vector orthogonal to the radius of the sphere (orthogonal to the propagation vector of the radiation from the embedded source). If however, the source is unresolved, the symmetry of the scattering screen will result in the observed radiation having a measured polarization of 0%.

The fact that the underlying structure affects the observed polarization implies that in some cases polarimetry can reveal the previously undetermined structure. The successful applications of this fact to understanding astronomical systems range from the studies of Seyfert galaxies (e.g. Miller and Antonucci 1983) to binary systems which include an AM Her star (e.g. Schmidt and Stockman 1991).

1.5 Superluminal Motion in BL Lacs

For BL Lac objects, interpreting the clues presented by the observed synchrotron radiation is complicated by the fact that the plasma producing the radiation not only has relativistic electrons but is moving with a relativistic bulk velocity. The presence of relativistic bulk flow is inferred from the observation of apparent superluminal motion in some BL Lacs and highly polarized quasars (e.g. Zensus and Pearson 1987 and references therein). The consequence of these large bulk velocities is that the synchrotron radiation is strongly beamed and the observed properties of the radiation is a strong function of the viewing angle to the beamed component (e.g. Blanford and Rees 1978; Blanford and Königl 1979; Björnsson 1982).

The presence of “beaming effects” was predicted by Blanford and Rees (1978) when they presented their relativistic “jet” model to explain the observed properties of BL Lacs. Their model (slightly modified by numerous researchers since its original publication, but remaining basically unchanged) is our working hypothesis to explain the observed properties of BL Lacs to the physical properties of the objects. We note, however, that this model is not universally accepted as an explanation for all of the observed properties of all BL Lacs (e.g. Ostriker 1989; Burbidge and Hewitt 1989). We also note that for the vast majority of BL Lac objects (including all of the x-ray selected BL Lacs we will discuss in this

work) there is currently no supporting evidence for superluminal motion or the need for relativistic bulk motion of the synchrotron emitting plasma. Nevertheless we will discuss the optical polarization properties of BL Lacs in the context of the beaming model and jets.

1.6 BL Lacs, HPQs, OVV's, Blazars, and Radio Galaxies:

Organizing the Active Galaxy Union

There is an apparent need among scientists to find underlying simplicity or structure in their explanations of the universe. This has led in astronomy to efforts to unify all or some of the classes of active galactic nuclei. Whenever classes of objects are observed to share certain properties, we immediately try to explain away any obvious differences.

Because BL Lacs are believed to be objects whose observed properties are aspect dependent and are dominated, over a small range of viewing angles, by a tremendously powerful active region, it is quite natural to speculate on what a BL Lac looks like when you are not looking along the relativistic jet. If we could characterize the properties of a misaligned BL Lac (observed at a large viewing angle to the jet ejection axis), the parent population of objects, of which observed BL Lacs are only a relatively tiny subset, could be identified. Since

this is difficult or impossible to determine directly by observing BL Lacs, it has been attempted by analogy. For example, there is evidence (e.g. superluminal motion) that BL Lacs have jets. Radio galaxies have huge radio lobes that look like they were produced by jets. This has led, quite naturally, to efforts to explain BL Lacs as radio galaxies (specifically Fanaroff-Riley I radio galaxies; Fanaroff and Riley 1974) viewed along the jet axis. Unifying these objects has attracted considerable attention from numerous researchers (e.g. Antonucci and Ulvestad 1985; Browne 1989; Padovani and Urry 1990). Efforts have also been made in the past to unify BL Lacs with highly polarized quasars (HPQs) and optically violent variables (OVV). This was again motivated by the observed similarities (variability and/or polarization) between the classes. Finally, there are numerous efforts to unify, to varying degrees, all AGN and radio galaxies. We will not, however, try to review all of the suggested ideas for unifying the various classes of AGN. We will also not review all of the literature presenting evidence for unification. Instead we direct the reader to the work of several authors that have used the observed similarities between classes to persuasively argue for unification. The following list is not a complete bibliography of the subject and we apologize if the favorite paper of these or other authors is left out of the list: Scheuer and Readhead 1979; Blandford and Königl 1979; Orr and Browne 1982; Antonucci 1984; Antonucci and Ulvestad 1985; Barthel 1989; Browne 1989; Miller 1989; Ulrich 1989. Because we will have to discuss the possible confusion in identifying HPQs as BL Lacs and vice versa throughout

this dissertation, we take this opportunity to present the observationally derived definitions of HPQ, OVV, and Blazar.

- A **highly polarized quasar (HPQ)** is a quasar that has been observed to be linearly polarized at values of P (the percent polarization) greater than 3%.

- An **optically violent variable quasar (OVV)** is an object capable of rapid (day to day) and large (greater than one to two magnitude) changes in its brightness.

- The definition of a **BL Lac** is given in §1.2 .

- The term **Blazar** was created to describe objects which have violently variable and highly polarized optical continua. The term is frequently used to refer to HPQs, OVVs and BL Lacs as a single group or class.

We will use all of the above terms throughout this dissertation, but we will try to avoid the term Blazar. This term first appeared in print in the introduction to the 1980 review article of Angel and Stockman. They attributed the creation of the term “Blazar” to Ed Spiegel in his banquet speech at the 1978 Pittsburgh meeting on BL Lac objects. Because at that time the highly polarized quasars and BL Lacs seemed to possess virtually all of the same observed properties (the obvious exception being strong and broad emission lines), it seemed natural to group these objects together. The term has now seen wide use and acceptance, despite the growing body of evidence that HPQs and BL Lacs have significant and

possibly fundamental differences. The most notable differences are the spectral shape of these objects' x-ray emission (Worrall 1989), the frequency dependence of their optical polarization (Smith *et al.* 1987), their distribution with redshift (Browne 1989), and possibly contrasting VLBI polarization properties (Gabuzda 1989). Furthermore, while all known HPQs are OVV's, not all BL Lacs have been observed to undergo the extremely large variations characteristic of being an OVV. To refer to all of these objects by a single term implies a unification which is not justified. It is not always possible, however to avoid the use of the term. In order to conclusively distinguish between an HPQ and a BL Lac, we need either x-ray observations or spectroscopy. Since HPQs are observed to have periods when the emission lines are not detectable (hidden by the bright nonthermal continuum), single epoch spectroscopy is not sufficient. Similarly BL Lacs and HPQs can undergo periods of similar frequency dependence in observed polarizations. Unless the differences are apparent on the first epoch of observation it is only through continued monitoring that proper classification can be made. When an extragalactic object is known to be variable and significantly polarized, but we do not know whether it is an HPQ or a BL Lac, other authors have chosen to classify the object as a Blazar. For consistency when we refer to such objects (or samples of objects) already described in the literature, we will refer to them as Blazars.

1.7 Are All BL Lacs the Same?

In order to understand an entire class of objects, we must first obtain a collection or sample of objects to study. The composition of the sample will be affected by the means used to compile the sample. Surveys for quasars have found objects with different mean properties depending on the wavelength regime in which the survey was conducted. Both radio loud and radio quiet quasars share many properties. But without extensive optical surveys (e.g. the Palomar-Green Survey, Green *et al.* 1986), the relative numbers and their contrasting properties with radio loud quasars could not be determined. Complete and thorough surveys at radio, optical and x-ray wavelengths have all proved valuable in obtaining a complete picture of the range of properties exhibited by quasars.

Compiling similarly selected samples of BL Lacs has proved more difficult. The first samples of BL Lacs were not selected in a uniform or systematic manner. Samples selected from radio surveys suffered from incomplete identifications of the radio sources. X-ray surveys have now succeeded in compiling samples of objects that have been classified as BL Lacs, but the vast majority of x-ray selected BL Lacs have been classified solely on the appearance of their optical spectrum, without confirming polarimetry. The first x-ray selected BL Lacs seem to have differences in their radio and optical properties from radio selected BL Lacs (see Chapter 2 and Chapter 6). This has led to questions about the relationship between the samples selected in the two different bands.

While x-ray and radio surveys have now both succeeded in finding BL Lac objects (see Chapter 3), optical surveys have continued to fail to find objects in large numbers (Chapter 7).

Since we wish to study the properties of BL Lacs in general, it became evident that the following problems needed to be addressed:

- Since x-ray selected BL Lacs were initially classified solely on the basis of their optical spectra, should they be called BL Lacs? (i.e.) Do they have optical polarization and how do their polarization properties compare with those of radio selected BL Lacs?
- Would an optical survey for BL Lacs find a previously unknown subset of BL Lacs?
- Could we distinguish between or rule out suggested beaming models for BL Lacs by obtaining an optically selected sample or by setting upper limits on the surface density of these objects?

We decided to pursue two programs:

1. A measurement and monitoring program of the optical polarization of x-ray selected BL Lacs.
2. An optical polarization survey for BL Lacs.

This dissertation presents the results from these two programs. In Part II we present the results of our program to measure and monitor the optical

polarization of x-ray selected BL Lacs. In Part III we present the results of our optical polarization survey.

PART II

THE OPTICAL POLARIZATION

PROPERTIES OF

X-RAY SELECTED

BL LACERTAE OBJECTS

CHAPTER 2

INTRODUCTION:

WHAT IS AN X-RAY SELECTED BL LAC?

We have been using the phrase “x-ray selected BL Lacs” to refer to those objects discovered through optical identification of sources detected in x-ray surveys. This does not mean that these objects could not have been found through the use of some other survey technique. X-ray satellite observations of previously known BL Lacs showed that some BL Lacs were strong x-ray emitters (Mushotzky *et al.* 1978; Schwartz *et al.* 1978; Hearn, Marshall and Jernigan 1979). As the number of BL Lacs detected at x-ray wavelengths increased, Schwartz *et al.* (1979) suggested that x-ray emission was a shared property of all members of the class. This has proven to be true (Madejski and Schwartz 1989). However, all known BL Lacs are also detectable radio sources (Stoeckert *et al.* 1990). Various meanings have therefore been associated with the phrases “x-ray selected” and “radio-selected” BL Lacs. Schwartz *et al.* (1989) adopted the terminology “x-ray” or “radio” discovered BL Lacs to try and lessen confusion. Recently Giommi *et al.* (1990) introduced the terms Q-BL Lac (for quasar-like BL Lac) and X-BL Lac (x-ray strong BL Lac) to describe the two subsets of the

class of BL Lacs by the differences in their overall spectral energy distributions as represented by their location in the α_{ro} vs. α_{ox} plane (α is a measure of the slope of the spectrum between two points in the electromagnetic spectrum and is an indication of the relative energy output between two different regions of the spectrum, with r, o, and x referring to the radio, optical, and x-ray regions of the spectrum respectively; see §6.1 for a detailed definition). This latter attempt to relate an object's classification to differences in observed properties is commendable, but the choice of names imposes an explicit association between BL Lacs with large α_{ro} and quasars. For now we prefer to use identifications that refer to an individual object's membership in a particular observationally defined sample. This means that an individual object (e.g. Mrk 501) could be a member of both groups. We will discuss more physically based divisions of the class in Chapters 5 and 6. The definitions we adopt are the following:

An object is an x-ray selected BL Lac (XSBL) if it is a member of a sample of BL Lacs selected from a survey for x-ray sources.

An object is a radio selected BL Lac (RSBL) if it is a member of a sample of BL Lacs selected from a survey for radio sources.

The first XSBLs were those discovered as part of the *HEAO* A-1 high galactic latitude survey (Piccinotti *et al.* 1982; *HEAO* stands for High Energy Astrophysics Observatory). These first four XSBLs were already well known sources. Their proper identification was not in doubt. Subsequent serendipitous

discoveries of XSBLs were of objects that had not previously been identified as BL Lacs (e.g. Chanan *et al.* 1982; Maccacaro *et al.* 1982; Feigelson *et al.* 1986; Halpern *et al.* 1986). They received their classification on the basis of essentially one criterion, that optical spectroscopy of objects within the x-ray position error box revealed an object that was “featureless” and presented some evidence of having a non-thermal continuum. Radio emission was specifically not used as a selection criterion because it was hoped that x-ray surveys might provide the first “radio quiet” BL Lacs (e.g. Chanan *et al.* 1982). For the first few identified XSBL candidates, no effort was made to obtain confirming polarimetry before classification. Unfortunately, a high percentage of the early identifications were based on spectra of inadequate signal to noise or insufficient wavelength coverage. For example 1E 1408+020 was classified as a BL Lac until subsequent improved spectroscopy showed it to be an AGN with a redshift of $z=0.20$ and strong $H\beta$, [OIII], and $H\alpha$ emission (Margon *et al.* 1986). Even with almost a decade of experience in the problems of distinguishing BL Lacs from their insidious spectroscopic doppelgängers (DC white Dwarfs and any faint emission lineless objects), mistakes are still made. For example MS 1603.6+2600, an extremely interesting x-ray binary (Morris *et al.* 1990a), was initially classified as a BL Lac candidate. In the case of 1E 1408+020, polarimetry would have easily shown the misidentification. For MS 1603.6+2600, our polarimetry gave one of the first clues that it was not a BL Lac. Later surveys have added variability, polarimetry,

and radio observations to aid in the classification of BL Lac candidates (Gioia *et al.* 1984; Stocke *et al.* 1985).

While BL Lacs were rare in the first x-ray surveys (described in Chapter 3), x-ray surveys have now been shown to be quite efficient at finding extragalactic objects with featureless optical spectra and significant variability (Stocke *et al.* 1989). If the surface density determined by the EMSS sample (Chapter 3, §3.1.d) proves accurate (all of the BL Lac candidates prove to be BL Lacs), then ROSAT will provide the largest known sample of BL Lacs. Radio selected BL Lacs will quickly become a small subset of the total class. While it was the RSBLs that provided us with our observational definition of a BL Lac, it is the XSBLs that have been used the most extensively and successfully to study the surface density, luminosity function, and evolution of all BL Lacs (e.g. Maccacaro *et al.* 1984; Maccacaro *et al.* 1989; Padovani and Urry 1990). It is therefore important to understand whether or not these objects are members of the same class of objects as the RSBLs.

While the first XSBLs have met our definition for classification as BL Lacs, evidence has been presented indicating that they have significant differences in their properties from RSBLs (Stocke *et al.* 1985). These differences included apparently less variable and less polarized optical emission (Stocke *et al.* 1985). This evidence was provided, however, from a sample of only eight objects.

Progress has been made over the past five years in studying the detailed properties of XSBLs. Work by other authors examines the optical spectra, optical variability, and radio properties of XSBLs (e.g. Stocke *et al.* 1985; Stocke *et al.* 1990; Morris *et al.* 1990). Our work presented in this dissertation is the most extensive, systematic, and thorough examination of the optical polarization properties of XSBLs. Together, these studies provide the data necessary to compare the two subclasses of objects. In particular, we will address the following three questions:

1. Are the x-ray selected objects classified as BL Lacs true members of the class?
2. How great are the differences and similarities between XSBLs and RSBLs?
3. What do the optical polarization properties of all BL Lacs tell us about the intrinsic physical nature of these spectacular objects?

In 1987 we began a program to measure and monitor as extensively as possible the optical polarization of the then known XSBLs. In particular we chose to study the complete sample being compiled as part of the Einstein Extended Medium Sensitivity Survey (EMSS, Gioia *et al.* 1990; Stocke *et al.* 1989; Stocke *et al.* 1990). In the chapters that follow, we will describe the details and results of our program. In Chapter 3 we describe the x-ray selected and radio selected samples of BL Lacs that we will use in our general study of the optical

polarization properties of BL Lacs. In Chapter 4 we describe the observing techniques and procedures used in obtaining our polarimetry and photometry data. In Chapter 5 we present the results of our photometry and polarimetry of XSBLs. In Chapter 6 we compare the optical polarization properties of XSBLs with RSBLs.

CHAPTER 3

EXISTING SAMPLES OF BL LACS AND HPQS

If we wish to determine accurately and understand the general properties of BL Lac objects, it is necessary to study representative objects of the class. How do we find representative objects? For a given BL Lac object, there is no a priori method of determining whether or not it is a "typical" object. In order for an object to be "characteristic," we have to have a large enough sample to identify the extreme objects as well as the typical. As we discussed in Chapter 1, BL Lacs as a class are unusual in their observed properties and yet are difficult to find. Obtaining a complete sample of BL Lac objects has proven to be very difficult (see Chapter 1 and Part III of this dissertation). Despite the difficulty in obtaining complete samples, they are important if we wish to study the general properties of the class and essential if we wish to study the spatial distribution, evolution, and parent population of BL Lac objects (Urry 1984). We are fortunate that 1990 sees the completion of two successful efforts to obtain complete samples of BL Lacs. The successful surveys found their candidates through the use of flux limited x-ray and radio surveys. The results of the most

extensive optical polarization survey so far undertaken are described in Part III of this dissertation.

In this chapter we will describe the BL Lac samples compiled through the follow up of x-ray (§3.1) and radio (§3.2) flux limited surveys. In §3.3 and §3.4, we also describe the selection and compilation of the other samples of quasars, Blazars and highly polarized quasars (HPQs) (see Chapter 1 for definitions) used in our study of the optical polarization properties of BL Lacs. Finally in §3.5 we detail the XSBLs included in our monitoring and measurement program.

3.1 X-ray Selected Samples of BL Lacs

In order to study the general optical polarization properties of XSBLs, we included in our measurement and monitoring program a complete sample of XSBLs. This sample was composed of the BL Lacs from the Einstein Extended Medium Sensitivity Survey (EMSS) and the *HEAO 1* A-2 samples. The latter smaller sample was added in order to include objects at the high end of the x-ray flux distribution, against which the EMSS is biased. In addition, we included a few other XSBLs which for a variety of reasons were not included in either the EMSS or *HEAO 1* A-2 samples. The details of these samples are described in the following sections.

a.) *The HEAO 1 A-2 High-Latitude Sample*

The *HEAO 1* satellite experiment A-2 high-latitude survey detected four BL Lac objects with x-ray fluxes above the survey limit of 3.1×10^{-11} ergs cm $^{-2}$ sec $^{-1}$ in the 2–10 keV band (Piccinotti *et al.* 1982). The survey covered the sky with $|b^{\text{II}}| > 20^\circ$. In addition to excluding the galactic plane, a 6° circle centered on the LMC was also avoided. The total survey area was 26,919 square degrees (8.2 sr). The entire survey area was observed at two epochs, separated by 6 months. The sensitivity of the second epoch is lower than the first and objects were included on the basis of their flux during the first epoch observations. All of the objects are 5 sigma detections. At the time the survey was published, 78 of the 85 detected sources had been identified. Of the identified sources, 61 are extragalactic objects. The four BL Lacs included in this survey are H 0548–322, H 1219+305, H 1652+398, and H 2154–304 (also known as PKS 2155–304). These objects were added to the Einstein Medium Sensitivity Survey BL Lacs (described below) to comprise the first flux limited sample of BL Lacs (Maccacaro *et al.* 1984).

b.) *BL Lacs from the HEAO 1 MC-LASS Catalog of Identified X-ray Sources*

There is an ongoing program to identify the x-ray sources listed in the Naval Research Laboratory's (NRL) all-sky catalog (Wood *et al.* 1984). The list of identified objects will be published as the *HEAO 1* MC-LASS Catalog of Identified X-Ray Sources (Remillard 1990). Using this data from the Scanning

Modulation Collimator (MC, A-3) on the first *HEAO 1* satellite, efforts are being made to compile a sample of XSBLs with fluxes $> 1.5 \times 10^{-11}$ ergs $\text{cm}^{-2} \text{s}^{-1}$ (Remillard *et al.* 1989; Schwartz *et al.* 1989). To date this sample is not complete; but as identifications and finding charts have become available, we have tried to add these sources to our observing program. Of the 659 x-ray sources contained in the Large Area Sky Survey (LASS), 631 have been identified. There are currently 27 BL Lacs and three BL Lac candidates included in this catalogue. The details of the source selection and these objects' optical and radio properties are described in Schwartz *et al.* (1989). They also discuss the optical polarization properties of these x-ray bright BL Lacs. We will return to them again in Chapter 5. At this time we note a few of the factors that affect the selection of objects for this sample. Besides an x-ray flux criterion, they also require that the candidates' optical identifications appear as ultraviolet excess objects on two color (U, B) Schmidt plates. Their U and B magnitude limits are different for each field, but are generally 17.5 and 18.0 respectively. The UV excess objects are generally selected by visual inspection of the plates (Remillard *et al.* 1986). Since BL Lacs can have relatively steep optical and UV spectra, UV excess is not necessarily a general property of the class (see Chapter 1) and this step of their selection process might cause the exclusion of some BL Lacs from their sample. They have also cross-referenced the positions of their x-ray detections with the positions of objects in catalogues of objects known to emit x-rays. To be classified as a BL Lac, they additionally require a subsequent

observation of an object to reveal a featureless optical spectrum and the detection of one of the following: radio emission, optical polarized emission, variability of total optical emission. Sources are drawn from the high galactic latitude sky ($|b^{\text{II}}| > 20^\circ$). Finally we note that Schwartz *et al.* (1989) argue that the surface density of BL Lacs derived from this survey is a large overestimate of the density which would be observed in an instantaneous snapshot of the sky. They feel that the rapid x-ray variability of BL Lacs (factors from 2 to 50 in flux on time scales of a few hours to a few days), the relatively long period of observation of each field (minimum four days), and the steep increase in the number of sources with decreasing x-ray flux combine to cause an overestimate of the surface density.

c.) *The Einstein Observatory Medium Sensitivity Survey*

The Einstein Observatory Medium Sensitivity Survey (MSS) explored the high-galactic latitude sky at fluxes between the Uhuru/Ariel V and Einstein Deep Survey limits. The survey looked for serendipitous sources, in the energy range 0.3-3.5 keV, detected with the Imaging Proportional Counter (IPC). The survey results were presented in two sections, the MSS 1 (Maccacaro *et al.* 1982; Stocke *et al.* 1983) and MSS 2 (Gioia *et al.* 1984). The flux limit varied for each IPC observed field, depending on the integration time of the pointed observations. The MSS 1 covered approximately 50 square degrees at flux levels $7 \times 10^{-14} \leq S_x \leq 5 \times 10^{-12} \text{ ergs cm}^{-2} \text{ sec}^{-1}$. The MSS 2 added an additional 40 square degrees. For both parts of the MSS, only IPC fields with $|b^{\text{II}}| > 20^\circ$ were

used. For each IPC image approximately 945 square arcminutes could be used for the survey. Two regions of each frame were excluded from the survey area. First, areas around the edge of the frame that might suffer from obscuration by the window and supporting structure were excluded. Second, a circle $5'$ in radius centered on the target object of each frame was also excluded from the survey. In all, the two medium sensitivity surveys covered 89.1 square degrees to a limiting flux of 2×10^{-12} ergs cm^{-2} sec^{-1} . A subset of the survey area, 72.3 square degrees in size, was surveyed to a limiting flux of 6.5×10^{-13} ergs cm^{-2} sec^{-1} . It is important to note that this survey effectively has an upper flux cutoff as well. Virtually every strong x-ray source in the sky was scheduled for a pointed observation by the *Einstein Observatory*. Since the MSS excludes the central regions of each IPC field (the target of the pointed observation), this survey is biased against strong x-ray sources (fluxes greater than 5×10^{-12} ergs cm^{-2} sec^{-1}). Further details of the selection of objects are included in the references mentioned above.

A total of 112 serendipitous x-ray sources were detected. Four BL Lac objects were found. These objects are 1E 1207.9+3945, 1E 1402.3+0416 (Macacaro *et al.* 1982), and 1E 0317+1835 and 1E 1235.4+6315 (Gioia *et al.* 1984). We note that at the time this survey was published, the authors were using a featureless optical continuum, detectable radio emission, and detectable optical polarization as their primary criteria for BL Lac classification. However, only one of the four objects (1E 1402.3+0416) actually met all three of their condi-

tions at the time of the publication of the sample. The defining criteria have been subsequently quantified and are described in §3.2. The optical and radio properties of this small sample are discussed by Stocke *et al.* (1985). We will examine the properties of these BL Lacs along with those of the other XSBLs in later chapters. Note that in the future, these four objects will be referred to by their Extended Medium Sensitivity Survey catalogue names (MS prefix).

d.) *The Einstein Observatory Extended Medium Sensitivity Survey*

The Einstein Observatory Extended Medium Sensitivity Survey (EMSS) was designed to greatly increase the survey area of the MSS and the total number of included objects. In addition to increasing the number of IPC fields, new reduction algorithms and background maps for each IPC field allowed the exploration of a greater portion of the outer edges of each previously examined IPC field. The details of the selection process and a discussion of the completeness of the survey are presented by Gioia *et al.* (1990). The final survey area covers 778 square degrees of the high galactic latitude sky with differing flux limits for each IPC field. Flux limits range from 5×10^{-14} to 3×10^{-12} ergs cm⁻² sec⁻¹ in the 0.3-3.5 keV IPC band. A total of 835 sources were detected. The details of the amount of area covered at a given flux limit will be presented in Morris *et al.* (1990b).

Thirty-four EMSS sources have been classified as BL Lac objects or candidates. Two classification criteria were used:

1. The x-ray emission must be point-like in the IPC observation. They note that there are four objects with possibly extended x-ray emission which were retained as members of the BL Lac sample of the survey. The detection of extended emission for these objects is tentative since all four sources have been detected at the edge of an IPC field. The affected objects are MS 0257.9+3429, MS 0922.9+7459, MS 1229.2+6430, and MS 2143.4+0704.

2. The object must have a featureless optical spectrum by which they mean:

“a) no emission lines with [observed] equivalent width $W_\lambda > 5\text{\AA}$ and

b) if a Ca II H and K “break” is visible due to the underlying galaxy, the strength of the break is much less than is typical for a cluster elliptical galaxy, ensuring the presence of a substantial non-thermal component; i.e. $[\text{flux}(4000\text{\AA}+) - \text{flux}(4000\text{\AA}-)] / \text{flux}(4000\text{\AA}+) \leq 25\%$.” (Gioia *et al.* 1990)

A third criterion, listed in Stocke *et al.* 1990, is the following:

3. If a redshift is obtained, z must be greater than 0.

This last criterion is to exclude any galactic objects which might somehow meet the prior two conditions.

Stocke *et al.* (1990) note that they currently only have spectra from 3400 to 6000Å, but are in the process of obtaining coverage out to 8500Å (Morris *et al.* 1990b).

Twelve of the 34 EMSS BL Lacs are classified as candidates because the signal-to-noise of the available spectroscopy is not yet sufficient to apply the second criterion at the 3σ level.

An additional division of the EMSS objects was made by Stocke *et al.* (1990). A subset of the survey was selected to include sources with x-ray fluxes $S_x > 5 \times 10^{-13}$ ergs cm⁻² sec⁻¹ and declinations $\geq -20^\circ$. This restricted area of the EMSS covers 634 square degrees. Three hundred and forty-eight sources meet these additional flux and location restrictions and all but four of them have been identified. Of these 348 objects, 22 are BL Lacs and comprise what is called the complete EMSS sample (C-EMSS; Stocke *et al.* 1990; Morris *et al.* 1990b). Firm redshifts (as designated by Morris *et al.* 1990b) have now been obtained for 14 of the 22 C-EMSS objects. Tentative redshifts have been determined for the remaining eight objects. An additional 14 objects are listed as candidate BL Lacs. Four of the candidates have firm redshifts. The x-ray, radio, and optical properties of these objects are discussed in Stocke *et al.* 1989, Stocke *et al.* 1990, and Morris *et al.* 1990b. We will discuss their optical polarization properties and their relationships to RSBLs in Chapters 5 and 6. We

will also examine whether or not our polarimetry confirms the classification of these objects as BL Lacs.

e.) *EXOSAT High Galactic Latitude Survey*

The EXOSAT observatory has also discovered XSBLs, but these objects were not available for inclusion in our monitoring program. The general properties of this sample are described in Giommi *et al.* (1989). So far 11 XSBL candidates have been found. All of these objects have featureless optical spectra and have been detected to be radio sources.

f.) *Future Samples of XSBLs*

There is yet another sample of BL Lacs to be compiled from data obtained by the Einstein Observatory. The Einstein All-Sky Slew Survey is in the process of being completed (Elvis 1990). It will have a brighter flux limit (8×10^{-12} erg cm $^{-2}$ sec $^{-1}$) than the EMSS, but covers a much greater area. This should provide yet another "complete", hopefully larger, sample of BL Lacs.

With the launch of ROSAT in 1990 and its apparent successful operation, we can also look forward to the largest complete sample of BL Lacs ever compiled. The ROSAT all-sky survey should find thousands of objects that are similar to the XSBLs in the EMSS (Maccacaro *et al.* 1989).

3.2 Radio Selected BL Lac Samples

a.) The 1 Jy 5 GHz Radio Selected BL Lac Sample

As we discussed in Chapter 1, we are fortunate finally to have a completely identified flux limited sample of radio selected BL Lacs (Stickel *et al.* 1989; Kühr and Schmidt 1990; Stickel *et al.* 1990a; Stickel *et al.* 1990b). The complete sample is based on optical followup and identification of the radio sources in the 1 Jy catalogue (Kühr *et al.* 1981b). The 1 Jy 5 GHz survey is virtually an all sky survey, excluding only the galactic plane and the LMC. The total area covered is 32,204 square degrees (9.81 sr), approximately 78% of the sky. The 1 Jy catalogue contains 518 radio sources selected to have 5 GHz radio fluxes greater than 1 Jy at the time of the survey. More than 50% of these are flat spectrum radio sources. The optical identification of those radio sources with $m_v < 20.0$ and flat radio spectra is virtually complete (Stickel *et al.* 1990a).

Because two different “complete 1 Jy BL Lac samples” have been presented in the literature, we will discuss each in turn. In the following subsections we describe the selection criteria for these two 1 Jy samples and specify how they will be referenced in the later chapters.

a.1.) The Stickel 1 Jy Sample: What we will call the Stickel 1 Jy sample was selected from the catalogue of 1 Jy radio sources (Kühr *et al.* 1981a; 1981b) according to the following criteria (explained in detail in Stickel *et al.* 1990a; Stickel *et al.* 1990b):

1. The object must have a flat or inverted radio spectrum with a spectral index (11 to 6 cm) of $\alpha_r \geq -0.5$ where $S_\nu \propto \nu^\alpha$.

2. The optical counterparts of the radio sources are brighter than twentieth magnitude on the Palomar Observatory Sky Survey (POSS) plates.

After the application of these first two criteria, 207 candidates were left in the sample (Kühr and Schmidt 1990).

3. The equivalent width in the rest frame of the strongest line is less than 5\AA . The observed range for most of their spectroscopy is ≈ 4000 to $\approx 7500\text{\AA}$.

There are thirty-four objects which meet these criteria. The polarimetry is taken from either Kühr and Schmidt (1990) or Impey and Tapia (1990) and references therein. This BL Lac subsample comprises 16% of the flat spectrum radio sources with $m_v < 20.0$. There are still 10 sources that meet criteria one and two Stickel *et al.* (1990a;1990b), but for which they do not have adequate spectra. They estimate that at most two BL Lacs will be added to the list once these objects are identified.

One of the great strengths of this sample is the large number of objects for which redshifts have been determined. Emission line redshifts have been

determined for 25 of the 34 RSBLs that comprise the 1 Jy Sample (Stickel 1990). Absorption lines (assumed to be produced by Mg II in intervening systems) provide lower limits for an additional four objects. The remaining objects have had lower limits of $z > 0.2$ assigned on the basis of their stellar appearance on direct images. Together with the complete x-ray surveys, this sample allows the direct study of the relationships between the optical polarization and other properties of BL Lacs. Redshifts for this sample were kindly provided in advance of publication (Stickel 1990), but should be published in 1991.

The optical spectra of these objects are presented in Stickel *et al.* (1989a; 1990b). Direct images are presented for some of the objects in Stickel *et al.* (1989b; 1990b).

a.2.) The Kühr and Schmidt 1 Jy Sample: Kühr and Schmidt (1990) have independently presented a list of BL Lacs from the 1 Jy catalog selected with slightly different criteria:

1. The object must have a flat or inverted radio spectrum with a spectral index (11 cm to 6 cm) of $\alpha_r \geq -0.5$ where $S_\nu \propto \nu^\alpha$.
2. The sources have $\delta > -20^\circ$ and $|b^{\text{II}}| > 10^\circ$.
3. The object must have a $m_v < 20.0$ at the time of spectroscopic and polarimetric followup.

4. They required that the initial spectroscopic followup revealed a spectrum with no features and a generally red continuum. Objects which subsequently showed strong emission lines were maintained in the sample. This means that some objects that other researchers would call HPQs were maintained in this BL Lac sample.

5. The optical polarization must exceed 3σ and $P \geq 3\%$.

Thirty-four objects met these criteria. The major qualitative differences between the Stickel, and Kühr and Schmidt 1 Jy samples is that the latter subgroup includes several objects with observed emission line strengths greater than the limit set by Stickel *et al.* (1990a). We have returned again, and not for the last time, to the problem of discriminating between BL Lacs and HPQs. A second, effectively moot point, is that Kühr and Schmidt required the detection of significant polarized emission from a candidate before classifying the object as a BL Lac. In practice, all but two of the Stickel 1 Jy sample have also been observed to emit significant polarized emission. This is not surprising considering the extensive overlap between the two samples. We will refer to the Kühr and Schmidt 1 Jy sample as the K-S 1 Jy BL Lac sample.

We note that the 1 Jy BL Lac samples described above were chosen without any reference to the optical morphology of the objects. This avoids discrimination against nearby objects, but results in the inclusion of objects which are not stellar in appearance (i.e., not quasars).

The polarization data for the 1 Jy samples were taken from Kühr and Schmidt (1990) and Impey and Tapia (1990).

b.) *The S5 5 GHz Radio Sample*

The S5 north polar region survey (Kühr *et al.* 1981a) contains 185 sources with 5 GHz radio fluxes greater than 0.25 Jy. Other selection criteria are the same as for the Kühr and Schmidt (K-S) 1 Jy sample. We will refer to this sample as the S5 BL Lac sample. The details of its selection are described in Kühr and Schmidt (1990). There are fourteen objects in this sample. Four of these objects are also in the 1 Jy sample.

3.3 Samples of Quasars

As we discussed in Chapter 1, it is often tempting to merge samples of highly polarized quasars with samples of BL Lacs and study the properties of an encompassing class, Blazars. In fact it is sometimes easier to conduct a followup optical polarization or variability survey of radio survey sources for objects which behave as Blazars (large amounts of variability and significant polarized emission) than it is to obtain the complete spectroscopic information necessary to distinguish between an HPQ and a BL Lac. In fact, such surveys have allowed the compilation of “complete Blazar” (or alternatively complete survey for polarized stellar objects) samples. Furthermore, the shared observed

properties of HPQs, OVV's, and BL Lacs and their proposed relationships in unification models necessitate that we compare the properties of BL Lacs to the properties of HPQs, QSOs, and OVV's (see Chapter 1 for definitions). In the subsections that follow, we describe the samples of these objects to which we later compare our observations of XSBLs. Additional studies in the literature are listed in the last subsection.

a.) *The Impey and Tapia Complete Quasar Samples*

Impey and Tapia conducted a polarization survey of two subsets of radio sources in the 1 Jy 5 GHz radio source catalogue (Kühr *et al.* 1981). The 1 Jy catalogue contains 518 sources. The two samples they define are the "2 Jy" and "1.5 Jy" quasar samples. The differences between these two samples are explained in the following two subsections. Both samples share several characteristics. They require that in order for a radio source to be classified as a quasar it had to have a stellar appearance on the POSS plates. Using their own data and observations in the literature, Impey and Tapia (1990) obtained polarimetric observations for 90% of the "quasars" (they use the term to apply to radio loud quasars and BL Lacs) in their samples. In order for an object to be classified as a Blazar, they require it have a polarization (P) greater than 3%. Since they do not require demonstrated variability, their polarization criterion amounts to selecting a sample of HPQs and BL Lacs and the effective definition of Blazar becomes the following: significantly polarized object with

a stellar optical morphology. No optical spectroscopic criteria were applied in selecting their sample. More detailed descriptions of the “2 Jy” and “1.5 Jy” samples follow. The major differences between these two samples and the 1 Jy Stickel and K-S samples are the lack of any spectroscopic criterion and the stellar morphological requirement.

a.1.) The 2 Jy Sample: The 2 Jy sample consists of the 90 quasars included among the 165 objects in the 1 Jy catalogue that are brighter than 2 Jy. Of the 165 sources, 62 are radio galaxies and 13 are unidentified. For this quasar sample no restriction was imposed on an object’s radio spectral index (α_r). Identifications and redshifts were available for, respectively, 97% and 83% of the 165 sources. Polarimetry was obtained for 92% of the quasars. We will discuss the properties of these objects in relationship to the properties of XSBLs in Chapters 6 and 7. We will refer to three subgroups of the 2 Jy sample. The 2 Jy HPQs are the 2 Jy quasars with observed polarization greater than 3% and emission lines more than 10% of the continuum. The 2 Jy BL Lacs are the 2 Jy quasars with observed polarization greater than 3% and emission lines less than 10% of the continuum. The 2 Jy Blazars (which we will refer to as the 2 Jy Combined Sample) include all the 2 Jy HPQs and BL Lacs with observed polarization greater than 3% (note this also includes two polarized objects for which adequate spectroscopy is not available to determine whether or not the object is an HPQ or BL Lac). For a few of the significantly polarized objects, a

good spectrum was not available. In our comparisons in later chapters, we only include these objects in the 2 Jy Combined (Blazar) group.

a.2.) *The 1.5 Jy Sample:* There are 220 sources in the 1 Jy catalogue with flux densities between 1.5 and 2.0 Jy. Of these sources, Impey and Tapia obtained polarimetry for 86% of the 50 quasars with flat radio spectra ($\alpha_r > -0.5$). Identifications and redshifts were available for, respectively, 94% and 82% of the 1.5 Jy radio sources. We will refer to three subgroups of the 1.5 Jy quasars, defined similarly to those for the 2 Jy sample (§4.2.a.2). They are the HPQ, BL Lac, and Blazar subsets of the 1.5 Jy sample of radio sources.

b.) *The Ledden and O'Dell HPQ and BL Lac Samples*

Ledden and O'Dell (1985) made the first extensive study of the radio-optical-x-ray spectral flux distribution of what they chose to call Blazars. At the time of their work there were no complete samples. Instead they depended on published compilations of BL Lacs and HPQs. By combining their own data with that in the literature, they were able to gather a sample of 99 HPQs and BL Lacs. For 77 of these they were also able to obtain x-ray observations. It will certainly become possible to obtain complete samples of HPQs for which x-ray data is available. At the time of this work, however, the Ledden and O'Dell sample (compiled mainly from Angel and Stockman 1980; Moore and Stockman

1981; Moore and Stockman 1984; Stockman, Moore, and Angel 1984) is as useful as any other available sample. In subsequent chapters we will refer to three groupings of objects from the Ledden and O'Dell paper. Ledden and O'Dell HPQs and Ledden and O'Dell RSBL Lacs refer respectively to the HPQs and BL Lacs (with the x-ray selected objects excluded) included in their paper. Ledden and O'Dell Combined (Blazars) will be used to refer to the combined set of HPQs and BL Lacs. It is important to note that Ledden and O'Dell samples are in no way complete and include objects with much lower observed radio fluxes than are included in the radio selected samples discussed in this chapter.

c.) *Polarization Studies of Incomplete Samples*

There have been several other efforts to study systematically the optical and/or infrared polarization properties of BL Lac objects. These studies were done when there were no existing complete samples, and therefore we must keep in mind that generalizing from these studies to all BL Lacs is difficult. We describe in the two following subsections two of the past studies of optical polarization properties of BL Lacs because they provide the only published extensive monitoring data of a relatively large number of RSBLs.

c.1.) Sitko, Schmidt, and Stein 1985: Sitko, Schmidt, and Stein (1985) monitored the polarization of a sample of 24 BL Lac objects and violently

variable quasars for approximately two and one third years (1982 to 1984). Their major objective was to study the wavelength dependence and variability of the percent polarization and position angle of BL Lacs and OVV's. The objects they included in their monitoring program were all well known and extensively studied BL Lac objects and OVV's or objects of extremely unusual properties. While their sample is neither complete nor homogeneous in its selection, the period of time the objects were observed is comparable to our monitoring of XSBLs, and when appropriate we will compare to the results of presented by Sitko *et al.* 1985.

c.2.) P. S. Smith 1986: For his Ph.D. dissertation, Paul S. Smith undertook an extensive monitoring program of the optical and infrared polarization of 19 BL Lacs and OVV's (Smith 1986; Smith *et al.* 1987). The objects were repeatedly observed for nearly two years. Again, the selection of the objects included in his study was not by any uniform process, other than they had bright enough optical magnitudes and were of high enough declination to allow frequent observation. The time period of their monitoring covers from 1982 to 1984, coincident to a large extent with the time period covered by Sitko *et al.* There is also an extensive overlap in the objects studied, 15 objects being in both samples. Together with data compiled by Angel and Stockman (1980) in their review paper on BL Lacs, the two studies described above give us the bulk of our data on the variability of the optical polarization of radio selected BL Lacs.

d.) *The Palomar-Green Bright Quasar Sample*

Berriman *et al.* (1990) have completed an optical polarization survey of all 114 QSOs from the Palomar-Green Bright Quasar Survey. No highly polarized quasars were found, consistent with the lack of powerful core dominated radio sources in the sample. Only eight of the 114 objects are radio loud QSOs. There are, however, many core dominated quasars with small ratios of radio flux to optical flux. There is evidence of a polarized synchrotron component (Impey *et al.* 1989) in the emission of one of the survey quasars, 3C 273. It does not however meet our definitions of HPQ or OVV (see Chapter 1). The details of the polarization properties of these UV excess selected quasars are in the paper by Berriman *et al.* (1990).

3.4 Radio Loud X-ray Selected Active Galactic Nuclei

Because the discrimination between a BL Lac object and a highly polarized quasar can sometimes seem arbitrary, we were concerned that during the classification of EMSS BL Lacs some BL Lacs or highly polarized quasars might have been missed. To examine this question, we observed the polarization of a “radio loud” sample of AGN from the EMSS (described in §3.1.d). We call these objects radio loud x-ray selected active galactic nuclei (RLXSAGN). The results of this study are described in Chapters 5 and 6. The objects we observed

are listed in Table 5.5. These objects met all of the requirements for inclusion in the EMSS (Gioia *et al.* 1990) and the following criteria:

1. While no information was available on the radio spectral index of these objects, 5 GHz radio flux densities were obtained by Stocke (1989b). We selected those objects with $\alpha_{\text{ro}} > 0.3$ (see Chapter 6 for the definition).

2. Our available telescopes and instrumentation forced us to impose the additional restrictions that members of our sample of RLXSAGN have $m_v < 18.5$ (as estimated from the POSS plates or CCD photometry, Stocke 1988) and $\delta > -20^\circ$.

A total of twenty-four objects were included in the sample.

3.5 Objects Included in Our Study

One of the main goals in our study of the optical polarization of BL Lacs is to confirm the classification of XSBLs by observing their optical polarization. We also wish to compare their properties to those of a complete sample of RSBLs. The XSBLs we chose for our observing program include the 22 members of the complete EMSS (C-EMSS), as many of the remaining EMSS BL Lacs and BL Lac candidates as we could observe (five more objects), the four *HEAO 1* A-1 high latitude survey objects, and a selection of six other XSBLs. These latter six objects include two serendipitous Einstein IPC sources that were in regions

excluded from the EMSS (1E 0514+064, Margon *et al.* 1986; 1E 1415.6+2557, Halpern *et al.* 1986) and four XSBLs identified in the *HEAO 1* LASS described above. The complete list of the XSBLs we observed as part of our program is listed in Table 5.1.

We also observed the polarization of the RLXSAGN described in §3.4. These objects were observed only until a limit of 4% was obtained for their white light polarization.

Finally we compiled from the literature a representative selection of studies of the optical polarization properties of RSBLs, HPQs, and Blazars. While there have been numerous efforts to study the polarization properties of RSBLs and Blazars, only recently have the studies of complete samples been published. We have summarized in §3.3 the selection criteria and general properties of the samples of radio selected objects to which we will compare the XSBLs and RLXSAGN. Other studies of the polarization properties of BL Lacs, HPQs, and Blazars are in the literature or are in preparation. Examples of other studies are the following: Ballard *et al.* 1990; Wills *et al.* 1990; Wills *et al.* 1989; Wills *et al.* 1990; Fugmann and Meisenheimer 1988.

CHAPTER 4

101 ARIZONA NIGHTS:

OBSERVING TECHNIQUES AND DATA REDUCTION

Determining the “typical” properties of intrinsically variable objects requires extensive monitoring and unusual amounts of telescope time. We were fortunate enough to obtain polarimetry and/or photometry of XSBLs on 101 nights between 1987 September and 1990 March. We obtained polarimetry and photometry using the UCSD 1.52 m, Steward Observatory (SO) 1.54 m, SO 1.52 m, and SO 2.3 m telescopes.

The vast majority of the observations were made with the “Two-Holer” polarimeter/photometer. We will describe “Two-Holer’s” design and operation below. More information about the instrument can be obtained from Gary Schmidt and from the following references: Sitko *et al.* 1985; P. S. Smith 1986; Schmidt 1982. A few observations were obtained using the Steward Observatory “Octopol” polarimeter. Efforts were also made to obtain measurements of the faintest XSBLs using a CCD and the Steward 2.3 m telescope. The balance of this chapter describes our observation techniques and data reduction procedures.

4.1 Polarimetry and Photometry with “Two-Holer”

a.) *The “Two-Holer” Polarimeter/Photometer*

In 1982 Gary Dean Schmidt commissioned the “Two-Holer” polarimeter/photometer. “Two-Holer” was built for and belongs to the University of Minnesota. It has been instrumental in the completion of at least two Ph.D. dissertations (P. S. Smith 1986 and the current work) and several extensive polarization studies of extragalactic objects (e.g. Sitko *et al.* 1985; Berriman *et al.* 1990; Kühr and Schmidt 1990). In the following two subsections, we describe the basic operation of the instrument and how it is used for polarimetry and photometry.

b.) *Polarimetry*

Detecting the Polarized Light: “Two-Holer” was modeled after the “Mini-pol” polarimeter (Freckler and Serkowski 1976). “Mini-pol” was extensively used in a great deal of the ground breaking polarimetry of BL Lacs and galactic objects in the late 1970’s and throughout the 1980’s (latest example, Impey and Tapia 1990). Like “Mini-pol”, “Two-Holer” uses a rapidly rotating (20.8 Hz) semi-achromatic half-wave retardation (180° phase shifter) plate to give uniform retardance across the entire range of observed wavelengths. A Wollaston prism then divides the light into ordinary and extraordinary rays.

Each ray is detected by a GaAs photomultiplier tube (RCA C31034). These two tubes respond with high quantum efficiency (10 to 20%) over a broad range of wavelengths (2500 to 8600 Å). The action of the rotating waveplate and the Wollaston prism produce a periodic modulation of the signal detected by each photomultiplier tube. The amplitude of the modulation is directly related to the fraction of the total source intensity which is linearly polarized. The frequency of the sinusoidal variation is 83.2 Hz (four times the frequency of the rotation of the half-waveplate). The phase shift of the functional fit to the data (relative to the fit of data on a polarization position angle standard) gives direct information on the position angle of the polarization. Each tube provides an independent measurement of the polarization. The two measurements are averaged together, weighted by the errors. Except for objects at low flux levels ($m_v > 20.0$), the errors are determined from photon statistics. We could not observe such faint objects with "Two-Holer" and the available telescopes. More of the details of the online data reduction and methodology are discussed by P. S. Smith (1986). The major change from the description in Smith (1986) is that the instrument and telescope motion during chopping are now controlled by an IBM compatible PC instead of an LSI-1103. The data reduction steps are described in sections below.

Dealing with the Variable Sky Background: The sky background and polarization are measured by chopping (wobbling) the telescope off of the object (in right ascension and/or declination) and observing blank sky every 15 to 30 seconds, depending on weather conditions and the phase of the moon.

Apertures: A Geneva wheel provides a selection of eight aperture plates located at the focal plane. The available apertures and their sizes in arcseconds at the various telescopes are listed in Table 4.1. Each plate is reflective and is tilted at an angle to allow viewing of the field with an off-axis intensified television camera. The camera allows the acquisition of objects as faint as $m_v \approx 20$. Guiding is done in general by the observer. At the Steward 2.3 m we occasionally were able to make use of an IBM PC controlled autoguider. During our polarimetry observations we usually used the smallest aperture possible (depending on the seeing or angular extent of the source) in order to minimize the contribution of the sky background, which can be highly polarized in the presence of moonlight.

Table 4.1: Apertures for “Two-Holer” and “Octopol”

Apt Code	Size in mm	“Two-Holer”			“Octopol”		
		SO 60" (f/16.0)	SO 61" (f/13.5)	SO 90" (f/16)	Size in mm	SO 61" (f/13.5)	SO 90" (f/9)
(1)	(2)	(3)	(4)	(5)	(6)	(7)	(8)
0	.51	4.3	5.1	2.9			
1	.94	8.0	9.4	5.3			
2	1.93	16.3	19.2	10.9			
3	3.8	32.2	37.8	21.5	.29	2.9	2.9
4					.36	3.6	3.6
5					.42	4.2	4.2
6					.48	4.8	4.8
7					.68	6.8	6.8

The entrees in Table 4.1 indicate the diameter in millimeters (columns (2) and (6)) or arcseconds (columns (3), (4), (5), (7), and (8)) of each aperture when used with the indicated telescope and instrument. Note the 61" telescope is in actuality a 60.56 inch telescope and is referred to in the text of the dissertation as the UAO 1.54 m telescope. The 60" telescope is referred to in the text as the SO 1.5 m. The 90" telescope is referred to in the text as the SO 2.3 m. The English unit designations are used in Table 4.1 because in the data tables in Appendix I, a code using the English units is used to designate which telescope and aperture were used for each observation. For example, in the tables of Appendix I “90-1” would indicate that the observation was made through a 5.3 arcsecond aperture since the 1 apt of “Two-Holer” was used while observing with the SO 90" (2.3 m) telescope.

Available Filters: “Two-Holer’s” electronically controllable filter-wheel has six positions and is located directly below the Wollaston prism. The wheel holds a set of glass filters including Johnson U , B , and V and Cousins R and I filters. The band passes and central wavelengths are listed in Table 4.2. The effective wavelength of each filter is λ_0 and the bandpass is $\Delta\lambda$ (Smith 1986). A_λ is the ratio of interstellar extinction at color X to the interstellar extinction at V . The values for A_λ are only approximate since they do not take into account the intrinsic spectral colors of the source (Smith 1990). C_λ is the flux density (in milli-Janskys) at a filter’s effective wavelength of a magnitude 15 A0 star (Smith 1990). The instrumental system is a close match to the photometric system defined by Bessell (1976). The sixth space in the filter wheel is left blank to allow for “white light” observations. The observed band pass then reflects the spectral response of the GaAs photomultiplier tubes (RCA C31034) and the atmospheric cutoff. Our “white light” measurements therefore span 3200 to 8600 Å.

Table 4.2: Filters Available with “Two-Holer”

Filter	λ_0 (μm)	$\Delta\lambda$ (μm)	C_λ	A_λ
U	0.36	0.06	1.68	1.53
B	0.44	0.10	3.90	1.32
V	0.55	0.11	3.64	1.00
R	0.64	0.16	3.08	0.84
I	0.79	0.14	2.55	0.62

Reducing the Polarimetry: The percent polarization should in theory be corrected for several effects:

First, any significant instrumental polarization should be removed. The instrumental polarization was measured by observations of non-polarized standard stars on three separate occasions during the three years of the monitoring program (once on each of the three Steward Observatory telescopes). On all occasions the two sigma upper limit on the instrumental polarization was 0.2%. Since we are always interested in polarizations or limits that are much larger than this small value, we make no correction for instrumental polarization.

Second, we must make a correction for the modulation efficiency of the semi-achromatic waveplate. The waveplate is not 100% efficient at modulating the incident polarized radiation and its efficiency is a function of wavelength. At the 2.3 m telescope, a glass lens is used to create the proper effective focal length, so the correction made for the B band is the most variable as a function of telescope. The lens changes the relative amount of light reaching the instrument across the B band. Since the efficiency of the waveplate changes across the B band, there is in principle a variable correction that should be made as a function of the spectral slope of the object being observed. In practice this correction is small and we utilize the single observed average modulation efficiency for the band. The efficiency corrections used for each color and telescope are presented

in Table 4.3. We also list the efficiency corrections for the few observations obtained with the “Octopol” polarimeter at the Steward Observatory 2.3 m. Note that the efficiency correction must also be applied to the error in the percent polarization (σ_p).

Table 4.3: Polarimetry Efficiency Corrections

Telescope	Instrument	Weff	Ueff	Beff	Veff	Reff	Ieff
SO 1.54	Two-Holer	.951	.934	.902	.949	.969	.953
SO 2.3 m	Two-Holer	.959	.947	.883	.951	.976	.964
UCSD 60"	Two-Holer	.948	.949	.909	.958	.973	.952
SO 1.52 m	Two-Holer	.960	.949	.900	.951	.973	.952
SO 2.3 m	Octopol	.824		.864	.874	.864	.844

Third, a correction for the “statistical bias” of percent polarization needs to be applied. The statistical bias correction is discussed in Wardle and Kronberg (1974) and in Simmons and Stewart (1985). Throughout this dissertation all quoted percent polarizations have been corrected for statistical bias unless otherwise indicated or the signal to noise ratio of the measurement (P/σ_p) is less than 1.5. In this latter case we do not apply the correction, but rather quote a two sigma limit to the polarization of $P_{\text{obs}} + 2 \times \sigma_p$. Whenever Stokes vectors are needed (for example for the Q/I *vs.* U/I plots in Appendix II) they have been properly calculated from the percent polarization corrected only for the modulation efficiency. The statistical bias correction used is

$$P_{\text{true}}^2 = P_{\text{obs}}^2 - \sigma_p^2.$$

The error in the polarization position angle is:

$$\sigma_\theta = 28.65^\circ \times (\sigma_p / P_{\text{obs}}).$$

The definition of the position angle error presented above is an underestimate when the measurements are of low signal to noise ratio. Throughout this dissertation we use the term polarization position angle to refer to the angle of the electric vector, \mathbf{E} . The measured polarization position angle needs to be referenced to a repeatable reference frame. This is accomplished by observing polarization position angle standards (which are generally stars with significant interstellar polarization or portions of reflection nebulae). At least one standard was measured each observing run and the corrections were very consistent. The numerous standards used were drawn from the lists provided in Krzeminski and Serkowski (1967), Mathewson and Ford (1970), and Turnshek *et al.* (1990). The position angles of the standards are generally known to better than one degree. The polarization position angle is defined to be 0° for the \mathbf{E} vector pointed north and increases toward the east. For example, an object with $\theta_p = 90^\circ$ has the \mathbf{E} vector of its polarized radiation pointed due east on the sky.

c.) *Photometry*

In order to monitor the flux variations of our program objects we made photometric observations whenever possible. A set of comparison stars for the XSBLs were observed and calibrated during five photometric nights between 1988 March and 1990 February. "Two-Holer" was used as either a dual or single channel photometer, depending on whether or not any polarimetry observations were being made during that night. The comparison stars and photometric standards were observed through 19.2" and 10.9" apertures at the SO 1.54 m and SO 2.3 m telescopes, respectively. The instrumental *ubvri* magnitudes of the comparison stars were transformed to the standard *UBVRI* system using observations of Landolt's (1983) equatorial photometric standard stars. Between 17 and 28 sets of *UBVRI* measurements of standard stars were made during each night. The transformation equations give root mean squares of the residuals for the standard stars. The values are the following: $\sigma_V = 0.014$, $\sigma_{B-V} = 0.012$, $\sigma_{U-B} = 0.025$, $\sigma_{V-R} = 0.009$, and $\sigma_{R-I} = 0.011$. These RMS values are those that result from averaging the five nights of data obtained for the calibration of the comparison stars.

The *UBVRI* magnitudes of the 76 comparison stars in the fields of XSBLs are given in Table 4.4. The identifications and finding charts for the comparison stars and XSBLs are provided in Appendix IV. In Table 4.4, the eight columns are respectively the object field name, comparison star ID, magnitude and error (listed in parentheses) for each color, and the number of nights each comparison

star was independently calibrated. The errors of the comparison star magnitudes were usually dominated by the systematic errors of the transformation from the instrumental *ubvri* to *UBVRI* magnitudes. These errors were determined from the residuals of the transformation for the photometric standards. A complete discussion of these comparison stars is presented by Smith, Jannuzi, and Elston (1991).

Table 4.4: *UBVRI* Comparison Stars in the Fields of X-ray selected BL Lacertae Objects.

Object	Star	<i>U</i> (σ)	<i>B</i> (σ)	<i>V</i> (σ)	<i>R</i> (σ)	<i>I</i> (σ)	<i>n</i>
MS 0122.1+0903	A	16.28 (0.07)	15.67 (0.02)	14.80 (0.01)	14.35 (0.01)	13.95 (0.02)	2
	B	16.67 (0.10)	16.47 (0.03)	15.60 (0.02)	15.08 (0.02)	14.63 (0.03)	2
MS 0158.5+0019	A	13.92 (0.02)	13.79 (0.01)	13.12 (0.01)	12.75 (0.01)	12.38 (0.01)	2
	B	15.05 (0.03)	14.29 (0.01)	13.30 (0.01)	12.76 (0.01)	12.26 (0.01)	2
MS 0205.7+3509	A	18.04 (0.32)	16.74 (0.04)	15.25 (0.02)	14.49 (0.02)	13.79 (0.02)	2
	B	14.74 (0.03)	14.65 (0.01)	13.95 (0.01)	13.57 (0.01)	13.17 (0.02)	2
MS 0257.9+3429	A	17.69 (0.22)	16.96 (0.05)	15.76 (0.02)	15.12 (0.02)	14.52 (0.02)	2
	B	16.46 (0.07)	16.04 (0.02)	15.19 (0.02)	14.60 (0.02)	14.09 (0.02)	2
MS 0317.0+1834	A	12.47 (0.02)	12.44 (0.01)	11.86 (0.01)	11.55 (0.01)	11.22 (0.01)	2
	B	15.03 (0.03)	14.62 (0.01)	13.76 (0.01)	13.33 (0.01)	12.87 (0.01)	2
H 0323+022	A	14.40 (0.03)	13.80 (0.01)	12.84 (0.01)	12.32 (0.01)	11.83 (0.01)	2
	B	14.94 (0.03)	14.97 (0.02)	14.40 (0.01)	14.02 (0.01)	13.61 (0.02)	2
MS 0419.3+1943	A	13.39 (0.03)	13.21 (0.02)	12.41 (0.01)	11.89 (0.02)	11.36 (0.02)	1
	B	14.42 (0.04)	14.16 (0.02)	13.28 (0.01)	12.73 (0.02)	12.15 (0.02)	1
1E 0514+064	A	13.84 (0.02)	13.84 (0.01)	13.24 (0.01)	12.89 (0.02)	12.53 (0.02)	1
	B	15.49 (0.04)	14.88 (0.02)	13.91 (0.02)	13.37 (0.02)	12.87 (0.02)	1
H 0548-322	A	13.84 (0.04)	13.88 (0.02)	13.36 (0.01)	13.02 (0.02)	12.71 (0.02)	1
	B	14.35 (0.05)	14.02 (0.02)	13.28 (0.01)	12.89 (0.02)	12.47 (0.02)	1

Table 4.4. (continued)

Object	Star	U (σ)	B (σ)	V (σ)	R (σ)	I (σ)	n
MS 0607.9+7108	A	16.73 (0.05)	16.29 (0.02)	15.47 (0.02)	14.95 (0.02)	14.50 (0.03)	1
	B	15.89 (0.05)	15.02 (0.02)	13.93 (0.02)	13.30 (0.02)	12.74 (0.03)	1
MS 0737.9+7441	A	13.19 (0.04)	12.58 (0.02)	11.70 (0.02)	11.24 (0.02)	10.82 (0.03)	1
	B	14.83 (0.04)	14.78 (0.02)	14.23 (0.02)	13.91 (0.02)	13.63 (0.03)	1
MS 0922.9+7459	A	13.98 (0.04)	13.49 (0.02)	12.69 (0.02)	12.24 (0.02)	11.85 (0.03)	1
	B	16.60 (0.07)	15.50 (0.02)	14.37 (0.02)	13.67 (0.02)	13.13 (0.03)	1
MS 0950.9+4929	A	14.02 (0.02)	13.76 (0.01)	13.05 (0.01)	12.64 (0.01)	12.27 (0.01)	3
	B	16.51 (0.06)	16.58 (0.03)	16.05 (0.03)	15.74 (0.03)	15.50 (0.04)	2
	C	14.37 (0.02)	14.26 (0.02)	13.61 (0.01)	13.27 (0.01)	12.91 (0.02)	2
MS 0958.9+2102	A	16.07 (0.05)	15.83 (0.02)	15.12 (0.02)	14.73 (0.02)	14.30 (0.02)	2
	B	16.78 (0.08)	15.91 (0.02)	14.35 (0.01)	13.34 (0.02)	12.52 (0.02)	2
H 1101-232	A	15.13 (0.04)	14.88 (0.02)	14.09 (0.02)	13.49 (0.02)	13.06 (0.02)	2
	B	15.82 (0.06)	15.32 (0.02)	14.40 (0.02)	13.77 (0.02)	13.34 (0.02)	2
MS 1133.7+1618	A	13.50 (0.03)	13.25 (0.01)	12.49 (0.01)	12.09 (0.02)	11.67 (0.02)	2
	B	16.78 (0.07)	15.46 (0.02)	14.13 (0.01)	13.27 (0.02)	12.50 (0.02)	2
MS 1207.9+3945	A	13.04 (0.02)	12.26 (0.01)	11.22 (0.01)	10.63 (0.01)	10.09 (0.01)	2
	B	13.52 (0.02)	13.59 (0.01)	13.05 (0.01)	12.75 (0.01)	12.42 (0.01)	2
H 1219+305	A	13.16 (0.02)	13.13 (0.01)	12.47 (0.01)	12.11 (0.01)	11.77 (0.01)	2
	B	14.71 (0.02)	14.65 (0.01)	14.01 (0.01)	13.61 (0.01)	13.22 (0.02)	2

Table 4.4. (continued)

Object	Star	U (σ)	B (σ)	V (σ)	R (σ)	I (σ)	n
MS 1221.8+2452	A	14.05 (0.02)	13.98 (0.01)	13.37 (0.01)	13.02 (0.01)	12.67 (0.01)	2
	B	14.48 (0.02)	14.50 (0.01)	14.51 (0.01)	14.51 (0.02)	14.54 (0.02)	2
MS 1229.2+6430	A	17.27 (0.11)	15.74 (0.03)	14.36 (0.02)	13.42 (0.02)	12.74 (0.03)	1
	B	14.80 (0.05)	14.58 (0.02)	13.91 (0.02)	13.57 (0.02)	13.26 (0.03)	1
MS 1235.4+6315	A	13.73 (0.04)	13.70 (0.02)	13.16 (0.02)	12.82 (0.02)	12.51 (0.03)	1
	B	15.90 (0.05)	15.51 (0.02)	14.65 (0.02)	14.20 (0.03)	13.84 (0.03)	1
MS 1402.3+0416	A	15.42 (0.03)	15.46 (0.02)	14.90 (0.02)	14.59 (0.02)	14.22 (0.02)	2
	B	11.89 (0.02)	11.88 (0.01)	11.37 (0.01)	11.03 (0.01)	10.73 (0.02)	2
MS 1407.9+5954	A	17.19 (0.07)	16.03 (0.02)	14.70 (0.01)	13.86 (0.01)	13.17 (0.02)	2
	B	14.28 (0.02)	13.63 (0.02)	12.67 (0.01)	12.10 (0.01)	11.61 (0.01)	2
1E 1415.6+2557	A	15.96 (0.03)	15.30 (0.02)	14.34 (0.01)	13.76 (0.01)	13.29 (0.02)	2
	B	14.88 (0.02)	14.80 (0.02)	14.16 (0.01)	13.84 (0.01)	13.46 (0.02)	2
H 1426+428	A	16.72 (0.07)	15.61 (0.03)	14.16 (0.01)	13.23 (0.02)	12.43 (0.02)	2
	B	15.80 (0.04)	15.47 (0.02)	14.61 (0.01)	14.17 (0.02)	13.79 (0.02)	2
	C	14.55 (0.04)	14.22 (0.02)	13.46 (0.02)	13.00 (0.02)	12.62 (0.03)	1
	D	16.26 (0.09)	16.14 (0.06)	15.53 (0.04)	15.20 (0.04)	14.82 (0.05)	1
MS 1443.5+6349	A	14.93 (0.05)	14.74 (0.02)	14.07 (0.02)	13.69 (0.02)	13.33 (0.03)	1
	B	13.62 (0.04)	12.85 (0.02)	11.90 (0.02)	11.38 (0.02)	10.91 (0.03)	1

Table 4.4. (continued)

Object	Star	U (σ)	B (σ)	V (σ)	R (σ)	I (σ)	n
MS 1458.8+2249	A	17.08 (0.05)	16.52 (0.03)	15.58 (0.02)	15.06 (0.02)	14.60 (0.02)	2
	B	13.25 (0.02)	13.18 (0.01)	12.57 (0.01)	12.23 (0.01)	11.89 (0.02)	2
MS 1534.2+0148	A	11.38 (0.02)	11.36 (0.01)	10.80 (0.01)	10.48 (0.01)	10.16 (0.02)	2
	B	14.48 (0.02)	13.68 (0.01)	12.71 (0.01)	12.14 (0.01)	11.67 (0.02)	2
MS 1552.1+2020	A	14.98 (0.02)	14.64 (0.01)	13.72 (0.01)	13.17 (0.01)	12.62 (0.01)	4
	B	10.97 (0.02)	10.64 (0.01)	9.83 (0.01)	9.40 (0.01)	8.94 (0.01)	3
	C	13.30 (0.02)	13.31 (0.01)	12.81 (0.01)	12.53 (0.01)	12.24 (0.01)	3
H 1652+398	A	14.23 (0.02)	13.55 (0.01)	12.61 (0.01)	12.11 (0.01)	11.63 (0.01)	3
	B	14.62 (0.02)	14.08 (0.01)	13.22 (0.01)	12.76 (0.01)	12.34 (0.01)	3
MS 1704.9+6046	A	13.06 (0.02)	12.76 (0.01)	11.98 (0.01)	11.53 (0.01)	11.10 (0.01)	2
	D	16.25 (0.03)	15.42 (0.02)	14.49 (0.01)	13.96 (0.01)	13.52 (0.01)	2
H 1722+119	A	14.37 (0.03)	13.86 (0.02)	12.95 (0.01)	12.45 (0.01)	11.99 (0.02)	2
	B	14.58 (0.03)	14.44 (0.02)	13.71 (0.01)	13.32 (0.01)	12.89 (0.02)	2
MS 1757.7+7034	A	15.70 (0.05)	15.50 (0.02)	14.88 (0.02)	14.49 (0.03)	14.17 (0.04)	1
	B	14.83 (0.05)	14.68 (0.02)	14.09 (0.02)	13.71 (0.02)	13.40 (0.03)	1
MS 2143.4+0704	A	14.80 (0.02)	14.58 (0.01)	13.93 (0.01)	13.55 (0.01)	13.19 (0.01)	3
	B	13.36 (0.02)	13.30 (0.01)	12.76 (0.01)	12.45 (0.01)	12.11 (0.01)	3

Table 4.4. continued

Object	Star	U (σ)	B (σ)	V (σ)	R (σ)	I (σ)	n
H 2155-304	2	12.92 (0.02)	12.71 (0.01)	12.03 (0.01)	11.62 (0.01)	11.26 (0.01)	2
	3	14.54 (0.03)	13.88 (0.01)	12.96 (0.01)	12.46 (0.02)	11.99 (0.01)	2
	C	13.17 (0.03)	13.16 (0.02)	12.58 (0.01)	12.22 (0.02)	11.87 (0.02)	1
MS 2336.5+0517	A	15.76 (0.04)	15.48 (0.02)	14.68 (0.01)	14.24 (0.01)	13.77 (0.02)	2
	B	15.56 (0.03)	14.96 (0.02)	14.03 (0.01)	13.55 (0.01)	13.09 (0.01)	2
MS 2342.7-1531	A	17.02 (0.10)	16.51 (0.04)	15.70 (0.02)	15.22 (0.02)	14.80 (0.03)	2
	B	15.68 (0.04)	14.95 (0.02)	13.95 (0.01)	13.42 (0.01)	12.94 (0.01)	2
MS 2347.4+1924	A	14.04 (0.02)	13.89 (0.01)	13.20 (0.01)	12.79 (0.01)	12.39 (0.01)	2
	B	13.46 (0.03)	13.28 (0.02)	12.55 (0.01)	12.16 (0.01)	11.73 (0.02)	1

4.2 Polarimetry with a CCD

Objects fainter than $m_v > 20.0$ are virtually impossible to observe with “Two-Holer” and telescopes smaller than 2.5 m. For this reason we have begun to obtain polarimetric observations using an instrument with a CCD as the detector. While our first efforts have only provided relatively high upper limits for several objects, the observations were made under relatively poor conditions. The system that we describe below has been successfully used to observe very faint objects, $m_v > 20.0$, (Jannuzi and Elston 1991) and we should be able to improve on the limits presented in Table IV in Appendix I.

Our CCD polarimeter has two configurations. The first uses four polaroid filters made from commercially available HN 38 sheet polaroid as the polarization analyzers and a TI 800² CCD as the detector. The polarizers were positioned with their transmission axes at position angles 0° , 45° , 90° , and 135° (North through East). This allows the measurement of both the Q and U Stokes parameters. Behind each polaroid was placed a quarter waveplate retarder with its fast axis rotated 45° with respect to the polaroid filter. This means that the CCD is always “seeing” circularly polarized light. This was done to minimize instrumental polarization. The second configuration uses a Savart plate (double calcite plate) as the polarization analyzer. Two exposures with the Savart plate

at 0° and 45° allow the measurement of both Q and U . The advantages of the Savart plate are that each exposure is a measurement of a single Stokes parameter and both Q and U can be determined with only two integrations (compared to the necessary four observations with the polaroid filter configuration). The major disadvantage is that the Savart plate produces two images of each object and overlapping of the images of adjacent objects can cause difficulties in measuring the polarization. Still, during poor weather conditions the Savart plate allows observations to be made. For both configurations the CCD was read out as a 400×400 array with a pixel scale of $0.297 \text{ arcsec pixel}^{-1}$ at the $f/9$ focus of the Steward Observatory 2.3 m. We used a "Nearly Mould" B filter to restrict our measurement to a region of the spectrum which is efficiently modulated by our polarization analyzers.

In order to obtain accurate flat fields, we used all of the sky-background limited exposures from the night in each configuration of polarization filter or Savart plate (i.e. one flat was generated for each of the polaroid filters and each of the two orientations of the Savart plate). The median of each group of frames (evaluated on a pixel by pixel basis) was taken to produce the flat field. The magnitudes of the objects in each image were measured for each filter combination using the IRAF APHOT task. The Stokes parameters we determine are the following: Q is determined by the difference between the 0° and 90° images, U is determined by the difference between the 45° and 135° images, I is the total intensity (sum of the four images divided by two). The percent

polarization is $P = \sqrt{(Q^2 + U^2)/I^2}$. The polarimetry errors are a combination of both photon statistics and the uncertainty in the sky level. It can be shown that the error in the percent polarization is then

$$\sigma_P^2 = \frac{2\sigma^2}{I^2} [1 + 2P^2] + \frac{\sigma_{sky}^2}{I^2}$$

where σ is the error in the photometry of the images (photon statistics), σ_{sky} is the product of the area in pixels of the aperture used for the photometry times the uncertainty in the sky background for an individual pixel (typically 0.1 of an ADU), and σ_P is the resulting error in the percent polarization.

CHAPTER 5

ARE XSBLs BL LAC OBJECTS?

POLARIMETRY AND PHOTOMETRY OF XSBLs

In this chapter we report on our observations of XSBLs. Our goal was to measure the polarization of all of the XSBLs in our sample and monitor their polarization as extensively as possible. The program objects are listed in Table 5.1 (see §5.1.a) and their selection is described in Chapter 3. Our observations have produced the largest and most systematically compiled database on the polarization of XSBLs. Every effort was made to observe all of the objects listed in Table 5.1 as extensively as possible. There are, however, very obvious disparities in the degree to which various objects were observed. This was the result of a variety of observational constraints. First, the bulk of our monitoring observations were made with the Steward Observatory (SO) 1.54 m telescope, which can not observe objects with declinations greater than 60° . Second, the fainter objects ($m_v > 19.0$) could not be observed at the SO 1.52 m and 1.54 m telescopes when the weather or seeing was less than excellent. Third, objects with low declinations were obviously not as easy to monitor as objects at higher declinations. Despite these problems, we were able to monitor extensively the

majority of the EMSS XSBLs. We note that our monitoring data is not biased by the past behaviour of the objects in the sample. It is well known that the early polarimetry of RSBLs (especially for the published data) is biased by the “hot object” effect. Objects which were observed to be highly polarized tended to be more extensively monitored than objects which had low polarizations when first observed. This problem is still affecting our knowledge of the polarization properties of HPQs and LPQs. In our study of XSBLs, we have made every effort to observe all of the program objects observable during each night of observations, regardless of their past polarization history. When possible, we have performed multicolor polarimetry in order to examine the frequency dependence of the percent polarization and position angle. Obviously we could not make such observations of the fainter objects. Hopefully other researchers with access to 4 m class telescopes and efficient polarimeters will be able to make these observations. When the weather permitted (55 of the 101 nights) accurate photometry, every effort was made to make a *V* band measurement. On some occasions multiband photometry was obtained for particular objects (see Appendix I).

In §5.1 we present the results of the optical polarimetry of XSBLs. We describe the detection, maximum observed polarization, duty cycle, variability, and frequency dependence of the polarization. In §5.2 we present the general results of our photometry including a discussion of detected variability. The complete listing of all of the data obtained for the program objects is contained in Appendix I. Detailed discussion of the properties of individual objects is also

contained in Appendix I. In §5.3 we discuss the proper classification of these objects. In §5.4 we describe our observations of radio loud x-ray selected AGN. In §5.5 we summarize the results of this chapter.

5.1 Polarimetry of XSBLs

5.1.a.) *Are XSBLs Polarized?*

Prior to our observations, the majority of our program objects had not been observed for polarized emission. We have observed thirty-seven objects, previously classified as XSBLs, for optical polarization (see Chapter 3 for details of classification process). Of these objects, thirty-one were observed to be polarized upon at least one occasion. We were able to make significant observations (a three sigma detection or a two sigma limit of $P < 4\%$) for twenty-one of the twenty-two members of the C-EMSS (see Chapter 3 for descriptions of samples). The choice of 4% as the cutoff for the polarization limit was to exclude the effects of interstellar polarization and because it was our chosen limit for use in calculating the duty cycle of polarization (see §5.1.c). Polarization measurements were made of nearby stars to check for interstellar polarization caused by dust along the line of sight. Often the stars checked included the photometry comparison stars described in §4.2. These observations are listed in Appendix I. If “ISP” appears in column (11) of Table 5.1, significant interstellar polarization was detected in the field of the object. For two objects (MS 0205.5+1454, MS 0419.3+1943)

the comparison stars were observed to be polarized with position angles agreeing with the polarization position angles of the objects. Conclusive variability in the polarization of the two objects was not detected. We do not consider either of these objects to have been shown to be intrinsically polarized. We discuss the proper classification of these two objects in §5.3. The complete listing of the data is presented in Appendix I. The polarization properties of the individual objects are summarized in Table 5.1. Column (1) lists the object's x-ray survey or catalogue name. Column (2) indicates to which x-ray selected sample the object belongs. HEAO-A1 means the object was taken from the *HEAO* A-1 high latitude sample. HEAO-NRL means the object was taken from the NRL *HEAO*-1 catalogue as identified by the Large Area Sky Survey (see Chapter 3). C-EMSS means the object is a member of the complete EMSS BL Lac sample. EMSS means the object is an EMSS candidate BL Lac. Columns three through ten refer to the polarization and photometry observations of the objects and will be explained in the following sections.

5.1.b) *Maximum Observed Polarization, P_{\max}*

We will be comparing in Chapter 6 the polarization properties of the XSBLs to various samples of RSBLs and HPQs. One of the properties we will compare is P_{\max} (or P_m), the maximum percent polarization ever observed for an object. Ideally we would always compare polarized fluxes or luminosities, but the advantage of percent polarization is that it is a quantity that can be

measured even under nonphotometric conditions and does not depend on the availability of a measured redshift for the object. When possible we also made photometric observations which allowed the determination of S_p , the polarized flux. The percent polarization (P) is therefore much more extensively monitored than S_p . We list in column (3) of Table 5.1 the maximum observed “white light” (see Chapter 4, §4.1.b, for definition) percent polarization, P_{\max} , for each of our program objects. The error in this measurement is listed in column (4). The variability of the object, thoroughness of monitoring, dilution of the nonthermal source by host galaxy starlight, and other factors affect this quantity. These issues will be discussed when we compare the maximum observed polarizations of XSBLs to those of RSBLs.

For eleven of the program objects we were able to make polarization measurements through color filters (see Chapter 4 for description of filters). In ten cases the maximum observed polarization at U or B was greater than the white light P_m . In column (5) of Table 5.1, we list the maximum observed percent polarization at any optical frequency if it was greater than the white light measurement. The errors for the observations listed in column (5) are not listed in Table 5.1 because of a lack of space, but can be found in Appendix I.

When a limit is listed for P_m (column 3), it is the best limit obtained for the polarization of the object. We define our two sigma limits as

$$P_{\text{obs}} + 2 \times \sigma_p.$$

Finally we note that the following objects were only detected to be polarized on one occasion or were marginal detections: MS 0607.9+7108, H 1101-232, MS 1229.2+6430, MS 1235.4+6315, MS 2336.5+0517, MS 2347.4+1924. For further discussion of each object see the "Notes on Individual Objects" in Appendix II.

Description of Table 5.1

We present in Table 5.1 a list of our program XSBLs and a summary of our polarimetry and photometry of these objects. The detailed explanations of the acquisition and derivation of the quantities presented in the table are contained in the various sections of this Chapter. For the next three pages we give a description of the contents of each column of the table and reference to which sections give a more complete description. The table follows the conclusion of this description.

Column (1): Contains the object name.

Column (2): Contains an abbreviation for the x-ray flux limited survey to which the object belongs. These surveys are described in Chapter 2. EMSS = Member of the Einstein Extended Medium Sensitivity Survey. C-EMSS = Member of the Complete EMSS survey. HEAO-A1=Member of the Piccinotti *HEAO* A-1 sample. HEAO-NRL = member of the Naval Research Lab *HEAO*-1 MC-LASS sample.

Column (3): The maximum observed white light percent polarization during our monitoring, P_m (§5.1.b).

Column (4): The one sigma error for the observations listed in column (3).

Column (5): The maximum observed percent polarization at any optical wavelength (§5.1.b). The one sigma error is given in parentheses.

Column (6): The V band magnitude of the object at the time that P_m was observed (§5.2). The errors are given along with all of our photometry in Appendix I. The one sigma error in our V band magnitudes is typically less than two hundredths of a magnitude.

Column (7): The brightest V band magnitude reached by the object, $m_{v,Br}$ (§5.2).

Column (8): The white light percent polarization of the object at the time of $m_{v,Br}$ (§5.2).

Column (9): The faintest V band magnitude reached by the object, $m_{v,Fa}$ (§5.2).

Column (10): This column contains a set of codes describing each object's known variability as confirmed by our observations. The symbols appearing in column 9 refer to polarization properties and are the following:

p = detected significant polarization intrinsic to the source, but no significant variation in the percent polarization has been observed.

P = detected significant polarization intrinsic to the source and the percent polarization has been observed to vary significantly ($\Delta P > 2\sigma_p$).

θ = the position angle of the polarization has been confirmed to be variable.

θ_{pref} = during the years of monitoring, the position angle of the polarization was not observed to vary significantly.

Θ_{pref} (Θ_{stable}) = during the years of monitoring, the position angle of the polarization was observed to vary significantly, but only over a limited range. We say that it has a stable polarization position angle if the object's behavior indicates a preferred position angle, but it does not meet our defined requirements to be designated as having a preferred angle of polarization (see §5.1.f for the exact definition).

Column (11): This column contains comments on the individual objects. If "ISP" appears, we detected significant interstellar polarization in the field of the object. If a "C" appears, it means we have confirmed the classification of the object as a BL Lac object. If "Marg Det." appears it means that only a marginal detection of polarized emission was made.

If a † appears next to a listed magnitude, it means that the value was obtained from Stocke *et al.* (1990) or Morris *et al.* (1990b) and was determined from CCD observations on Mount Hopkins with a 24" telescope. The errors are reported to be less than one tenth of a magnitude.

Table 5.1: Summary of Polarimetry and Photometry of XSBLs

Object	Sample	P_m (%)	σ_p	P_m (%)	m_v	$m_{v,Br}$	P_w (%)	$m_{v,Fa}$	Variable	Comment
(1)	(2)	W (3)	(4)	Color (5)	at P_m (6)	(7)	$m_{v,Br}$ (8)	(9)	(10)	(11)
MS 0122.1+0903	C-EMSS	≤ 3.50				20.07	≤ 6.25			
MS 0158.5+0019	C-EMSS	3.03	0.88		18.30	18.30	≤ 3.60	18.60	M p	C
MS 0205.7+3509	C-EMSS	3.59	1.04		19.27	?18.38	≤ 4.00	19.32	M?	ISP
MS 0257.9+3429	C-EMSS	6.25	1.14		18.61	18.42	2.20	18.71	M P θ_{pref}	C
MS 0317.0+1834	C-EMSS	5.20	0.67			18.13	3.90		P Θ_{pref}	ISP, C
H 0323+022	HEAO-NRL	10.01	0.63	13.15	16.23	16.23	10.17	17.03	M P Θ_{pref}	C
MS 0419.3+1943	C-EMSS	≤ 2.90				$\dagger 20.26$				ISP
1E 0514+064		5.80	1.70		19.25	18.35	≤ 2.50	19.25	M P θ	C
H 0548-322	HEAO-A1	3.21	0.70	3.32	15.54	15.48	1.41	16.13	M P Θ_{pref}	C
MS 0607.9+7108	C-EMSS	4.82	0.67			$\dagger 19.60$			p	C
MS 0737.9+7441	C-EMSS	2.70	0.29		17.06	17.06			P Θ_{stable}	C
MS 0922.9+7459	C-EMSS	≤ 3.90				20.02	≤ 6.00			
MS 0950.9+4929	C-EMSS	5.19	1.03		18.82	18.45	4.27	18.85	M P θ	C
H 1101-232	HEAO-NRL	1.33	0.42		18.35	18.35	1.33		p	
MS 1133.7+1618	EMSS	≤ 15.00				$\dagger 20.04$				
MS 1207.9+3945	C-EMSS	≤ 4.00				≥ 20.00				
H 1219+305	HEAO-A1	6.83	0.70			15.30	4.92	16.48	M?P θ	C
MS 1221.8+2452	C-EMSS	11.86	0.61	14.26	17.34	17.33	2.08	18.17	M P Θ_{pref}	C
MS 1229.2+6430	C-EMSS	2.28	0.35			17.41	≤ 1.84	17.47	M p	C
MS 1235.4+6315	C-EMSS	2.62	0.98		18.83	18.53	≤ 4.00	18.83	M	Marg Det.
MS 1258.4+6401	EMSS	≤ 20.00				$\dagger 19.50$				

Table 5.1 continued: Summary of Polarimetry and Photometry of XSBLs

Object	Sample	P_m (%) W	σ_p	P_m (%) Color	m_v at P_m	$m_{v,Br}$	P_w (%) $m_{v,Br}$	$m_{v,Fa}$	Variable	Comment
(1)	(2)	(3)	(4)	(5)	(6)	(7)	(8)	(9)	(10)	(11)
MS 1402.3+0416	C-EMSS	9.52	0.44	11.40	17.14	16.46	6.78	17.30	M P Θ_{pref}	C
MS 1407.9+5954	C-EMSS	8.64	1.80		19.36	19.36	8.64		p	C
1E 1415.6+2557		7.53	0.74	8.60	17.08	16.69	5.73	17.08	M P Θ_{pref}	C
H 1426+428	HEAO-NRL	2.48	0.55			16.51	2.35		p	C
MS 1458.8+2249	C-EMSS	7.03	0.42	7.59	16.67	16.28	2.75	17.03	M P θ	C
MS 1534.2+0148	C-EMSS	4.51	1.10			18.73	3.78	18.80	p θ	C
MS 1552.1+2020	C-EMSS	5.95	1.14		17.32	17.32	5.95	17.90	M P Θ_{pref}	C
H 1652+398	HEAO-A1	4.18	0.15	7.77	13.60	12.90	3.02	13.85	M P Θ_{pref}	C
MS 1704.9+6046	EMSS	≤ 3.10				19.21	≤ 3.10	19.86	M	
H 1722+119	HEAO-NRL	15.54	0.35	18.04	15.47	15.24	4.33	15.57	M P Θ_{stable}	C
MS 1757.7+7034	C-EMSS	3.70	0.85			[†] 18.27			p θ	C
MS 2143.4+0704	C-EMSS	10.83	1.01	11.60	18.05	17.74	5.45	18.26	M P Θ_{pref}	C
H 2154-304	HEAO-A1	10.80	0.12	11.20	13.07	13.05	10.33	13.38	M P Θ_{pref}	C
MS 2336.5+0517	EMSS	5.13	1.69		19.53	19.53	5.10		p	Marg Det.
MS 2342.7-1531	EMSS	6.33	1.24		19.81	19.81	6.33		p	C
MS 2347.4+1924	EMSS	3.09	0.92			19.93	≤ 3.10	p		

5.1.c) *The Duty Cycle of Polarization*

If we make the assumption that all of the XSBLs in the C-EMSS are intrinsically members of the same class of object, then a single set of polarization measurements of this sample gives us a “snapshot” determination of the duty cycle of polarization for XSBLs. We interpret the duty cycle as the fraction of the sample that for a given epoch of observation has percent polarizations above a given cutoff level. The duty cycle is observationally defined as what fraction of the time a member of the class is highly polarized (above the cutoff value). We are making the assumption that the temporal distribution of polarization in a single object is equivalent to the distribution of polarization measured in all objects in the class. Similar calculations have been done for RSBLs (Kühr and Schmidt 1990) and Blazars (Impey and Tapia 1990; Fugmann and Meisenheimer 1988). Because the majority of our observed two sigma limits for nondetections are at four percent, we have chosen that value as the dividing line in our duty cycle calculation. This is slightly higher than the conventional boundary of 3% for detection of significant polarization (e.g. Moore and Stockman 1985). The three percent value was chosen as an aid in discriminating against objects polarized by interstellar dust (typical interstellar values are less than one percent; Mathewson and Ford 1970). Neither the calculation for Blazars nor RSBLs is significantly changed if we change the limit to 4%. We will compare the duty cycles of the various samples in Chapter 6. For now we concentrate on the various values of the duty cycle for XSBLs.

For the C-EMSS we have multiple significant observations for twenty of the twenty-two objects. We have computed the duty cycle for the first, second, and last epoch of observation of the C-EMSS sample. Remember that the C-EMSS is a complete x-ray flux limited sample (Chapter 3). For some objects the first, second, or last epoch of observation is only an upper limit. For objects that were detected to be polarized on at least one occasion (for the C-EMSS sample, seventeen), we have assumed for the duty cycle calculation that the object was polarized at the limit value. For objects that were never observed to be polarized (for the C-EMSS sample, five), we have considered two possibilities. We first assume that these objects are BL Lacs and that we have just failed to detect the polarization. Under this assumption we have used the limit values as the observed polarization. The second possibility is that these objects are misclassified and we have also calculated the duty cycle for the sample without the inclusion of these objects. For a very few members of the sample, we do not have three epochs of observation and we have assumed that the object had a percent polarization greater than 4%. For example, we were never able to observe MS 1443.5+6349 and we have assumed for the calculations below that this object had a polarization greater than 4%. We have calculated the duty cycle of the C-EMSS XSBLs in a manner to avoid at all costs underestimating the amount of time spent at large values of percent polarization. Consequently, we have almost certainly overestimated the duty cycle. We calculated the errors by considering the one sigma range of observations for each object. If an object

was observed to be 3.5% polarized with an error of 0.7%, the object was counted as less than four percent, but contributed to the positive error.

The computed values for the three epochs are $41^{+14}_{-27}\%$, $32^{+14}_{-14}\%$, and $46^{+10}_{-14}\%$. If we restrict ourselves to those objects in the C-EMSS which were observed on at least one epoch to have intrinsic polarized emission, the sample size decreases to sixteen objects and the new duty cycle estimates are $44^{+6}_{-31}\%$, $25^{+19}_{-6}\%$, and $50^{+13}_{-13}\%$. The EMSS is biased against objects of high x-ray flux (see Chapter 2). If we add the HEAO A-1 objects to the C-EMSS, the duty cycles calculated from the first and last epochs of observation are $38^{+11}_{-23}\%$ and $42^{+8}_{-12}\%$ (and excluding objects never detected to be polarized, $38^{+5}_{-23}\%$ and $48^{+10}_{-10}\%$). For the entire program sample (34 objects with detections or two sigma limits of better than 4%), the first and last epoch duty cycles are $32^{+9}_{-9}\%$ and $47^{+9}_{-26}\%$. If we restrict the calculation to those objects with confirmed detections on at least one epoch, our sample size drops to twenty-nine objects and the resulting duty cycles are $38^{+10}_{-10}\%$ and $45^{+10}_{-21}\%$. We adopt 40% as the duty cycle of XSBLs for comparison to the duty cycle of RSBLs (see Chapter 6).

Consistent with the similarity of all the calculated duty cycles, the individual objects are variable (§5.1.d) and spend differing amounts of time above and below the 4% cutoff. Furthermore, the measured duty cycles are not the consequence of some small population of highly polarized ($P > 4\%$) XSBLs mixed in with a group of objects that are not capable of being highly polarized. The

majority of the program objects were observed to be highly polarized on at least one occasion (20 out of 34, 60%). If we restrict our consideration to the objects with detected polarized emission (the confirmed BL Lacs), $69^{+13}_{-10}\%$ (20 out of 29, with the error reflecting the fact that some objects were within one sigma of the dividing line of 4% polarization) were observed to be highly polarized at least once.

5.1.d) *Variability of Polarization*

Our polarization measurements determine both the percent polarization and position angle for the observation epoch. For the majority of the program objects, particularly those with declinations less than 60° , we have multiple observations and can examine whether or not the percent polarization and/or position angle vary with time. We will examine the total flux and polarized flux variations in §5.2 and §6.7 respectively. Our observing runs were in general a few days in duration and spaced at roughly monthly intervals.

Column (10) of Table 5.1 contains a set of codes describing for each observed object its known variability as confirmed by our observations. The symbols appearing in column (10) referring to polarization properties are the following:

p = detected significant polarization intrinsic to the source, but no significant variation in the percent polarization has been observed.

P = detected significant polarization intrinsic to the source and the percent polarization has been observed to vary significantly ($\Delta P > 2\sigma_p$).

θ = the position angle of the polarization has been confirmed to be variable.

θ_{pref} = during the years of monitoring, the position angle of the polarization was not observed to vary significantly.

Θ_{pref} (Θ_{stable}) = during the years of monitoring, the position angle of the polarization was observed to vary significantly, but only over a limited range. We say that it has a stable polarization position angle if the object's behavior indicates a preferred position angle, but it does not meet our defined requirements to be designated as having a preferred angle of polarization (see §5.1.f for the exact definition).

Determining the time scales of variability for the entire sample is more difficult than listing which objects are demonstrated to be variable. We note that in our data the shortest observed period of time for a significant change in P and θ is one day.

5.1.e) *Frequency Dependence of Polarization*

We were able to obtain multicolor polarimetry for eleven of our program objects. The data are presented in Table II of Appendix I. In Figures II.1

through II.4 of Appendix II we plot the selected data for four objects. A range of frequency dependent behavior is observable. Some objects show no significant frequency dependence to their percent polarization or position angle, while other objects show strong frequency dependence. In all of these latter cases, the percent polarization increases with increasing frequency. While our monitoring of the multicolor polarization of these objects is not extensive, on 24 January 1988 we observed in H 0323+022 the first reported rotation of the position angle of an XSBL with frequency (see Appendix I for data).

Table 5.2 summarizes the observed frequency dependence behavior of the polarization for the eleven observed objects. We will discuss further the significance and interpretation of these multicolor polarimetry data in Chapter 6.

Table 5.2: Frequency Dependence of the Polarization of XSBLs

Object	Sample	Frequency Dependence Observed	No. Obs
H 0323+022	HEAO-NRL	Strong dependence, always	7
H 0548-322	HEAO-A1	No significant dependence	2
H 1219+305	HEAO-A1	No significant dependence	5
MS 1221.8+2452	C-EMSS	Both types of behavior	4
MS 1402.3+0416	C-EMSS	Both types of behavior	5
1E 1415.6+2557		Strong dependence, always	2
MS 1458.8+2249	C-EMSS	No significant dependence	1
H 1652+398	HEAO-A1	Detectable dependence,	13
H 1722+119	HEAO-NRL	Strong Dependence, usually	7
MS 2143.4+0704	C-EMSS	No significant dependence	2
H 2154-304	HEAO-A1	No significant, usually	16

5.1.f) *Preferred Polarization Position Angles*

A substantial number of the XSBLs in our monitoring program have exhibited a preference for a limited range of angles. The behaviour we are describing is different from the time scale or amount of variability. We describe an object as having a preferred polarization position angle if during our three years of monitoring the observed position angles are concentrated to a limited range of angles (We give a specific and quantitative definition below). This does not mean that these objects might not lose this preference over time or develop a new preferred position angle in the decades ahead. To test for such behavior, even longer periods of monitoring are required. We are reporting the relatively stable behavior of the position angle for a large number of objects in our sample. We must keep in mind that while observing runs were usually separated by a month or more, many of the objects were observed repeatedly during a two to five day run. It could convincingly be argued that observations within one week are not "independent" and that we should not let four or five observations in one week skew our impression of the stability of the polarization position angle. Unfortunately there is no a method for deciding what is enough separation in time to call two observations "independent". We can however still address the question of preferred position angles over the time period of our study by limiting ourselves to considering well-studied objects. We consider an object to be well-studied for position angle variability if the following criteria are met:

1. The object must have been observed to be significantly polarized during at least six separate observing runs. Observing runs are generally two to seven days in length and are separated by at least three weeks.

2. We must have a significant baseline of observations of the object. We choose the arbitrary number of 20 months separation between the first and last observation.

Table 5.3 lists the XSBLs which meet these criteria and are therefore well-studied. The objects MS 0737.9+7108 and H 1722+119 are also included in Table 5.3 for reasons explained below. The individual columns of Table 5.3 contain the following information: (1) object name, (2) sample membership, (3) variability code as defined for Table 5.1, (4) the number of observation epochs (nights observed), (5) the number of observing runs during which the object was significantly polarized, (6) the observed range of the polarization position angle (θ), (7) the mean position angle calculated by including only one observation from each observing run, (8) the variance of the observed distribution of position angles, (9) the average deviation from the mean, (10) the time in months between the first and last observations of the object.

For our study, we describe objects which meet the following criteria as having preferred position angles: (1) They are well observed for position angle variability (defined above), (2) They have average deviations from the mean angle of less than 20° . This last criterion is a quantitative means of expressing the

Table 5.3: The Longterm Variability of the Polarization Position Angles of XSBLs

Object	Sample	Variability	No. of Obs	No. of Runs	Obs θ	$\bar{\theta}$	σ_{θ}	Avr. Dev.	Time Baseline in months
(1)	(2)	(3)	(4)	(5)	(6)	(7)	(8)	(9)	(10)
MS 0257.9+3429	C-EMSS	M P θ_{pref}	13	6	153-185	170	11	8	24
MS 0317.0+1834	C-EMSS	M P Θ_{pref}	16	9	118-192	169	25	20	29
H 0323+022	HEAO-NRL	M P Θ_{pref}	34	17	116-204	173	15	10	29
H 0548-322	HEAO-A1	M P Θ_{pref}	17	10	167-215	12	14	11	24
MS 0737.9+7441	C-EMSS	P Θ_{stable}	4	4	148-174	164	12	10	4
H 1219+305	HEAO-A1	M P θ	31	13				52	29
MS 1221.8+2452	C-EMSS	M P Θ_{pref}	21	8	0-80	48	20	15	26
MS 1402.3+0416	C-EMSS	M P Θ_{pref}	19	10	35-145	97	25	17	25
1E 1415.6+2557		M P Θ_{pref}	17	10	4-32	18	8	6	25
MS 1458.8+2249	C-EMSS	M P θ	15	10	0-180			37	25
MS 1552.1+2020	C-EMSS	M P Θ_{pref}	14	9	44-73	52	8	6	23
H 1652+398	HEAO-A1	M P Θ_{pref}	38	22	91-130	115	10	9	29
H 1722+119	HEAO-NRL	M P Θ_{stable}	17	8	85-140	104	8	6	12
MS 2143.4+0704	C-EMSS	M P Θ_{pref}	26	11	35-56	46	8	6	22
H 2154-304	HEAO-A1	M P Θ_{pref}	21	9	110-180	140	18	15	25

observation that the range of variability of the position angle is limited. What we mean by limited range of θ is best exemplified by the data for MS 2143.4+0704. Examination of Figure 5.1 shows that over twenty-two months of observation, the position angle of the polarization did not vary by more than twenty degrees.

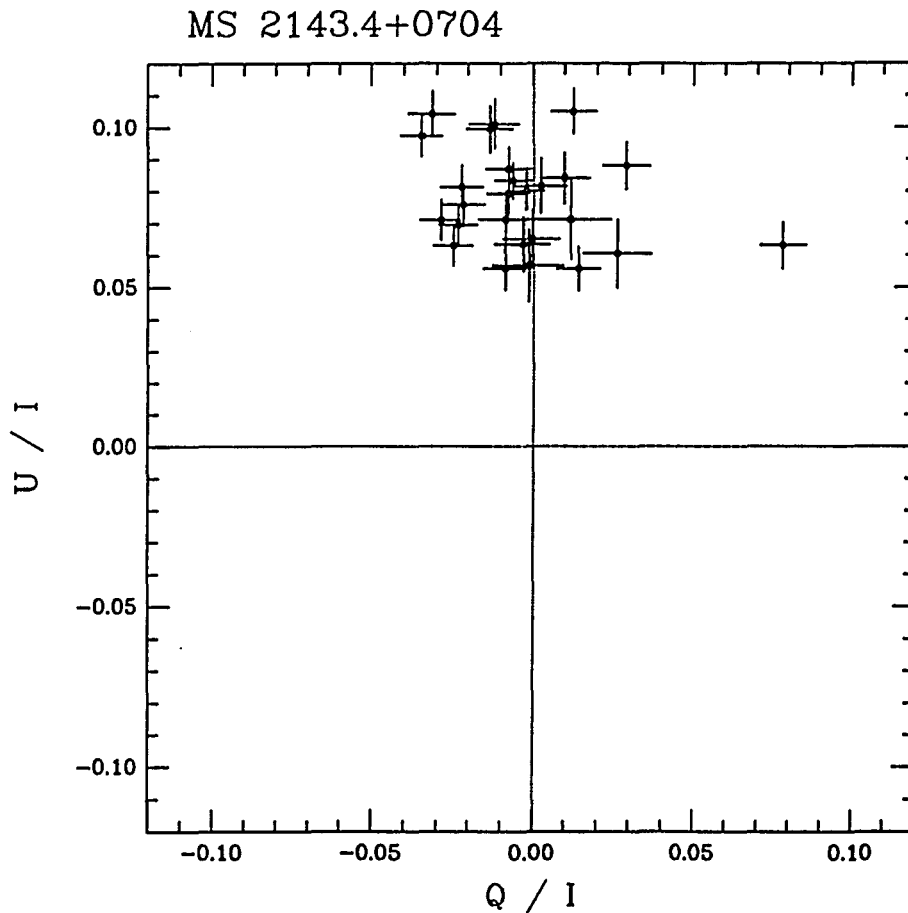


Figure 5.1—Our white light polarization observations of MS 2143.4+0704 are plotted. The x and y axes are the normalized Stokes Q and U parameters. The one sigma error bars are indicated by the vertical and horizontal lines centered on each data point. The data (listed in Appendix I) was obtained during our monitoring program and covers a time baseline of twenty-two months. Although the position angle of the polarization (position angle of the electric field vector E) is variable, this object has a preferred position angle.

Under this definition, eleven of the fifteen objects in Table 5.3 have preferred position angles. MS 0737.9+7441 and H 1722+119 have observed position angles which do not vary over a wide range, but do not meet the first criterion listed above. We describe them as having stable position angles. We only have four epochs of detected polarized emission for MS 0737.9+7441 and the baseline of observations for both MS 0737.9+7441 and H 1722+119 is only one year. H 1722+119 was added late to our study when its identification as an XSBL was available in 1989 (Brissenden *et al.* 1990). H 1722+119 has the highest observed percent polarization of any XSBL.

Of the twenty-two C-EMSS BL Lacs, seven are included in our well-studied sample. An amazing six out of seven (86%) have preferred position angles! In fact 85% of the entire well-studied sample (11 out of 13) have preferred position angles. All but one of the objects (MS 0257.9+3429) have confirmed variable position angles, but the range of variation is limited. Figures II.5 through II.20 of Appendix II are plots of the normalized Stokes parameters (Q/I vs. U/I) for the objects in the well studied sample. We have plotted all of our white light polarization observations for each object. In Chapter 6 we will compare these objects to RSBLs and discuss further the implications of the remarkable stability of their polarization position angles.

5.2 Are XSBLs Photometric Variables?

Photometry of XSBLs

One of the defining criteria of a BL Lac is that the object exhibit variability in its flux. Our photometry of XSBLs allows us to look for variability and to determine polarized fluxes from our polarimetry. The photometry data is presented in Appendix I. The data reduction and calibration of comparison stars is discussed in Chapter 4. While we tried to obtain photometry when possible, our main observational goal was to monitor the polarization of our program objects. This meant that we occasionally passed up the opportunity to obtain a photometry measurement of an object if, by doing so, we could obtain a polarization measurement of an additional object. Additionally if the conditions did not allow the measurement of the object's polarization, we did not try to measure its total flux. For example, if an object appeared on the television monitor to have $m_v > 20$, and the seeing was greater than one arc second, we knew that we would not be able to obtain efficiently an accurate polarimetry observation and we would move on to the next object. For these reasons, we are not complete in our photometric observations of the sample. Other researchers have been observing these objects however. Rudy Schild and John Stocke (1990) report that all of the C-EMSS BL Lacs show variability. In column (10) of Table 5.1 we indicate with an "M" objects for which we

have confirmed variability. We consider that two photometric observations of an object which differ by more than 2σ confirm the variability of the object. If an “M?” appears it means that there is a question about the significance of the variability and the notes on individual objects in Appendix II should be consulted. Our data combined with the observations of Schild *et al.* (1990) allow the determination that all of the objects in Table 5.1 are variable except for MS 0419.3+1943, H 1101–232, MS 1207.9+3945, H 1426+428, MS 2336.5+0517, MS 2342.7–1531, and MS 2347.4+1924. Continued or improved monitoring might detect variability in these later objects since the long term (greater than two years) behavior of XSBLs is unknown.

We did not observe any large or rapid changes in the brightness of these objects. When we did detect variability, the change in brightness was always less than 1.2 magnitudes (peak to peak). None of the observed objects could be considered to be optically violent variables (see Chapter 1 for definition). Our photometry is not extensive enough to examine in detail what time scales are typical for photometric variability.

When we do have photometry, we can use our polarimetry and the observed redshifts to calculate the polarized fluxes and luminosities of our objects. We will discuss these properties in more detail as part of our comparison of the XSBLs to RSBLs. We note here that we have examined our data set to answer the following question: Are increases in percent polarization accompanied by

an increase in total and/or polarized flux? There is no fixed rule. Objects are observed to get brighter, have the polarized flux increase, and have P decrease. Objects are observed to get fainter, have the polarized flux decrease, and have P increase. On other occasions, an increase in unpolarized flux is accompanied by a relative increase in polarized flux, resulting in an increase of brightness, but no change in the percent polarization. While a range of behaviour is observed, there is a tendency for the maximum observed percent polarization to indicate when the object is experiencing a period of maximum production of polarized flux.

This can be demonstrated directly. The data supporting the discussion below is presented in Appendix I and in the following columns of Table 5.1: (6) m_v of object when P_m observed, (7) the brightest magnitude reached by the object, $m_{v,Br}$, (8) the white light percent polarization of the object at the time of $m_{v,Br}$, (9) the faintest magnitude observed for the object. When one of these columns has no value it means there are insufficient data. If a value is given for $m_{v,Br}$ but not for $m_{v,Pa}$, the value in column (7) is not the brightest magnitude, but whatever V band photometry we had available. We have the necessary polarimetry and photometry for eighteen objects. We have compared the polarized flux at the epoch of maximum observed percent polarization (P_m) and the polarized flux when the object is at its observed brightest ($m_{v,Br}$). For nine objects we observe P_m at the same time as $m_{v,Br}$. For nine objects the epochs of P_m and $m_{v,Br}$ do not correspond. For two of these, the polarized flux

was greater at the time of m_{v,B_r} despite a lower observed percent polarization (P at time of $m_{v,B_r} < P_m$). For the other seven objects the polarized flux was greater at the time of P_m even though the corresponding m_v is greater than m_{v,B_r} . In Table 5.4 we summarize these results. The behavior of two specific objects is worth detailed attention. MS 1221.8+2452 has displayed a great range in polarization at the same brightness. On two occasions this object had an m_v of 17.3. The polarizations, however, were quite different, 11.86 (± 0.61) and 2.08 (± 0.28) %. 1E 1415.6+2557 had its largest output of polarized emission when it was at its faintest. We do not have a clear picture of what happens to these objects at low total and polarized fluxes, because it is not easy to obtain adequate data when these objects are faint and/or weakly polarized. There was also a bias on the part of the observers always to obtain photometry when the object was at a record high percent polarization. This might bias the above discussion.

In general, however, it seems that XSBLs are variable in total and polarized emission but that total flux increases are not necessarily accompanied by an increase in polarized flux.

5.3 Are XSBLs Really BL Lacs?

We have obtained a large amount of data on the polarizations and flux variations of our study sample of XSBLs and can use these data to examine

Table 5.4: Relationship between P_m , Pol Flux and $m_{v,Br}$

Less Pol Flux at $m_{v,Br}$	The Same Pol Flux	More Pol Flux at $m_{v,Br}$	
MS 0257.9+3429	H 0323+022	MS 1552.1+2020	MS 0950.9+4929
1E 0514+064	MS 0737.9+7441	H 2154-304	H 1652+398
H 0548-322	MS 1402.3+0416	MS 2336.5+0517	
MS 1221.8+2452 [†]	MS 1407.9+5954		
MS 1458.8+2249	1E 1415.6+2557		
H 1722+119	H 1426+428		
MS 2143.4+0704			

the objects' classifications as BL Lacs. As we discussed in Chapter 1, BL Lac objects must exhibit flux variations and produce polarized emission in addition to the spectroscopic restriction of having no strong emission or absorption features. We can now reevaluate the classification of each of the objects, independent of considerations of the physical nature of XSBLs and the properties shared by all of the objects in our study sample,

The usual dividing line for "significant" polarization or membership in the class of highly polarized quasars or Blazars is $P > 3\%$ (Impey and Tapia 1990; Kühr and Schmidt 1990). If we rigorously apply this threshold, several of the objects which were detected to be polarized would have to be excluded from our list of XSBLs. However, the main purpose of the polarization criterion of our BL Lac definition is to confirm the synchrotron source contribution to the flux of the candidate BL Lac. Since we checked for interstellar polarization and in light of the low duty cycle of XSBLs (§5.1.c), we will retain the objects with low polarizations unless significant interstellar polarization was detected.

After applying our definition of a BL Lac to our study sample, we are left with twenty-seven confirmed BL Lacs. We indicate in column (11) of Table 5.1 whether or not the object is a confirmed (C) to be a BL Lac (see Appendix II for discussion of individual objects). Of the twenty-two C-EMSS BL Lacs we can only confirm the classification of fifteen. Of the remaining seven, one was not successfully observed for polarization. The other six objects failed to

have detectable polarized emission despite repeated observations. Of the twelve EMSS candidate BL Lacs, we have detected polarized emission from three of the six observed objects (MS 2336.5+0517, MS 2342.7–1531, MS 2347.4+1924).

5.4 Polarimetry of RLXSAGN:

The Search for X-ray Selected HPQs

Independent of the presence of strong emission lines, forty percent of compact radio selected AGN are observed to have high optical linear polarization (Impey and Tapia 1989). The EMSS contains a variety of objects including a large number of quasars. We have observed a sample of twenty-four radio loud x-ray selected quasars from the EMSS to search for highly polarized quasars and check on the BL Lac classification procedures of the EMSS (see Chapter 3 for selection of sample). For this study, we rarely made repeated observations of the sample objects. We observed each object until a two sigma upper limit of 4% was placed on the white light polarization. Table 5.5 presents a summary of our polarization measurements of RLXSAGN. All of the data are contained in Appendix III. None of the RLXSAGN were significantly polarized ($P > 3\%$; $P/\sigma_P > 3$). We cannot rule out the possibility that one of these objects was temporarily in a low polarization state when measured. Observations of radio selected highly polarized quasars seem to indicate long time scales for variability

and extensive periods of time at very low polarizations (P. S. Smith 1990). It is still surprising, however, that not a single object in this sample was significantly polarized.

Description of Table 5.5

In Table 5.5 we present data for the radio loud x-ray selected AGN. All of the data provided in this table was supplied by John Stocke, except for the two sigma limits on the white light percent polarization (determined as part of this dissertation). Since this data was presented prior to publication, no reference to this dissertation should be made when refering to this data and we caution that the journal papers which will be published (Stocke *et al.* 1991) should be consulted for the definitive values of the x-ray and radio emission from these objects. The contents of the collumns are as follows: (1) Oject name; (2) two sigma limit on the white light percent polarization (this work); (3) x-ray flux in units of 10^{-13} erg cm $^{-2}$ s $^{-1}$, computed in the 0.3 to 3.5 keV band; (4) *V* band apparent magnitude, if followed by an e it is an estimate off of the Palomar Sky Survey Plate; (5) 6 cm radio flux density in mJy; (6) the redshift of the object; (7) α_{ro} (as defined by Stocke *et al.* 1989); (8) α_{ox} (as defined by Stocke *et al.* 1989); (9) Comments on the radio structure.

Table 5.5: The Properties of RLXSAGN

Object (1)	P (2)	$f_x(10^{-13})$ (3)	m_v (4)	$f_{\theta cm}$ (5)	z (6)	α_{ro} (7)	α_{oz} (8)	Comments (9)
MS 0012.5-0024	< 3.6	2.4	18.5e	24.0	1.695	0.45	1.33	
MS 0038.7+3251	< 4.7	3.1	18.5	2.4	0.225	0.28	1.27	
MS 0038.8-0159	< 2.9	3.1	16.9	322.0	1.675	0.54	1.55	4C,triple
MS 0136.3+0606	< 4.7	2.7	18.5	16.3	0.450	0.43	1.31	
MS 0226.8-1041	< 3.0	2.5	18.3	96.2	0.620	0.56	1.36	triple
MS 0232.5-0414	< 1.2	7.2	18.0e	523.0	1.450	0.66	1.23	PKS dble
MS 0311.8-0801	< 3.0	3.4	18.5e	8.2	1.244	0.37	1.26	
MS 0449.4-1823	< 4.1	8.4	18.3	1.1	0.338	0.20	1.16	
MS 0521.7+7918	< 2.1	5.5	18.5e	22.1	0.503	0.46	1.17	pnt sr.
MS 0815.7+5223	< 4.0	3.2	19.2	1.5	0.624	0.29	1.17	
MS 0822.0+0309	< 3.5	1.5	17.9	315.0	0.577	0.44	1.50	triple
MS 0833.3+6523	< 2.3	3.8	18.2	30.0	1.112	0.45	1.29	
MS 0850.2+2825	< 2.6	1.4	18.3	38.0	0.922	0.47	1.47	
MS 0952.3+4412	< 2.0	5.4	18.0e	11.3	0.465	0.36	1.29	pnt sr.
MS 1003.6+1300	< 3.0	2.8	17.5	125.0	1.958	0.50	1.47	
MS 1138.6+6553	< 4.3	1.3	18.4	133.0	0.805	0.59	1.47	triple
MS 1234.9+6651	< 3.0	5.4	18.0	142.0	0.860	0.56	1.29	triple
MS 1326.6+2546	< 2.5	2.4	18.5e	45.6	0.960	0.51	1.35	
MS 1340.7+2859	< 2.9	4.9	17.1	250.0	0.905	0.54	1.45	
MS 1442.8+6344	< 1.8	2.9	17.2	445.0	1.380	0.59	1.52	pnt sr.
MS 1623.4+2712	< 2.6	7.8	18.4	43.0	0.500	0.50	1.16	
MS 1640.0+3940	< 3.7	4.4	18.2	31.0	0.540	0.46	1.31	
MS 2134.0+0028	< 2.6	8.7	18.0	922.0	1.936	0.89	1.19	PKS
MS 2141.2+1730	< 1.1	8.9	15.5	417.0	0.213	0.47	1.55	

5.5 Summary of Results

Our polarimetry observations confirm that x-ray flux limited surveys find objects that meet the definition of being BL Lacs. Repeated observations of the candidate BL Lacs proved vital and should be continued for those objects we have not extensively monitored. If we had used only the first epoch observations, only 35% of the sample would have been confirmed to be BL Lacs.

While these objects are polarized, we have learned that they have a low duty cycle, 33%. Not only are they seldom highly polarized, but the maximum observed polarizations are only around 10%. Some of the objects are observed to have strong frequency dependence in their percent polarization, but frequency dependence of the position angle is very rarely observed. There is no rule relating an increase in total flux with an increase or decrease in polarized flux, although usually an observed maximum in percent polarization accompanies the maximum production of polarized flux.

While our photometric monitoring is not extensive, we have confirmed the variability of many of the objects in our sample. We have not observed any examples of the large and rapid fluctuations typical of optically violent variable quasars or well known radio selected BL Lacs.

Polarimetry of a sample of radio loud x-ray selected AGN failed to discover a single HPQ. This supports the success of the EMSS at not mistakenly

classifying as a quasar an object that is more similar to a BL Lac. It is puzzling, however, that objects with otherwise similar spectral energy distributions would be so different from the XSBLs in their polarization properties, while among radio selected quasars at least ten percent are found to be HPQs as the result of a single epoch survey.

In Chapter 6 we will compare the observed properties of XSBLs with those of other extragalactic objects which exhibit significant variable polarization. We will discuss further the relationships between quasars and BL Lacs and examine the possible relationships between the intrinsic physical properties and the observed properties BL Lacs.

CHAPTER 6

COMPARISON OF THE POLARIZATION PROPERTIES OF XSBLs AND RSBLs

In this chapter we compare the polarization properties of XSBLs (determined in Chapter 5) with those of RSBLs and HPQs. We will also examine how the polarization properties of all BL Lacs depend on their other properties. In §6.1 we define what we mean by α_{ro} , α_{ox} , and α_{rx} and discuss the spectral energy distributions of the various samples of AGN described in Chapter 3. In §6.2 we will compare the observed maximum polarizations (P_m) of XSBLs and RSBLs. Section 6.3 is a discussion of the relationship between observed P_m and characteristics of the spectral energy distribution of BL Lacs. In §6.4 we consider the consequences of dilution of the intrinsic polarization of the synchrotron component of BL Lacs by host galaxy starlight. We consider the effects on the observed and derived properties of both XSBLs and RSBLs. Section 6.5 is a discussion of the duty cycles of XSBLs, RSBLs, and HPQs. In §6.6 we again discuss the amazingly strong tendency of XSBLs to have preferred position angles and compare this result to what is known about RSBLs. Section 6.7 is a discussion of the total flux variations of BL Lacs. In §6.8 we examine existing models and

explanations for the observed polarization properties of BL Lacs. We propose in §6.9 our hypothesis for the relationship between the observed properties and the physical mechanisms and geometry producing the observed radiation from BL Lacs. In §6.10 we briefly reexamine a few of the differences between BL Lacs and quasars. Section 6.11 is a summary of the results in this chapter.

6.1 The Spectral Energy Distribution of BL Lacs

BL Lacertae objects, optically violent variables (OVVs), and highly polarized quasars (HPQs) are all intrinsically variable objects from radio to x-ray frequencies. This makes an accurate determination of the spectral energy distribution of these objects difficult. We would like to know at which frequencies these objects emit the bulk of their energy. We would also like to know what physical mechanism dominates the observed emission at each wavelength. Single epoch optical and radio observations are available for all of the objects in our study and comparison samples (see Chapter 3 for description of samples). X-ray flux measurements are available for some of the radio selected objects. EXOSAT and ROSAT observations should soon provide x-ray data for all of the 1 Jy BL Lacs and the 2 Jy and 1.5 Jy Impey and Tapia quasars. Even when we have observations in all three wavelength regimes, they are very rarely simultaneous. This means that for individual objects or small samples we might be slightly misled in our understanding of the overall energy budget by the variability of

the sources at all of the observed wavelengths. Nevertheless, by combining the data in the literature with our own observations, we can compare the properties of our various samples and extract useful insights.

Since redshifts are not available for all the objects we wish to compare, we will usually use distance independent quantities to compare the spectral properties. Specifically we will use the quantities α_{ro} , α_{ox} , and α_{rx} (defined below) which are measures of the relative energy output of the object at the specified wavelengths. We will then plot the positions of the various samples' objects on the α_{ro} vs. α_{ox} plane in a manner similar to that of Stocke *et al.* (1989). We have chosen to define α in a slightly different manner from that of other authors (Stocke *et al.* 1989; Stocke *et al.* 1990; Schwartz *et al.* 1989), and this explains the differences in our figures compared to similar plots in other papers. Our spectral indices, α , measure the relative energy output of an object at two different observed wavelengths. We define $\alpha_{ab} = \log(S_a/S_b)/\log(\nu_a/\nu_b)$, where a and b represent the observed wavelength bands, S_a is the observed flux in the "a" band, and ν is the frequency of observation. We chose 6 cm, 5500 Å, and 2 KeV as our observation wavelengths in the radio, optical, and x-ray bands. Since we do not have redshifts for all of the objects, we prefer to compare the samples by using values of α defined at the observed wavelengths. Other authors have chosen to use rest frame wavelengths, but this has required that a spectral index be assumed and that a redshift is available for the object. (By calculating α at the observed wavelengths, our values of these quantities are no longer distance

independent. In fact, the vast majority of BL Lacs with known redshift (the majority of the x-ray selected and radio selected BL Lacs in the complete samples discussed in Chapter 3) are not extremely distant objects (redshifts are less than 1) and the effective scatter in our calculated values of α is small.) We have adopted the following sign conventions in an effort to be consistent with other published work. The following definitions are used:

$$\alpha_{ro} = -\log(S_r/S_o)/\log(\nu_r/\nu_o) = \log(S_r/S_o)/5.0375$$

$$\alpha_{ox} = \log(S_o/S_x)/\log(\nu_o/\nu_x) = \log(S_o/S_x)/-2.947$$

$$\alpha_{rx} = \log(S_r/S_x)/\log(\nu_r/\nu_x) = \log(S_r/S_x)/-7.984$$

For the EMSS XSBLs the data used for calculating the above values were our own V photometry supplemented by the data of Schild *et al.* (1990), the x-ray fluxes measured by the Einstein Observatory (Gioia *et al.* 1990), and the radio fluxes measured by Stocke *et al.* (1990; 1989; 1985). The data for the HEAO A-1 and NRL HEAO samples were obtained from Schwartz *et al.* (1990; 1989). The data for the radio selected samples were obtained from Ledden and O'Dell (1985), Angel and Stockman (1980), Kühr and Schmidt (1990), Impey and Tapia (1990), and Stickel *et al.* (1990). The values of α most likely to be incorrect for an individual object are α_{ox} and α_{rx} , since they depend on the observed x-ray flux, which is the most variable of the three components for all of the objects we are discussing (e.g. Schwartz *et al.* 1989; Giommi *et al.* 1990). Despite these uncertainties, one of the benefits of examining regions of a log *vs.*

log plane is that even factors of two to five in flux variability will not make large differences in the placement of the objects.

We begin our study of the differences between our samples by looking at their relative placement in the α_{ro} vs. α_{ox} plane. It is clear from an examination of Figures 6.1, 6.2, and 6.3 that the x-ray and radio surveys currently find different objects. This is not at all surprising. In general, a survey in a wavelength band will certainly be most efficient at finding the objects that are “loud” in that band. Consequently the x-ray surveys find objects with small α_{ox} and the radio surveys find objects with large α_{ro} .

Figure 6.1— The samples of XSBLs, RSBLs, and HPQs described in Chapter 3 are plotted in the α_{ro} vs. α_{ox} plane. The definitions for α_{ro} and α_{ox} are given in §6.1. The solid circles indicate the XSBLs from the EMSS, Einstein, HEAO-A1, and HEAO-NRL samples. The solid squares indicate the positions of the RLXSAGN sample taken from the EMSS. Empty circles include the RSBLs from the Ledden and O'Dell, Stickel, Kühr and Schmidt, and Impey and Tapia samples. Empty squares are the radio selected HPQs from the Ledden and O'Dell, and Impey and Tapia samples. All of these samples are described in Chapter 3. Not all of the members of these samples could be plotted due to a lack of x-ray data for some of the objects.

Figure 6.2— The samples of XSBLs and RSBLs are plotted on the α_{ro} vs. α_{ox} plane (see Figure 6.1). Solid symbols indicate the positions of XSBLs. Empty symbols are the positions of RSBLs. The various symbol shapes indicate the sample to which the object belongs: empty triangles are BL Lacs from 1 Jy Stickel, empty circles are objects from the S5, empty pentagons are from Ledden and O'Dell, solid triangles are from HEAO-A1 and HEAO-NRL, solid circles are from EMSS and other objects discovered with the *Einstein Observatory*.

Figure 6.3— The complete samples of XSBLs and RSBLs are plotted on the α_{ro} vs. α_{ox} plane. The empty triangles are objects from the 1 Jy Stickel sample. The empty circles are objects from the S5. The solid circles are the objects from the C-EMSS (samples are described in Chapter 3).

X-ray and Radio Selected BL Lacs and Quasars

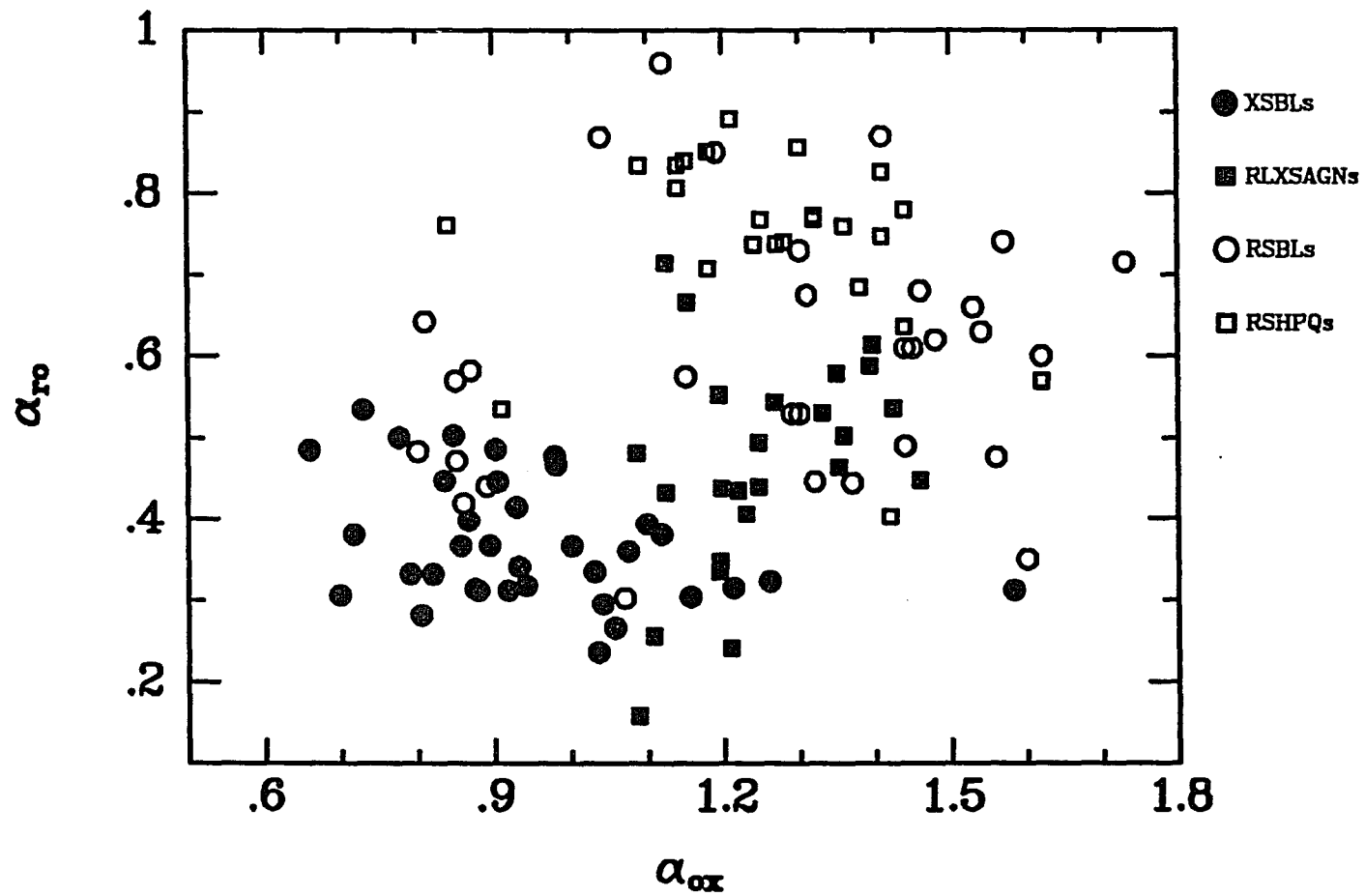


Figure 6.1

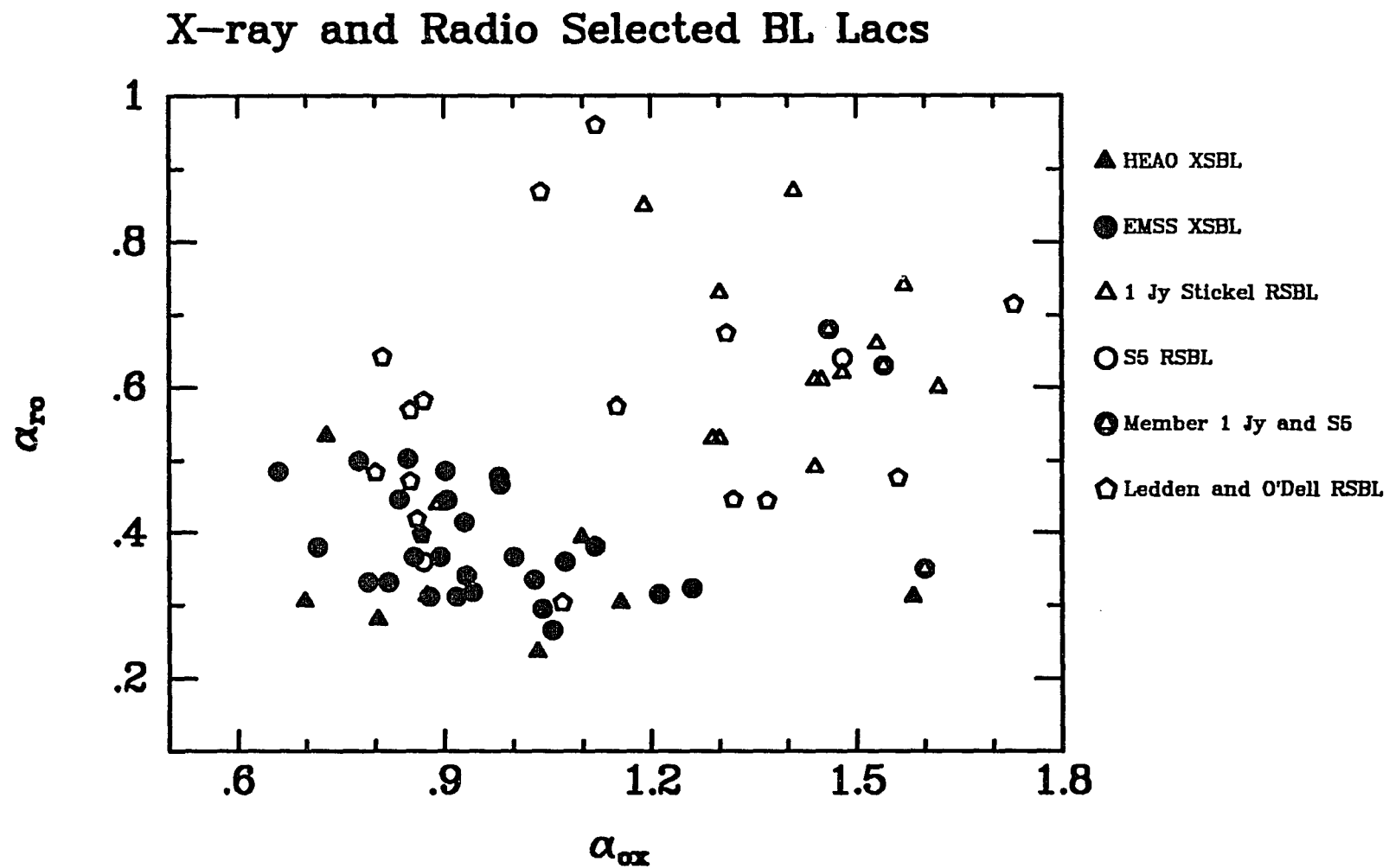


Figure 6.2

Complete Samples of X-ray and Radio Selected BL Lacs

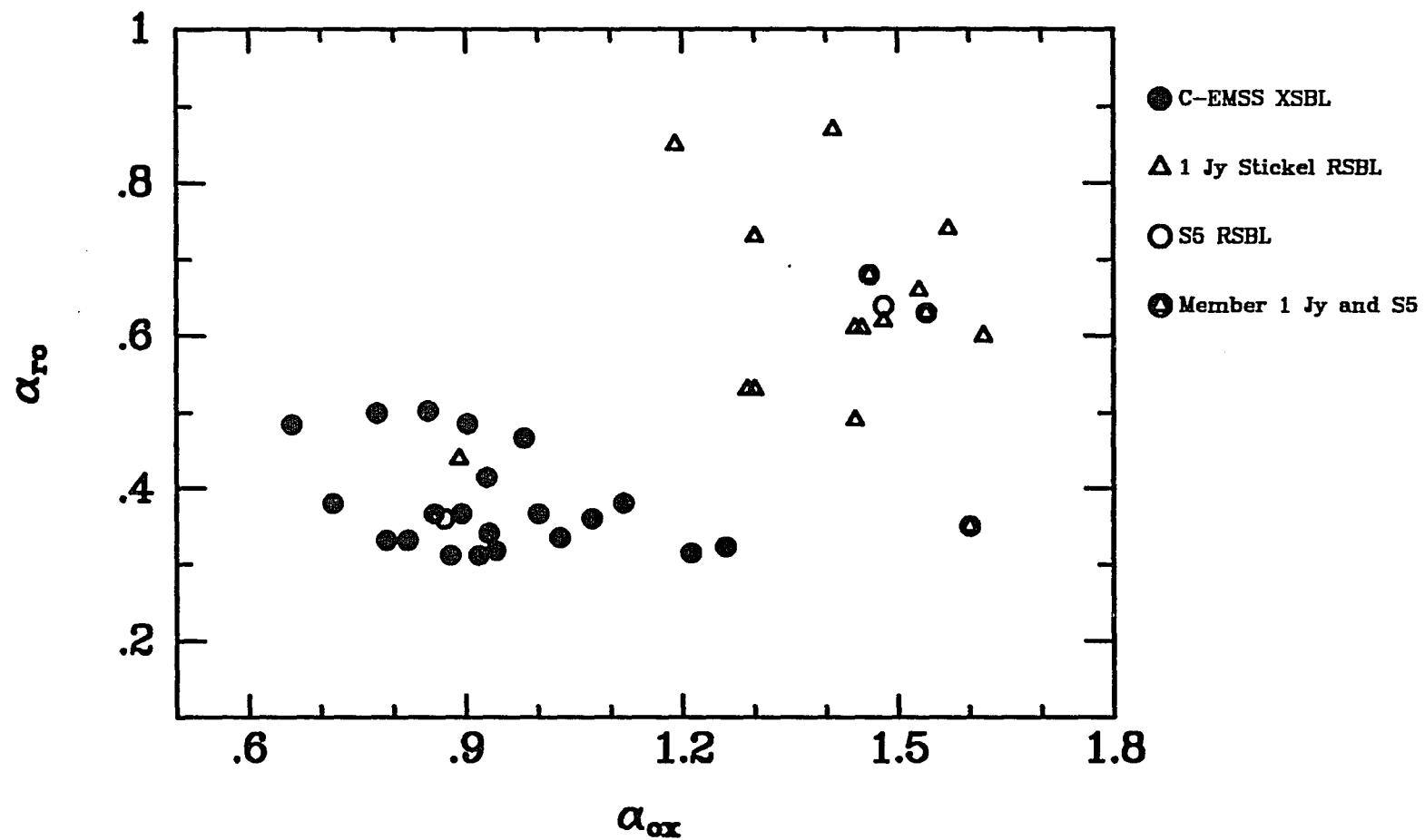


Figure 6.3

Despite the selection biases of flux limited surveys in a particular waveband, the differences between the two groups of BL Lacs are not just a function of selection effects. It is evident that there is a definite structure to the distribution of objects as a function of α_{ro} and α_{ox} . There is a lack of objects with $\alpha_{ro} > 0.6$ and $\alpha_{ox} < 1.2$ among the complete samples (the C-EMSS and 1 Jy Stickel) and only a few objects if we include all the objects from the various samples. As we discussed in Chapter 3, the terms “x-ray selected” and “radio selected” refer to the frequency of the flux limited survey to which a particular object belongs. All of the RSBLs would be included in an x-ray survey of sufficiently faint limiting flux and no bias against previously discovered objects. Similarly, if radio surveys were conducted down to 10 mJy flux levels, all of the x-ray selected objects would be found. The lack of objects in the previously defined region ($\alpha_{ro} > 0.6$ and $\alpha_{ox} < 1.2$) and with $\alpha_{ro} < 0.4$ and $\alpha_{ox} > 1.3$ is not a result of survey technique. Neither is the apparent separation of the BL Lacs into two regions of the plane. Even though there are two “radio” selected objects located in the same region as the XSBLs, there is a noticeable segregation of the two samples. This has been previously discussed by others including Stocke *et al.* (1989; 1990), Schwartz *et al.* (1989), and Giommi *et al.* (1990). The vast majority of the known HPQs can be found in the region of the plane populated by the 1 Jy BL Lacs. The RLXSAGNs form a “bridge” between the two regions of the plane, but are the only objects plotted that have not been observed to be significantly polarized.

This is in spite of the fact that they share continuum and emission line properties with many of the radio selected HPQs.

We can also look at the absolute fluxes and luminosities of the XSBLs and RSBLs as functions of α_{ro} . In Figures 6.4 and 6.5 we display the Log of the radio and optical luminosities of BL Lacs and HPQs *vs.* α_{ro} . The luminosities were calculated for those objects for which we had redshifts and the required flux observations. All distance dependent calculations were calculated assuming $H_0 = 50 \text{ km sec}^{-1} \text{ Mpc}^{-1}$, $q_0 = 0$, and $\alpha_{opt} = -1.5$. Optical luminosities (L_{opt}) were calculated for 5500 Å in the rest frame. Radio luminosities were calculated at 6 cm in the rest frame with $\alpha_r = -1$. In order to calculate luminosities without knowledge of the properties of the jets of the BL Lacs, we have made the unrealistic assumption that the BL Lacs are isotropic emitters of their radiation. While not accurate, it allows us to compare the luminosities of the different objects and include our knowledge of the objects redshifts in the analysis. Redshifts for the XSBLs were taken from Morris *et al.* (1990) and from the previously listed references that provided the radio and optical flux data. Redshifts for the RSBLs are from Stickel *et al.* (1990). Redshifts for the Ledden and O'Dell list of HPQs are from the references listed in Ledden and O'Dell (1985). The combined samples compose a sample of BL Lacs and HPQs with a continuous distribution of optical and radio luminosities as a function of α_{ro} . The radio selected objects have radio luminosities which, on average, are greater than the radio luminosities of the x-ray selected objects. For all of the BL Lacs,

the optical luminosities are also greater for the objects with larger α_{ro} . Figures 6.6, 6.7, and 6.8 are plots of the x-ray luminosities of the XSBLs as a function of α_{ro} , α_{ox} , and α_{rx} . No trend is evident in these plots. This reflects the fact that all BL Lacs, x-ray and radio selected, have the same mean x-ray luminosities (Maraschi *et al.* 1986).

Figure 6.4— The Log of the radio luminosity is plotted against α_{r0} for a selection of XSBLs, RSBLs, and HPQs. The XSBLs plotted are our program objects (see Chapter 3). The RSBLs are the 1 Jy and S5 samples and the HPQs are from the Ledden and O'dell sample. Only objects for which redshifts were available were plotted. (see Chapter 3 for a description of the samples). The luminosities are calculated assuming the sources are emitting their radiation isotropically. The 6 cm radio flux measurements were used for all objects.

Figure 6.5— The Log of the optical luminosity is plotted against α_{r0} for a selection of XSBLs, RSBLs, and HPQs. The XSBLs plotted are our program objects (see Chapter 3). The RSBLs are the 1 Jy and S5 samples and the HPQs are from the Ledden and O'dell sample (see Chapter 3 for a description of the samples). The luminosities are calculated assuming the sources are emitting their radiation isotropically. Only objects for which redshifts were available were plotted. The V band measurements were used for all objects.

Figure 6.6—The Log of the x-ray luminosities of the XSBLs from our monitoring program are plotted against α_{r0} . The luminosities are calculated assuming that the source is emitting isotropically. Only objects for which redshifts were available were plotted. The values for α_{r0} were calculated as described in Chapter 5.

Figure 6.7—The Log of the x-ray luminosities of the XSBLs from our monitoring program are plotted against α_{ox} . The luminosities are calculated assuming that the sources are emitting their radiation isotropically. Only objects for which redshifts were available were plotted. The values for α_{ox} were calculated as described in §6.1.

Figure 6.8—The Log of the x-ray luminosities of the XSBLs from our monitoring program are plotted against α_{rx} . The luminosities are calculated assuming that the sources are emitting their radiation isotropically. Only objects for which redshifts were available were plotted. The values for α_{rx} were calculated as described in §6.1.

X-ray and Radio Selected BL Lacs and Selected HPQs

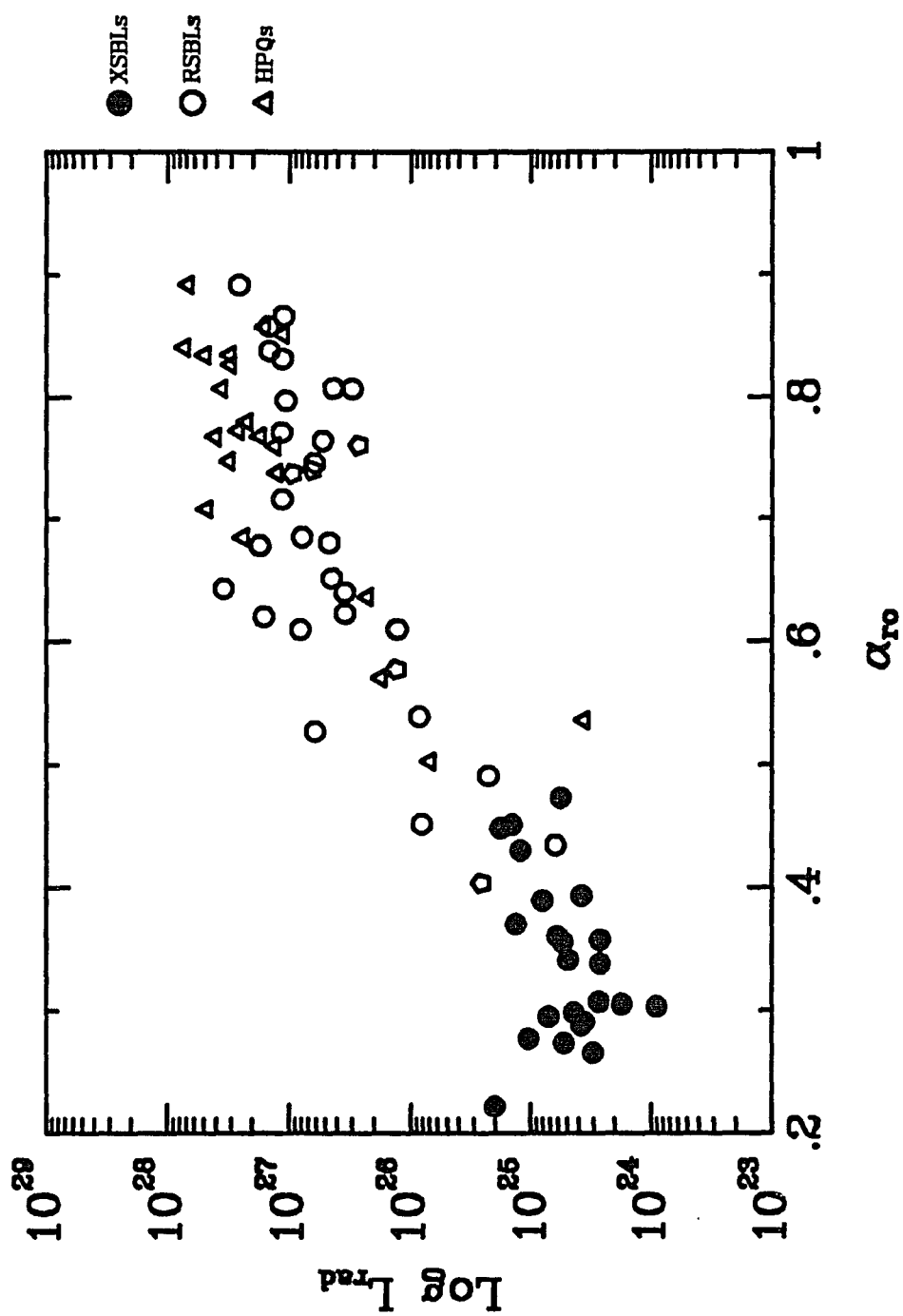


Figure 6.4

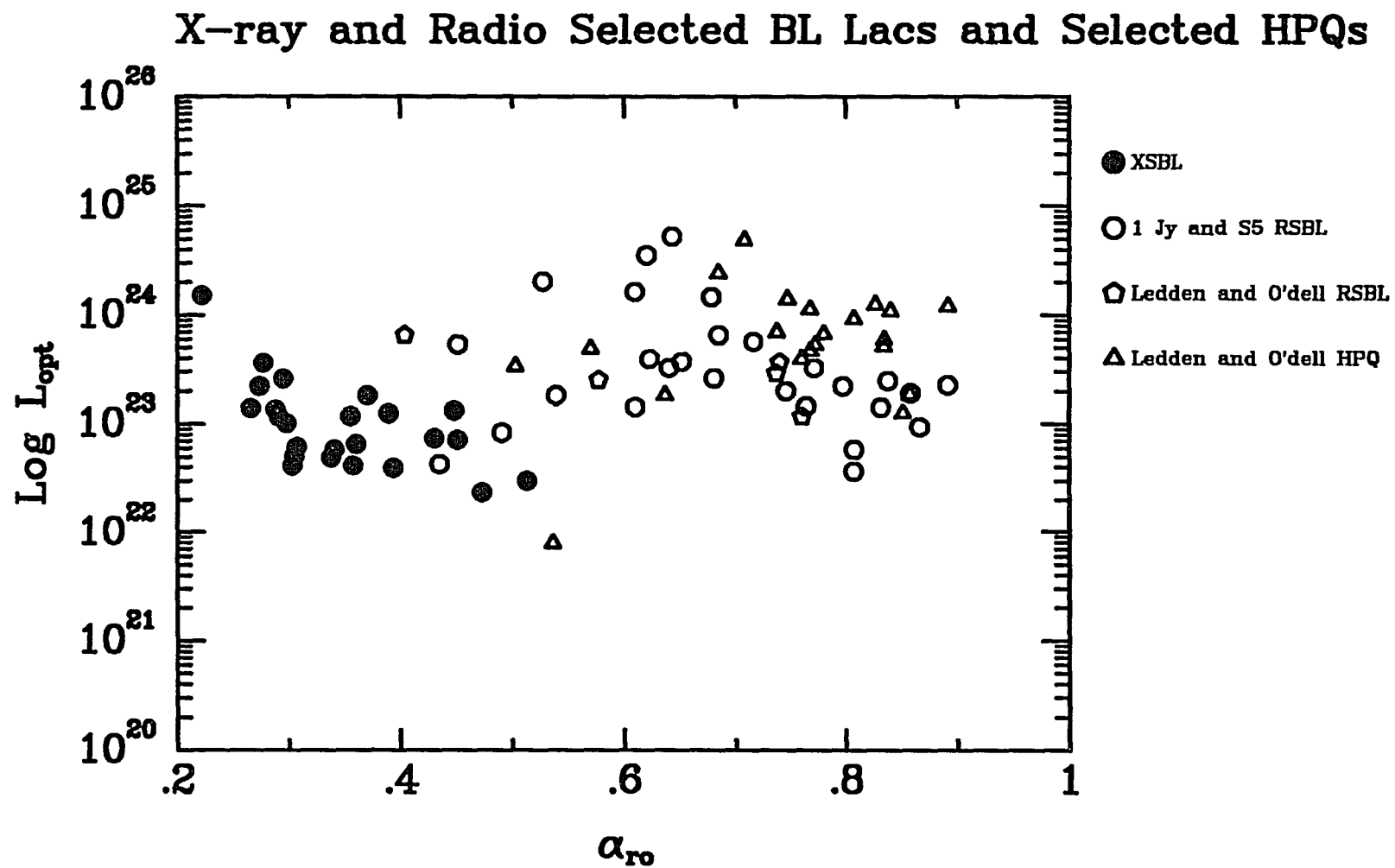


Figure 6.5

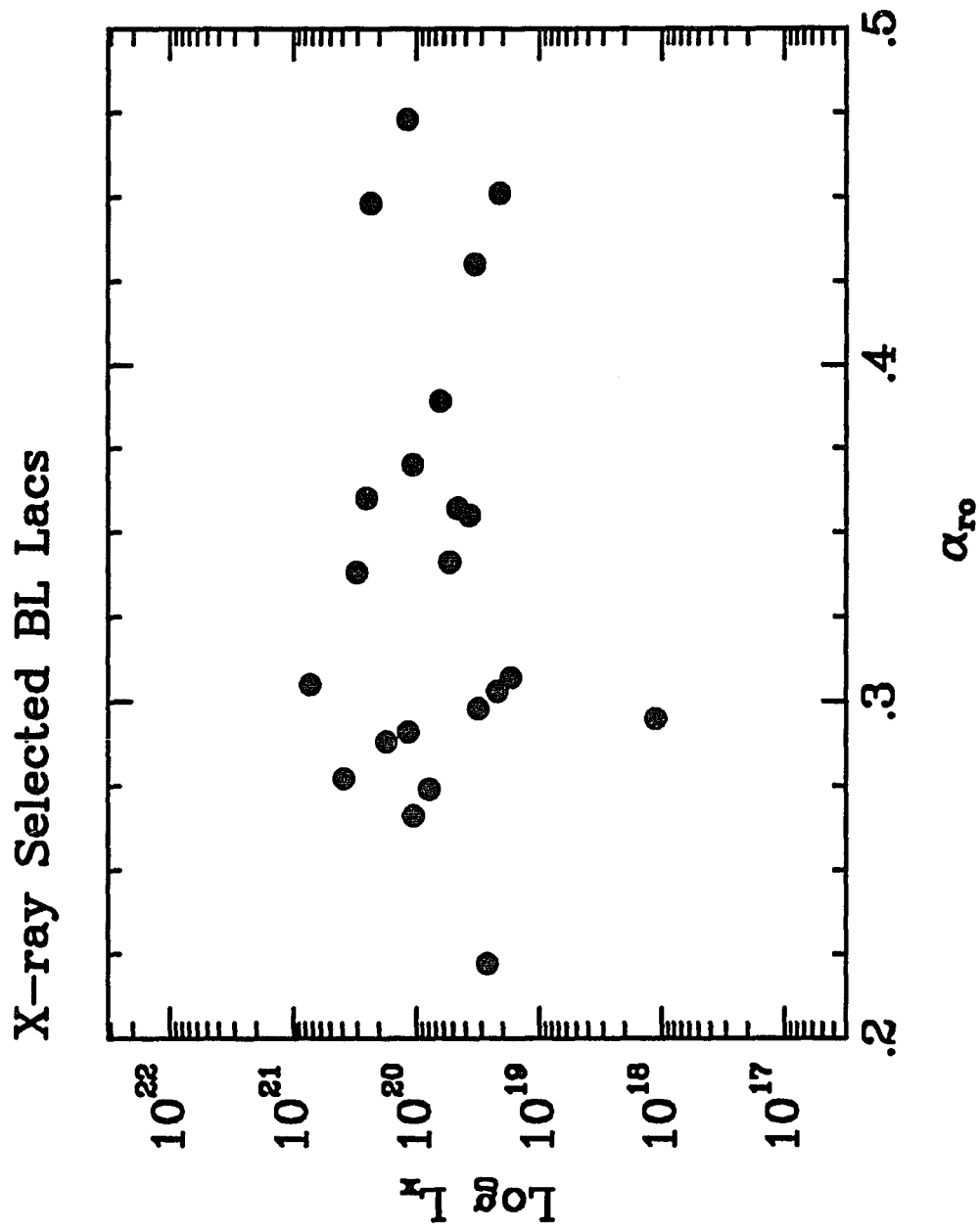


Figure 6.6

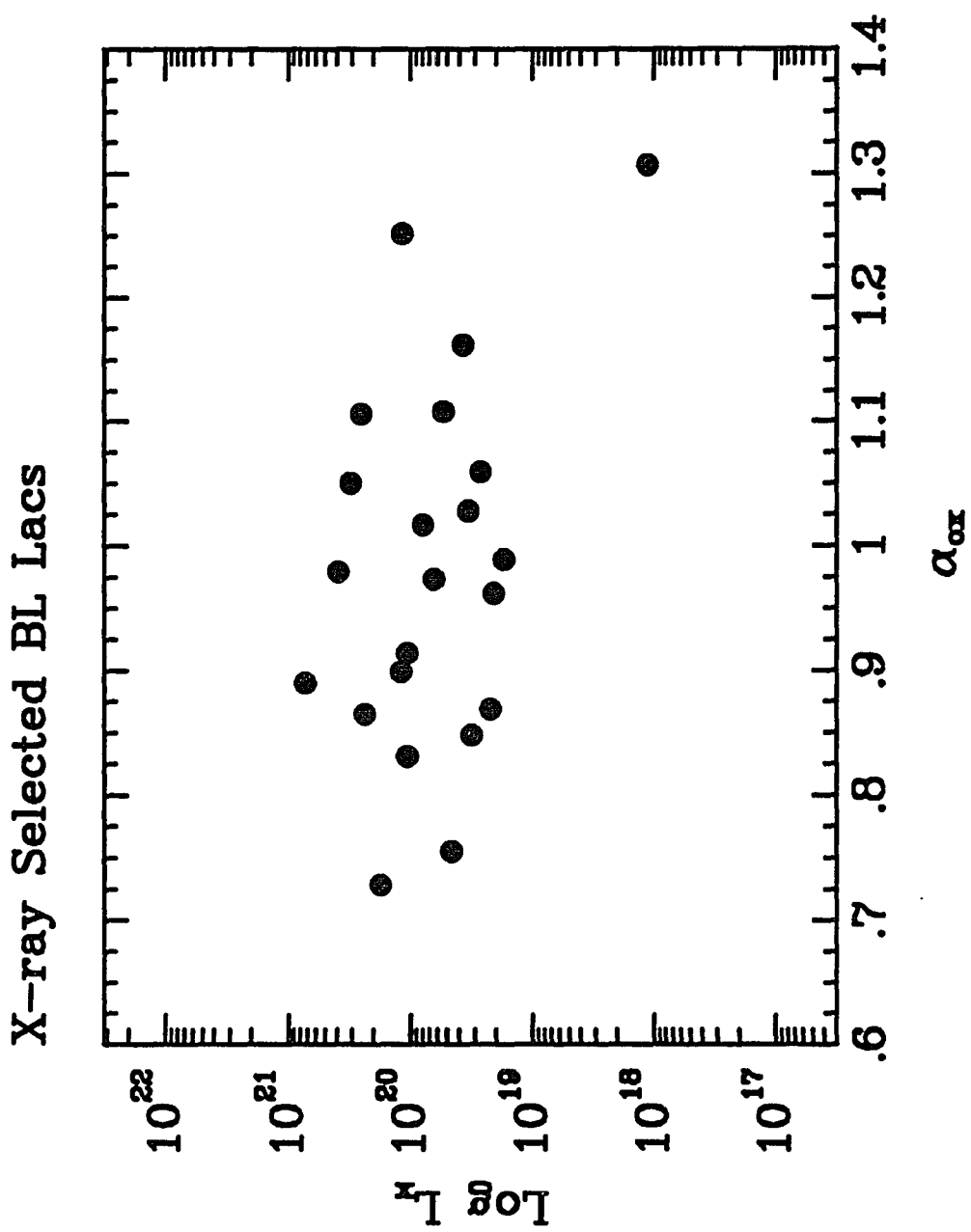


Figure 6.7

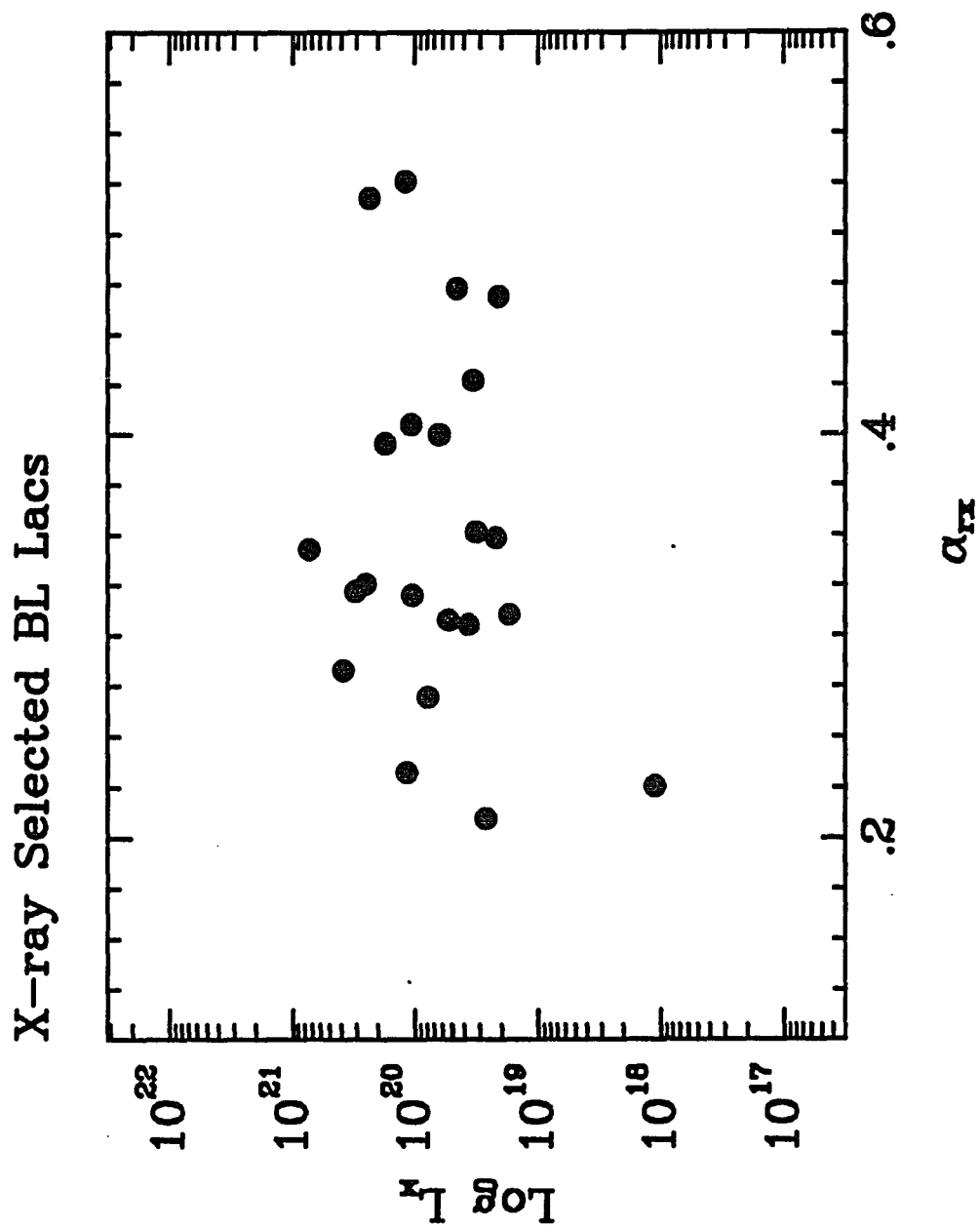


Figure 6.8

It is tempting to interpret the changing ratio of radio to optical flux with increasing optical and radio luminosity as a modulation of the relative amounts of boosting of the two components. This modulation could be caused by a distribution of viewing angles to or range in dynamical properties of (resulting in a range of properties due to relativistic aberration) the relativistic jet producing the optical and radio synchrotron emission. To be consistent with the data, the radio luminosity would have to be a stronger function of the viewing angle than the optical luminosity. The x-ray emission would have to be much more isotropic, reflected in the lack of a dependence on α_{ro} . Our working hypothesis (discussed in Chapter 1) is that BL Lacs are objects that have their observed properties dominated by the effects of a relativistically beamed synchrotron component. At short radio wavelengths the emission from these objects is dominated by the beamed component, while at optical wavelengths there is the addition of the host galaxy's thermal and unpolarized starlight. It is appealing to try to relate the observed distribution in the α_{ro} vs. α_{ox} plane to the relative importance of the beamed component to the x-ray emission. If the x-ray emission is more isotropic, for whatever reason, then x-ray surveys are the best way to find objects that have large viewing angles to their relativistic jets. We will return to this picture in later sections.

6.2 The Maximum Observed Percent Polarizations

of XSBLs and RSBLs

We will explore in this section the observed contrasts between the percent polarizations of x-ray selected and radio selected BL Lacs. The RSBLs have larger observed maximum observed polarizations (P_m or P_{max}) than the XSBLs. This is qualitatively quite clear by inspection of the distributions of P_m in Figures 6.9 through 6.14. We can make a more quantitative test of the differences between the observed distributions of P_m by performing Kolmogorov-Smirnov tests between various samples of BL Lacs and HPQs. We have performed these tests between the various samples described in Chapter 3. The results are summarized in Table 6.1. Figures 6.15a and 6.15b are representative plots of the cumulative distributions between two of the compared sample pairs. The samples in the first column are various subgroupings of the XSBLs. The first row contains the abbreviated names of the various radio selected subsamples. In each cell, the top number is the maximum difference in the cumulative distributions and the bottom number is the probability that the null hypothesis is accepted. In other words, it is the probability that the two samples could have been drawn from the same underlying population. There is no doubt that the observed distributions are different.

Notes for Table 6.1

In this table we list the results obtained from Kolmogorov-Smirnov tests run between the distributions of maximum observed percent polarization for various samples of objects. In columns (2) through (8) are the results of tests between the samples in column (1) and the samples in row (1). In each cell, the top number is the maximum difference in the cumulative distributions and the bottom number is the probability that the null hypothesis is accepted. In column (1) are listed the various samples of x-ray selected BL Lac samples used in the analysis. In row 1 are the names of the radio selected BL Lac samples used. In the list which follows we provide brief descriptions of the samples whose abbreviated names appear in Table 6.1. The number of objects in the sample is indicated in square brackets after the name. "All XSBLs" [29] refers to all of the objects observed and detected in our monitoring program. "EMSS" [19] refers to BL Lacs from the Einstein Medium Sensitivity Survey which were observed and detected. "C-EMSS wLim" [22] refers to all of the BL Lacs from the Complete EMSS sample assuming that those objects for which we only had limits had maximum values of polarization equal to our worst two sigma limit (for each individual object). "C-EMSS" [16] refers to BL Lacs from the Complete EMSS Sample which were detected on at least one occasion to be polarized. "Einstein" [27] includes all BL Lacs discovered by the *Einstein Observatory*. "HEAO" [8] includes the eight HEAO XSBLs. "All RSBLs" [54] refers to the RSBLs in the S5 5 GHz, 1 Jy, 2 Jy, and 1.5 Jy samples described in Chapter 3 (objects in

more than one survey where only included once). “Stickel” [32] refers to the 1 Jy sample as defined by Stickel. “Kühr/Schmidt” [34] refers to the 1 Jy sample as defined by Kühr and Schmidt (see Chapter 3). “S5 Sample” [14] refers to the S5 5 GHz sample as presented by Kühr and Schmidt (see Chapter 3). “2 Jy BL Lac” [18] and “2 Jy HPQ” [38] are the samples of BL Lacs and HPQs described by Impey and Tapia (see Chapter 3). “2 Jy Comb” [60] is the combination of the previous two samples plus four objects which, while they are optically polarized flat spectrum radio sources, were not classified as either BL Lacs or HPQs because spectroscopic data was not available.

Table 6.1: Results of KS Tests Between X-ray and Radio Selected Samples

X-ray Selected	All RSBLs	Stickel	Kühr/ Schmidt	S5 Sample	2 Jy BL Lac	2 Jy HPQ	2 Jy Comb
(1)	(2)	(3)	(4)	(5)	(6)	(7)	(8)
All XSBLs	0.653 2.03E-7	0.744 9.90E-8	0.730 1.13E-7	0.616 1.55E-3	0.703 3.41E-5	0.485 8.59E-4	0.542 2.06E-5
EMSS	0.685 3.70E-6	0.760 2.10E-6	0.765 1.28E-6	0.647 2.36E-3	0.734 9.50E-5	0.553 8.73E-4	0.589 8.83E-5
C-EMSS wLim	0.698 7.85E-7	0.765 7.21E-7	0.765 5.10E-7	0.667 1.14E-3	0.754 3.28E-5	0.563 3.82E-4	0.610 1.91E-5
C-EMSS	0.685 1.85E-5	0.750 1.23E-5	0.765 5.95E-6	0.607 8.13E-3	0.694 5.66E-4	0.533 3.34E-3	0.550 9.60E-4
Einstein	0.741 5.28E-9	0.775 4.49E-8	0.779 2.35E-8	0.709 1.89E-4	0.796 2.25E-6	0.584 4.24E-5	0.635 5.96E-7
HEAO	0.597 1.39E-2	0.688 4.72E-3	0.669 6.06E-3	0.482 0.187	0.611 3.19E-2	0.401 0.238	0.425 0.156

Can we interpret the observed difference as an intrinsic difference in the percent polarization produced by the synchrotron component? We know that the XSBLs have stronger evidence of the underlying host galaxy in their optical spectra as demonstrated by stronger absorption features and stronger 4000Å breaks (Stocke *et al.* 1985; Morris *et al.* 1990). It has been suggested that the lower observed polarizations of the XSBLs result from dilution of the polarization of the nonthermal synchrotron source by the thermal and unpolarized starlight of the host galaxy (Stocke *et al.* 1985). This would be consistent with the flux contribution of the beamed synchrotron component being less for the x-ray selected objects. We contend that while the host galaxy is definitely a greater fraction of the optical emission of the XSBLs, dilution by starlight is not enough to explain the observed differences between the x-ray selected and radio selected BL Lacs. There are two arguments in support of this view.

First, for most of the XSBLs with redshifts greater than $z = 0.2$ and assuming that the host galaxy is an elliptical galaxy, U and B band polarimetry measures the polarization shortward of the 4000 Å break in the rest frame of the object. Shortward of the break, the object's emission will be composed of a much higher fraction of the nonthermal emission and the observed percent polarization is an indication of the intrinsic polarization of the nonthermal source. We have B or U polarimetry observations for five XSBLs with redshifts greater than 0.2. In every case, the maximum observed polarization at U and B is within a few percent of the white light value. The observed differences between

the 1 Jy and C-EMSS samples are too great to overcome by shifting the observed P_m distribution of the XSBLs by only a few percent.

Second, we can model the observed flux of the XSBLs and derive the polarization of the nonthermal component. When a similar procedure is performed for the RSBLs, we can compare the polarizations of the two samples' synchrotron components free of the effects of dilution by the host galaxies. We have made corrections for the effects of dilution for the objects in our two most nearly complete samples of BL Lacs, the C-EMSS (corrections also done for all XSBLs) and 1 Jy Stickel samples. For both of these samples we restricted ourselves to objects for which we had redshifts, photometry, and polarimetry. We then calculated the observed polarized flux by multiplying the coincidentally measured V band flux by the V (when available) or white light percent polarization. In general, for the XSBLs and RSBLs the V band and white light polarizations are very close. For each BL Lac, we then calculated the observed V band flux for a brightest cluster elliptical galaxy at the same redshift. We followed the procedure of Sandage (1972) to determine the aperture correction (adjusting to the aperture used to observe the BL Lac) and a fit to the observations of Kristian, Sandage, and Westphal (1978) to determine the V band flux of the brightest cluster ellipticals as a function of redshift. We are assuming that all of the BL Lacs are in the brightest possible host galaxies. The host galaxy flux is then subtracted from the total observed flux. We call the residual flux the total nonthermal flux. The corrected percent polarization is then the

polarized flux divided by the nonthermal flux. We have made the assumption that the starlight is not polarized (for example any scattering of the starlight by dust is assumed to be insignificant or symmetrically distributed and therefore does not contribute significantly to the observed polarization). We have compared the resulting distributions of polarizations for the C-EMSS and 1 Jy Stickel samples. In Table 6.2 the corrected x-ray sample is called “Dilution Corrected XSBLs”. The corrected radio selected sample is called “Dilution Corrected RSBLs”. While the difference between the two cumulative distributions has decreased, there is still only a 0.3% chance that these two samples are drawn from the same underlying distributions! We are forced to conclude that the synchrotron components of BL Lacs in these two samples have different distributions of *observed* percent polarization.

Table 6.2: Results of Further KS Tests Between Samples

	Dilution Corrected 2 Jy BL Lac RSBLs		Stickel
Dilution Corrected XSBLs	0.556 8.16E-4	— —	— —
Dilution Corrected C-EMSS	0.576 3.05E-3	— —	— —
2 Jy HPQ	— —	0.366 0.076	0.339 0.037

Notes for Table 6.2

In this table we present the results from additional KS tests between samples of objects. In all cases it is the distributions of maximum observed optical polarization which are compared. The names “2 Jy BL Lac”, “Stickel”, and “2 Jy HPQ” have the same meaning as in Table 6.1. “Dilution Corrected XSBLs” and “Dilution Corrected RSBLs” refer to the distributions of percent polarization (corrected for the dilution by the unpolarized host galaxy star light) of the C-EMSS and Stickel samples (see discussion above). We note that there is an indication from the comparison between the HPQs and RSBLs that they are not drawn from the same underlying population. In other words, this is additional evidence (although perhaps not as strong) that the two populations should not be grouped together under the name “Blazars”.

6.3 The Relation of P_m to Other Observed Properties

We have shown in §6.2 that the observed distributions of P_m for samples of XSBLs and RSBLs are entirely different. This is not the only difference we have noted between the two groups of samples. We have also seen that they populate different ranges of α_{ro} and α_{ox} . Together, the various samples of BL Lacs cover a wide range in observed properties. We can examine the relationships between the observed polarization properties and the other observable properties

of these objects. We present in Figures 6.9 through 6.14 plots of P_m vs. α_{ro} and α_{ox} for various samples of BL Lacs and HPQs. The distribution of objects in these plots reflects the observed properties we have already described in the previous sections. The XSBLs have smaller values of P_m and α_{ro} while the RSBLs cover a wider range of P_m , but have larger values of α_{ro} . If we consider the combined sample of BL Lacs, it is clear that objects with small values of α_{ro} do not reach large values of P_m . This relationship is even more evident if we only consider the complete samples of BL Lac objects (Figure 6.11). The plots of P_m vs. α_{ox} have fewer objects because x-ray flux measurements are available for only some of the RSBLs. Nevertheless, if we consider only the complete samples of BL Lacs, we see a strong trend for objects with smaller α_{ox} to have a more limited range and smaller values of P_m .

Figures 6.9 through Figure 6.11—The maximum observed percent polarization is plotted against α_{ro} for a variety of samples of polarized objects. The values of α_{ro} were calculated as described in §6.1. The samples are described in Chapter 3.

Figures 6.12 through Figures 6.14—The maximum observed percent polarization is plotted against α_{ox} for a variety of samples of polarized objects. The values of α_{ox} were calculated as described in §6.1. The samples are described in Chapter 3.

Figure 6.15—The cumulative distributions of XSBLs (solid line) and RSBLs (dotted line) are plotted as a function of maximum observed percent polarization. In Figure 6.15a we show the distributions for all of the XSBLs in our monitoring program and all of the 1 Jy and S5 RSBLs. In Figure 6.15b we show the distributions for the C-EMSS XSBLs (including only those objects which were detected to be polarized on at least one epoch; solid line) and the Stickel Sample of 1 Jy RSBLs (dotted line).

X-ray and Radio Selected BL Lacs and Quasars

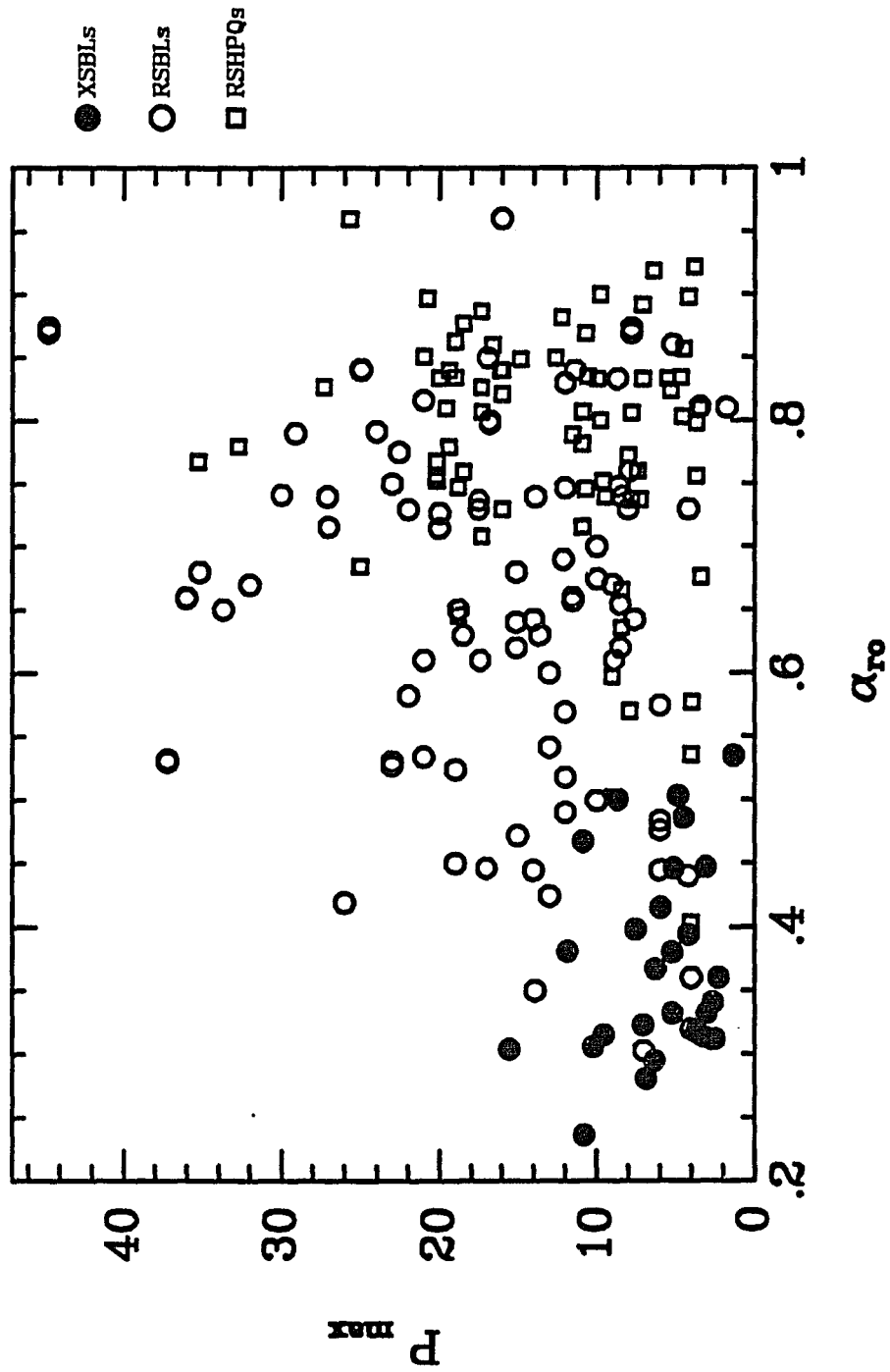


Figure 6.9

X-ray and Radio Selected BL Lacs

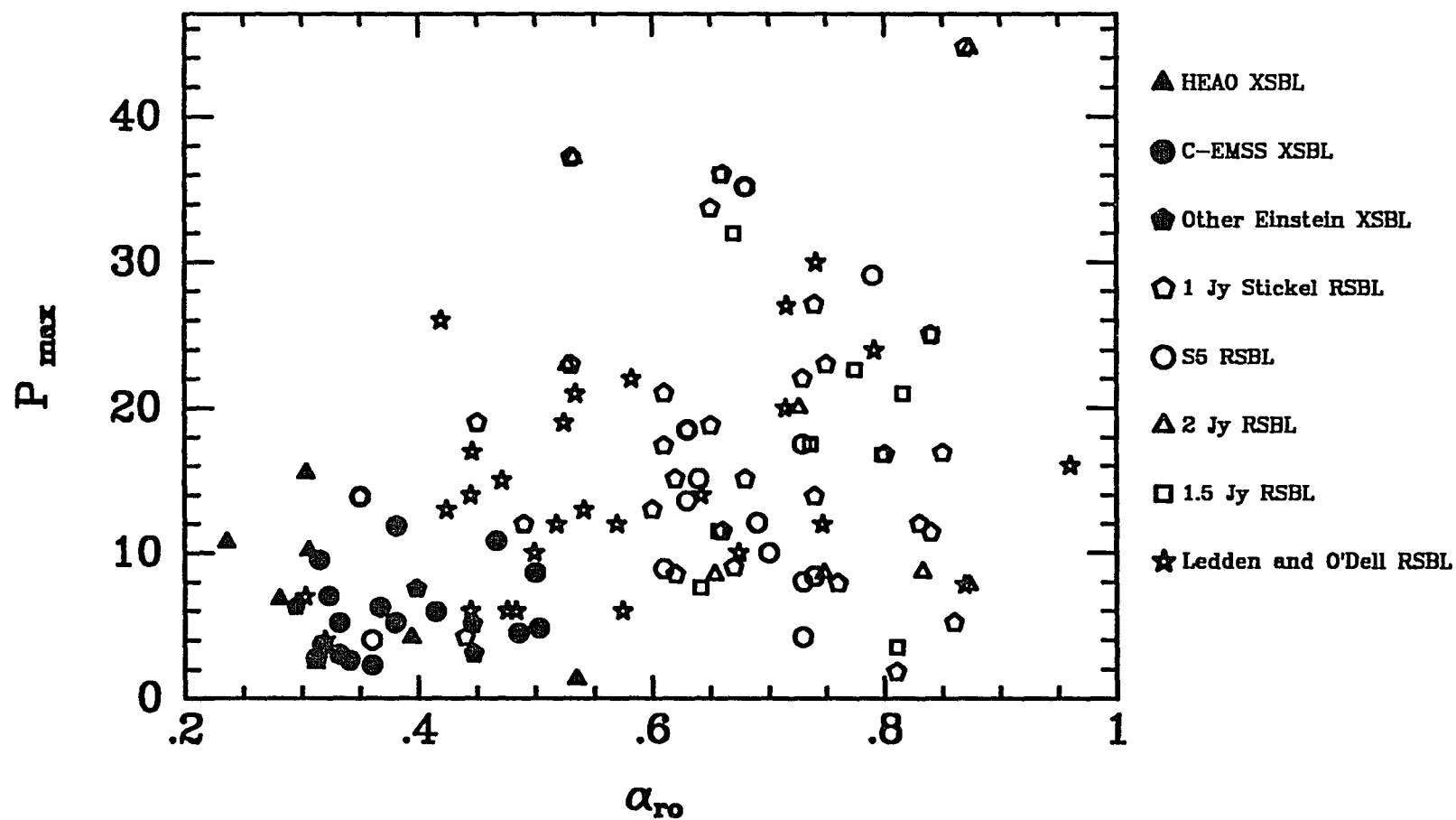


Figure 6.10

X-ray and Radio Selected BL Lacs, Complete Samples

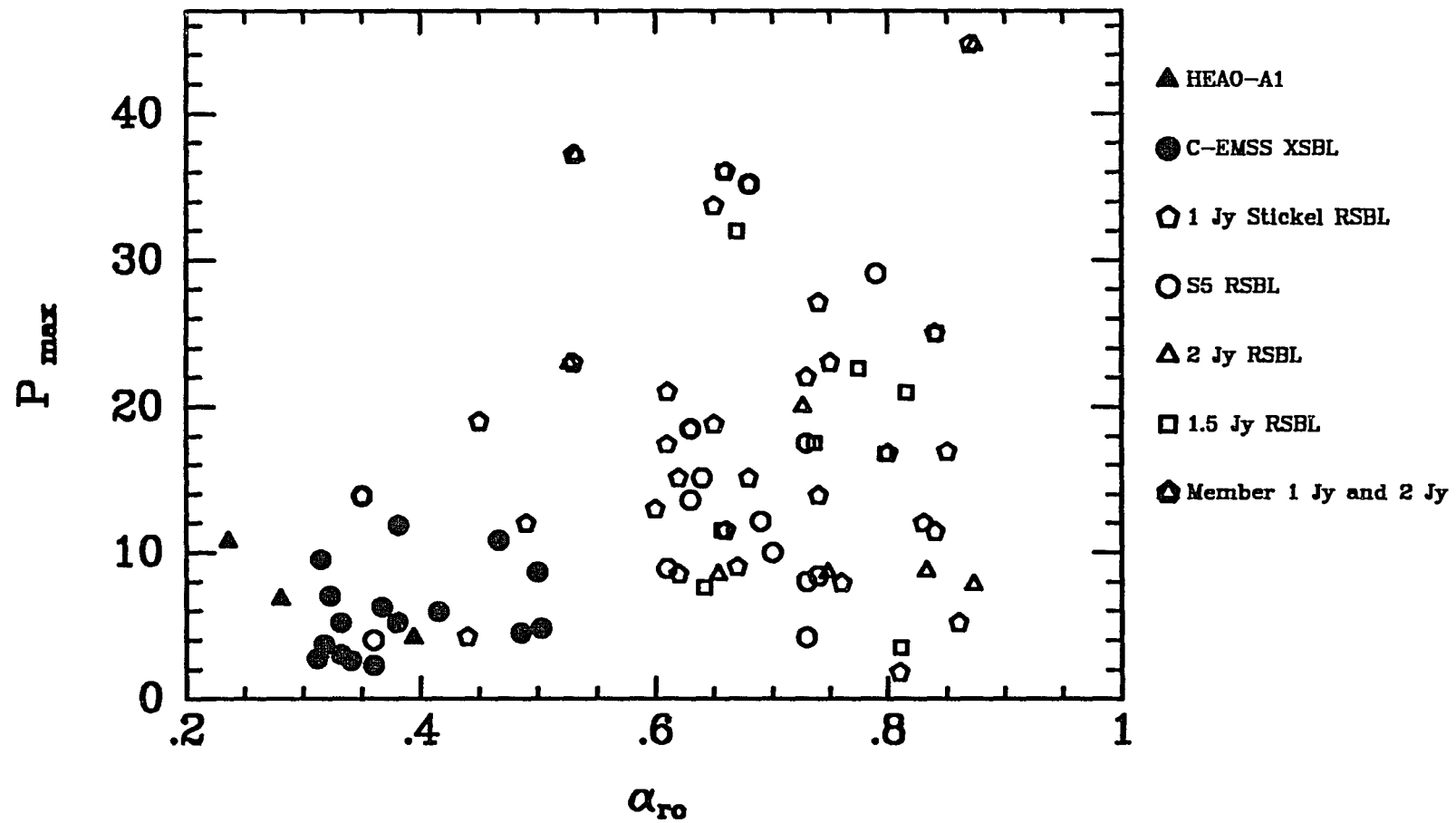


Figure 6.11

X-ray and Radio Selected BL Lacs and Quasars

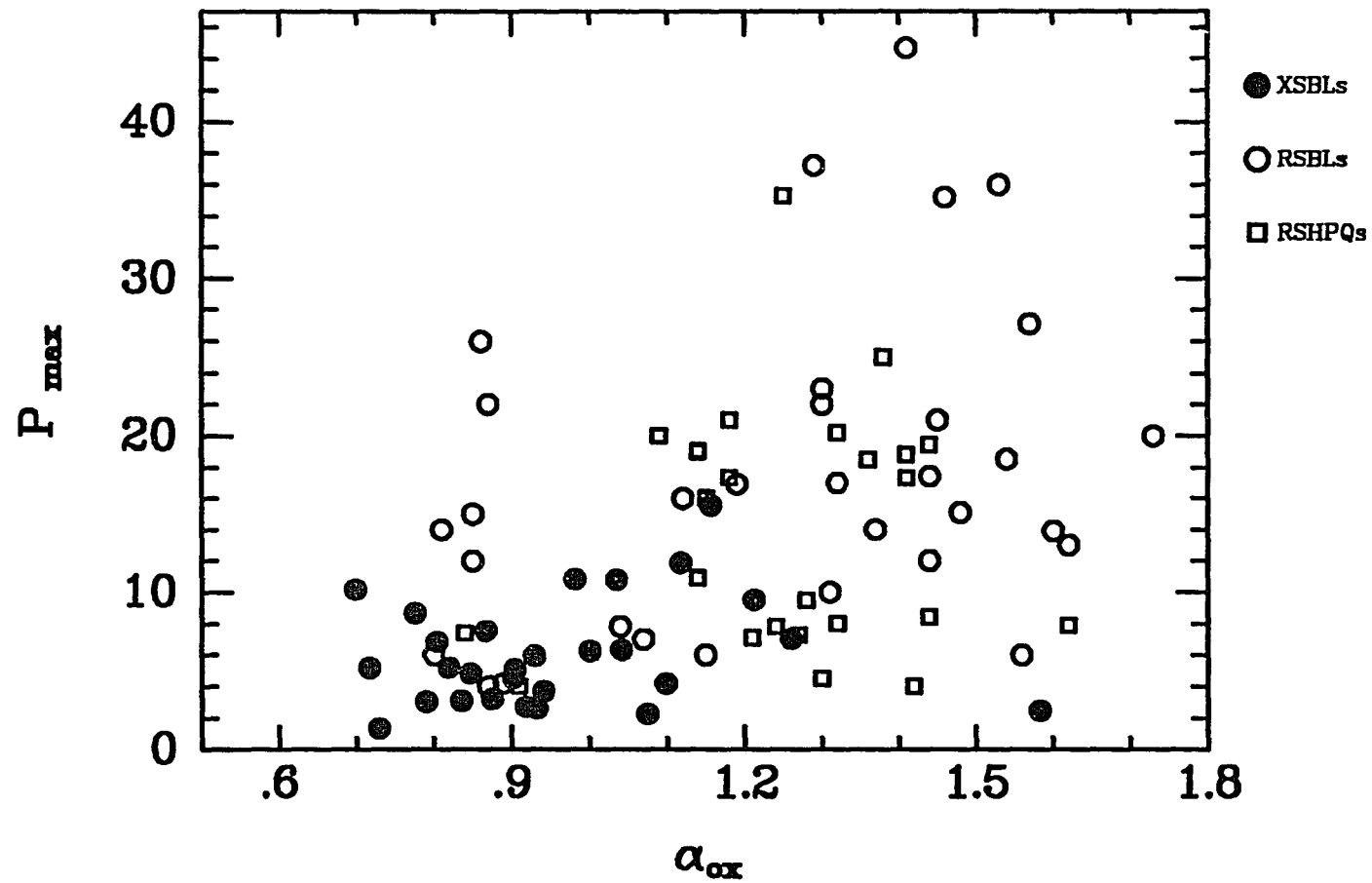


Figure 6.12

X-ray and Radio Selected BL Lacs

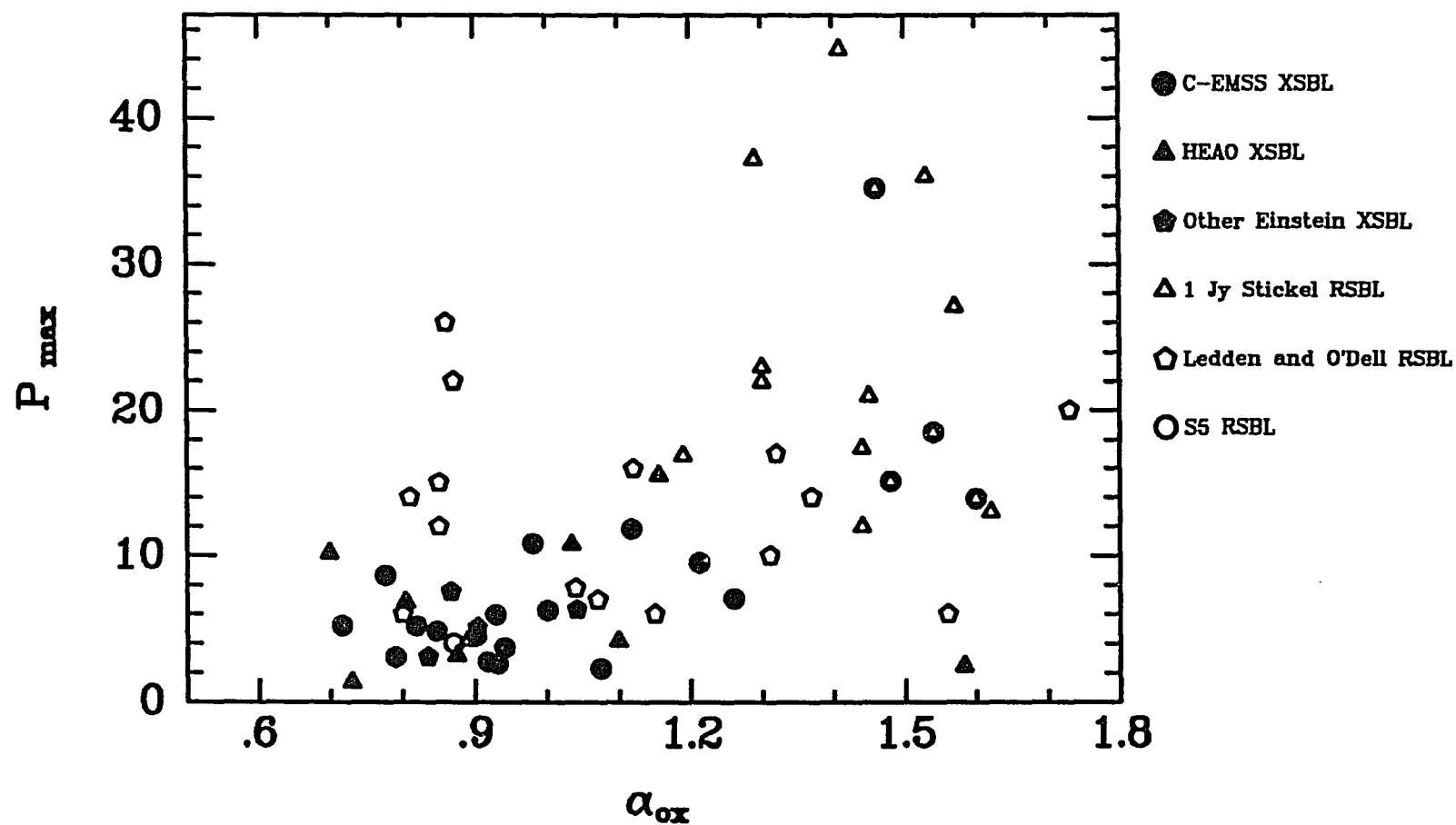


Figure 6.13

Complete Samples of X-ray and Radio Selected BL Lacs

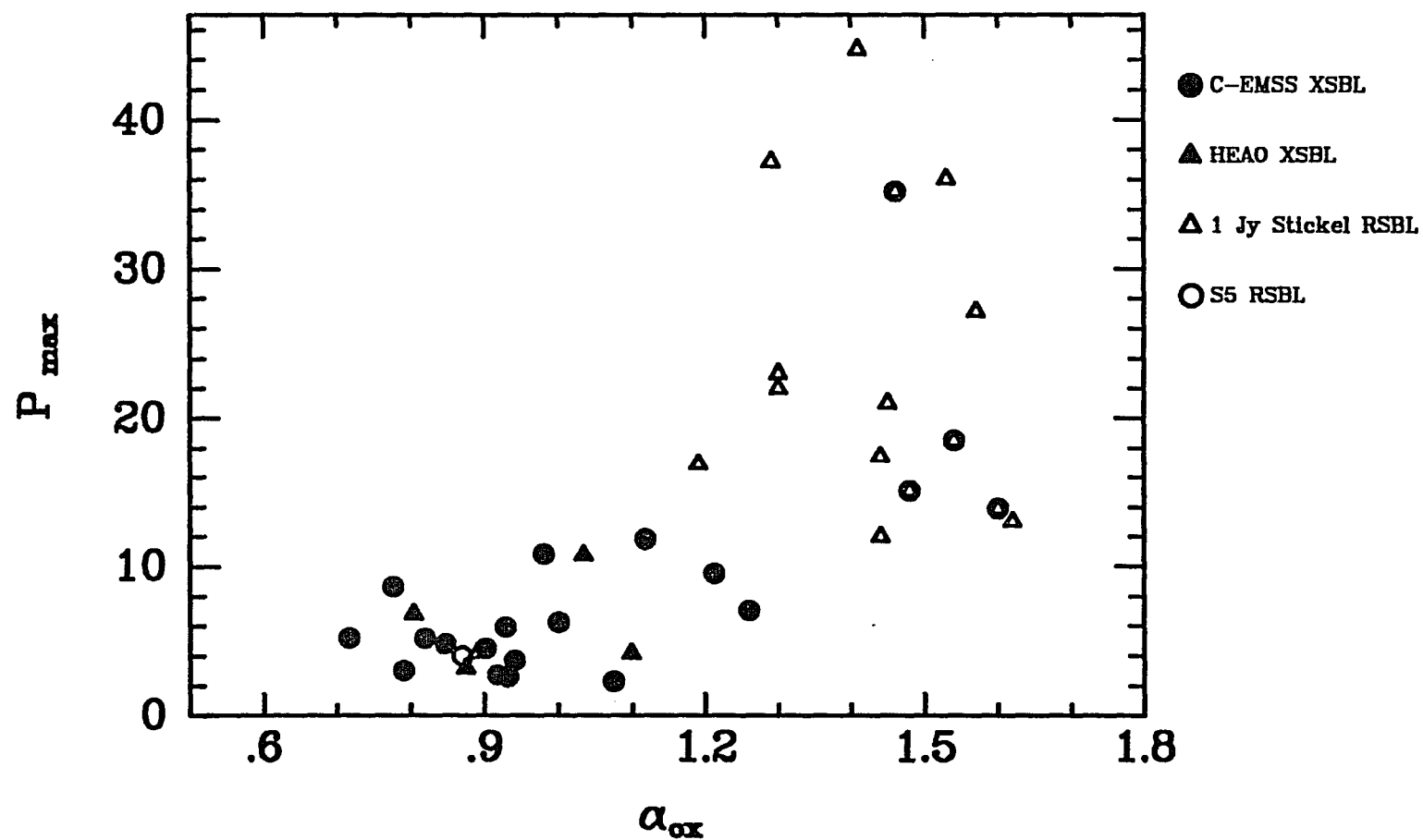


Figure 6.14

XSBLs compared with 1 Jy and S 5 RSBLs

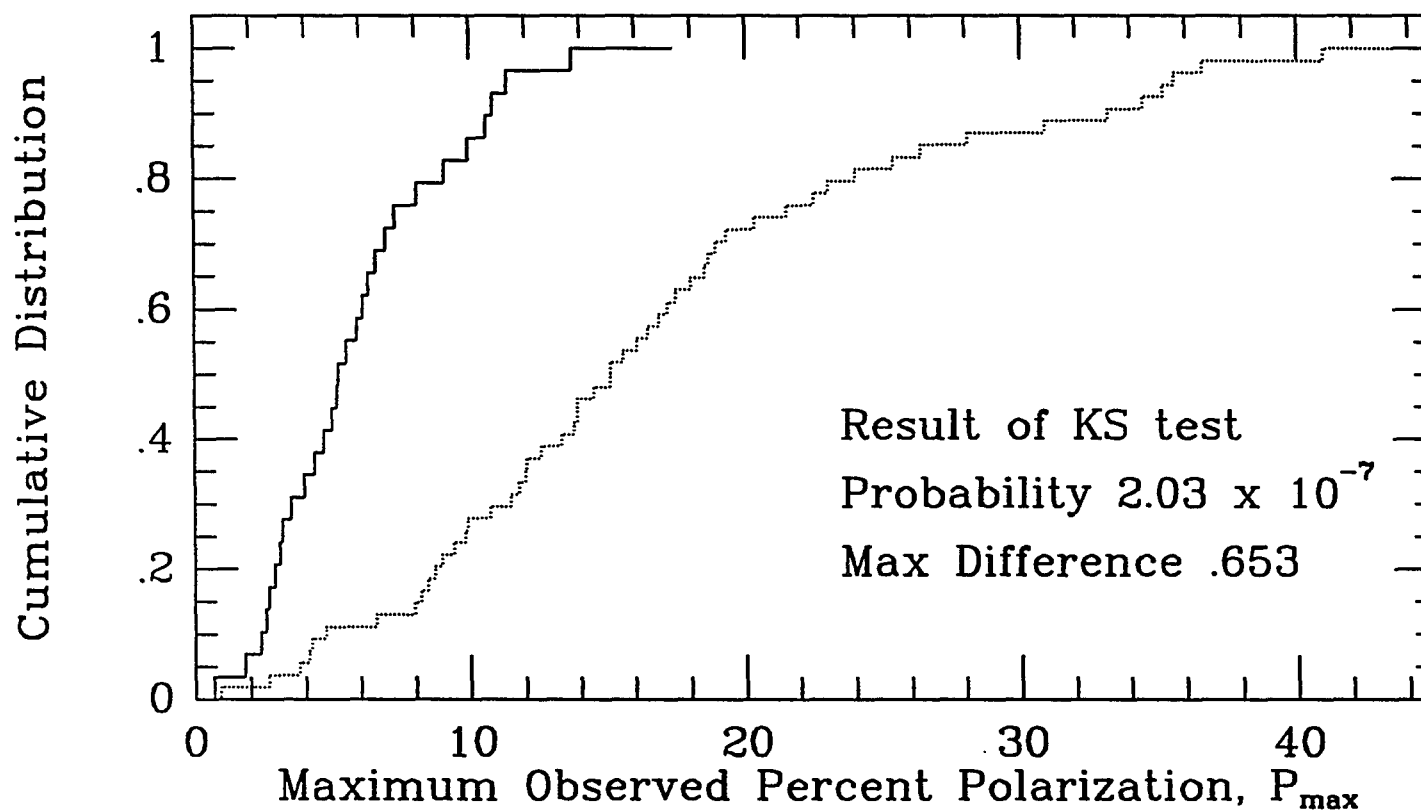


Figure 6.15a

C-EMSS XSBLs compared with Stickel 1 Jy RSBLs

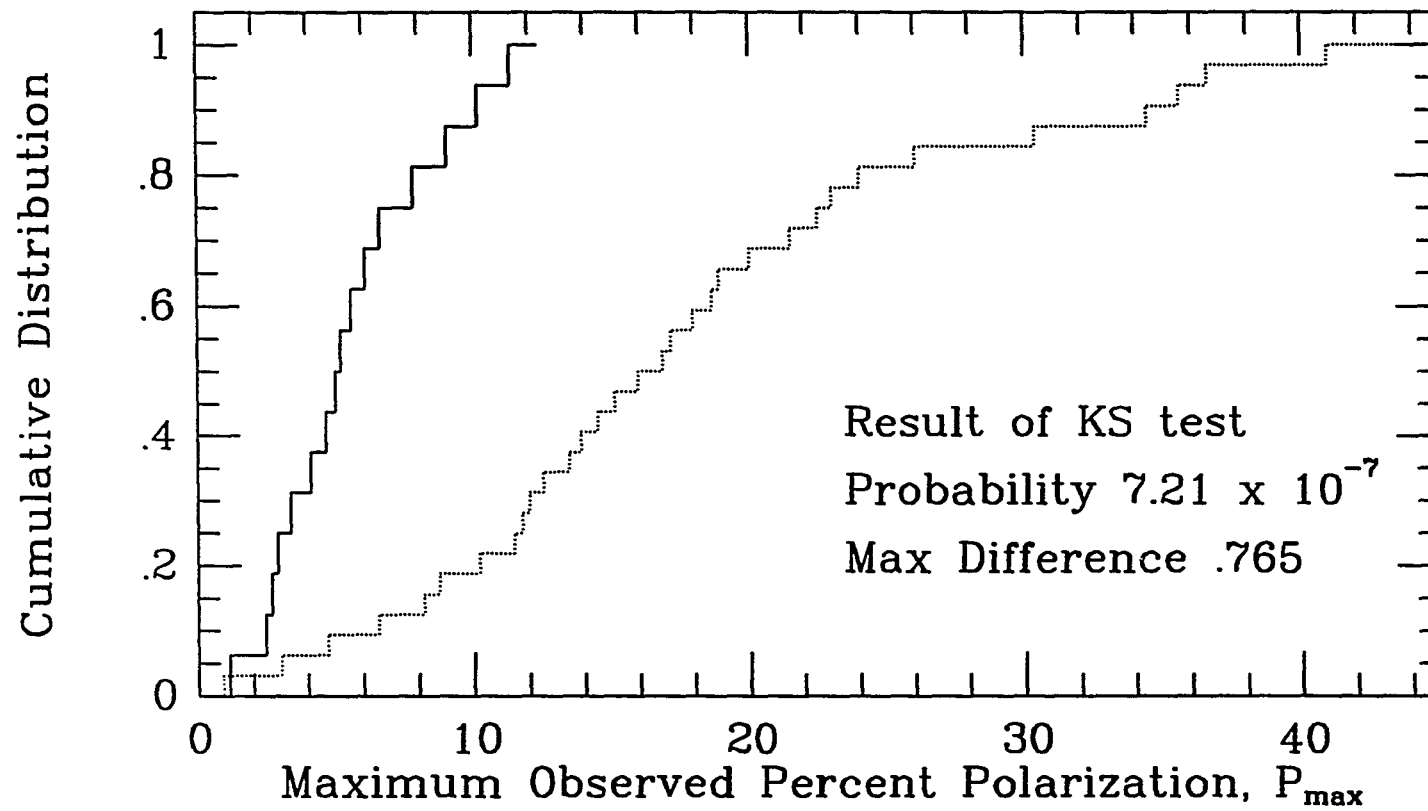


Figure 6.15b

Since we have redshifts for the majority of the EMSS XSBLs and 1 Jy Stickel RSBLs, we can also examine how the polarized luminosities (L_{pol}) depend on α_{ro} and α_{ox} . Figures 6.16 through 6.18 are plots of $\log L_{\text{pol}}$ vs. α_{ro} , α_{ox} , and α_{rx} for various samples of BL Lacs and HPQs. Despite the smaller number of objects in these plots, the observed trend for BL Lacs with larger α_{ro} to have larger polarizations is still present in Figure 6.16. Even more striking is the relationship between α_{ox} and $\log L_{\text{pol}}$. Here we see a stronger segregation of the objects than was evident in the plot of P_{m} vs. α_{ox} . No object with α_{ox} less than 1.1 has a polarized luminosity within a factor of ten of the mean polarized luminosity of the objects with α_{ox} greater than 1.1.

Figures 6.16 through 6.18—The Log of the polarized luminosity is plotted against α_{ro} , α_{ox} , and α_{rx} for a variety of samples of polarized objects. The polarized luminosity was calculated assuming the sources emit their radiation isotropically.

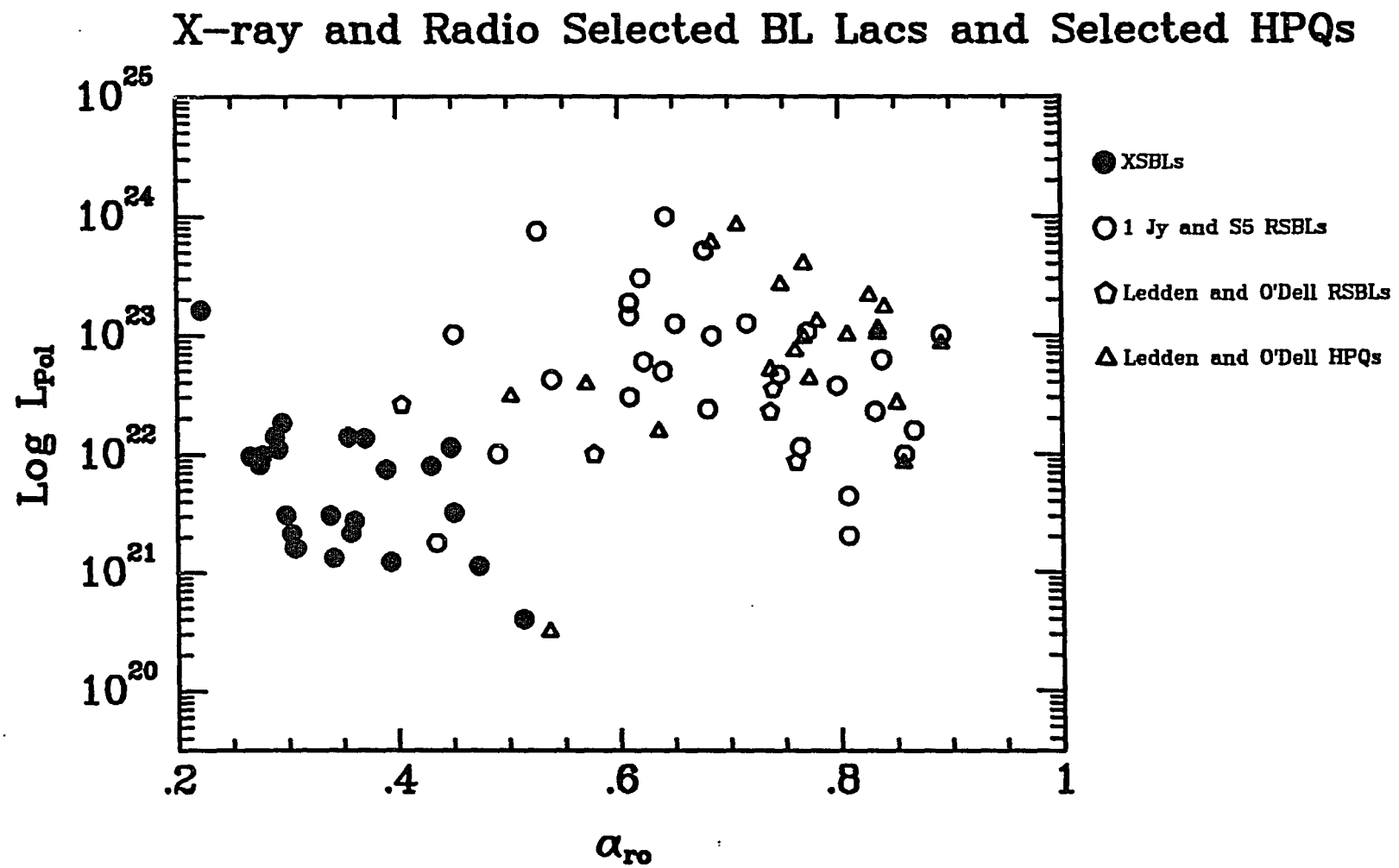


Figure 6.16

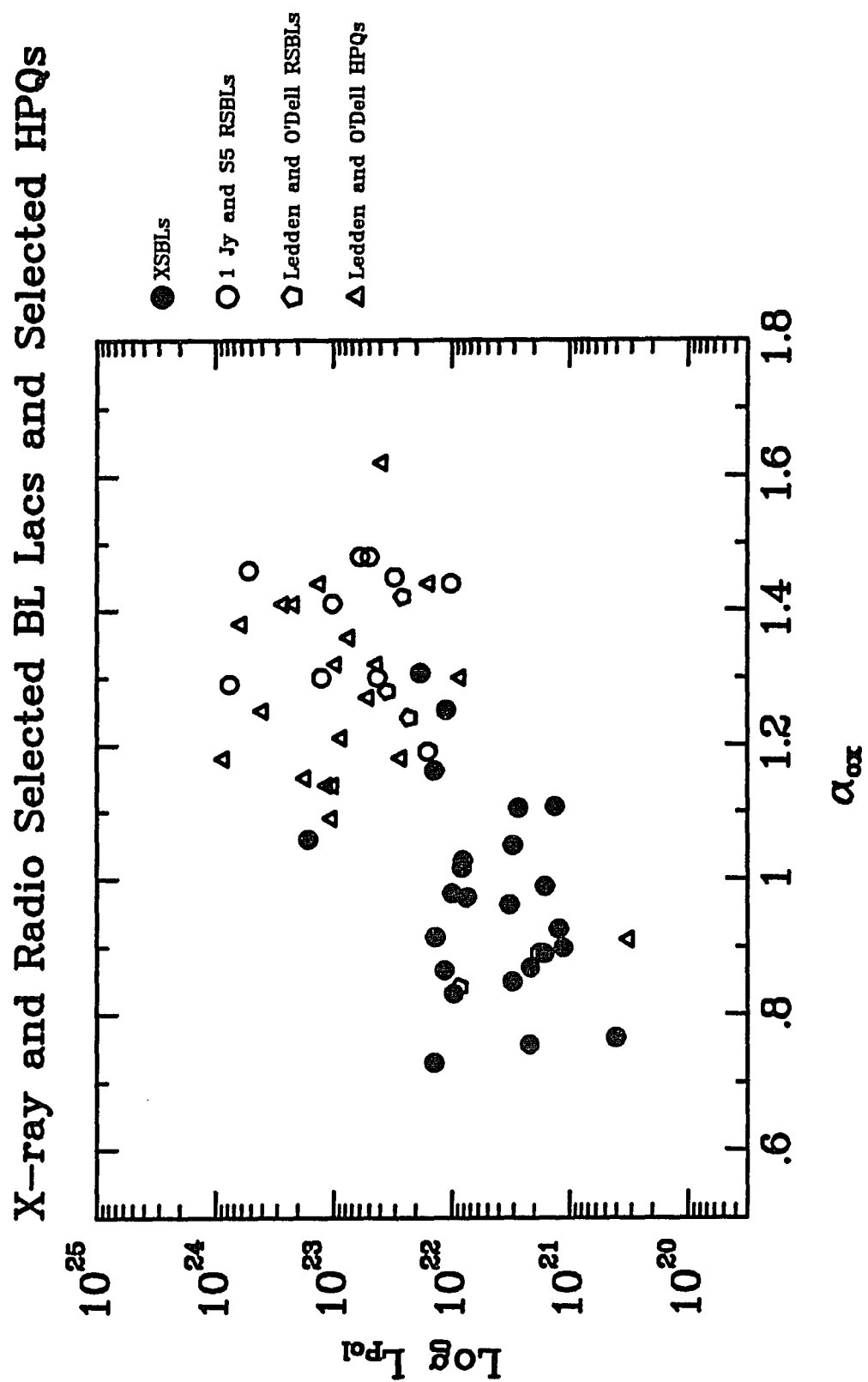


Figure 6.17

X-ray and Radio Selected BL Lacs and Selected HPQs

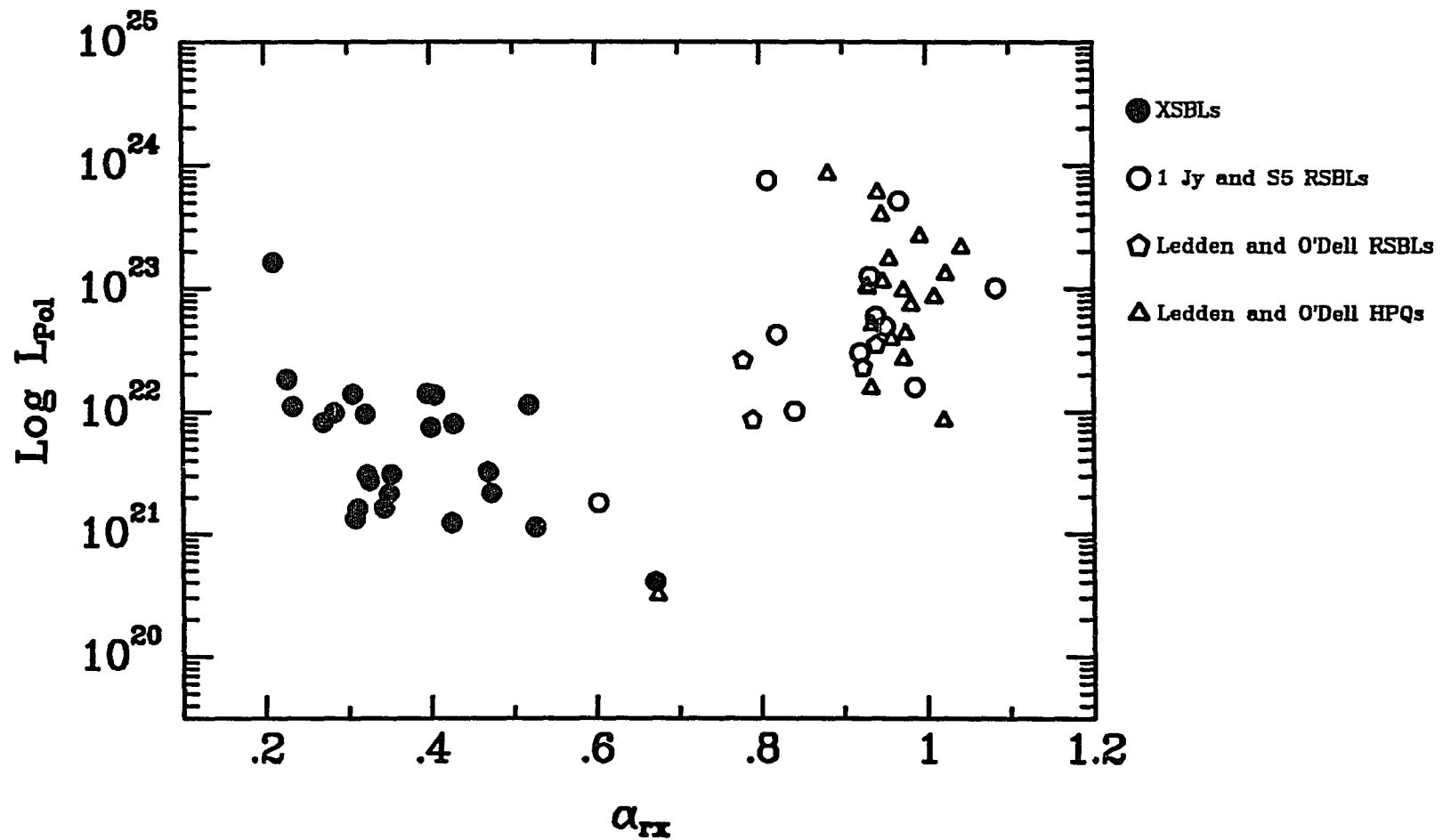


Figure 6.18

The distributions of objects in these plots reflect the previously identified differences between the x-ray selected and radio selected objects. They are also consistent with the beaming model of BL Lacs. If we consider the entire sample of BL Lac objects presented by both the x-ray and radio selected samples, we can qualitatively describe the observed trends or correlations as consequences of a range of viewing angles to the relativistic or beamed component of the BL Lacs. When the viewing angle is small, the radio and optical fluxes are boosted relative to the more isotropic x-ray emission. This is consistent with the lack of any strong correlation in observed x-ray luminosities as a function of α_{ro} , α_{ox} , or α_{rx} .

Alternatively, the differences between these two samples might reflect fundamental differences between the two groups of objects. For example they might reflect differences in evolutionary history or other properties of RSBLs, XSBLs, and quasars. We have mentioned before that HPQs and RSBLs, despite observed similarities, have significant differences which do not support unifying them into a single class (e.g. Chapter 1; Browne 1989). We can not rule out the possibility that the XSBLs also represent a distinct class of objects. Remember that there is at this time no confirmation of the existence of relativistic bulk motions occurring in XSBLs. Such evidence would certainly strengthen our treatment of both the XSBLs and RSBLs as representatives of a common parent population.

We have also learned that the maximum observed percent polarization of the nonthermal component of BL Lacs increases, independent of the question of dilution, with increasing α_{ro} . This can also be attributed to a range of viewing angles within the sample of BL Lacs. The change in polarized flux is not directly proportional to the change in total optical nonthermal flux as a function of α_{ro} or α_{ox} . While both increase with increased α_{ro} , α_{ox} , or α_{rx} (i.e. with an increased beamed component), the rates of increase are different. This is evident in Figures 6.19 through 6.24 which are plots of the total nonthermal luminosities and unpolarized luminosities determined as part of our discussion above and in §6.4 on the dilution of the observed polarization by starlight. Comparison of Figures 6.17 and 6.22 shows that the rates of change as a function of α_{ox} of the total nonthermal component and the polarized component are different. This is just another way of interpreting the observed difference in P_m for BL Lacs with different values of α_{ro} and α_{ox} .

Figure 6.19 through Figures 6.24—The Log of the unpolarized nonthermal luminosity and the Log of the total nonthermal luminosity are plotted against α_{ro} , α_{ox} , and α_{rx} for XSBLs and RSBLs. The values for the unpolarized and nonthermal radiation were calculated assuming that all of these objects had brightest cluster ellipticals as their host galaxies. (see §6.3 and §6.4).

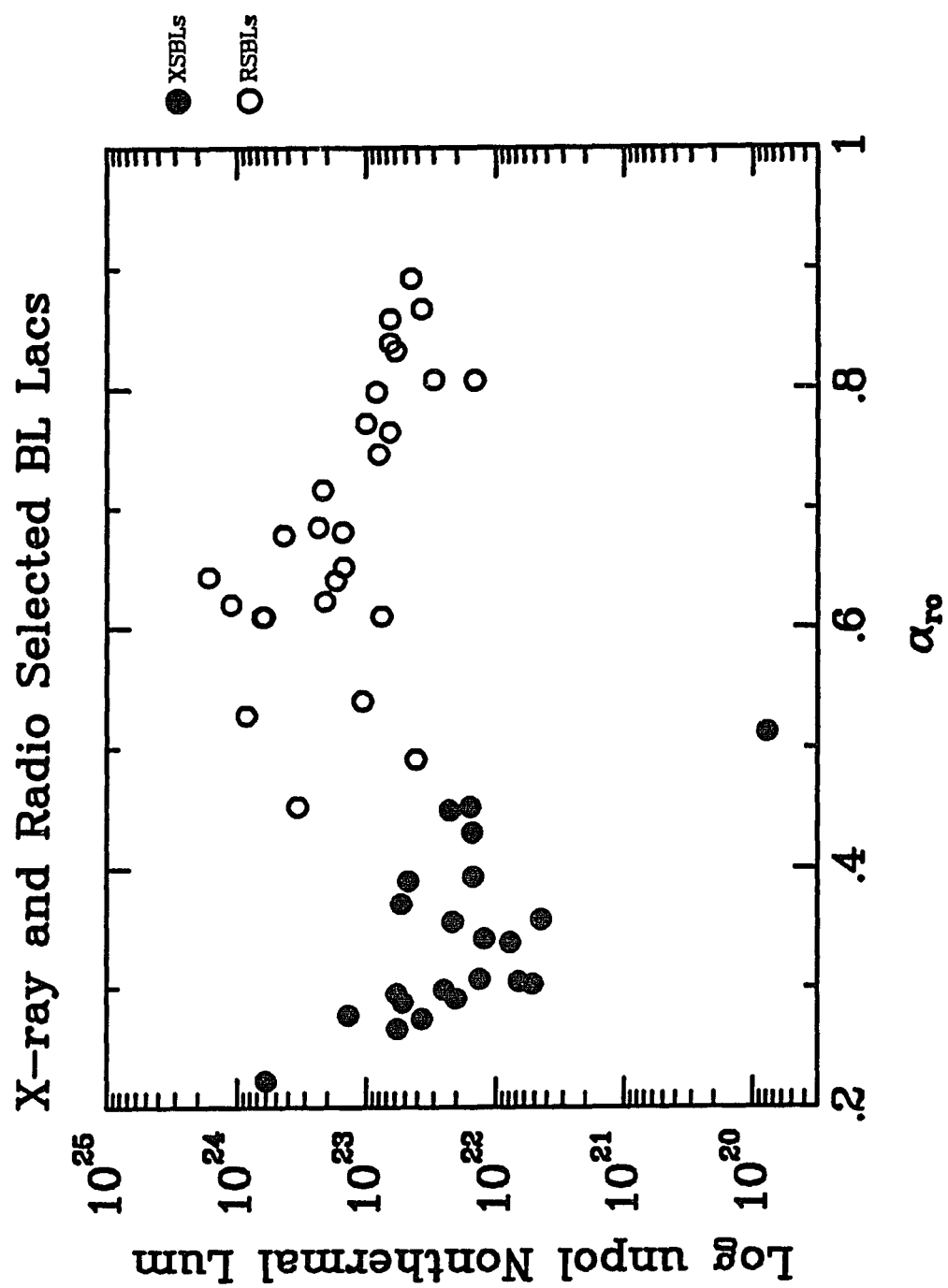


Figure 6.19

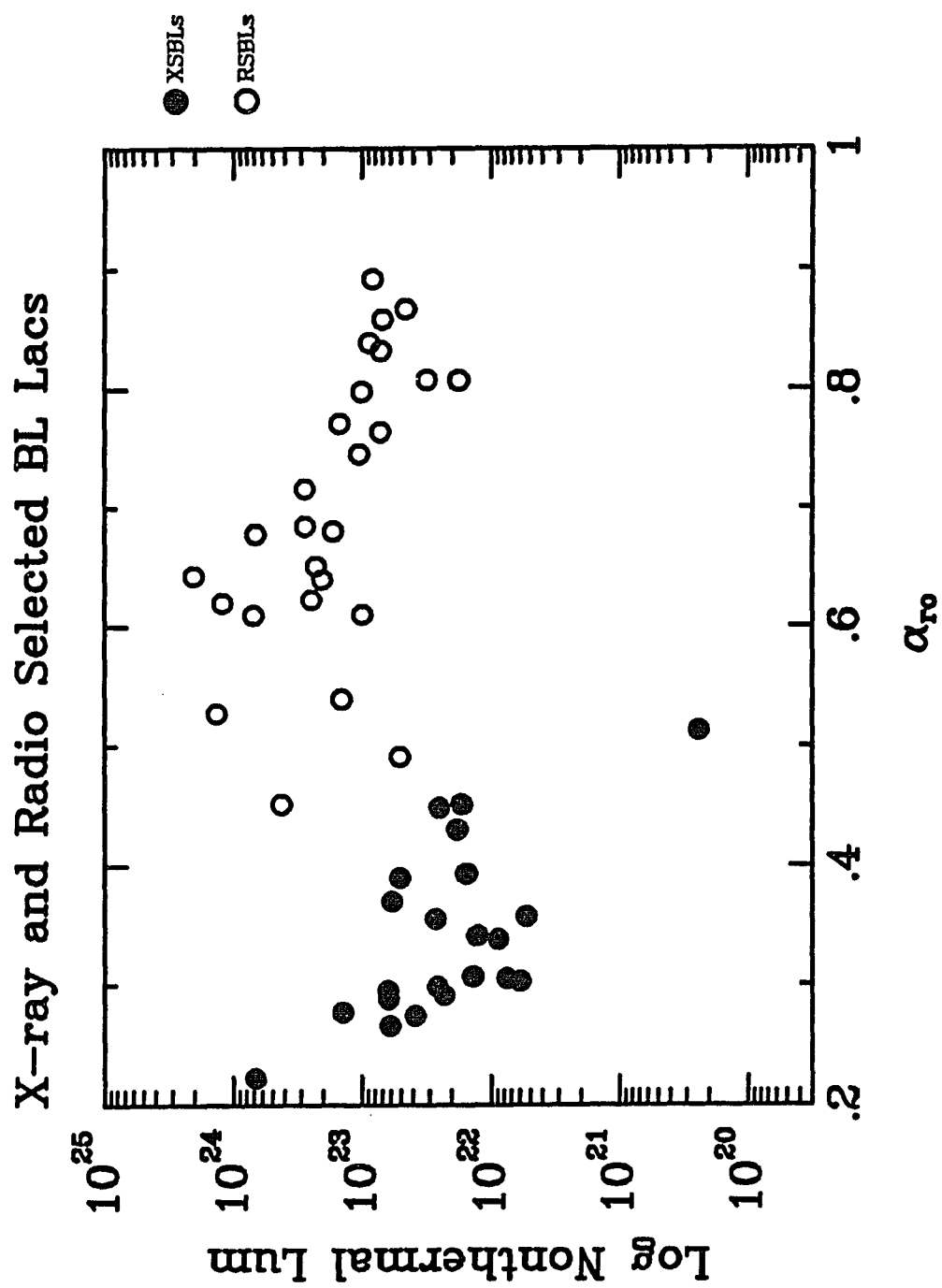


Figure 6.20

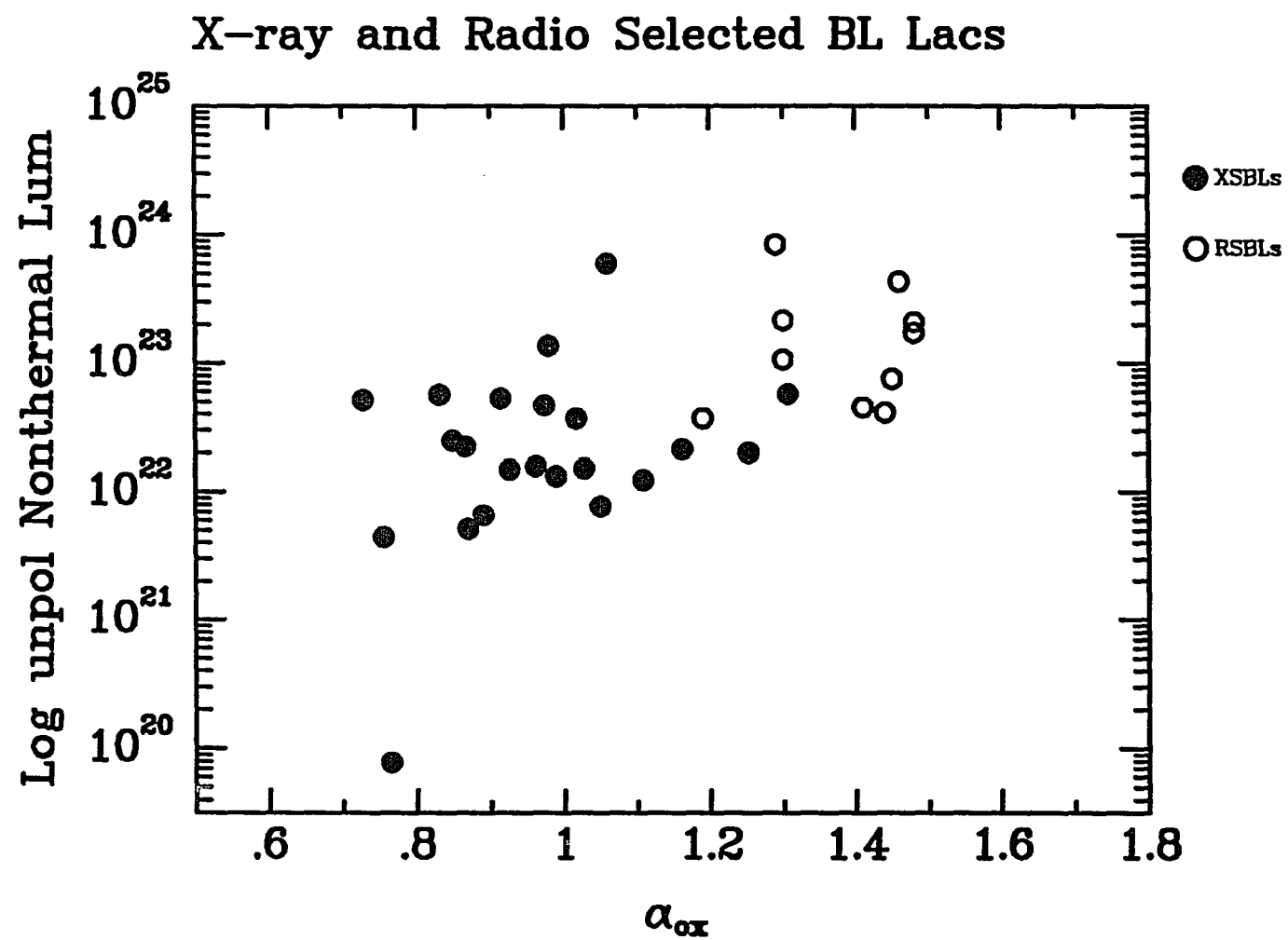


Figure 6.21

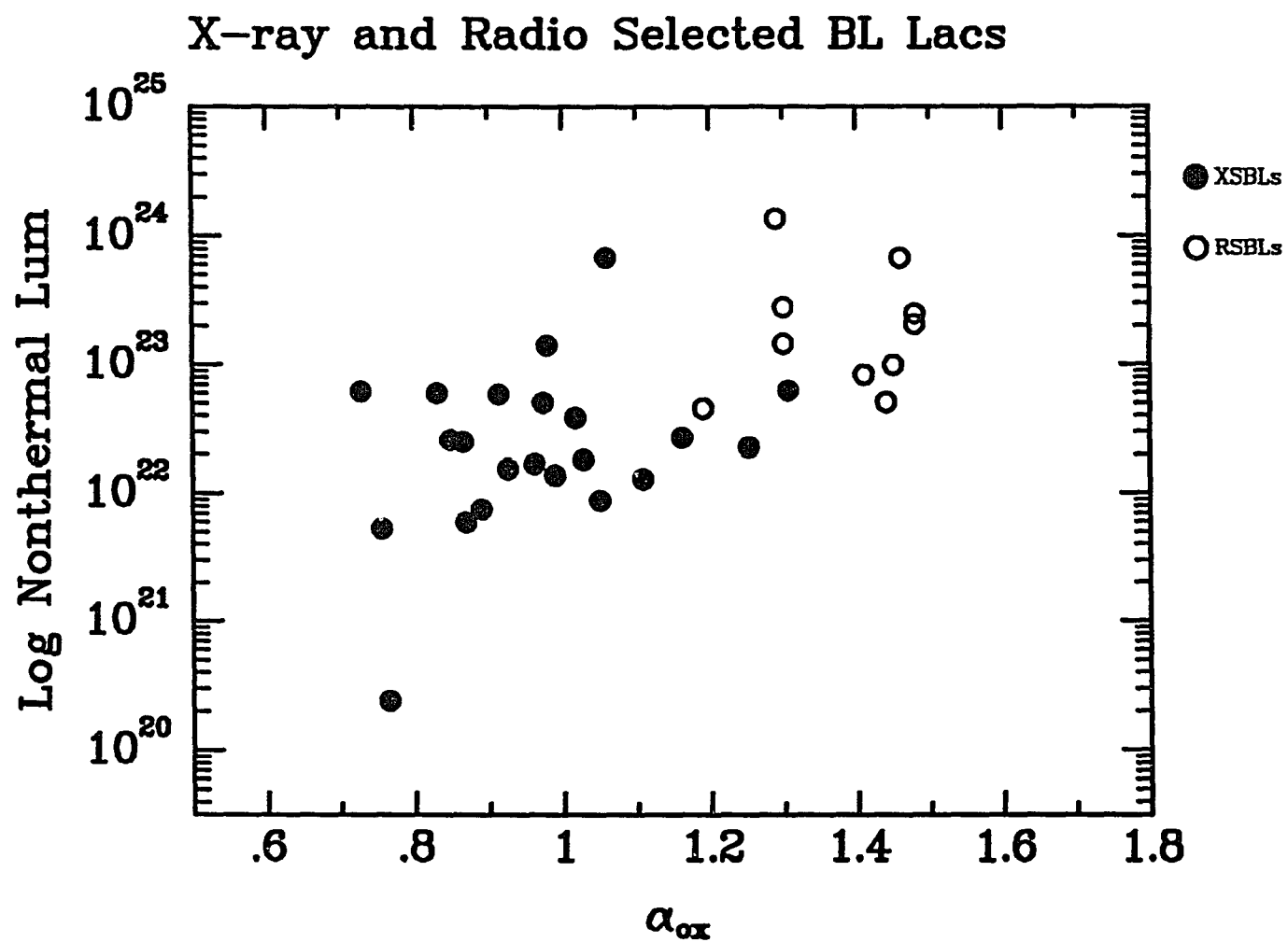


Figure 6.22

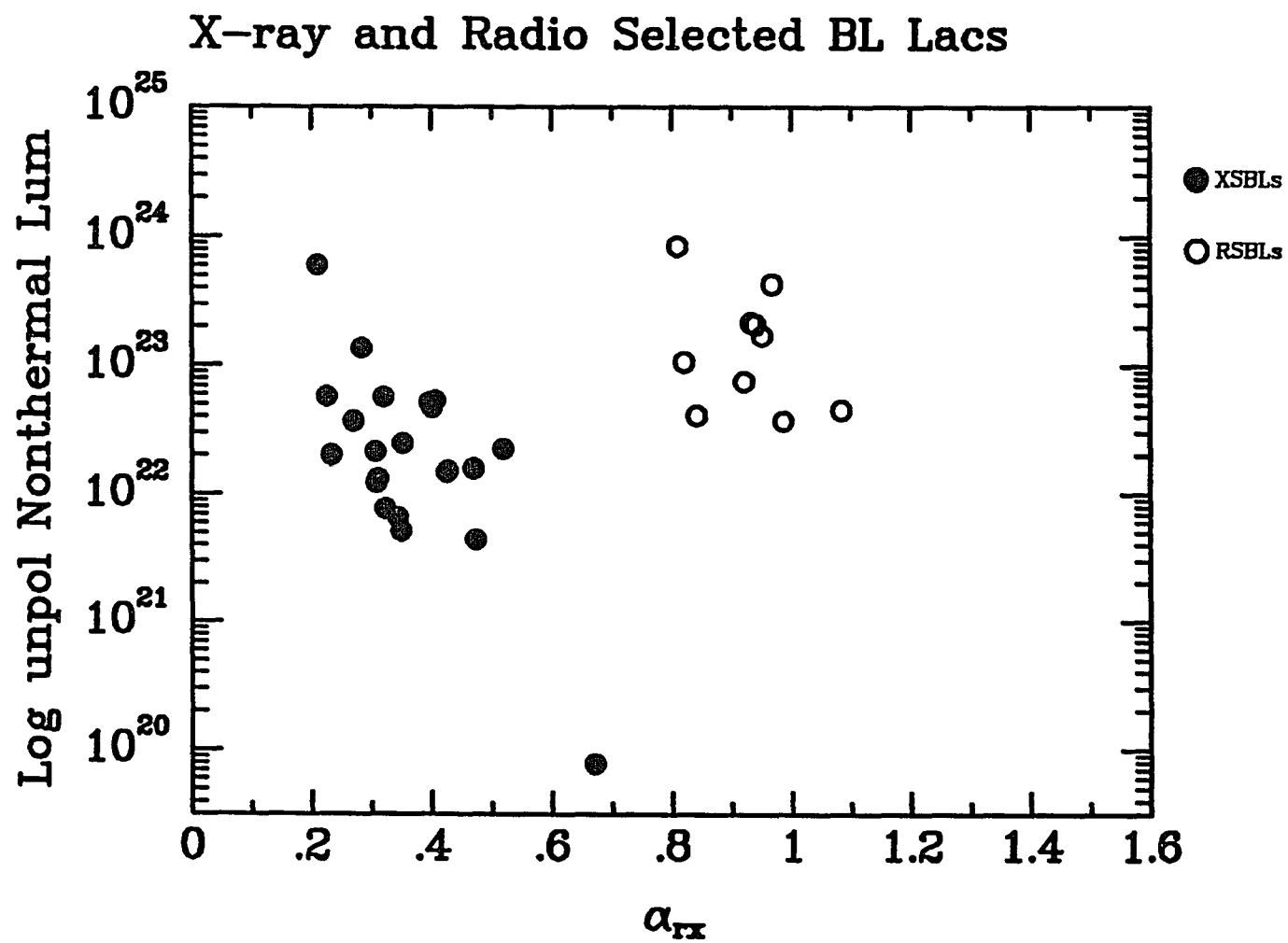


Figure 6.23

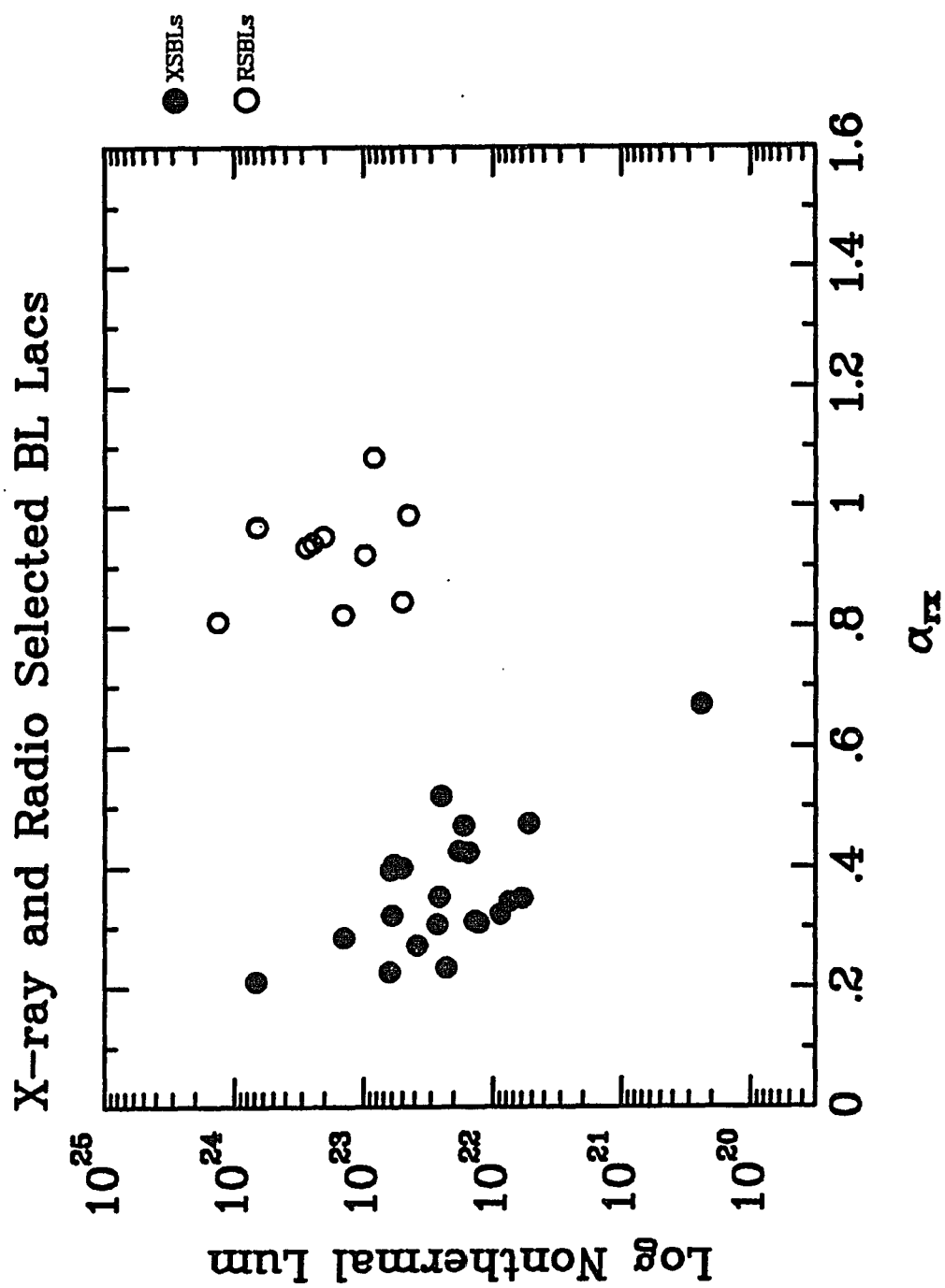


Figure 6.24

6.4 The Frequency Dependence of The Polarized Emission

and Dilution by the Host Galaxy

While we do not have spectra for the XSBLs and RSBLs in the complete samples (the publication of the spectra is in preparation: Morris *et al.* 1990; Stickel *et al.* 1990), we can consider the effects of dilution of the polarization of the synchrotron component by the host galaxy. If all BL Lacs have giant ellipticals as their host galaxies (see Chapter 1; Ulrich 1989), then we would expect the unpolarized stellar light to dilute the polarization of the nonthermal synchrotron component at longer wavelengths. This is precisely what is observed. For all of the objects in our monitoring program, whenever frequency dependence in the polarization was detected the *B* band polarization was larger than the *I* band measurement. Similar results have been found for RSBLs (Smith *et al.* 1987). This is in marked contrast to the frequency dependence of HPQs. HPQs have been observed to have lower polarizations at *U* and *B* than at *V*, *R*, and *I*. This has been interpreted as the result of a hot thermal component (usually modelled as an accretion disk) diluting the polarization at short wavelengths (Smith *et al.* 1986). No evidence of an analogous component in BL Lac objects has been observed.

6.5 The Duty Cycle of Polarization for BL Lacs

In addition to our examination of the difference in the cumulative distributions of P_m for the XSBLs and RSBLs, we can compare the duty cycles of polarization for both groups. In Chapter 5 we determined that the duty cycle of polarization for XSBLs is 40%. Similar calculations have been made for samples of RSBLs and Blazars (Kühr and Schmidt 1990; Impey and Tapia 1990; Fugmann 1988). For RSBLs, the various independently determined values all find roughly the same value of 60%. Considering our complete set of BL Lacs, it is evident that the objects with large α_{ro} , large P_m , and larger polarized luminosities also spend more of their time at levels of significant polarizations. Correspondingly, the objects with low values of α_{ro} and P_m spend the majority of their time at low levels of polarization. Note that the duty cycle determined by Impey and Tapia for Blazars considers a sample of objects including both RSBLs and HPQs. If BL Lacs and HPQs are intrinsically different objects then we would want to exclude the HPQs from this sample for comparison to the XSBLs. In practice, this makes no difference since the studies of BL Lac samples find the same duty cycle.

6.6 BL Lac Objects with Preferred

Polarization Position Angles

As the number of known RSBLs began to increase and the amount of polarization data for these objects grew, a few of these intrinsically variable objects were observed to have position angles which clustered around a “preferred value”. In fact the first member of the class, BL Lac, has a preferred position angle. It was also noticed that these few objects were less polarized and less variable than the majority of BL Lacs being found during the optical followup of radio surveys (Angel and Stockman 1980; Sitko *et al.* 1985).

In general however, the vast majority of RSBLs have unpredictable polarization position angles. If we consider the data of Sitko *et al.* (1985) and Smith *et al.* (1987), we see that virtually all of the RSBLs they monitored have widely varying position angles, the exception being BL Lac and perhaps OJ 287. Mrk 501 (H 1652+398) is another well known BL Lac with a preferred position angle. Still, among RSBLs this behavior is not a general characteristic. For example, if we plot the measured polarizations over two years of monitoring for 0735+178 and OI 090.4 (data from Smith 1986), we see that the polarization of these RSBLs can range over the entire Q,U plane (Figures 6.25 and 6.26).

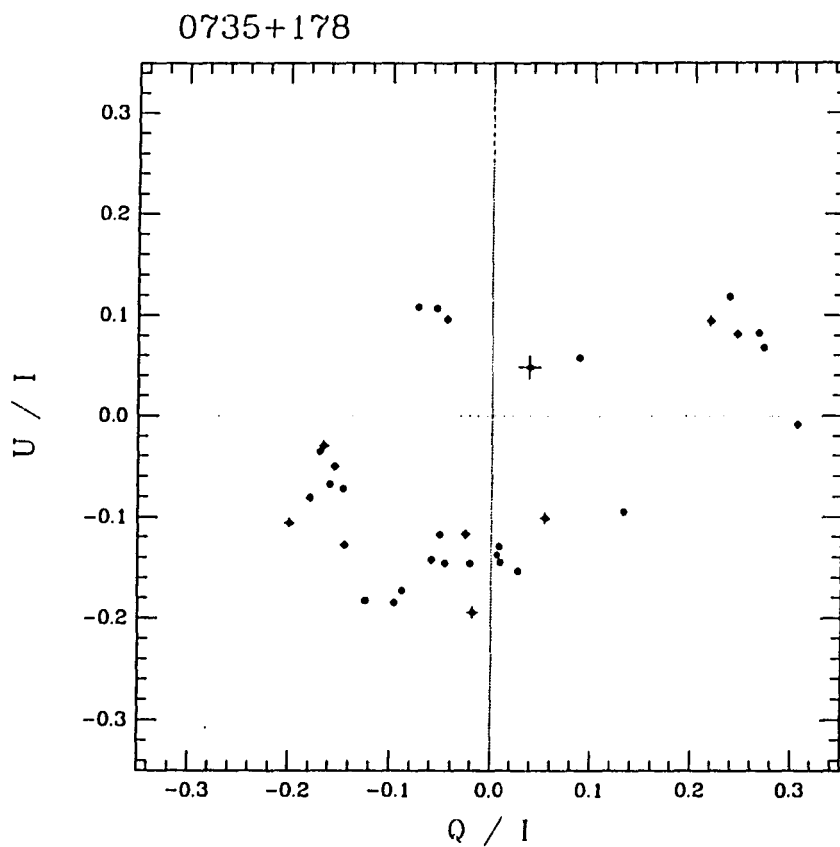


Figure 6.25—We have plotted the R polarimetry data of Smith *et al.* 1987 for the radio selected BL Lac object 0735+178. The x and y axes are the normalized Stokes Q and U parameters. The one sigma error bars are indicated by the vertical and horizontal lines centered on each data point. The data were obtained during a time baseline of approximately two years.

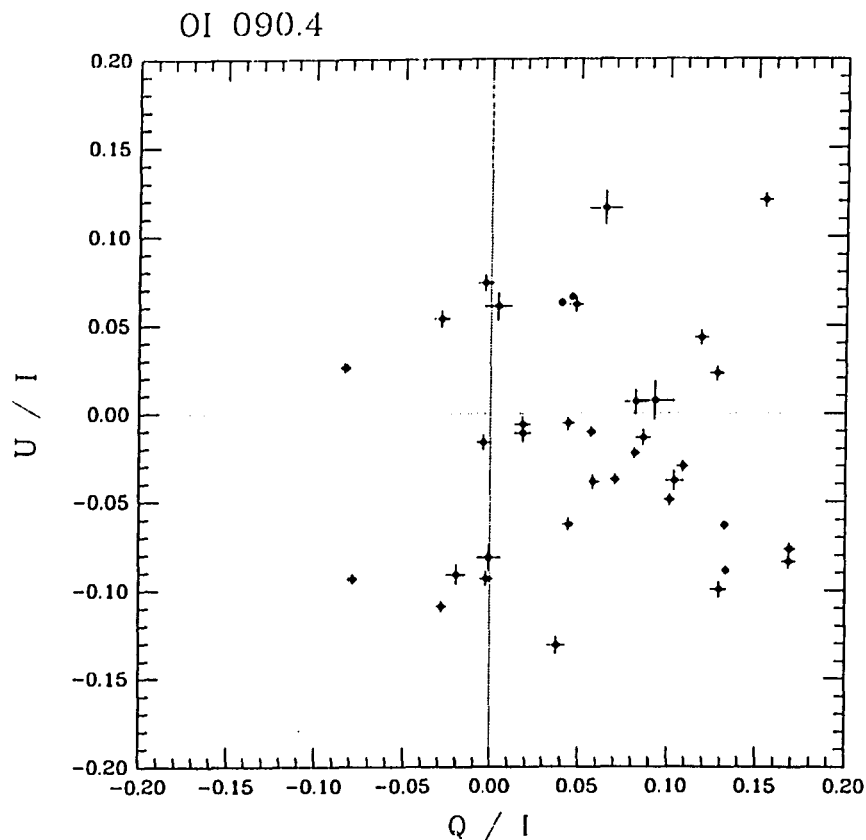


Figure 6.26—We have plotted the R polarimetry data of Smith *et al.* 1987 for the radio selected BL Lac object OI 090.4. The x and y axes are the normalized Stokes Q and U parameters. The one sigma error bars are indicated by the vertical and horizontal lines centered on each data point. The data were obtained during a time baseline of approximately two years.

Rusk (1988) has compiled a list of those BL Lacs with observed radio “jets” (observed with either VLBI or the VLA). Only eight out of all the then known RSBLs are described by Rusk as having a preferred position angle for their optical polarization. Unlike our definition or preferred position angle (Chapter 5), Rusk (1988) allows a much wider range of variability in the position angle.

This means the number of RSBLs that meet our definition is even less. Table 6.3 presents the data on the RSBLs with preferred position angles as classified by Rusk. The objects marked with a † or ‡ are members of the 1 Jy RSBL sample (see Chapter 3). The object marked with a ‡, H 1652+398 (Mrk 501), is also an XSBL and was extensively observed by us during our monitoring program.

Table 6.3: RSBLs with Preferred Polarization Position Angles

Object	Range of P (%)	Range of θ	Preferred Angel
0219+428	6-22	170- 45	24
0316+413	1- 6	100-160	151
0422+004	6-22	140- 30	174
0851+202	1-37	0-180	75
1101+384	0- 7	150-185	173
1400+162	4-14	80-100	180
1652+398 [‡]	2- 4	124-145	136
1807+698 [†]	0-12	65-100	85
2200+420 [†]	2-23	0-180	24

Angel and Stockman (1980) provide in their review paper a heterogeneous compilation of the BL Lacs known at that time and also indicate for some of those objects that they have “preferred” position angles. The monitoring data available at that time was not extensive, and is still not available for a large complete sample of RSBLs. Nevertheless, monitoring of partial samples of RSBLs, while showing some objects with preferred position angles, does not find this to be

a trait shared by a majority of the objects studied (Sitko *et al.* 1985; Smith *et al.* 1986).

The XSBLs are much more likely to show a preferred position angle. We learned in Chapter 5 that 70 to 80% of the XSBLs might have preferred position angles. This difference between the two samples might also be explained as a consequence of a range of viewing angles (or equivalently a range in relativistic bulk velocities for the jets) to the beamed component of the BL Lacs' radiation. For objects observed at a large viewing angle (hypothetically most of the XSBLs) the projected angle on the sky of the \mathbf{E} vector will be more stable, even if the polarization is intrinsically as variable. The resulting range of position angle variations will be considerably smaller and limited to perhaps one quadrant of the \mathbf{Q}, \mathbf{U} plane. Figures 6.27 and 6.28 (as well as Figure 5.1 and Figures II.5 to II.20 in Appendix II) are examples of the behavior of the polarization position angles of XSBLs.

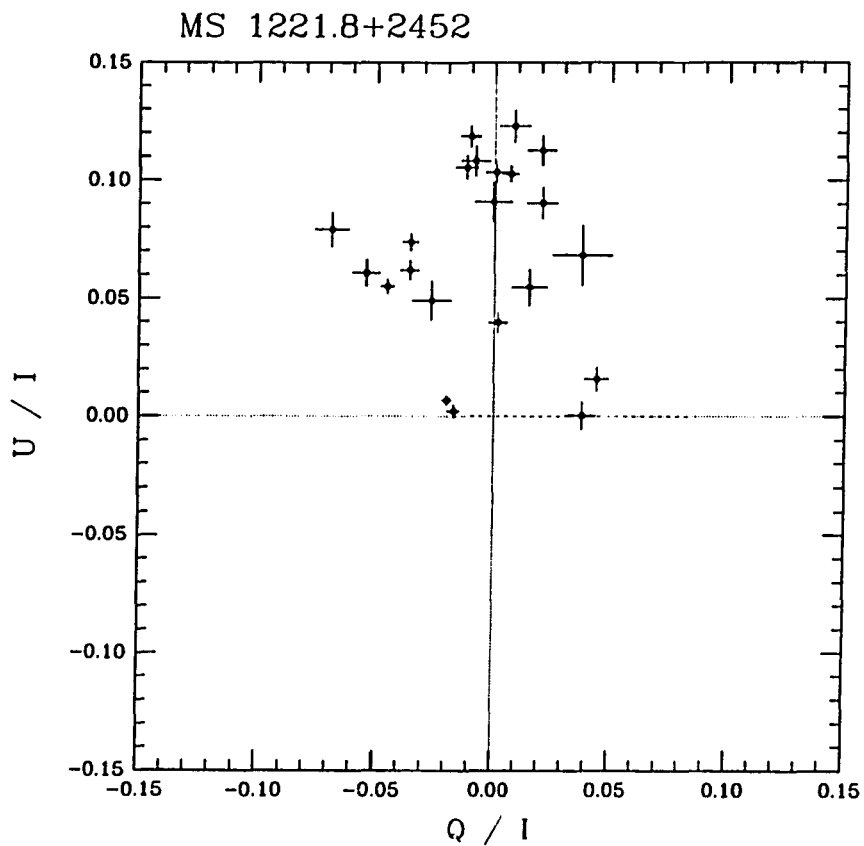


Figure 6.27—We have plotted our white light polarization observations of the XSBL MS 1221.8+2452. The x and y axes are the normalized Stokes Q and U parameters. The one sigma error bars are indicated by the vertical and horizontal lines centered on each data point. The data (listed in Appendix I) were obtained during our monitoring program and covers a time baseline of twenty-six months.

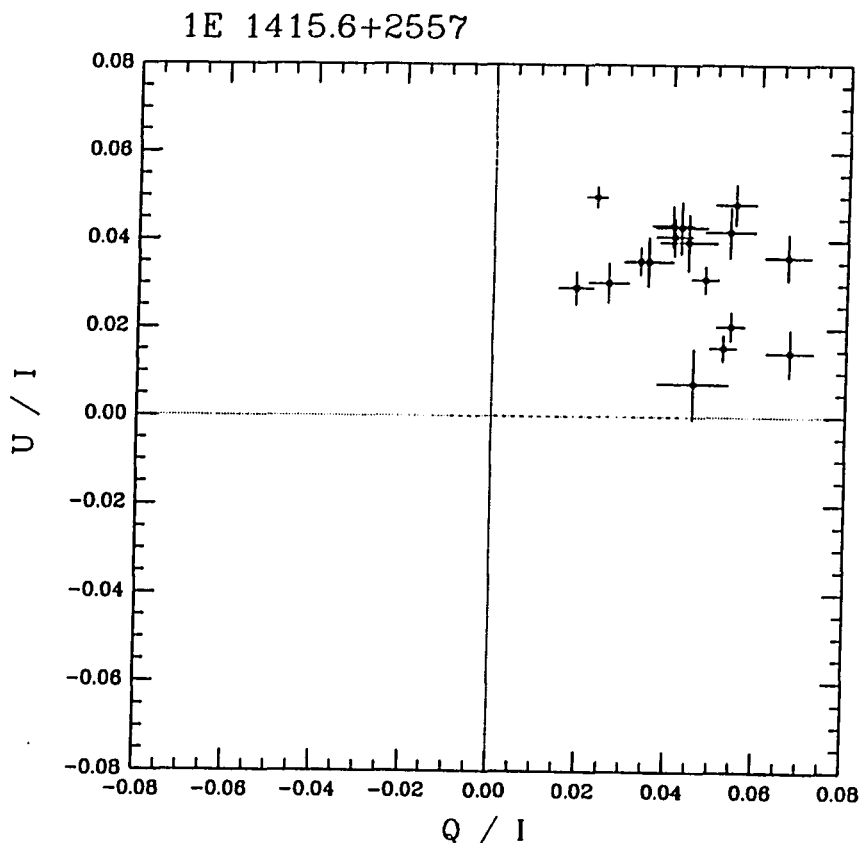


Figure 6.28—We have plotted our white light polarization observations of the XSB 1E 1415.6+2557. The x and y axes are the normalized Stokes Q and U parameters. The one sigma error bars are indicated by the vertical and horizontal lines centered on each data point. The data (listed in Appendix I) were obtained during our monitoring program and covers a time baseline of twenty-five months.

Having a preferred position angle is related to other observed properties for both RSBLs and XSBLs. Compared to the entire family of BL Lacs, the objects with preferred position angles have lower values of P_m , α_{ro} , and α_{ox} . Among RSBLs with preferred angles, the optical polarization position angle (the electric field vector, \mathbf{E}) is aligned with the position angle on the sky of the radio

emission observed with VLBI or the VLA (this refers to the direction of elongation of the radio emission and not the direction of the radio emission polarization position angle; Antonucci and Ulvestad 1985; Rusk 1988; Gabuzda *et al.* 1989). One of the best examples of this behavior is H 1652+398. We note that this object's optical polarization position angle is aligned (parallel) with the VLBI radio emission ($\theta_{VLBI} = 128^\circ \pm 5^\circ$; Rusk 1988). The alignment is interpreted as demonstrating a relationship between the optical and radio components and the orientation on the sky of the "jet" and magnetic field. Specifically the projection of the magnetic field direction on the sky is perpendicular to the ejection axis of the jet. If this is true for all BL Lacs with preferred position angles, then we would expect a large fraction of the XSBLs to have radio morphologies elongated at the position angle of their optical polarization. We have recently obtained VLA observations of seven of the XSBLs with preferred position angles in an effort to address this question in the near future. Besides looking for evidence of asymmetry in the radio emission, we will also study of the flux in any extended emission and follow an analysis similar to that done for RSBLs by Antonucci and Ulvestad (1985).

We note that Gabuzda and her collaborators have reported that HPQs might have contrasting alignment properties. They note that quasars have their radio polarization position angles perpendicular to the VLBI jet's axis (Gabuzda 1989). This is one of the observed differences between the two classes of objects.

6.7 The Total Flux Variations of BL Lacs

The historically well studied RSBLs have been observed to undergo rapid and large variations in their total and polarized flux. XSBLs have not been observed to undergo similar outbursts. In Figure 6.29 we plot the maximum observed polarization (white light or V band observation) *vs.* the difference between $m_{v,Br}$ and $m_{v,Fa}$ for x-ray and radio selected BL Lacs. The points plotted for the XSBLs (solid circles) are derived from our own data. The points for the RSBLs (empty circles) were determined from the observations of Sitko *et al.* (1985) and Smith *et al.* (1986). Both of these quantities (P_m , and Δm_v) were determined during two year monitoring periods for these objects. In order to increase the number of RSBLs on this plot, we have also included six other RSBLs for which polarimetry and variability data is available (polarimetry reference Impey and Tapia 1990; photometry reference Pica *et al.* 1988). These objects (plotted as squares), while not monitored as uniformly (time baselines for these objects range from one to more than four years) do provide additional information.

Even a cursory examination of Figure 6.29 reveals that there is an obvious correlation between observed large amplitude variability and large values of polarization. The physical explanation is not necessarily as obvious. If large increases in flux require the propagation of a strong shock through a sizable volume of the jet, a natural consequence might be a compression and ordering of

the magnetic field resulting in a larger observed percent polarization. However, we have already noted that there is no rule, even for individual objects, relating changes in total flux with changes in polarized flux.

Figure 6.29—For the XSBLs (solid circles) in our monitoring program and RSBLs from Smith *et al.* 1986 (empty circles) we have plotted the maximum observed polarization against the difference in magnitudes of the maximum and minimum observed magnitudes during two years of monitoring. The squares are additional RSBLs taken from Pica *et al.* 1988.

6.8 Models of the Polarization Properties of BL Lacs

Ostriker and Vietri (1983; 1985; 1990) have repeatedly proposed that the observed properties BL Lacs can be produced by the microlensing of a small region of the nucleus of a highly polarized quasar. The broad line region of the lensed quasar, being so much larger in size than the relativistic jet producing the optical synchrotron emission, is not lensed. This would then explain both the lack of emission lines in BL Lacs and the apparent lack of BL Lacs at high redshift. One of several objections to this model is the contrasting x-ray spectral slopes of BL Lacs and HPQs (Worrall 1989). Despite this and other problems with explaining all BL Lacs as the artifacts of gravitational lenses, some of the most luminous objects are possible candidates for examples of lensing events (Stickel 1990).

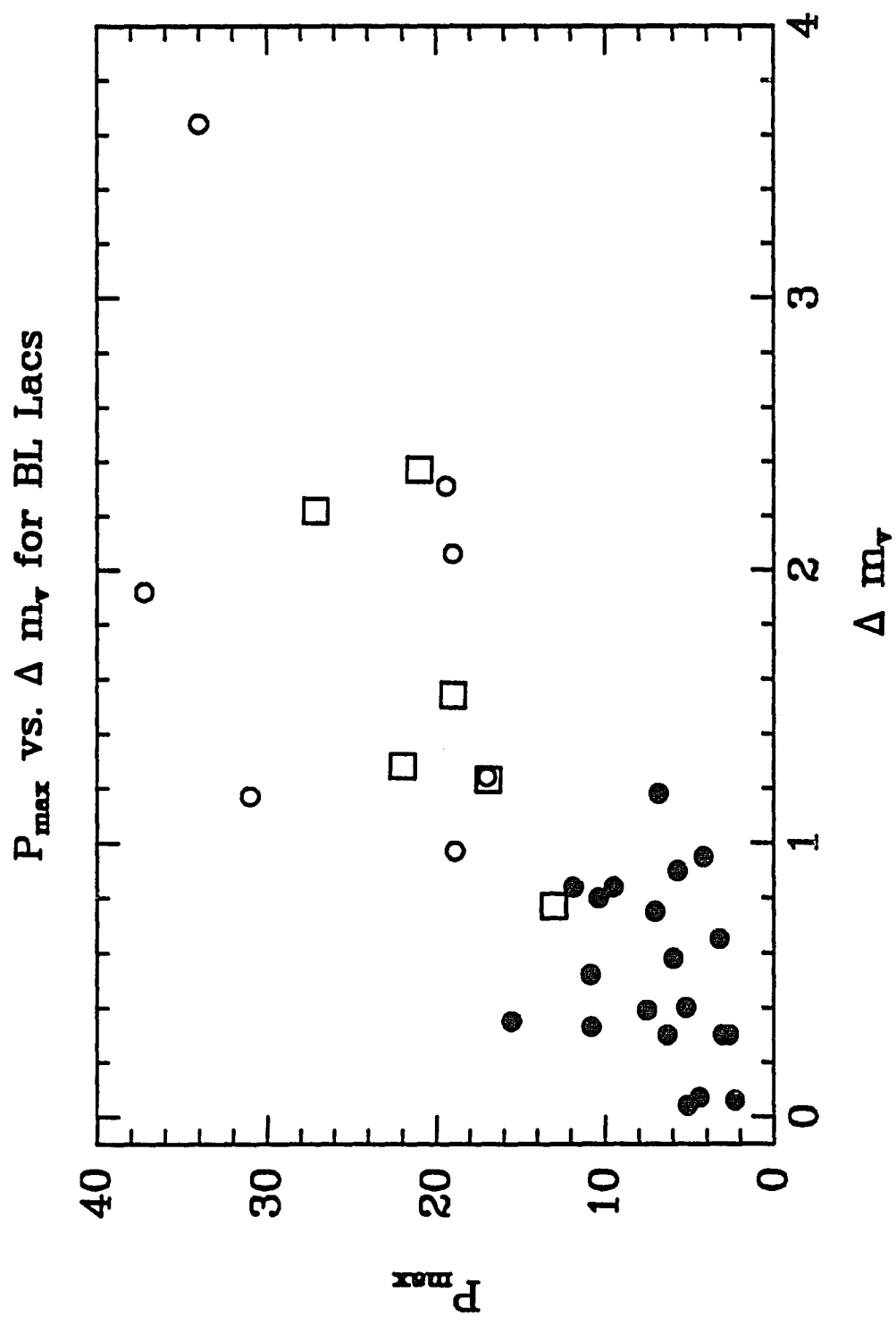


Figure 6.29

More conventional models of the relativistic jets and the consequences on the observed properties have been developed by a variety of authors (e.g. see the numerous papers in the Como conference proceedings and references therein, Maraschi *et al.* 1989). The effects of the viewing angle to the jet (or equivalently the dynamics of the relativistic jet) on the observed degree of polarization as a function of magnetic field symmetry and orientation to the jet axis have been examined in detail by Claes-Ingvar Björnsson (1982). The orientation and distribution of the magnetic field in the jet have profound consequences on the observed polarization. In Björnsson's models, changes in the jet speed are parameterized as a change in the viewing angle to the jet-magnetic field system. Polarization changes due to changes in jet dynamics are analogous to the changes that would be observed in a stable jet with changing viewing angle. His models therefore have implications for not only the behavior and interpretation of the long term behavior of individual objects, but also for the predicted distribution of polarizations of a class.

Björnsson demonstrates that the observed polarization properties are sensitive to the viewing angle to the relativistic component (or equivalently they depend on the changing velocity of the jet) For a distribution of magnetic field that has rotational symmetry (with respect to the ejection axis of the jet), the position angle of polarization seen by an observer viewing the jet at an angle θ (in the rest frame of the jet) is determined solely by the projection onto the plane of the sky of the symmetry axis of the magnetic field. Depending on the specific

assumed distribution of the magnetic field, the observed percent polarization will be a function of viewing angle to the jet (see Figure 3. in Björnsson 1982).

6.9 The Range of Polarization Properties Explained as

the Effect of a Distribution of Viewing Angles

We propose that XSBLs and RSBLs are both samples of a larger parent population of objects. All of these objects meet our definition for being a BL Lac (Chapter 1). The observed properties of BL Lacs are then consistent with a simple physical picture. A BL Lac is a relativistic jet of plasma with an associated magnetic field sitting in a host galaxy (most probably a giant elliptical; Ulrich 1989). The observed optical through radio properties will depend on the viewing angle to the relativistic jet and the Lorentz factor (beaming factor) of the jet. Objects viewed along the jet will have the largest α_{ro} (not strictly required, but consistent with the optical component consisting of both a beamed and unbeamed component while the radio emission is a purely beamed component), radio luminosities, the most core dominated radio sources, largest optical luminosities, largest maximum optical polarizations, the least amount of frequency dependence in their polarization, the shortest time scales of variability, no preferred position angle to the polarization, no or little dilution of the polarization at long wavelengths, and smallest surface and space density. With

increasing viewing angles the domination of the observed properties by the beamed component will decrease. A BL Lac viewed at increasing viewing angles should look more like the x-ray selected objects and other small α_{ro} BL Lacs. Preferred position angles are a consequence of the increasing stability of the projection of the magnetic field as the viewing angle to the velocity vector of the jet increases (It is assumed in this picture that perturbations are propagated as shocks along the jet and that the magnetic field has rotational symmetry about the jet axis). The similarity of x-ray luminosities of both XSBLs and RSBLs supports the contention that the x-ray emission is the most isotropic spectroscopic signature of BL Lac activity (Maraschi *et al.* 1986). The polarization data is an excellent constraint for models of the magnetic field distribution and dynamics of BL Lac jets (e.g. the models of Björnsson).

All of these objects therefore share the following intrinsic properties:

1. BL Lacs have relativistic jets which produce synchrotron radiation detectable at optical and radio wavelengths.
2. The BL Lac nucleus is contained in a host galaxy that can affect the observed polarization properties by diluting the polarization of the nonthermal synchrotron component at longer wavelengths.

We have not shown in this work that the above physical picture is required by the observational data. In fact, as we discussed in Chapter 1, there is currently no evidence for “jets” or relativistic motions among the vast majority

of the XSBLs; the population we suggest is being viewed at a “larger angle to the jet” than BL Lacs with large α_{ro} . We hope to more fully develop this model for BL Lacs in future work. This will include radio observations of the XSBLs in order to study their extended radio properties and more extensive modeling of the aspect dependence of the flux and polarization from a relativistic jet.

6.10 Why aren't BL Lacs more like QSOs?

In Chapter 1 we discussed that the most striking spectroscopic difference between QSOs and BL Lacs is the lack of strong emission lines in the spectra of the latter. Why do BL Lacs not have strong emission lines? Is this difference related to the other observed differences between BL Lacs and HPQs? While it is not the goal of this dissertation to explain the observed differences between AGNs or to try and unify the various classes, it is important to keep in mind several of the proposed explanations for the observed differences. In particular, if we still hope that both BL Lacs and quasars have the same monsters in their cores, we need to identify the cause of their different spectroscopic appearances. Without in-depth analysis or support we now describe three of the possible explanations. One, two, or all three of the following might explain the appearance of some objects classified as BL Lacs.

- It is possible that some of the known BL Lacs have “hidden” broadline regions. For these objects the nonthermal component is so luminous it dominates the observed spectrum. In effect, these BL Lacs would have the same line emitting regions as quasars, but they have not been detected because the lines have very small equivalent widths. It has been clearly demonstrated that for some objects this is possible. For example, two objects classified by Kühr and Schmidt (see Chapter 3) as BL Lacs have subsequently been reclassified as HPQs (Stickel *et al.* 1990a). Both of these objects had a featureless spectrum during the first epoch of spectroscopy, but at later epochs (when the contribution of the nonthermal continuum had decreased) had detectable strong line emission. While this is a possible explanation for some objects, it does not work as well for the majority of XSBLs and some RSBLs. In these objects the 4000 Å break is quite noticeable. As previously discussed, this break is interpreted as the effect of the light from the host galaxy star light present at a comparable luminosity to that of the nonthermal component. It is difficult to impossible to put a broadline region characteristic of most quasars in such an object and not be able to detect the lines. Finally, Stickel has detected line emission from many of the RSBLs in the 1 Jy sample and found that the line luminosities are at the low end of the range exhibited by quasars (Stickel 1990).

- A second explanation is that the host galaxies of BL Lacs are poor in gas. Without hot gas which is cooling by line emission there can be no strong emission lines. If all BL Lacs are in elliptical host galaxies (which compared to

spirals are gas poor) this might be a viable explanation. Possible problems with this picture include describing a mechanism to “feed” the monster (assumed to be an accreting Black Hole) without producing a broadline region. Such a model is the third suggestion which we will describe (below).

- The third possibility we will consider is the suggestion by Guilbert, Fabian, and McCray (1983) that because of their steep x-ray spectra (relative to Seyfert galaxies and quasars), BL Lacs can not develop the clouds of cooling gas that would produce the broad emission lines seen in Seyferts and quasars. The comparatively flat x-ray spectrum produced by Seyfert and quasar nuclei causes Compton heating of the gas accreting onto the central black hole. In their paper they show that the heating produces a thermal instability resulting in a two-phase gas. The “hot” gas has a temperature of $\approx 10^8$ K and compresses the cold phase gas (with a temperature of $\approx 10^4$ K) into clouds which produce the broad emission lines. BL Lacs have steeper x-ray spectrum and can not heat the gas enough to produce a two-phase gas. The gas in BL Lacs stays stable and at temperatures below 10^6 K, without developing colder clouds which are able to continue to cool through line emission. Further more, in their model, if the hardness of the x-ray spectrum of an object (either BL Lac or Seyfert) changes, the appearance of (and resulting classification) of the object can change. Unfortunately the time scales for the cooling (heating) of the gas and the resulting disappearance (creation) of the broadline region is about 100 years. While the inability of a BL Lac to effectively heat its gas might explain the lack of emission lines, there are

differences in the observed radio properties (e.g. range of luminosities) which make unification of Seyfert galaxies and BL Lacs difficult.

6.11 Summary

We have shown that XSBLs and RSBLs have distinct differences in their observed spectral energy distributions and polarization properties. Despite these differences, the objects all meet our definition of being a BL Lac. The observed properties are consistent with these objects all being members of a single class of objects which can have their observed properties dominated by the effects of a relativistically beamed synchrotron component. The wide range of observed properties is possibly the consequence of a distribution of viewing angles (and/or bulk velocities for the jet material) to the relativistic jet.

PART III

THE HUNTING OF THE OPTICALLY SELECTED BL LAC

AN OPTICAL POLARIZATION SURVEY

CHAPTER 7

AN OPTICAL POLARIZATION SURVEY FOR BL LACS

*"They sought it with thimbles, they sought it with care;
They pursued it with forks and hope;
They threatened its life with a railway-share;
They charmed it with smiles and soap."*¹

7.1 Introduction

When our optical polarization survey began in October of 1979, there were no complete samples of BL Lacertae Objects. The known BL Lacs had all been found as the result of the partial followup of radio surveys or as interlopers in optical surveys for variable stars or quasars. Basic fundamental questions about BL Lacs were unanswerable. What is the surface density of BL Lacs? Is it possible to determine whether or not they comprise an evolving population? What range of properties do they possess? How many are there? How are these objects related to other AGN? Are there any BL Lac analogues to the "radio

¹ From Lewis Carroll's *The Hunting of the Snark*.

quiet" quasar? In order to address these and other questions, it was evident that two general tasks should be performed. First, complete samples of BL Lacs needed to be compiled. Second, surveys for BL Lacs at other wavelengths should be undertaken to probe the range of characteristics exhibited by the class.

In 1978, a year before Dr. Richard Green exposed the first plate in our optical polarization survey, the *HEAO-2* satellite (also known as the *Einstein Observatory*) was launched. Although it did not perform an all sky survey, *Einstein* was successfully used to perform an extensive survey for previously unknown x-ray sources (*HEAO-1* did make an all sky survey and the ROSAT satellite launched in 1990 will perform the most extensive deep survey to date). While previous x-ray satellites had quickly established that BL Lacs were x-ray sources (e.g. Schwartz *et al.* 1978; Piccinotti *et al.* 1982), it took the Einstein Medium Sensitivity Survey to provide us with our first complete sample of BL Lacs (see Chapter 3). This BL Lac subsample consisted of only four objects. It has taken until 1990 for the Extended Medium Sensitivity Survey (EMSS) to provide a sizable (twenty-two BL Lacs) complete sample of x-ray selected BL Lacs (XSBLs).

In 1981 Dr. Howard French exposed the last Schmidt plate to be used in our optical polarization survey and the 1 Jy Catalogue of radio sources was published (Kühr *et al.* 1981). Over the past decade, there has been an extensive effort to identify the optical counterparts of the radio sources (Kühr and Schmidt

1990; Stickel *et al.* 1990a; see Chapter 3). A complete sample of radio selected BL Lac objects (RSBLs) is one of the products of this completely identified radio survey (see Chapter 3; Stickel *et al.* 1989a, 1989b, 1990b).

In this chapter we present the results of our own efforts to compile a complete sample of BL Lac objects. One of the major differences between our survey and the two mentioned above is that it is a survey at optical wavelengths. This difference is important. All known BL Lac objects are relatively strong radio sources. The vast majority of the objects known were discovered as the result of radio surveys. However, even the XSBLs have an α_{ro} greater than those of “radio quiet” quasars (Stoeckel *et al.* 1990) (see Chapters 5 and 6 for definition of α_{ro} and discussion). We have learned that the BL Lacs found in the x-ray surveys have significant differences in their polarization and other observable properties from RSBLs (see Chapters 5 and 6). We have also discussed the possibility that the difference in the two subclasses of objects are the result of the viewing angle to the beamed component of the optical emission (see Chapter 6). Both radio and x-ray surveys found BL Lacs, but the differences in the observed properties of the two samples have provided new insights into the properties of all BL Lacs.

Is there another population of objects that, while still meeting our definition of being a BL Lac, has significantly different properties from objects found in the existing surveys? Is there a BL Lac analogue to the radio quiet

quasar? Is there a radio/x-ray quiet BL Lac? We now know that for the existing samples of BL Lacs, the presence of strong radio emission is correlated with the presence of a significantly polarized optical continuum. Nevertheless, an optical survey allows a direct test for radio quiet BL Lacs and further explores the range of properties exhibited by the entire class. An optical survey also provides additional constraints on a variety of physical models explaining the observed properties of the class (e.g. Ghisellini and Maraschi 1989; Padovani and Urry 1990).

Optical color surveys for quasars have found very few BL Lacs (e.g. Green *et al.* 1986). Does this indicate a lack of objects or the difficulty of optically selecting BL Lac objects? It is the combination of the lack of emission lines and steep/red optical spectral energy distributions that conspire to make both wide-field spectroscopic and color surveys inappropriate or difficult as methods of finding optically selected BL Lacs. It is possible that high redshift BL Lacs might be found by optical surveys (for example grism surveys) which can detect objects with large breaks (discontinuities) in their spectrum. A high redshift BL Lac might have such a break caused by the Lyman limit of intervening clouds or systems. So far no BL Lacs have been found in this way. Similarly, multi-color surveys that are capable of finding objects which are red and have a power-law spectrum should be able to find BL Lac objects (e.g. Warren 1990).

The intrinsically strong optical linear polarization and variability of RSBLs suggest an alternative method of surveying for these objects; look for polarized and/or variable objects. Such surveys make use of some of the defining characteristics of all BL Lacs and also allow for the inclusion of other objects with polarized or variable continuum emission (e.g. highly polarized quasars, HPQs). To date, variability surveys have not provided a significant sample of objects (e.g. Usher 1978). Optical polarization surveys have been attempted by two groups of researchers with no success at finding any polarized objects (Impey and Brand 1983; Borra and Corriveau 1984).

We have undertaken the most extensive optical polarization survey to date. It was designed to obtain an optically selected sample of highly polarized objects. The initial phase of the survey required obtaining polarization measurements of the vast majority of objects over a large area of the sky. This was accomplished by obtaining pairs of 48" Schmidt telescope plates exposed through polaroid filters (§7.2). Plates were obtained covering approximately 680 square degrees of the sky. In the second phase, followup observations were made of the detected candidates to cull the objects that were modulated by measurement error and not by the changing relationship between the polarization analyzer's transmission axis and the position angle of the incident radiation.

There were two original goals when the survey was undertaken. The first was to test for a population of radio quiet BL Lacs with high optical

polarizations (i.e. $P > 20\%$). The second was to obtain a sample of optically selected BL Lacs and/or set meaningful limits on their surface density. In §7.2 we describe how the photographic polarization survey was made. In §7.3 we discuss the selection of candidate objects and the results of our spectroscopic and polarimetric followup observations. In §7.4 we discuss the implications of our survey.

7.2 The Palomar 48" Schmidt Telescope Polarization Survey

There have been two other attempts to use the optical polarization of BL Lacs as a means of finding them in an optical survey. The results of an optical polarization survey of ten square degrees down to a B magnitude of 19 were published in 1982 by Impey and Brand. Borra and Corriveau made a polarization survey of only 1.84 square degrees, but it was complete to a B magnitude of 20. The techniques, errors, and results of these two surveys are described in their respective papers. Neither survey found a polarized object.

Our survey, begun contemporaneously with the two above, covers a much larger area of the sky (560 square degrees included in the final survey) to comparable magnitude and improved polarization limits. The details of how the photographic survey was undertaken are described in following the subsections.

7.2.a.) *The Schmidt Plates*

The Palomar 48" Schmidt Telescope was used to observe nineteen high galactic latitude fields. The plate material was Kodak IIIaJ baked in forming gas. The plate scale is the same as for the POSS, 67" per millimeter. Each plate provides approximately 33 square degrees of useful sky coverage. No filters were used other than the polarization analyzers.

We list in Table 7.1 the observed fields and information related to the observations. Two plates were taken of each field. Each plate was exposed three times. Each exposure generally lasted 30 minutes and was taken with a different sheet of Polaroid's commercially available HN 42 linear polarizer in front of the plate. The sheets of polaroid were each placed so that their transmission axis was at a different position angle (0° , 60° , and 120° respectively). Between each of the three exposures, the telescope was moved 10" to 25". Two different patterns for the images were tried and are described in the explanatory notes for Table 7.1. The second plate of each field was normally exposed immediately after the first. The order of the polaroid filters was generally reversed for the second plate; 120° , 60° , 0° (reason explained in §7.3). If there was a problem with one of the plates (trailed etc.), a replacement was obtained within two days.

By placing all three images on one plate, we improved the accuracy of the polarization measurement by making it independent of all types of plate to plate variations. By comparing objects on a quadrant by quadrant basis, we were

relatively unaffected by any large scale variations on an individual plate. The noise in the measurement of each individual image is, of course, increased since the background is three times the background of a singly exposed plate. By having two plates for each field, we were able cut down on the number of objects we would need to followup by requiring that candidate objects be detected as modulated in the same sense on both plates. By choosing to observe with only three position angles of the polarization analyzers, we sacrificed being able to uniquely determine the Stokes Q and U parameters for a decrease in the necessary integration time to detect modulated objects. The method of recovering the polarization of the object from our three measurements is described in §7.2.d.

Despite the general uniformity and high quality of the final plates, individual fields suffered from various problems (scratches, satellite trails, fogged emulsion, etc.). We have carefully accounted for these effects while determining the usable area of the survey. Two fields are not included in the final survey (noted in Table 7.1) because the separation of the three images was not sufficient to provide accurate measurement over the entire field when the plates were later scanned with the Monet Machine at Kitt Peak (§7.2.b).

Explanation of Table 7.1: Optical Polarization Survey Fields

Column (1): Contains the individual plate identification numbers.

Columns (2) and (3): The right ascension and declination in Epoch 1950 for the center of the observed field.

Columns (4) and (5): The galactic coordinates of the field center.

Column (6): The UT Date of the observation.

Column (7): The length of time in minutes that the plate was exposed at each position angle. The total exposure time for the plate is therefore three times the number in this column.

Column (8): The order in which the exposures at each position angle were made for the particular plate. The numbers 0, 60, and 120 indicate the position angle (measured North to East) of the transmission axis of the HN 42 linear polarizer.

Column (9): The hour angle of the first exposure on each plate.

Column (10): Comments. Two fields are not included in the final analysis because two of the three images were too close together for accurate measurement of image moments. The symbols L and C indicate which pattern of spacing was used in shifting the plate center between exposures. L indicates that all three images were aligned east west with 13" and 25" spacing between the images. C indicates that the images roughly formed a right triangle with the second exposure offset 12" east or west. The third image of each object was offset 12" east (or west) and 12" north (or south) from the first.

† The third exposure of plate PS 28280 was stopped because of approaching clouds after twenty-five minutes and thirty-nine seconds.

Table 7.1: Optical Polarization Survey Fields

Plate ID	RA	DEC	Gal	Coord	UT Date	Exposure	Polaroid	Hour	Comment
(1)	Epoch	1950	l^I	b^I	(6)	Time (min)	Order	Angle	(10)
(1)	(2)	(3)	(4)	(5)	(6)	(7)	(8)	(9)	(10)
PS27575	00:01:25	+06:13:36	102.4	-54.5	80.10.09	30	0,60,120	1E01	C
PS27576					80.10.09	30	120,60,0	0W49	C
PS27565	01:13:17	+06:46:29	133.6	-55.3	80.10.07	30	0,60,120	0E22	C
PS27566					80.10.07	30	120,60,0	1W25	C
PS27570	01:39:03	+06:17:21	144.6	-54.2	80.10.08	30	0,60,120	0E56	C
PS27571					80.10.08	30	120,60,0	0W52	C
PS26580	01:42:08	+12:39:42	161.1	-41.6	79.10.23	30	120,60,0	2W12	C
PS26584					79.10.25	30	120,60,0	0E05	C
PS27577	02:26:03	+06:08:28	161.6	-49.1	80.10.09	30	0,60,120	0W14	C
PS27578					80.10.09	30	120,60,0	2W03	C
PS27567	02:49:53	+06:25:62	168.3	-45.3	80.10.07	30	0,60,120	1W41	C
PS27572					80.10.08	30	0,60,120	1W28	C

Table 7.1 (continued): Optical Polarization Survey Fields

Plate ID	RA	DEC	Gal	Coord	UT Date	Exposure	Polaroid	Hour	Comment
(1)	Epoch (2)	1950 (3)	l^{II} (4)	b^{II} (5)	(6)	Time (min) (7)	Order (8)	Angle (9)	(10)
PS26581	03:19:45	+06:21:40	175.9	-40.3	79.10.23	30	0,60,120	2W51	C
PS26585					79.10.25	30	0,60,120	0W08	C
PS27031	10:53:31	+29:44:10	200.8	64.8	80.06.13	30	0,60,120	0W01	C
PS27032					80.06.13	30	120,60,0	2W13	C
PS28263	11:11:39	+35:56:20	184.4	67.7	81.03.14	30	120,60,0	0E32	L
PS28277					81.03.14	30	120,60,0	0W32	L
PS27035	11:17:38	+29:21:49	202.0	69.8	80.03.14	30	0,60,120	0E04	C
PS27036					80.03.14	30	120,60,0	1W55	C
PS28264	13:01:24	+30:27:50	82.2	85.9	81.03.10	30	0,60,120	0E30	L
PS28265					81.03.10	30	120,60,0	1W22	L
PS28278	13:53:35	+30:00:18	47.3	75.6	81.03.11	30	0,60,120	0E17	Trailed, L
PS28279					81.03.11	30	120,60,0	1W32	L
PS28280					81.03.12	†30	0,60,120	1E03	L

Table 7.1 (continued): Optical Polarization Survey Fields

Plate ID	RA	DEC	Gal	Coord	UT Date	Exposure	Polaroid	Hour	Comment
(1)	Epoch	1950	l^I	b^I	(6)	Time (min)	Order	Angle	(10)
(1)	(2)	(3)	(4)	(5)	(6)	(7)	(8)	(9)	(10)
PS27033	14:44:05	+30:22:40	46.7	64.7	80.06.13	30	0,60,120	0W21	C
PS27034					80.06.13	30	120,60,0	2W09	C
PS27037	15:10:04	+29:18:13	45.0	59.0	80.06.14	30	0,60,120	0W04	C
PS27038					80.06.14	30	120,60,0	1W59	C
PS28484	15:37:08	+30:09:47	47.6	53.3	81.05.30	30	0,60,120	1E15	L
PS28485					81.05.30	30	120,60,0	1W11	L
PS27563	22:49:48	+06:10:05	77.9	-45.8	80.10.07	30	0,60,120	1E38	Not in, C
PS27564					80.10.07	30	120,60,0	0W12	Complete, C
PS27574					80.10.09	30	120,60,0	1E35	Survey, C
PS26579	22:56:15	+07:30:19	80.9	-45.7	79.10.23	30	0,60,120	2W55	Not in, C
PS26583					79.10.25	30	0,60,120	0W37	Complete, C
PS27568	23:14:26	+06:04:25	85.1	-49.5	80.10.08	30	0,60,120	2E07	C
PS27669					80.10.08	30	120,60,0	0E18	C
PS27436	23:37:55	+12:05:75	97.1	-46.9	80.08.19	25	30,150,90	0E32	C
PS27437					80.08.19	25	90,150,30	1W12	C

7.2.b.) *Scanning of Plates*

The images on all plates were measured with the Monet PDS/IIS Measuring Engine of Kitt Peak National Observatory. Each plate was scanned in overlapping quadrants. The Monet Machine, developed by David Monet (1984), uses a CCD camera mounted on the PDS measuring engine. The polarization survey plates were scanned from 1985 to 1989 and made use of several different incarnations of the Monet Machine. Most of the changes involved which computer controlled the processing of the images (a change from sharing a VAX with an IIS to a dedicated MicroVAX). The only major change involved a switch of CCD cameras in 1989 (hence forth known as OldCam and NewCam respectively). OldCam had rectangular pixels that projected onto 12.6 micron by 10.39 micron areas of the plate. This corresponds to pixels 0.84" by 0.689" in size. OldCam was used to scan all of the plates in the final survey. NewCam has square pixels which are 1.01" on a side (15.8 microns on a side). NewCam was used to complete the scanning of POSS plates used for comparison to our polarization plates. As part of our efforts to quantify our completeness, we tested the effects of multiplying the universe by three (triple images) by comparing as a function of magnitude how many objects were lost due to overlapping images on the plates (§7.3., §7.4). The switch in cameras does not affect this procedure.

It took four scanning sessions to scan each plate. The 33.07 square degree plates were each scanned in four 9.35 square degree segments or quadrants (NE, NW, SW, SE). When each quadrant was scanned, we made sure to scan a

large enough region to overlap the scanning of the other three quadrants. During the scanning of an individual quadrant, the CCD camera would successively image partially overlapping regions each approximately 26 square arcminutes in size. Successively imaged fields overlap by approximately ten percent. Multiple frames at each position are coadded. The IIS then digitizes the image to an 8-bit precision (the new system does not use the IIS, but has its own frame grabber). After each frame was obtained, the digitized frame was processed on the fly, objects were identified, image moments and locations were determined, and the results were stored for later analysis. For each scanning run (scanning a quadrant), an individual flat field was obtained. With OldCam the flat field was obtained by making an out of focus image of the plate. With NewCam the flat field was obtained by making an exposure through neutral density filters chosen to match the background density of the plate. The rotation matrix that relates the CCD coordinates to the PDS machine coordinates is also determined prior to scanning each quadrant by the procedure described in the "User's Manual" available at Kitt Peak National Observatory. Real time processing of each frame proceeds as follows.

Approximate positions and image sizes of "objects" are defined.

The positions and centers are then refined.

The following parameters are then computed and stored:

x and y position in microns

M, the instrumental magnitude of the image. This magnitude is calculated by giving full weight to the inner three rings of pixels and then weighting subsequent rings as one over the ring number.

R, a measure of the image roundness or elongation as defined by Jarvis and Tyson (1981).

The maximum difference of image pixels is also a stored parameter for each image.

After the images are identified and measured, the digitized frame is discarded. Finally, duplicate observations of objects (remember that each frame field overlaps with adjacent fields) are removed from the output list of objects.

When care is taken to provide enough illumination through the plate and consistent set up procedures are followed, the Monet Machine provides extremely repeatable measurements. We tested this directly by comparison of overlap regions and by repeated scanning of the same quadrant. Furthermore, the same candidate objects were found in the overlap regions of the four quadrants. The uniform RMS for the entire plate (§7.2.d), independent of the scan, is an additional demonstration of the stability of the Monet Machine system.

7.2.c.) *Photometric Calibration of Survey*

It is important to determine the transformation from measured instrumental magnitudes to a well defined and commonly used system. Although our

exposures were taken without any color filter, the response of the IIIaJ plates and the HN 42 polaroid filters is close to being a blue or B band measurement. Determining the B magnitudes is necessary in order to define the bright (saturation) and faint (loss of objects at threshold) end detection limits. It is also necessary in order to transform the measured differential magnitudes (for a given object) into a true polarization measurement (§7.2.d).

We have calibrated the plates using a model of the cumulative star counts as a function of B magnitude and our corrected observed image counts. The success of this calibration is verified by direct comparison to the stars in the Guide Star Photometric Catalog (GSPC; Lasker, Sturch, *et al.* 1988) and faint sequences determined by Borra *et al.* (1985).

The procedure used to calibrate the magnitudes is as follows. A transformation is determined for each scanning session. The transformation was determined by a direct mapping of the observed (corrected) cumulative image counts as a function of Monet Machine magnitude (the measured magnitude) against the predicted star counts as a function of B as determined from the Bahcall and Soneira model of our Galaxy (Bahcall and Soneira 1980). Equation B1 of their Appendix B was used to generate the counts as a function of limiting B magnitude and galactic latitude (b^{II}) and longitude (l^{II}). This model applies for B magnitudes between 12 and 20. The stability of the scanning and uni-

formity of the plates resulted in virtually indistinguishable transformations being determined for all quadrants of a given plate.

Three corrections were made to the observed image counts before the magnitude transformation could be determined:

1. Non-stellar images were removed by culling objects above the stellar loci in the roundness vs. magnitude diagram (Figure 7.1). This correction was not applied at the bright end because the diffraction spikes of the brighter images cause them to be quite elongated. For the brightest objects ($B < 11$), the images merge together and are either rejected by the processing software as not being an object (because the entire CCD frame is filled with the merged stellar images) or recorded as a single image. Since we need to keep count of these bright objects, we do not remove them by applying a roundness cutoff brighter than instrumental magnitude 10.8. An examination of Figure 7.1 will make clear the procedure. Figures 7.1a and 7.1b are plots of the roundness vs. instrumental magnitude of the images detected on two of our plates (images from only one quadrant are plotted). For these plates, representative of the plates retained in the final survey, there is a well defined locus of stellar images. The effect of having triple images is demonstrated by comparison to Figure 7.1c, a plot made after scanning Palomar Observatory Sky Survey plate O-531. While an increase in extended objects is noticeable at instrumental magnitude 12, there is no flaring in the plot at bright magnitudes. The lack of very extended objects at faint instrumental

magnitudes is a result of the faint large scale extended emission from galaxies falling below the plate threshold. Figure 7.1d shows what happened when the size of the shift in plate center between exposures was not adequate to allow accurate measurement. The ridge of elongated objects comes from the merging of two of the three images for a large number of the objects in the quadrant. This field was not included in the final survey. While elongated objects were excluded at faint magnitudes, the effect of this correction was small. The change in the transformation caused no more than 0.2 of a magnitude shift at the faintest end of our survey ($B \approx 19.5$). Galaxies do not begin to contribute significantly to the cumulative counts until $B > 18$.

2. An empirical correction was applied at the bright end by inspection of the plates and comparison to the results of the Monet Machine scanning of the corresponding POSS O plate. Consider the merging of saturated images of bright stars. The brighter objects are counted as single or double images instead of the three images obtained for the majority of the objects. When the image counts were divided by three to convert to star counts, the bright end was divided by a slightly smaller number, determined on a plate by plate basis.

3. Some plates had plate defects that artificially raised the number of images at bright instrumental magnitudes. A correction was applied in a manner similar to the correction applied for merged images.

Figure 7.1— The roundness of each image is plotted against the measured magnitude (instrumental). Each plot is for a single quadrant of a polarization or POSS plate. Figures 7.1a and 7.1b are plots of the data from the northeast quadrant of the polarization survey plates PS28280 and PS28284. The flaring in the stellar loci at the bright end is due to the merging of the multiple images of the bright stars. No similar effect is present in the data for scanned POSS plates on which each object has only one image. Figure 7.1c is a plot of the data from the northeast quadrant of POSS O-531. The data presented in Figure 7.1d demonstrates the effect of inadequate spacing between images on the polarization plates. For this plate the second and third images have merged together and the result is inaccurate measurement of the objects' magnitudes and modulations.

The results of the magnitude transformation are evident in Figures 7.2 and 7.3 where we have plotted the transformations for several representative plate quadrants. Also plotted are the position of photometric standards taken from Guide Star Photometric Catalog (Lasker, Sturch, *et al.* 1988) and Borra *et al.* (1985). The agreement at the faint end is excellent. At the bright end, the small number of expected stars per square degree causes greater inaccuracy in the mapping of the observed to predicted counts. In addition, saturation and image crowding make the measurement of the bright images difficult. The observed steepening of the transformation at the bright end is a consequence of information being gained from unsaturated diffraction spikes. Since we can not make polarimetry measurements of the saturated and merged images, we are not greatly affected by the inaccuracies at the bright end. We impose a bright end cutoff for each plate. This is easily determined from the flattening of the transformation caused by saturation. The plates respond linearly and are

PS28280ne

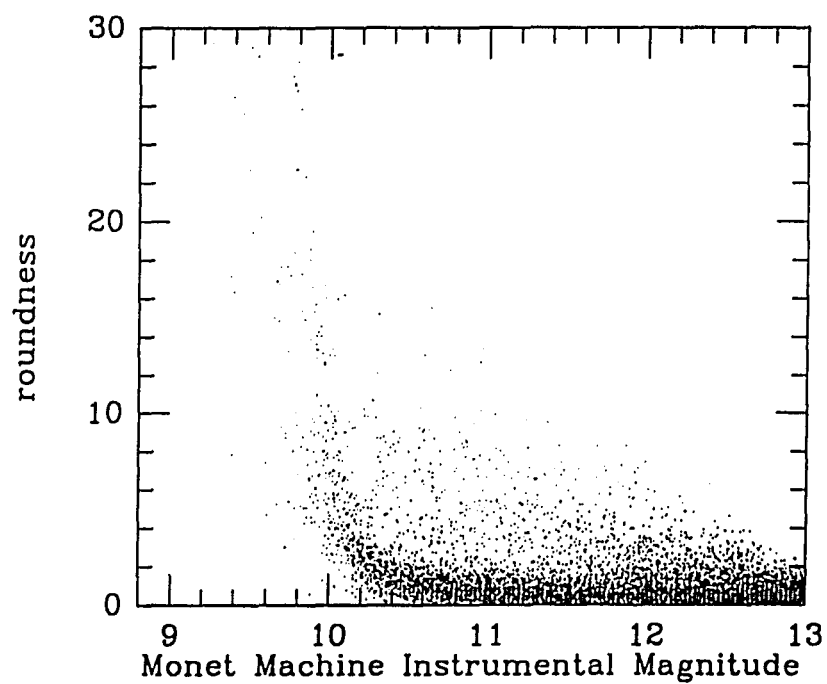


Figure 7.1a

PS28484ne

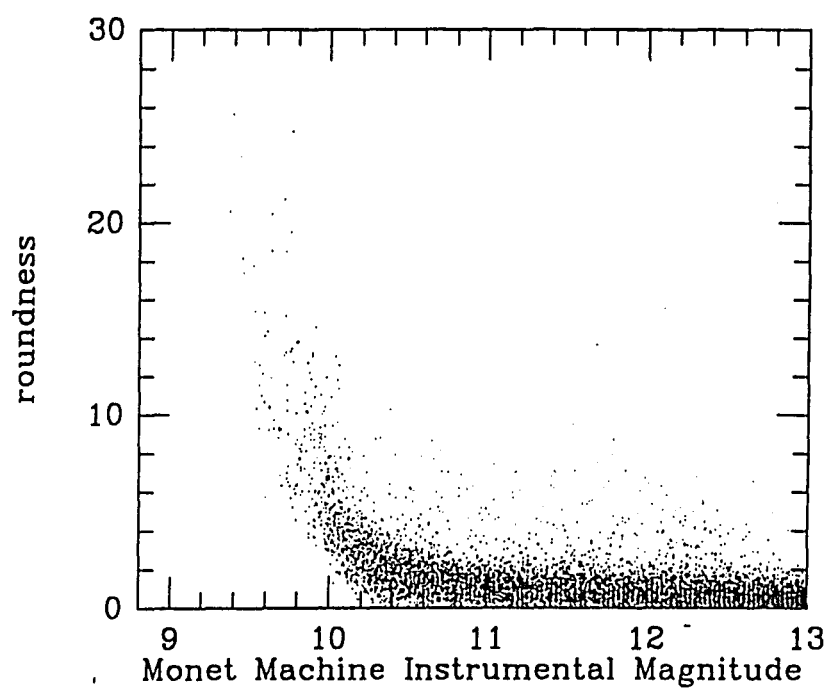


Figure 7.1b

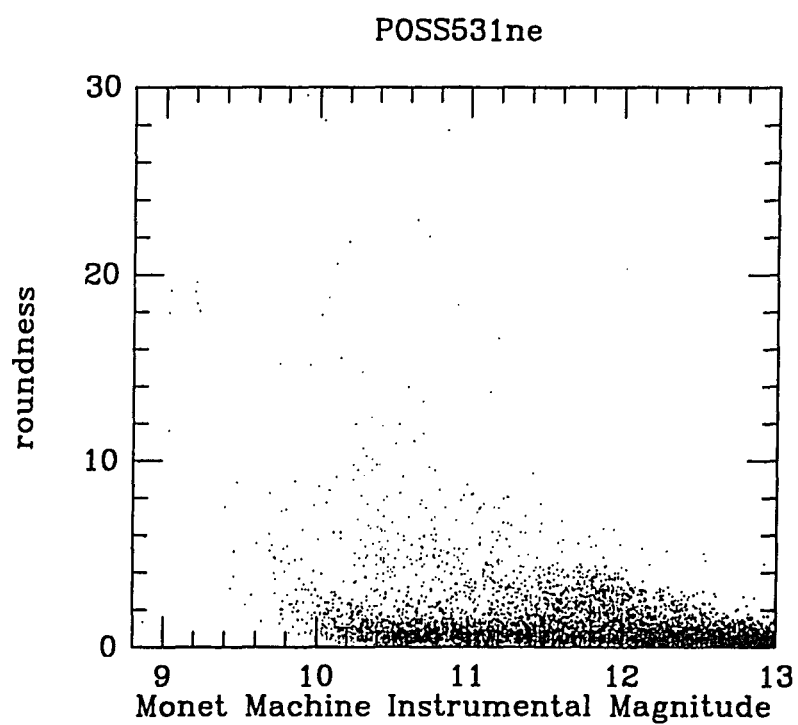


Figure 7.1c

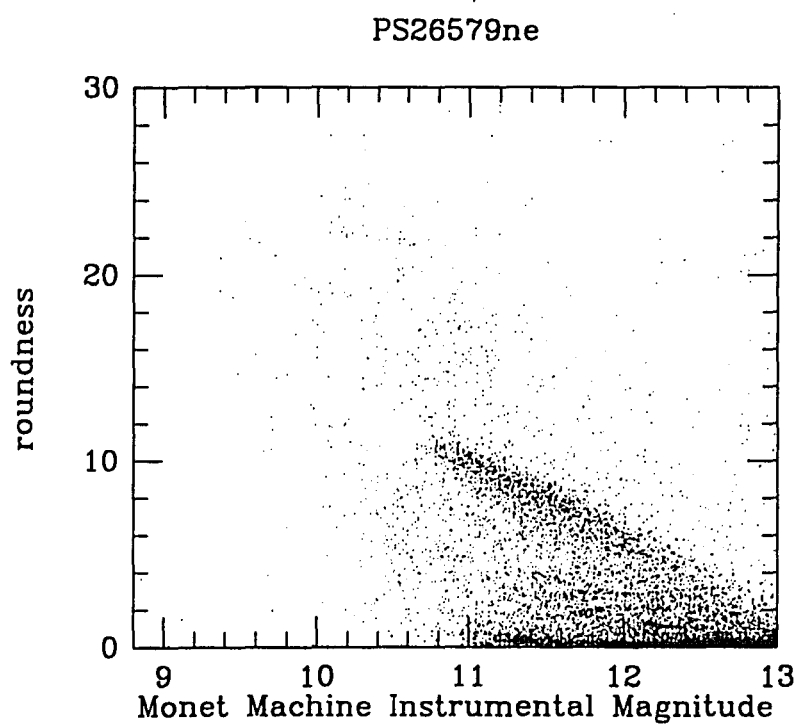


Figure 7.1d

generally complete past $B > 20$. However we impose $B = 20$ as our magnitude limit, because we are unable to make followup observations of fainter objects. For some plates we had to set brighter lower limits, ranging from $B = 18.5$ to 19.5 (for example some plates that did not respond as well to the baking to increase their sensitivity or were taken under poorer seeing conditions). The transformation of the errors is discussed in §7.2.d.3.

In general when the magnitude transformation derived from observed star counts is applied to the observed photometric standard stars, the agreement between the derived and published B magnitudes is excellent. It is important to remember that we measure every object three times and that since we correct our counts by converting the number of images to a number of objects, we are averaging over our three measurements.

Figure 7.2—The magnitude transformation from Monet Machine instrumental magnitude to B magnitude was determined by using the observed starcounts as a function of instrumental magnitude compared to the predicted starcounts as a function of B magnitude (Bahcall and Soneira 1980). The solid line is the direct mapping of instrumental to B magnitude determined as described in §7.2.c. The solid squares are the positions of measured photometric standards. The numbered stars are faint photometric standards observed by Borra *et al.* 1985. The plotted stars are from the second and third north galactic pole fields. The printed numbers indicate the field and star number (e.g. 3,2 would mean NGP3 field, star 2). The lettered stars are from field P322 of Lasker, Sturch, *et al.* 1988. The plotted transformation is for the southeast quadrant of polarization survey plate PS28264.

Figure 7.3—The magnitude transformations are plotted for four representative polarization survey plate quadrants. The transformations were determined as described in §7.2.c and are represented by the solid line. The solid squares are the positions of measured photometric standards. The lettered stars are from the Guide Star Photometric Catalog (GSPC) (Lasker, Sturch, *et al.* 1988). The stars plotted for PS27033ne (7.3a, top), PS27037ne (7.3a, bottom), and PS28263se (7.3b, top) are from GSPC fields P326, P327, and P264 respectively. The numbered stars plotted in 7.3b (bottom) are faint photometric standards observed by Borra *et al.* 1985. These stars are from the first north galactic pole field (NGP1). The printed numbers indicate the star number.

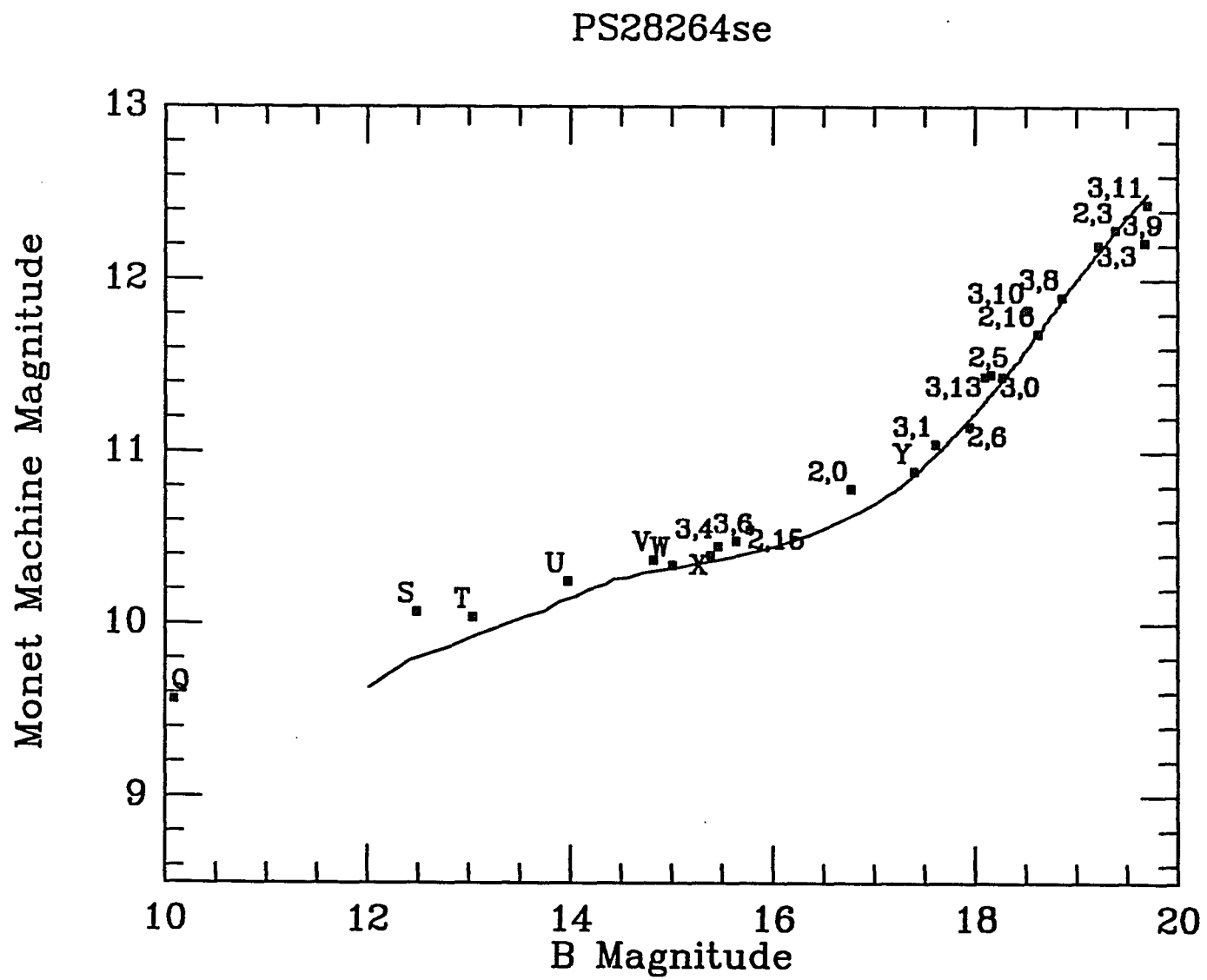
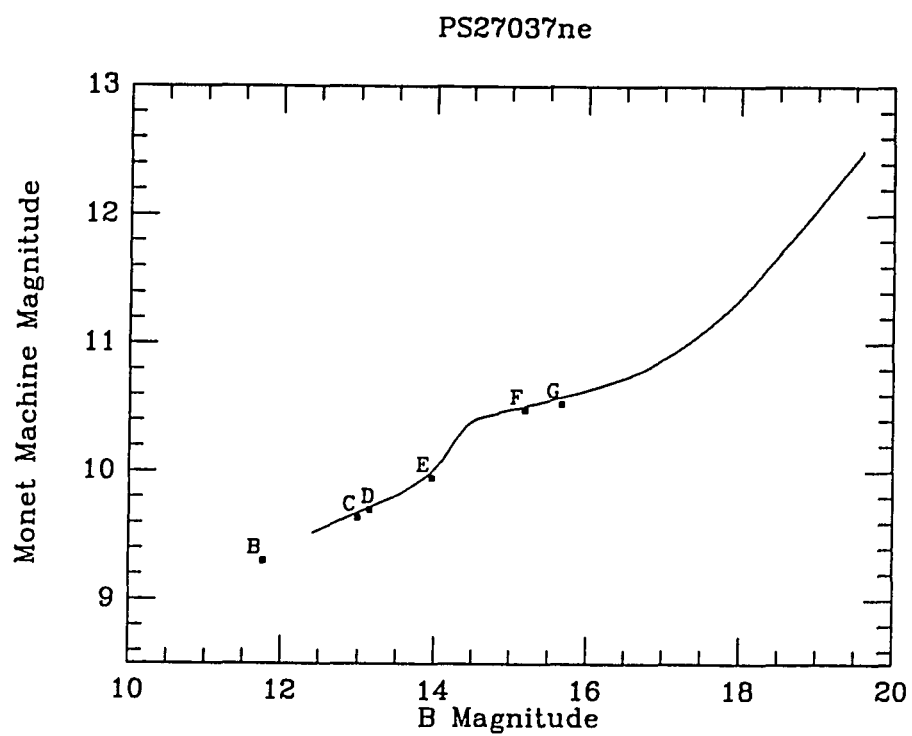
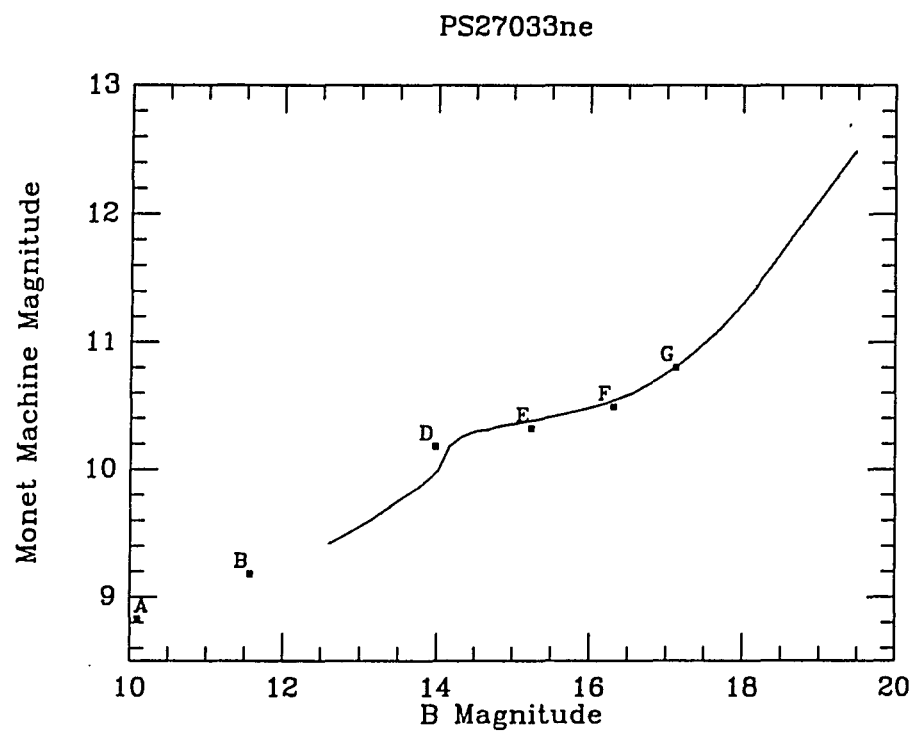
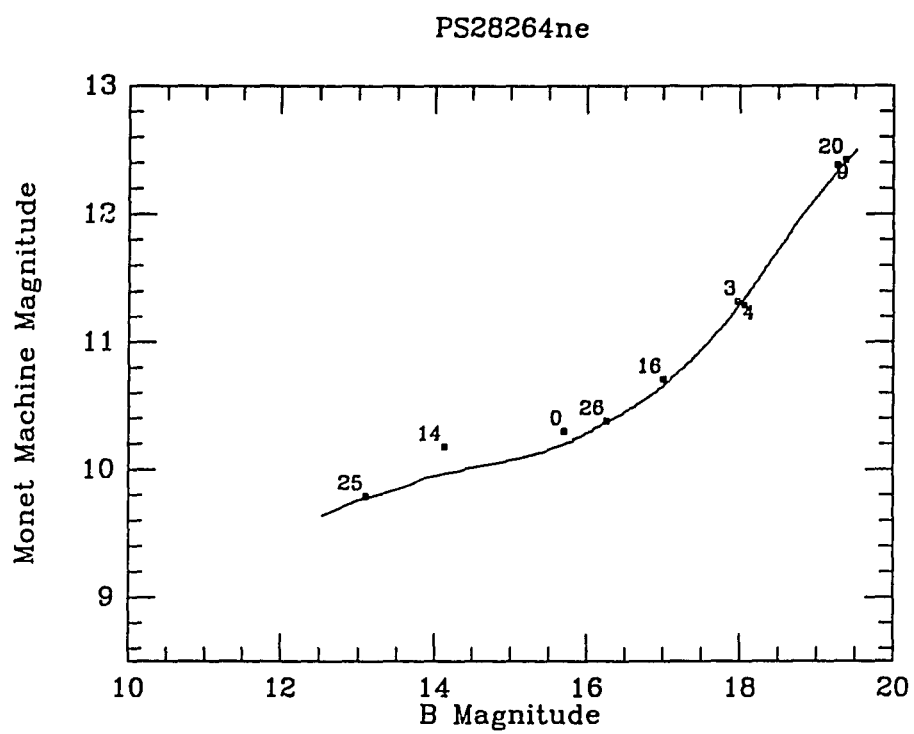
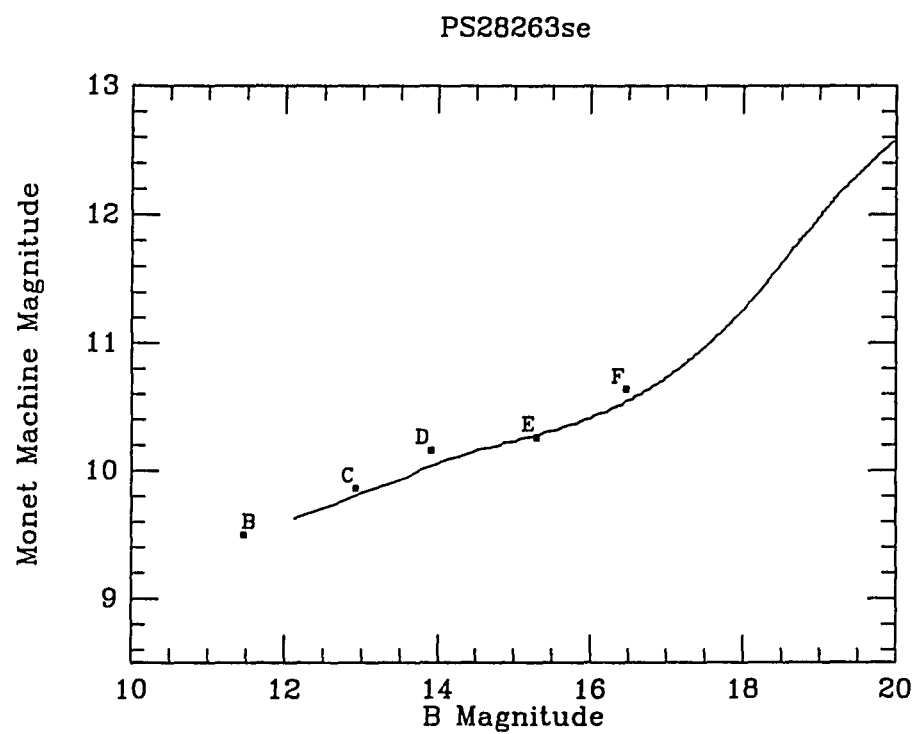


Figure 7.2

**Figure 7.3a**

**Figure 7.3b**

7.2.d.) *Measuring the Photographically Determined Polarization*

After scanning the plates with the Monet Machine, a list of images and associated image parameters must be transformed into a list of objects and their measured modulation. The images are matched together for each object and the differences computed. This difference is directly related to the linear polarization of the object, but is also affected by a variety of sources of error. After the modulation is calculated for each object, the objects are grouped by instrumental magnitude and statistics on the magnitude differences are computed. The distribution of magnitude differences is gaussian over the range of magnitudes included in the survey. At the bright end, as saturation and other effects increase in importance, the errors are not gaussian and these objects are not included in the survey. The selection of these candidate objects and our followup observations are described in §7.3. In this section we examine the relationship between the incident polarized radiation and the observed modulation and the sources of error in this measurement. At the end of this section, we discuss how the RMS in the magnitude differences is related to the error in the measured modulation of intrinsically polarized objects.

d.1.) *Matching Up the Images:* For each scan, the numerous images must be grouped together as objects. From a set of known object triples (provided

after inspection of the scan data), an initial second order mapping of the 2nd and 3rd images onto the coordinates of the 1st image is computed. A maximum coordinate difference is also supplied. For each image, all possible combinations of being matched to neighboring images (those images within 600 microns, maximum separation of images from the same object is 400 microns) are examined and the deviation from the predicted mapping computed. After this set of triple images has been identified, a new transformation is determined, constrained by the new larger set of triples. This process is performed interactively until the number of new triples with increasing allowed error in the mapping is small. Although the image spacing changes with radial distance from the plate center, the scanned files were split into smaller segments and transformations applied for the subgroups. In this manner the vast majority of objects that were not in extremely crowded fields had all three images properly identified. The actual number of unmatched images varied from field to field, but in general more than 80% of the images became matched as part of a triple.

d.2.) *The Observed Modulation for a Given Incident Polarization:*

We used Polaroid's commercially available HN 42 sheet polaroid as our linear polarization analyzer. Three separate filters (made from the same batch of polaroid) were mounted in frames (so that they could easily and repeatably be placed in the optical path) with their transmission axes at position angles of 0° , 60° , and 120° (measured North to East). Three exposures provide three

images, each through a different orientation of the polaroid, of every object. Neglecting the effects of seeing, changing opacity, and other conditions that vary for the entire plate, the differences in the measured brightness of the three images will be the result of measuring error and the modulation of any linearly polarized component of the radiation from an individual object.

Following the discussion of Serkowski (1974), we can describe the effects of the sheet of polaroid on the incident radiation. The electromagnetic radiation from a given object can be described with the Stokes parameters, I , Q , U , and V . These vector quantities fully describe the polarization state of the incident radiation. They are directly related to the percent linear polarization, p , the linear polarization position angle (angle of the electric field vector), θ , and the percent circular polarization, q .

$$I = \text{total intensity}$$

$$Q = I p \cos 2\theta$$

$$U = I p \sin 2\theta$$

$$V = I q$$

where I , Q , U , and V are the Stokes vectors of the incident radiation.

For convenience we will label the magnitudes of the three images m_0 , m_{60} and m_{120} . These three images were formed with the analyzer at position angles $\varphi = 0^\circ, 60^\circ, 120^\circ$. For a perfect polarization analyzer $k_1=1.0$ and $k_2=0$, where k_1 is the transmission along the transmission axis and k_2 is the transmission

perpendicular to k_1 (i.e. the amount of leakage of light with the orthogonal and unwanted sense of polarization). The light recorded on the plate is related to the incident radiation as follows:

$$\begin{pmatrix} I' \\ Q' \\ U' \\ V' \end{pmatrix} = 1/2 \begin{pmatrix} 1 & \cos 2\varphi & \sin 2\varphi & 0 \\ \cos 2\varphi & \cos^2 2\varphi & \frac{1}{2} \sin 4\varphi & 0 \\ \sin 2\varphi & \frac{1}{2} \sin 4\varphi & \sin^2 2\varphi & 0 \\ 0 & 0 & 0 & 0 \end{pmatrix} \begin{pmatrix} I \\ Q \\ U \\ V \end{pmatrix}$$

$$I'_\varphi = (1/2)(I + Ip \cos 2\theta \cos 2\varphi + Ip \sin 2\theta \sin 2\varphi)$$

The intensity incident on the plate for each φ is the following.

$$I'_0 = (\frac{1}{2})I(1 + p \cos 2\theta)$$

$$I'_{60} = (\frac{1}{2})I(1 + (\frac{-1}{2})p \cos 2\theta + (\frac{\sqrt{3}}{2})p \sin 2\theta)$$

$$I'_{120} = (\frac{1}{2})I(1 + (\frac{-1}{2})p \cos 2\theta + (-\frac{\sqrt{3}}{2})p \sin 2\theta)$$

The observed difference in magnitudes between the images is then related to the transmitted intensities as follows.

$$m_{60} - m_0 = -2.5 \log(I'_{60}/I'_0)$$

$$m_{120} - m_0 = -2.5 \log(I'_{120}/I'_0)$$

$$m_{120} - m_{60} = -2.5 \log(I'_{120}/I'_{60})$$

The difference in magnitudes between a pair of images is related to the polarization of the incident intensity as follows (we only present the results for one of the possible three difference, which are derived analogously).

$$m_{60} - m_0 = -2.5 \log \left(\frac{(1 + p \cos 2\theta(-1/2) + p \sin 2\theta(\sqrt{3}/2))}{(1 + p \cos 2\theta)} \right)$$

Let $A = 10^{\left(\frac{m_{60}-m_0}{-2.5}\right)}$ then

$$p = (1 - A)/(A \cos 2\theta + (1/2) \cos 2\theta - (\sqrt{3}/2) \sin 2\theta)$$

In Figure 7.4 we plot the observed differences in magnitudes as a function of θ for a given percent polarization. The three curves correspond to the three magnitude differences it is possible to compute, $m_{60}-m_0$, $m_{120}-m_0$, and $m_{120}-m_{60}$. In order to find highly polarized objects, we are interested in determining the

maximum modulation for each object. In computing the maximum observed modulation for each object, we made an error in our original analysis procedure and only compared the differences $m_{60}-m_0$ and $m_{120}-m_0$ for all objects. For objects with polarization position angles in two ranges (30° to 60° and 120° to 150°) we did not "measure" as large a modulation as we should have been able to detect. In practice this becomes a small source of additional incompleteness which can be explicitly accounted for in our analysis. In Figures 7.4c and 7.4d we present plots of the calculated maximum measurable modulation as a function of θ for a given percent polarization. The line with solid circles indicates what we would measure from our use of two of the possible differences. The line with empty circles indicates the range of position angles that would be improved if all three magnitude differences had been used. In Figure 7.5 we plot the mean maximum modulation (maximum detected modulation as function of polarization averaged over θ) for our comparison of two magnitude differences (solid line) and the theoretically obtainable value if all three differences had been used.

Figure 7.4—The measured magnitude difference as a function of polarization position angle (θ) for a particular percent polarization is plotted in Figures 7.4a and 7.4b. These were calculated according to the procedure described in §7.2.d.2. In Figure 7.4a the line with solid circles corresponds to the difference between m_{60} and m_0 ($m_{60}-m_0$) and the line with empty circles is $m_{120}-m_0$. In Figure 7.4b the line with solid circles is $m_{60}-m_0$, empty circles is $m_{120}-m_0$, empty squares is $m_{120}-m_{60}$. In Figures 7.4c and 7.4d are plotted the absolute values of the maximum magnitude difference. The lines with solid circles correspond to the maximum value when only the differences $m_{60}-m_0$ and $m_{120}-m_0$ are considered. The lines with empty circles indicate the maximum difference when $m_{120}-m_0$ is included in the comparison. Figures 7.4a and 7.4c (7.4b and 7.4d) were calculated for an object with a percent polarization of 15% (5%).

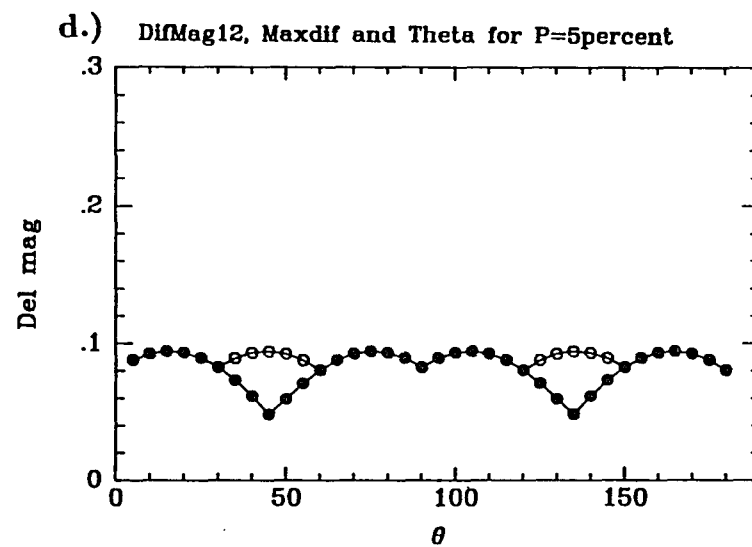
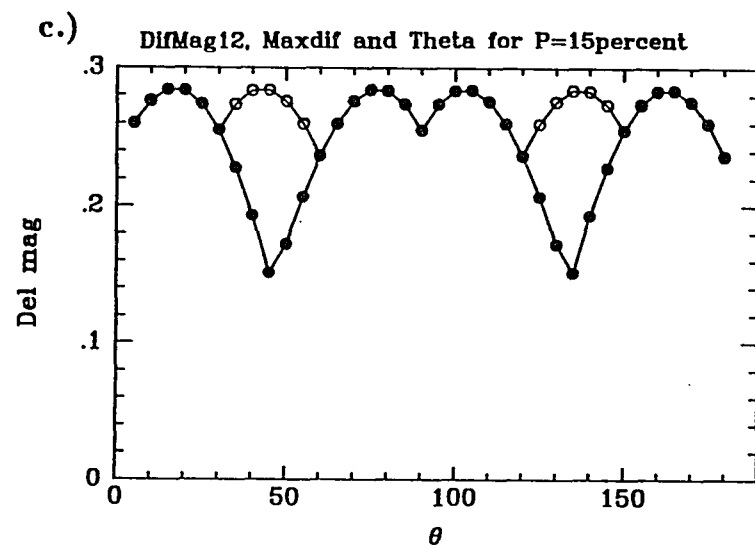
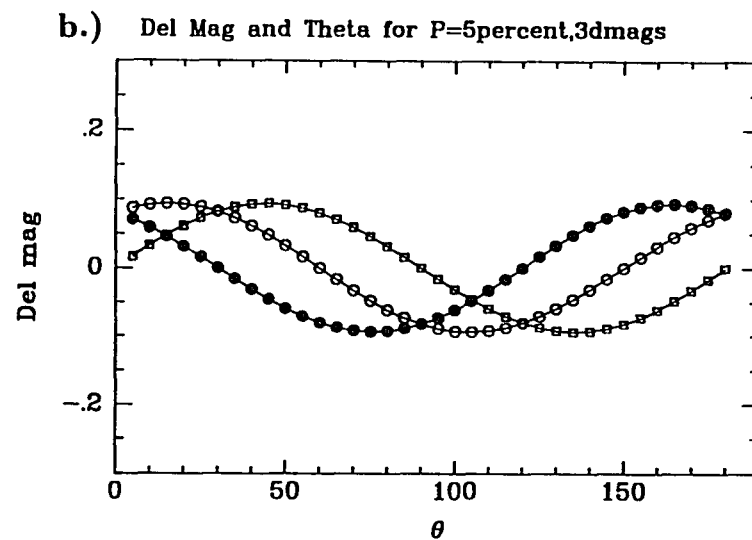
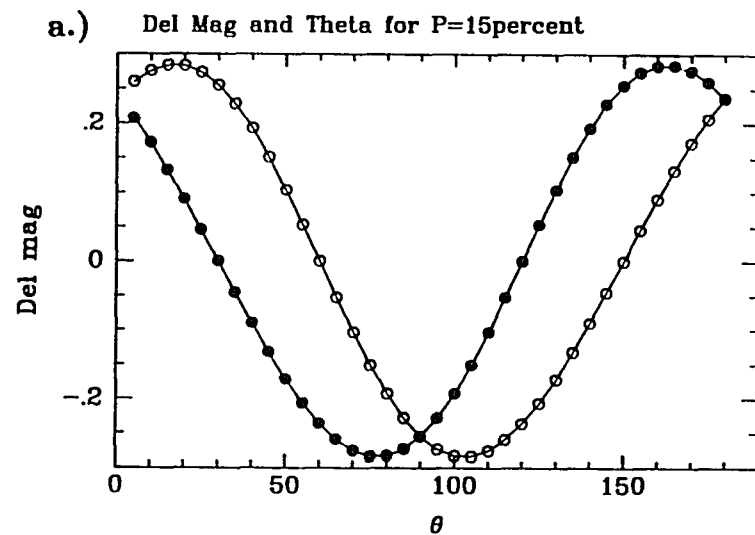


Figure 7.4

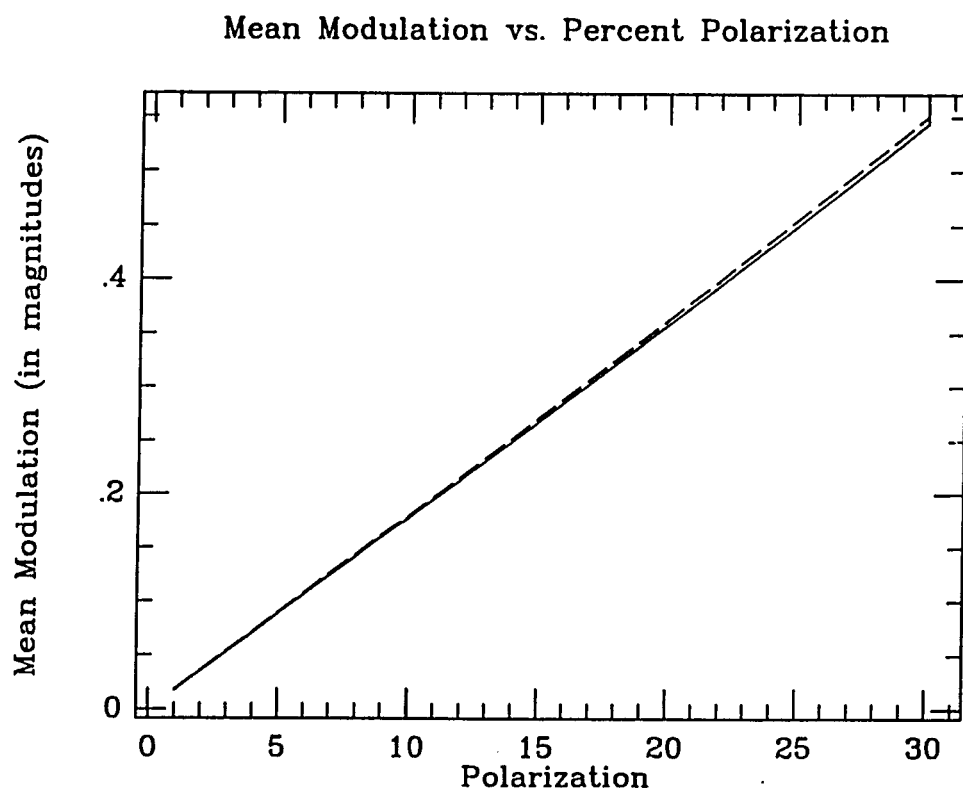


Figure 7.5—We have plotted the mean maximum modulation (maximum detected modulation as function of polarization averaged over θ) for our comparison of two magnitude differences (solid line) and the theoretically obtainable value if all three differences had been used (dotted line). See §7.2.d.

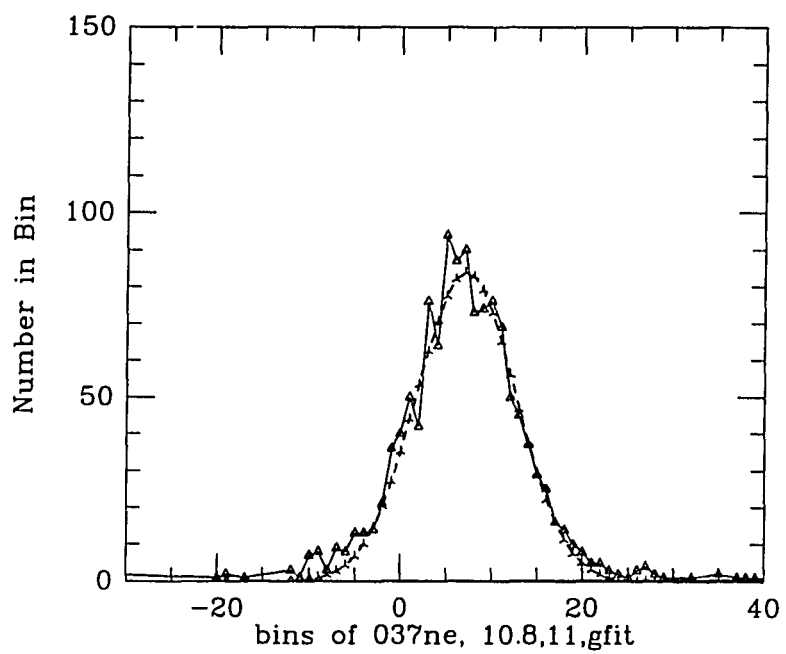
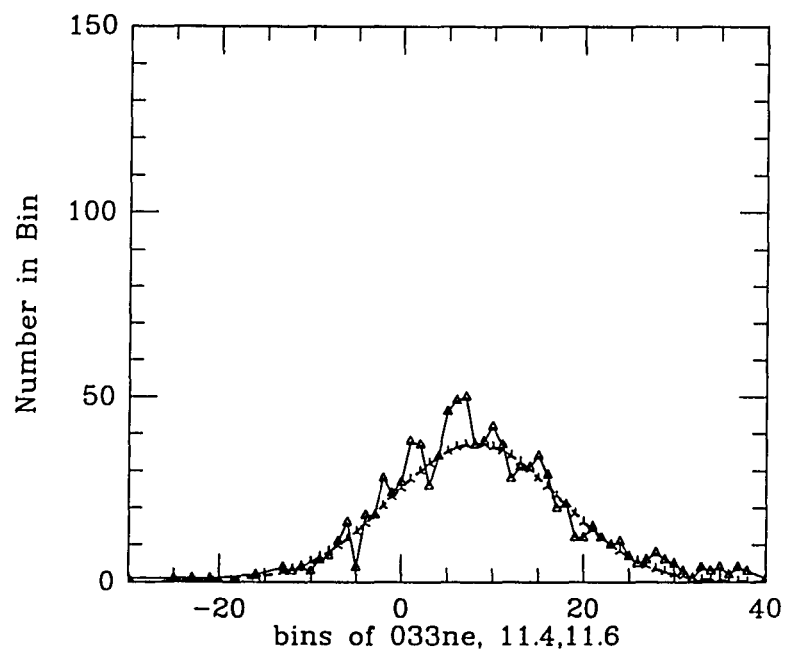
d.3.) *Determining the Error in the Measured Modulation:* In order

to calculate the error in the measured modulation, it is necessary to examine the distribution of magnitude differences as a function of instrumental magnitude. In Figure 7.6 we present plots of the distribution of magnitude differences for selected instrumental magnitude ranges. We have also plotted Gaussian fits to the distribution. For the range of magnitudes included in our survey (in general $16 < B < 20$) the errors in the magnitude differences are Gaussian.

In Figure 7.7 we present the transformed errors as a function of B magnitude. The square of the transformed error (σ_B) is related to the square of instrumental magnitude error (σ_{ins}) by the slope of the transformation function at a given instrumental magnitude. The direct mapping used to calibrate the instrumental magnitudes (described in §7.2.c) is not a functional fit. It proved cumbersome to determine the slope of the transformation function at an arbitrary point. For this reason a third order least squares fit was made for the faint end of each transformation. This slope of the fit was then used for the slope of the transformation function and the appropriate scaling of the RMS. The resulting RMS as a function of B magnitude is relatively constant. The larger values at bright magnitudes result from the increasing uncertainty as the plate response leaves the linear regime and the images begin to saturate.

Figure 7.6—We have plotted the distributions of magnitude differences for two ranges of instrumental magnitude (the magnitude difference is in units of hundredths of a magnitude). The data used comes from the northeast quadrant of polarization survey plates PS27033 and PS27037. In both plots the distribution of magnitude differences is plotted with empty triangles and the Gaussian fit is the dotted line. The top plot is of the distribution of the difference in magnitudes of the first and second images of objects with instrumental magnitudes between 11.4 and 11.6 (B magnitudes 18.1 to 18.3). The bottom plot is of the distribution of the difference in magnitudes of the first and second images of objects with instrumental magnitudes between 10.8 and 11.0 (B magnitudes 17.3 to 17.6).

Figure 7.7—In both 7.7a and 7.7b the top plot is the magnitude transformation for the given plate quadrant. The solid line is the direct transformation determined from star counts (see the caption for Figures 7.2 and 7.3 and §7.2.c). The dotted line is a third order least squares fit to the transformation. The slope of this fit was used to scale the RMS of the magnitude differences from instrumental to B magnitudes. The labeled squares are the positions of photometric standards that were on these plates (see the caption for Figures 7.2 and 7.3). We present in the bottom plot of both 7.7a and 7.7b the RMS of the magnitude differences. The solid line is the RMS of the B magnitude differences. The dotted lines are the RMS of the instrumental (before transformation of the magnitudes) magnitude differences. The jumps in the curves are due to the necessity of binning the objects by magnitude in order to determine the RMS of the magnitude differences.

**Figure 7.6**

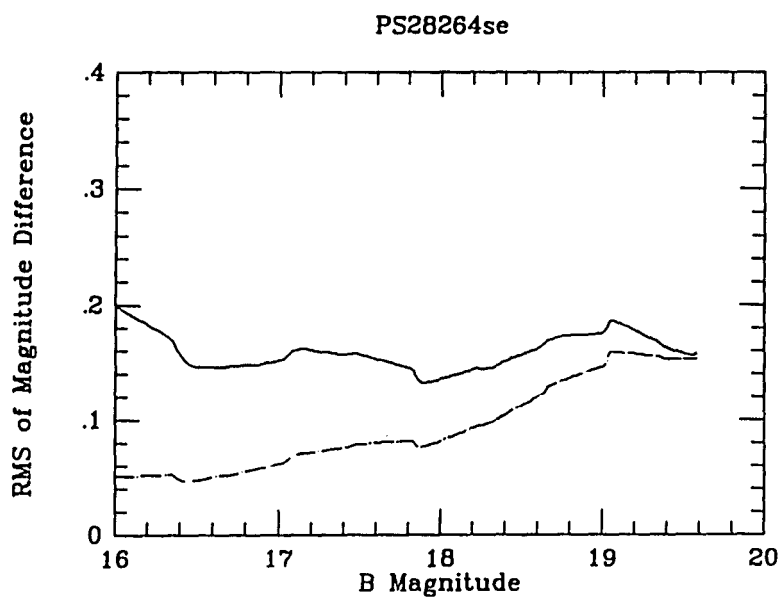
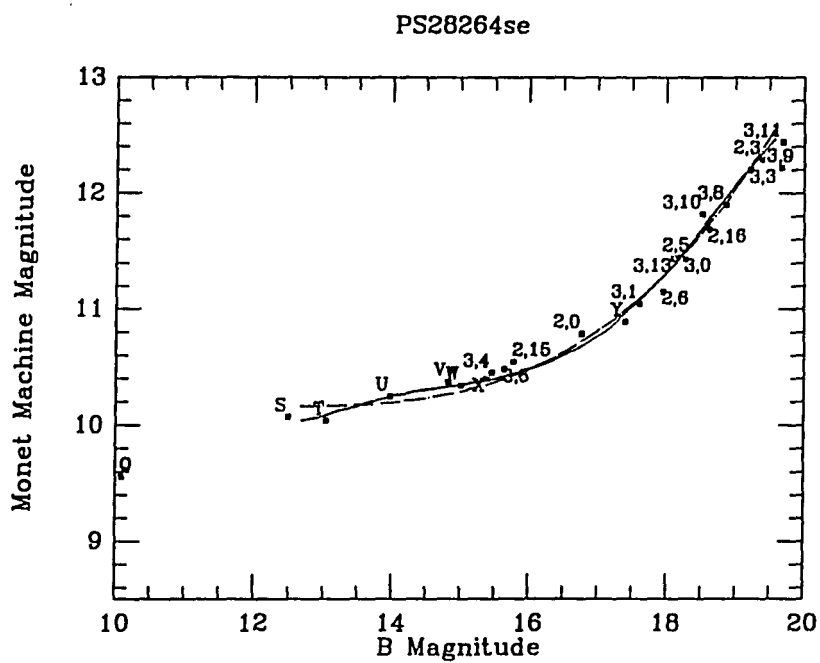


Figure 7.7a

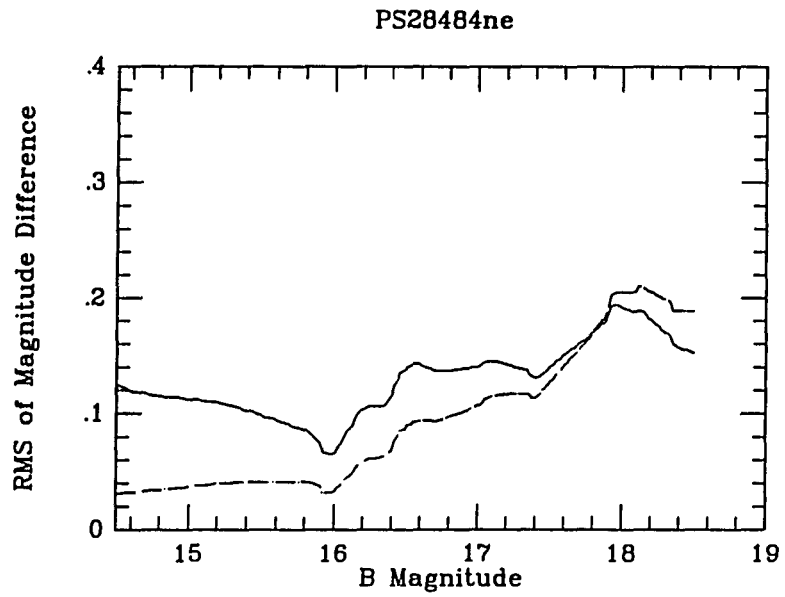
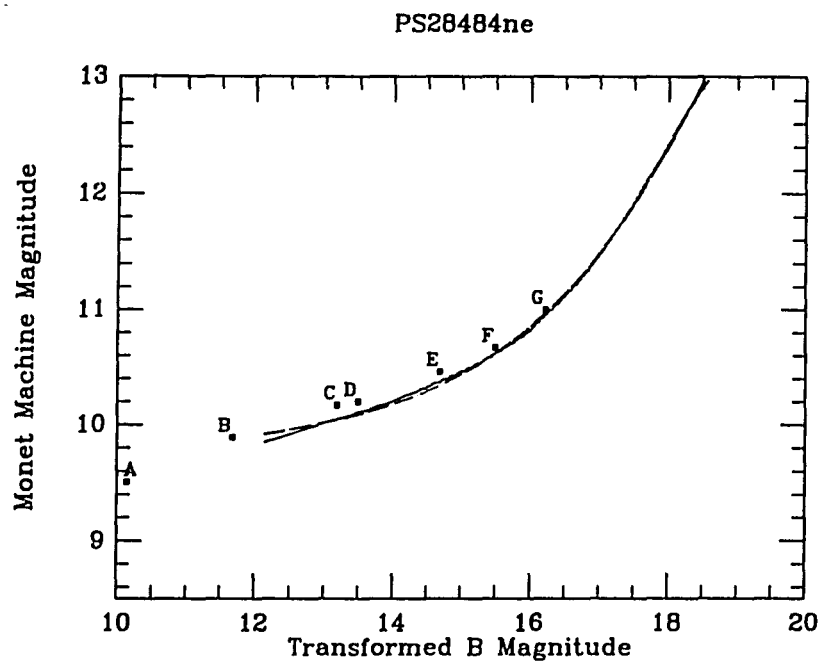


Figure 7.7b

7.3 Selection and Followup of Candidate Polarized Objects

7.3.a.) *Selecting Candidates*

Despite the advantages of using differential magnitudes computed from three images which are all on the same plate (we avoid plate to plate variations), there are still conditions that can induce a measured modulation, even if the object is unpolarized (§7.2.d.2). Fortunately, most of these problems affect the entire plate and just induce a shift to the distribution of differential magnitudes (i.e. the difference of any pair of instrumental magnitudes is no longer zero). In fact we have seen in the previous section that the RMS of the transformed differential magnitudes are Gaussian, but have variances ranging between 0.1 to 0.25 magnitudes over the magnitude range measured by our plates. The relatively large error requires us to observe deep into the error distribution if we wish to be able to be sensitive to objects with polarizations as low as 10%. In order to limit the number of objects which had to be observed as part of our followup program, we adopted several procedures to cull objects for which we could attribute the modulation of the images to causes other than intrinsic polarization of the objects.

Two plates were taken of each field and the order of exposures (order of filters) was generally reversed on the second plate. For unpolarized objects

at a given magnitude, the measurement errors will distribute the measured modulations of the objects equally around the mean difference. Measurements of truly polarized objects would also be affected by errors in our photometry of the individual images. Repeated measurements of a truly polarized object would detect amounts of modulation clustered around the value measured by a perfect system. We make use of this fact and our two measurements (two plates) by imposing our "Law of Two". All objects which, when compared to other objects on the plate of comparable brightness, are at least 2.2 sigma detections on both plates and in the same sense of modulation (has the same sign, which is required if the polarization and position angle are stable during the two measurements) are considered candidates for followup observations. By imposing this requirement, we run the risk of losing real objects which are detected on one plate and missed on the other. We gain, however, a tremendous reduction in the number of objects which must be inspected for systematic error (e.g. overlapping images, plate defects), or observed spectroscopically. For an individual object there is only a 0.019% chance that random errors will cause the object to appear as a 2.2 sigma detection on both plates and in the same sense of polarization. The order of the filters was reversed (in general) for the second exposed plate to help select against flare stars and other variable objects.

After an object's initial identification as a candidate, the scanning data, polarization plates, and POSS plates were inspected for any indications of overlapping images, nearby companions, or plate defects that might have induced

a measured modulation for the candidate. The candidate selection software tried to reject such objects. For example, objects with grossly non-stellar images (objects with roundness values greater than 10, see Figure 7.1 for an example of the distribution of image roundness for a scanned plate) were rejected.

7.3.b.) *The Followup Observations*

For candidates that survived this culling process, we made every effort to obtain spectroscopic identifications and photopolarimetric measurements of their polarization. BL Lacs are intrinsically variable objects (see Chapter 1). Because the polarization plates were exposed nearly a decade before the followup observations, spectroscopic identifications are particularly valuable. The duty cycle of polarization for XSBLs is low (see Chapter 5) and the duty cycle of RSBLs is not as high as was believed in the early 1980s (see Chapter 6 compared to the data presented in Angel *et al.* 1978). A single null detection from a polarization measurement in 1988 indicates that the object was not polarized at the epoch of observation, it does not rule out activity eight to ten years before. However, if a spectrum shows the object to be a normal B star, it can be safely removed from our list of candidates. Polarimetry measurements are not pointless, however. The detection of polarized emission is necessary to confirm a spectroscopically promising candidate. In addition, a good polarization limit can be used to argue that an object is not capable of being highly polarized, although it is not definitive. It was easier for us to obtain telescope time to make polarization

measurements than spectroscopic observations (large amounts of telescope time on small telescopes was available while the smallest available telescope with a spectrograph were the relatively oversubscribed S.O. 2.3 m and KPNO 2.1 m). Nevertheless we were able to obtain spectra for the vast majority of the candidates. Polarimetry and spectroscopic followup observations were made concurrently from April 1988 to January 1990. Spectroscopic observations were made using the Steward Observatory 2.3 m with the B and C spectrograph with the TI CCD and the Kitt Peak 2.1 m with the Gold Cam spectrograph. Polarimetry observations were made with the "Two-Holer" Polarimeter/Photometer and the S.O. 2.3 m, S.O. 1.5 m, and SO 1.54 m. If spectroscopy indicated a stellar identification and the candidate had not already been observed for polarization, it was generally not observed for polarization. The exceptions were two white dwarfs, which were examined to rule out the unlikely event that a highly magnetic white dwarf had been found in the survey. All galaxies detected as candidates were observed for polarization.

7.3.c.) *Results of the Followup*

All but one of the 171 candidate objects were observed either spectroscopically or polarimetrically. Of the observed candidates, spectra were obtained for all but twenty. Nineteen of these objects were observed with "Two-Holer" for evidence of polarized emission. Strong two sigma limits were set for all but one object. The breakdown on the number of objects at each polarization limit

follows (number of objects $<$ two sigma limit): 1 $<$ 6%, 2 $<$ 5%, 5 $<$ 2.0%, 3 $<$ 2.5%, 8 $<$ 3.5%. We do not believe that any of these objects is a BL Lac or a highly polarized quasar, although without a spectrum it is not possible to rule out the possibility. There is only one candidate for which we were not able to obtain followup observations.

While the polarimetric followup failed to find any confirmed BL Lacs or HPQs, spectroscopy did discover two objects which we consider to still be candidates, although there is no evidence of polarized emission from either object. Our observations of these two objects are discussed in §7.3.d and §7.3.e.

Before we discuss these two objects, we will describe in slightly more detail the results of the followup of the other candidates. It is important to keep in mind that the errors on each of our individual photographic polarization measurements are quite large (5 to 10%). In order to be able to detect even strongly polarized objects we had to dig into the noise of our data (hence our decision to work at the 2.2 sigma level on each plate). The vast majority of candidates (and possibly all of them) were the result of random errors (normal distribution as shown in Figure 7.6) on two separate measurements masquerading as a detection of "polarized emission". The objects which were observed spectroscopically were found to be normal stars or nearby galaxies. The most numerous interlopers at the faint end were G, K, and M dwarfs and elliptical galaxies. At the bright end the most numerous false detections were caused by M giants. The rarest

objects found included one DA white dwarf (unpolarized) and two galaxies with strong and narrow emission lines associated with HII regions (also unpolarized). The results of the followup observations of the 171 candidates follows: 1 quasar (see below), 1 candidate BL Lac (see below), 39 galaxies (all ellipticals or except for the two emission line galaxies mentioned above), 1 DA white dwarf, 1 B star, 1 A star, 6 F stars, 41 G stars, 27 K stars, 34 M stars, 19 objects for which only polarization limits could be set (all were stellar on the sky survey plates), and one unobserved object. There is no obvious bias in this sample. We note that the overrepresentation of ellipticals in the sample is probably a result of seeing variations causing errors in our photometry for these slightly extended, round, and compact objects.

7.3.d.) *A Candidate HPQ, OP 0229+06*

The candidate polarized object OP 0229+06 is a quasar with a redshift of 1.42. The identification of this object was reported in Jannuzi and Green (1989). After final calibration of our plates, we present revised values for this object's photographically measured B magnitude and polarization. On 9 October 1980 UT, this object had a $B = 19.2 \pm .2$ and a modulation consistent with a polarization of $24 \pm 10\%$. Our spectrum of the object (Figure 7.8) does not show an unusually strong continuum. The object's position (α 02^h 29^m 05.1^s; δ + 06° 29' 27") does not correspond with any previously identified radio source. Followup polarimetry has been performed repeatedly and failed to confirm

that this object is polarized. Two sigma limits of four percent were set on ten occasions from September 1988 to November 1989. This does not rule out the possibility that this object is an HPQ. Some previously identified HPQs have been observed to go through extended periods of time without exhibiting significant ($> 4\%$) polarization (Smith 1990). We will continue to periodically monitor this object, but do not consider it an HPQ until confirming polarimetry is obtained. A finding chart for this object is provided in Appendix IV. Finally we note that since we had candidate objects which we now know to be basically a random sample of objects down to a B of 20, it is quite possible that this object is also just a randomly selected unpolarized object.

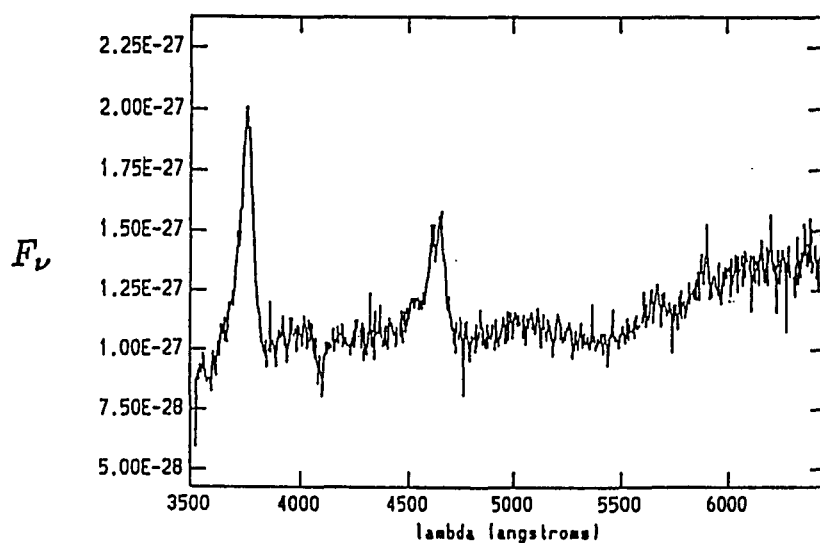


Figure 7.8—We have plotted our spectrum of the quasar OP 0229+06. The redshift of this quasar is 1.42. It was discovered during our spectroscopic identification of candidate polarized objects. This object is discussed in §7.3.d.

7.3.e.) *A Candidate BL Lac, OP 1106+36*

The candidate object OP 1106+3654 is our best remaining candidate to be a BL Lac object. It was as a 2.5 sigma detection on both plates. Spectra obtained 12 April 1989 UT (Figure 7.9) and 27 November 1989 (Elston 1990) show no evidence of any absorption or emission features. On our polarization plates, the object has a $B = 19.4 \pm 0.3$ (the error is larger than the RMS of the magnitudes of the individual images because the object has such a large modulation, easily visible on the polarization plate) and a modulation consistent with a percent polarization of $18 \pm 8\%$. While the object appears to be stellar on our plates, CCD polarimetry obtained at the Steward 2.3 m on 24 February 1990 UT clearly shows the object is extended and at least four arcseconds in size. The object is round and of uniform brightness. Because the object is faint and extended, followup polarimetry has been difficult to obtain. Our best limit to date was obtained during our imaging polarimetry observing run on 24 February 1990 UT. Our two sigma limit is $p < 9.5\%$. Karen Visnovsky, Chris Impey, and Craig Foltz (1990) were kind enough to observe this object as part of their radio observations of quasars. On 28 May 1989 UT, VLA observations at 8.44 GHz in C array detected the object at the 2.8 sigma level. The object has a peak flux density of 2.8145×10^{-4} Jy. The RMS noise was 9.84×10^{-5} Jy. The radio and optically determined positions are in excellent agreement (Optical Position: $\alpha 11^{\text{h}} 06^{\text{m}} 47.9^{\text{s}}$; $\delta + 36^{\circ} 54' 43''$; Radio Position: $\alpha 11^{\text{h}} 06 47.963^{\text{s}}$;

$\delta + 36^\circ 54' 42.75''$). The optical and radio measurements would give this object an α_{ro} of 0.89 (α_{ro} defined in Chapter 6, but in this case calculated at 8.44 GHz and the B band). If this object proves to be a BL Lac object, it would have the smallest value of α_{ro} ever observed. Therefore, in the discussion which follows we do not consider this object to be a detection of a BL Lac and the number of objects found in the survey is considered to be zero.

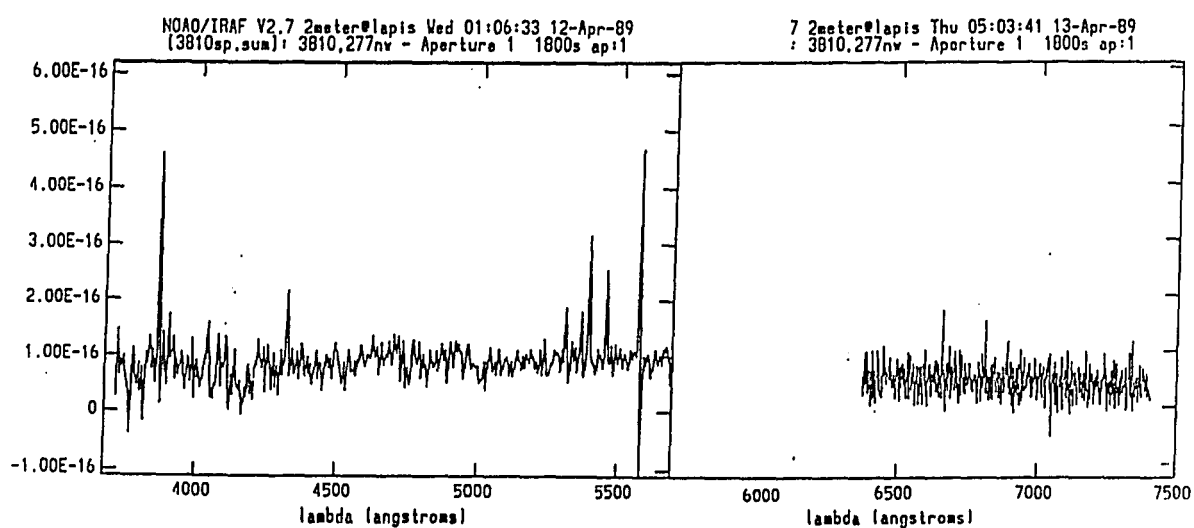


Figure 7.9—We have plotted our spectrum of the object OP 1106+36. It was discovered during our spectroscopic identification of candidate polarized objects. This object is discussed in §7.3.e. The sharp spikes in the spectrum were caused by cosmic rays.

7.4 Setting a Useful Limit

Although we were not able to compile a sample of optically selected BL Lacs, we can set the best limits to date of any optical polarization survey. In §7.4.a we determine our limits on the surface density of BL Lacs as a function of magnitude and polarization. We compare our results with past surveys and the known surface densities of radio and x-ray selected BL Lacs in §7.4.b. In §7.4.c we examine several theoretical predictions on the optically derived surface density of BL Lacs in the context of our work. Finally we address the question of whether or not there are any radio and/or x-ray quiet BL Lacs.

7.4.a.) *Using Monte Carlo Simulations to Determine our Survey Limits*

Because our probability of detecting a truly polarized object is a complicated function (of many variables) that varies from plate to plate, we use Monte Carlo generated data sets and a model of our known errors to provide limits to the surface density of BL Lacs drawn from various assumed distributions of polarization and magnitude. We have set limits on the surface density of objects of a given polarization as a function of magnitude. We are also able to determine limits on the surface density of BL Lacs with the optical polarization properties of radio and x-ray selected BL Lacs.

Each of the simulations we performed consisted of two parts. First, a dummy data set of objects was generated. Each “object” was assigned a B magnitude, percent polarization, and polarization position angle. The values assigned depended on the proposed parent distribution being used or tested. After the polarization and position angle (always randomly assigned) were determined, the maximum observed modulation was calculated using the equations in §7.2.d.²

Each dummy data set usually consisted of 10000 to 20000 “objects”. The objects were then randomly assigned to various fields in our survey area. Each field received equal weight. Once assigned to a field, two sets of “observations” (one for each plate) were generated using the errors determined for the given field (these were occasionally plate dependent, depending on the field). Following our Law of Two (§7.3), “objects” which were 2.2σ events on both plates in the same sense of polarization were considered to be “found”. We took into account the fractions of each field which were unusable by including a finite probability for each plate that object “landed” on these regions. The final result is the fraction, as a function of magnitude and polarization, of the dummy population that we would have detected.

In order to get an actual limit, the normalization of the dummy or test population has to be set from our actual survey results. Despite the fact that we

² Note that we included the minor effect of our error when the candidates were selected of only considering two of the possible differences available from our three images. See §7.2.d.

still have three objects that have not been finally rejected as possible BL Lacs or HPQs (the quasar, the BL Lac candidate, and one object for which we have not obtained either polarimetry or spectroscopy), we have no confirmed identifications of polarized objects found by the survey and as discussed in §7.3.e, we take zero as the number of detected objects. Since the mean number of objects detected in the “found, not found” problem obey Poisson statistics, we can use the confidence limits for small numbers of events determined by Gehrels (1986), the area of our survey, and our Monte Carlo calculations to obtain surface density limits,

$$N_{CL} = UL_{CL}/(f \times Area)$$

where N_{CL} is the surface density at the desired confidence level, UL is the Poisson single-sided upperlimit taken from Gehrels 1986 for a mean of 0 and a confidence level of CL , $Area$ is the area of our survey (560 square degrees), and f is the fraction of the real objects that would be found in our survey. In this way, the complex, but relatively well-determined errors can be translated into well-understood limits on the surface density.

It is important to note the kinds of errors and sources of incompleteness we have included in our model of the survey. The errors we have determined directly or assumed for our survey are the following:

1. The bright and faint end cutoffs for each plate (discussed in §7.2.c).
2. The error in the magnitude difference of two images of an object and its relationship to measured polarization. This is a function of magnitude

and is different for each plate. This was explicitly calculated for each quadrant. We only consider magnitudes and regions of the survey where the distribution of the errors in the magnitude differences are well approximated by a normal distribution (discussed in §7.2.d).

3. We have assumed that the error in the transformed magnitude is directly related to the error in the magnitude difference ($\sigma_{\text{mag}}^2 = (0.5) \times \sigma_{\text{diff}}^2$) and is applied to the test objects as a function of true magnitude and plate on which the test object falls.

4. Corrections were made for the loss of an object because of image overlaps, lost images, and incorrectly identified triples of objects. There are a variety of ways that images can be lost or the measurement of the modulation adversely affected. We have accounted for all of the multiple causes of image overlap etc. by making completeness corrections. The corrections were determined by comparing our polarization plates to the POSS plates and by direct inspection of the scanning data. For seven of the fields in our survey, we scanned the corresponding POSS O plates. The detected objects were then matched to those detected on our polarization plates. The objects identified on the POSS plates were also matched with our list of measured objects (the objects for which three images could be identified and accurately measured). These comparisons provided an empirically derived correction factor (as a function of instrumental magnitude) for the seven fields. Our survey consists of fields at high galactic lat-

itude, 40 to 85 degrees. The POSS plates scanned range from 40 to 70 degrees in galactic latitude. For those fields that we did not scan the corresponding POSS plate, we have assumed that the losses due to overlap are similar to those of the plate with the closest galactic latitude (it is the absolute value of the galactic latitude that is used because what is important is that the plates have similar numbers of objects per square degree). We also checked by visual inspection the scanning results of 0.3 square degrees of each plate to account for the losses due to not finding or failure to properly group all three images of an object. This was also computed as a function of instrumental magnitude and found to be indistinguishable from the results determined from the scanning of and comparison to the POSS plates. On the polarization plates, objects included in the survey ranged from Monet instrumental magnitudes of 10 to 13.0 (in general this corresponds to B magnitudes of 15 to 20). On average, greater than 85 percent of the objects between instrumental magnitudes 10.4 and 11.5 (in general B of 16 to 18.5) were successfully measured for modulation (see definition above). Between instrumental magnitudes 11.5 and 13.0, losses increase but are relatively consistent from plate to plate. At an instrumental magnitude of 12.5 (B of 19.5), only 40 percent of the objects are well-measured. In addition to overlap losses, we are also losing objects that have one or more of the three images lost because it is not bright enough to be detected. Note that at the flux limit of our survey we are actually less sensitive to very highly polarized objects because it is possible that some of the images will be too faint to be included in the survey.

In order to set a limit on the surface density of objects at a given polarization and magnitude, we created a series of dummy data sets with all of the objects fixed at a given polarization and uniformly distributed from B equals 15 to 20. In Table 7.2 we present the resulting surface density limits at the 99.95% and 90.0% confidence levels.

Table 7.2: Limits on the Surface Density of Polarized Objects

No. of Polarized Objects per Square Degree as a Function of Percent Polarization												
<i>B</i> Magnitude	5%		10 %		15 %		20 %		30 %		40 %	
Range	.9995	.90	.9995	.90	.9995	.90	.9995	.90	.9995	.90	.9995	.90
15.0, 15.5	.129	.0391	.0744	.0225	.0589	.0178	.0549	.0167	.0375	.0114	.0310	.0094
15.5, 16.0	.092	.0279	.0521	.0158	.0488	.0148	.0449	.0136	.0321	.0097	.0286	.0087
16.0, 16.5	.210	.0637	.0655	.0198	.0510	.0155	.0386	.0117	.0301	.0091	.0270	.0082
16.5, 17.0	.556	.1684	.1953	.0592	.0914	.0277	.0589	.0179	.0279	.0085	.0272	.0082
17.0, 17.5	.082	.0249	.0633	.0192	.0495	.0150	.0348	.0105	.0285	.0086	.0260	.0079
17.5, 18.0	.093	.0283	.0597	.0181	.0526	.0159	.0396	.0120	.0302	.0091	.0274	.0083
18.0, 18.5	.135	.0410	.0705	.0214	.0532	.0161	.0355	.0108	.0277	.0084	.0265	.0080
18.5, 19.0	.278	.0841	.0824	.0250	.0588	.0178	.0415	.0126	.0292	.0088	.0280	.0085
19.0, 19.5	.201	.0609	.0969	.0294	.0785	.0238	.0547	.0166	.0345	.0105	.0280	.0085
19.5, 20.0	.132	.0400	.1018	.0308	.0686	.0208	.0509	.0154	.0332	.0100	.0272	.0082
Total	.1398	.0424	.0746	.0226	.0581	.0176	.0435	.0132	.0307	.0093	.0276	.0084

7.4.b.) *What Should We Have Found?*

We note that there are no known BL Lacs in our survey fields. There are, however, certainly BL Lacs located along the direction of these fields. Why did we miss them? The two previously mentioned optical polarization surveys (Impey and Brand; Borra and Corriveau) inferred limits to the surface densities by convolving their detection limits and what little was known then (the only monitoring data at the time was Angel *et al.* 1978) about the relative distribution in B and polarization of BL Lacs. Since those surveys were published we have learned a great deal about the polarization and magnitude distributions of not only radio but x-ray selected BL Lacs (see Chapters 5 and 6). In this section we present the results of models predicting how many objects similar to those in the 1 Jy and EMSS BL Lac samples we should have detected (see Chapter 2 for a description of the samples).

Dummy data sets were constructed of “radio” and “x-ray” selected BL Lacs. For the dummy RSBLs we smoothed the magnitude and polarization distributions of the 1 Jy RSBL sample of Stickel *et al.* (1990a;1990b). The polarimetry data was taken from Kühr and Schmidt (1990) supplemented (when necessary) by the observations of Smith (1986). The first epoch of data (listed in the two references) for all objects was assumed to be a sampling of the true underlying distribution for all BL Lacs. We also assumed that the distribution in polarization was independent of apparent magnitude. This step in our procedure is very similar to our discussion of the duty cycle of polarization in Chapters 5

and 6. The added complexity is that we are trying to understand not just the fraction of time or number of objects with polarizations greater than 4%, but the relative distribution over all polarizations. Even though we now have sizable samples of BL Lacs (20 to 30 objects in the two complete samples), we still suffer for a lack of a complete sampling of the underlying distribution. While it has been suggested that there is a redshift dependence in the polarization of highly polarized quasars (Wills 1989), there is no evidence of any such dependence in the 1 Jy sample.

For the dummy XSBLs we used our own data on the EMSS and HEAO A-1 samples, with the HEAO objects' contribution weighted by their observed lower surface density. Again, the first epoch observations were taken as a sampling of the underlying true distribution. Our study of the XSBLs has provided a considerably more extensive database for the EMSS sample than the data available for the 1 Jy sample. We were able to include the last epoch of observation as an additional sampling of the distribution function. The apparent V magnitudes were converted to apparent B by assuming $B - V = 0.6$.

The Complete *Einstein* Extended Medium Sensitivity Survey sample of BL Lacs consists of 22 objects in a survey area of 634 square degrees. The 1 Jy sample of Stickel consists of 34 objects distributed over 32,204 square degrees. The limits derived from our "observations" of our Monte Carlo generated dummy RSBL and XSBL data sets are presented in Table 7.3. Normalizing the

distributions with the known surface densities and our survey area, we should have detected 1.27 “XSBLs” and 0.122 “RSBLs” for a total of 1.39 BL Lacs. This is certainly within our errors. The computed limits on the surface density are 0.0199 (0.0655) per square degree for RSBLs and 0.0630 (0.2078) per square degree for XSBLs at the 90% (99.95%) confidence level. In all we should have found 1.23 BL Lacs.

The bottom line is that BL Lacs are rare beasts. If we had been able to have a polarization limit of 0.5 percent we would have greatly increased the number of detected objects. When we began this survey, it was believed that BL Lac were not only highly polarized, but spent a large fraction of their time at high levels of polarization. This was prior to any systematic monitoring of a complete sample (e.g. our work for XSBLs presented in Chapter 5; Sitko *et al.* 1985; Smith *et al.* 1986). We now know that most BL Lacs do not spend very much time at polarizations as high as 30%. Our limits do constrain the surface density of linearly polarized objects.

7.4.c.) *What Have Others Predicted We Should Find?*

Urry and Padovani (1990) have considered in detail the various implications of FR I radio galaxies being the parent population of BL Lacs. The number of BL Lacs found in radio, x-ray, and optical surveys is then determined

Table 7.3: More Surface Density Limits

<i>B</i> Magnitude Range	Dummy Data Set			
	EMSS .9995	XSBLs .90	1 Jy .9995	RSBLs .90
15.5, 16.0	0.0000	0.0000	0.0678	0.0206
16.0, 16.5	0.0950	0.0288	0.0671	0.0203
16.5, 17.0	0.0000	0.0000	0.0957	0.0290
17.0, 17.5	0.1402	0.0425	0.0505	0.0153
17.5, 18.0	0.1829	0.0554	0.0585	0.0177
18.0, 18.5	0.1753	0.0531	0.0630	0.0191
18.5, 19.0	0.2583	0.0783	0.0637	0.0193
19.0, 19.5	0.2780	0.0843	0.0931	0.0282
19.5, 20.0	0.2151	0.0652	0.0764	0.0232
15.0, 20.0	0.2078	0.0630	0.0655	0.0199

Note For Table 7.3

The limits for each magnitude range were calculated assuming that the distribution of percent polarizations is independent of luminosity. We also assumed an apparent luminosity distribution consistent with the complete samples discussed in Chapter 3. The zeros in the table indicate the need for larger samples to smooth out our model distribution. We are in the process of testing assumed functional distributions in our simulations.

directly by the assumed model for the beamed component and the luminosity function (or surface density) of the parent population. Their model would predict (from their analysis of existing data, their assumed model for the beamed and unbeamed components, and their derived range of Lorentz factors for the beamed optical emission, $8 < \gamma < 20$) that in the area covered by our survey there should have been 9 to 56 objects down to a B of 18.5. This corresponds to a surface density of 0.0156 to 0.0937 per square degree. Our 90 percent confidence level limit down to 20th is 0.082 objects per square degree and down to 18.5 is approximately 0.06 objects per square degree. Unfortunately our limit is not quite strong enough to strongly constrain the value of γ (under the assumptions of the model of Padovani and Urry) for the relativistic component dominating the optical emission.

Ghisellini and Maraschi (1989) have also presented arguments that predict that an optically selected sample of BL Lacs will have a surface density in between the values determined by the radio and x-ray selected samples. This is a consequence of their proposed model for the relativistic component of BL Lacs and the resulting amount and distribution of emitted radiation. In their model the BL Lac's "jet" has an increasing bulk velocity with increasing distance from the core of the object. At the same time, the inner regions (those with low bulk velocities) dominate the observed emission at high frequencies while the radio emission is dominated by the material at greater distance (high bulk velocities). This apparently ad hoc assumption leads to the natural consequence that the

radio emission is the most beamed while the x-ray emission is the most isotropic. If we could improve our limit on optical surface density, then we would be able to directly test this model. Since our limits are above the observed XSBL surface density, we are not in conflict with nor confirm their model.

7.4.d.) *Can We Rule out the Existence of Radio Quiet BL Lacs?*

It is impossible to prove radio quiet BL Lacs do not exist. We can say, as Stocke *et al.* did in the title of a 1990 *Ap. J.* article, that there is “no evidence for radio quiet BL Lacs”. With our survey we can also do something that radio surveys and x-ray surveys can not accomplish; set an upper limit on the maximum surface density these objects can have. By definition BL Lacs are linearly polarized objects (see Chapter 1). Radio and x-ray emission are not required. Evidence of a synchrotron component is required. While we do not know the range of polarizations that our hypothetical radio quiet population might have, we have placed the best constraint to date on the surface density of all polarized objects. It is important to remember that the numbers in Tables 7.2 and 7.3 are the limits for the combined surface density of BL Lacs (all flavors) and HPQs. Radio loud quasars are outnumbered by radio quiet quasars by at least a factor of ten. If there is a BL Lac analogue to the radio quiet quasar, it does not exist in analogous numbers! If it did, we should have found 12 to 14 radio quiet BL Lacs.

CHAPTER 8

FIT THE EIGHTH: SUMMATION

“A fool ... is a man who never tried an experiment in his life.”
– *Erasmus Darwin*

BL Lacertae Objects are unique. They are the only extragalactic objects with featureless, variable, and polarized optical spectra. Since their discovery, they have proved to be enigmatic and difficult to understand. However, we are making progress in understanding these objects by bring together a variety of powerful diagnostic tools. These include determining the overall spectral energy distributions from x-ray to radio frequencies, observing the structure of these objects on the smallest observable scales (with VLBI), identifying isotropic components of their emission, monitoring the flux variability over all time scales, and studying their polarization properties. In this chapter we summarize both our work and our current understanding of BL Lacs with particular emphasis on the contributions of this dissertation.

8.1 Summary of Our Observational Programs

In this dissertation we presented the results from two programs. In Part II we presented the results of an extensive monitoring program to measure and monitor the optical polarization of x-ray selected BL Lac candidates. In Part III we presented the results of the most extensive optical polarization survey so far undertaken.

Our study of the optical polarization properties of XSBLs confirms that the BL Lac candidates found in x-ray surveys like the Einstein Extended Medium Sensitivity Survey meet the requirements for membership in the class of BL Lacs. In addition to having featureless optical spectra, the majority of the XSBLs are also variable in their emission and have variable (and intrinsic) polarized emission. Although x-ray selected BL Lac candidates have proven to be BL Lacs, the characteristics of their optical polarized emission are different from those of the classical radio selected BL Lacs. The XSBLs have lower maximum percent polarizations, a lower duty cycle, smaller variations in flux, and a greater tendency to have preferred angles of polarization than radio selected BL Lacs.

Our optical polarization survey is the most extensive survey of its kind ever undertaken. We did not find any confirmed BL Lacs or highly polarized quasars, but we are able to constrain the surface density of the various populations of polarized objects. The survey is complete to a B magnitude of 20 and covers

560 square degrees. Our sensitivity to polarized objects is a function of survey field.

We have shown that optically polarized emission is accompanied by significant radio emission. This is demonstrated by two facts. First, the that all known BL Lacs (XSBLs and RSBLs) are strong radio sources (Stoche *et al.* 1990) and have significant optical polarization (this work). Second, we found no evidence of a radio quiet population of optically polarized objects. Our optical polarization survey constrains the surface density of various populations of polarized objects. In particular we are able to rule out at the 90.0% confidence level the presence of a population of radio quiet BL Lacs or highly polarized quasars (with optical flux and polarization properties similar to radio selected BL Lacs) that would have a cumulative surface density of 0.03 per square degree down to a B magnitude of 20.

8.2 Constraining The Emission Mechanism of BL Lacs

Measuring the polarization of these objects provides a powerful diagnostic of the physical mechanisms which govern these objects. Combined with studies of the overall spectral energy distribution of these objects, measurements of the polarization allow us to constrain the mechanism of emission. The most common models for the radio through optical emission are variations on the synchrotron

and inverse-Compton model (e.g. Königl, A. 1989; Ghisellini and Maraschi 1989). These models are able to explain the general spectral energy distribution and polarizations at radio through optical wavelengths. Their greatest problems arise in trying to explain the steepening of the spectrum at UV wavelengths and the x-ray emission. The x-ray emission is, in particular, the most poorly understood. Models for the x-ray emission range from synchrotron self-Compton emission to modified thermal emission from a nuclear accretion disk (e.g. Königl 1989). Our optical polarization survey can be and has been used to constrain beaming models for the optical emission by synchrotron radiation in these objects (Padovani and Urry 1990).

Recently an alternative model has been suggested for the production of the observed spectrum of BL Lacs. Loeb, McKee, and Lahav (1990) demonstrate that the Comptonization of a very soft photon spectrum by semi-relativistic electrons in an expanding medium leads naturally to a log Gaussian spectrum of the form observed in BL Lacs. Loeb *et al.* do not investigate whether the polarization properties of RSBLs can be reproduced by their model. The range of polarization properties and variability of the polarization are stringent constraints on all of these models and we are investigating whether or not the Comptonization model can produce both range of observed polarizations and variability.

Our data (Chapter 5 and Chapter 6) indicates that the optical polarization of BL Lacs is correlated with the amount of nonthermal optical and

radio emission observed from the objects. We also showed that this is consistent with emission from relativistic jets (we considered the case where the emission is produced by optically thin synchrotron sources) viewed at different viewing angles to the jet (Chapter 6; Björnsson 1982). We hope in the future to improve on the existing models by using our data to constrain both the synchrotron and Comptonization models.

8.3 Determining The Source Geometry

VLBI and VLA observations of BL Lacs have detected both “jets” and extended emission from RSBLs (e.g. Rusk 1988; Gabuzda 1989; Antonucci and Ulvestad 1985). Together with studies of the radio properties of quasars and radio galaxies, these data have been used to support not only the beaming model of Blandford and Rees (1978), but also the efforts to unify various classes of AGN (e.g. Antonucci and Ulvestad). In all of the beaming and unification models, BL Lacs are objects viewed nearly along their relativistic jets. The observed properties of these objects are dominated by the relativistic beaming and small viewing angle. Direct support for this model can be found in the VLBI observations of some HPQs and BL Lacs. Some of these objects show evidence for apparent superluminal motion in their jets. This is directly explainable in the beaming model (whether the emission mechanism is synchrotron radiation or Comptonization).

Evidence of apparent superluminal motion is not available for the majority of BL Lacs (with so far no XSBL examples) and we must look elsewhere for evidence of a jet. For most of the unresolved RSBLs there are now VLBI or VLA radio maps which show strong cores sometimes surrounded by relatively weak extended radio emission (e.g. Antonucci and Ulvestad 1985; Rusk 1988). If we consider the double radio lobe morphology of many radio galaxies, it is a logical hypothesis that the BL Lacs are radio galaxies viewed along the "jet" (e.g. Barthel 1989). At this time we do not have comparable data available for the XSBLs, although we and Stocke and his collaborators are in the process of obtaining such observations.

Our measuring and monitoring of the polarization of XSBLs together with existing data on RSBLs also provides clues to the underlying physical structure of all BL Lacs. In either the synchrotron or Comptonization models, the fact that these objects have detectable polarization requires asymmetry or anisotropy in the emission region or emission process. Further more, our detection of preferred angles for the optical polarization of the XSBLs requires stability in the large scale geometry of these objects.

If we make the assumption that all of the objects we have considered as BL Lacs (both radio and x-ray selected) are intrinsically the same object, then the relativistic "jet" model is consistent with and helps explain the range of observed properties of the entire class of BL Lacs. As we discussed in Chapter 6,

such a model requires that objects viewed the most closely along the jet will have the largest α_{ro} and radio luminosities. They will be the most core dominated radio sources, have the largest optical luminosities, the largest maximum optical polarizations (for a properly chosen magnetic field geometry; Björnsson 1982), the least amount of frequency dependence in their polarization, the shortest time scales of variability, no preferred position angle to the polarization, no or little dilution of the polarization at long wavelengths, and the smallest surface and space density. With increasing viewing angles to the jet, the domination of the observed properties by the beamed component will decrease. A BL Lac viewed at increasing viewing angles should look more like the x-ray selected objects and other small α_{ro} BL Lacs. Preferred position angles are a consequence of the increasing stability of the projection of the magnetic field as the viewing angle to the velocity vector of the jet increases (It is assumed in this picture that perturbations are propagated as shocks along the jet and that the magnetic field has rotational symmetry about the jet axis).

8.4 Identifying the Parent Population

The optical emission from BL Lacs is dominated by a nonthermal and polarized continuum. If this radiation is strongly beamed, then observed BL Lacs are only the observed subset of a much larger group of objects. Since we have identified these objects by their beamed properties, it has been difficult to identify the “misdirected” objects. This has led various researchers to suggest

the use of more isotropic components of the radiation from BL Lacs and possible parent populations as a means of understanding these objects. The first attempts have used the diffuse radio emission and the properties of the host galaxies as probes of the isotropic properties of these objects (e.g. Antonucci and Ulvestad 1985; Ulrich 1989). The general conclusion is that radio galaxies or suitably chosen subsets of radio galaxies could be the parent population of BL Lacs (e.g. Barthel 1989; Browne 1989).

We have shown in this thesis that the optical polarization properties and the optical and radio luminosities are relatively independent of the x-ray luminosities. This supports the suggestion (e.g. Maraschi *et al.* 1986; Ghisellini and Maraschi 1989; Ghisellini *et al.* 1986) that the x-ray emission is more isotropic. If this is true, then we should consider the RSBLs as a subset of the XSBLs.

While using the isotropic emission to try and understand the evolution and nature of BL Lacs is important and fruitful, we have shown that by studying the optical polarization properties of BL Lac objects we can also test and provide constraints for models that try to identify the parent population of these objects. In particular, our optical polarization survey can be used to constrain beaming models and the resulting requirement for a parent population of BL Lacs (e.g. Padovani and Urry 1990). Future models for BL Lacs will have to explain the range of polarization behavior exhibited by the entire class (both RSBLs and

XSBLs) and not come in conflict with our constraints on the surface density of optically polarized objects (Chapter 7).

8.5 Future Work

Future work needs to address the following questions (plus, we are sure, numerous others):

Are all BL Lacs in the same kind of host galaxy? This is a very important problem which has implications not only on the lensing model of Ostriker and Vietri, but on explaining the observed differences between BL Lacs and quasars. Currently, all of the known host galaxies of BL Lacs are ellipticals.

Is there further supporting evidence for jets and/or beaming in XSBLs? In particular, will radio observations of XSBLs show strong flat spectrum cores and/or evidence for superluminal motion? This is important as a means of finalizing the apparent relationship between XSBLs and RSBLs.

What is the cause of the segregation in the α_{ro} vs. α_{ox} plane of the XSBLs and RSBLs? The apparent real gap needs to be definitively explained. In our plots in Chapter 6 it is important to remember that the XSBLs are under represented (sample drawn from a smaller region of the sky), but there still appears to be a real separation in the plane. Improved theoretical modeling is needed to help explain this separation.

Are BL Lacs and HPQs closely related or intrinsically different objects?

The duty cycle of the optical polarization of HPQs is poorly known and new observations of a complete sample of these objects is needed. The apparent differences between the radio (VLBI polarimetry) and x-ray emission (steepness of x-ray spectrum) of BL Lacs and HPQs need to be confirmed. The relationship between BL Lacs and HPQs needs to be understood if we hope to develop any successful unification scheme for AGN.

In addition to the above questions about BL Lacs, we will also use our optical polarization survey to constrain the local volume density of highly polarized white dwarfs and the fraction of radio loud quasars that are highly polarized quasars.

Finally, we end with the hope of all of us who study BL Lacertae objects. If some day we can understand these extreme examples of AGN, we might begin to understand the monsters lurking in the hearts of quasars.

APPENDIX I

POLARIMETRY AND PHOTOMETRY OF X-RAY SELECTED BL LACERTAE OBJECTS

Notes For Appendix I

In this appendix we present our polarimetry and photometry of XSBLs. The data is presented for each individual object and the objects are ordered by right ascension. For each object there can be up to three separate tables. Each table is identified by object name and a roman numeral. The roman numeral indicates the type of data presented in each table. For some objects only one or two tables are present because we were not able to obtain the appropriate data. The descriptions of the three types of tables follow below. After the descriptions of the tables, the data is presented.

Description of Three Table Types

Table I: For each object there is a table labeled Table I which contains our white light (unfiltered) polarimetry and when available *V* band photometry obtained immediately following or prior to the polarization measurement. The individual columns contain the following information: (1) UT Date of the observation, (2) the code indicating the telescope and instrument aperture (of "Two-Holer" unless otherwise noted in the Comment section) used for the polarimetry (not the photometry) observation (see Table 4.1 for explanation of the code), (3) the percent polarization corrected for both the efficiency of the instrument and statistical bias (see Chapter 4), (4) the one sigma error in the percent polarization measurement, (5) the position angle of the polarization (measured north to east this is the position angle of the electric field of the polarized radiation), (6) the

one sigma error in the position angle, (7) the V band apparent magnitude of the object on the night the polarimetry observation was made, (8) the one sigma error in the V magnitude, (9) a space for comments about the individual observations.

In the Comment column the following entrees appear (listed here with their explanations):

“UC 60”, the data was obtained with the UCSD/Minnesota 60" telescope;

“Octopol”, the data was obtained with the Octopol polarimeter and the aperture indicated in column (2) refers to an aperture of this instrument;

“Star A, (V)ISP” indicates that the polarization measurement refers to the polarization of a star in the field of the BL Lac Object (see Appendix IV for finding charts and identifications of the stars). The listed interstellar polarization measurements were made unfiltered except when noted by the presence of a V before the ISP (interstellar polarization).

“twilight” means that this observation was made during or after the beginning of 18° astronomical twilight.

Table II: For each object for which we have filtered polarimetry we include a table II. The individual columns have the following information: (1) UT Date of the observation, (2) the code indicating the telescope and instrument aperture (of “Two-Holer” unless otherwise noted in the Comment section) used for the polarimetry (not the photometry) observation (see Table 4.1 for explanation of the code), (3) the filter through which the observations were made (see Chapter

4 and table 4.2 for a description of filters), (4) the percent polarization corrected for both the efficiency of the instrument and statistical bias (see Chapter 4), (5) the one sigma error in the percent polarization measurement, (6) the position angle of the polarization (measured north to east this is the position angle of the electric field of the polarized radiation), (7) the one sigma error in the position angle, (8) the apparent magnitude of the object on the night the polarimetry observation was made, (9) the one sigma error in the magnitude, (10) a space for comments about the individual observations (see notes above for Table I).

Table III: For each object for which we have photometry we include a table III. The individual columns have the following information: (1) UT Date of the observation, (2) the code indicating the telescope and instrument aperture (of "Two-Holer" unless otherwise noted in the Comment section) used for the photometry (not the polarimetry) observation (see Table 4.1 for explanation of the code), (3) the filter through which the observation was made (see Chapter 4 and table 4.2 for a description of filters), (4) the comparison star used for the observation (see Chapter 3, Table 4.4, and Appendix IV), (5) the difference in magnitudes between the object and the comparison star, (6) the one sigma error in the magnitude difference listed in column 5, (7) the apparent magnitude of the object, (8) the one sigma error in the apparent magnitude.

Table IV: In last table of this appendix, Table IV, we list limits obtained with CCD polarimetry on the polarization of some of the objects in our monitoring

program. The columns are as follows: (1) the name of the object, (2) the UT date of the observation, (3) the two sigma limit on the B band percent polarization, (4) the polarization analyzer that was used for the observation. All observations were made using the Steward Observatory 2.3 m.

Table I: MS 0122.1+0903

UT Date	Tel-Apt	P (%)	σ_p	θ	σ_θ	m_v	σ	Comment
(1)	(2)	(3)	(4)	(5)	(6)	(7)	(8)	(9)
88.10.06	90-1	≤ 3.50						.
89.01.09	90-1	≤ 6.25				20.07	.15	
89.10.23	90-0	≤ 3.81						

Table III: MS 0122.1+0903

UT Date	Tel-Apt	Filter	Comp Star	Δm	σ	m	σ
(1)	(2)	(3)	(4)	(5)	(6)	(7)	(8)
89.01.09	90-2	V	STAR A	5.265	.154	20.07	.15

Table I: MS 0158.5+0019

UT Date (1)	Tel-Apt (2)	P (%) (3)	σ_p (4)	θ (5)	σ_θ (6)	m_v (7)	σ (8)	Comment (9)
87.11.29	90-5	≤ 2.10						Octopol
88.01.23	90-0	≤ 2.76						
88.09.16	61-0	2.85	.99	12.56	9.93			Avr 9.16, 9.17
88.09.17	61-0	6.00	1.91	45.90	9.11			
	61-0	3.03	.88	23.97	7.98			
88.09.18	61-0	≤ 3.60				18.30	.05	
88.10.06	90-1	≤ 2.60						
88.11.02	61-0	≤ 3.60						
88.11.03	61-0	≤ 2.50						
88.11.12	61-0	≤ 4.90						
89.02.04	61-0	≤ 5.50						
89.10.27	61-0	≤ 3.10				18.60	.08	
89.10.28	61-0	≤ 3.60						
89.11.03	61-0	≤ 0.46						Star A,ISP
89.11.03	61-0	≤ 0.49						Star B,ISP

Table III: MS 0158.5+0019

UT Date (1)	Tel-Apt (2)	Filter (3)	Comp Star (4)	Δm (5)	σ (6)	m (7)	σ (8)
88.09.18	61-1	V	STAR A	5.176	.048	18.30	.05
89.10.27	61-1	V	STAR A	5.480	.077	18.60	.08

Table I: MS 0205.7+3509

UT Date (1)	Tel-Apt (2)	P (%) (3)	σ_p (4)	θ (5)	σ_θ (6)	m_v (7)	σ (8)	Comment (9)
88.01.23	90-1	3.59	1.04	122.79	8.33	19.27	.07	
88.01.24	90-0	1.91	.05	115.31	.73			
88.09.18	61-0	≤ 4.00				18.38	.08	
88.10.06	90-1	2.29	1.50	117.53	18.75			
88.11.13	61-0	≤ 4.80				19.32	.07	
89.11.02	61-0	≤ 15.00						
88.01.24	90-1	1.81	.19	109.07	2.98			Star A, ISP
88.10.06	90-1	1.66	.07	117.90	1.21			Star C, ISP
88.10.06	90-1	1.68	.13	115.20	2.22			Star D, ISP

Table III: MS 0205.7+3509

UT Date (1)	Tel-Apt (2)	Filter (3)	Comp Star (4)	Δm (5)	σ (6)	m (7)	σ (8)
88.01.23	90-2	V	STAR A	4.024	.074	19.27	.07
88.09.18	61-1	V	STAR B	4.427	.078	18.38	.08
88.11.13	61-1	V	STAR A	4.072	.071	19.32	.07

Table I: MS 0257.9+3429

UT Date (1)	Tel-Apt (2)	P (%) (3)	σ_p (4)	θ (5)	σ_θ (6)	m_v (7)	σ (8)	Comment (9)
87.11.13	60-0	≤ 4.40						UC 60
88.01.23	90-1	≤ 2.10						
88.09.18	61-0	6.25	1.14	168.69	5.23	18.61	.04	
88.10.01	61-0	2.21	1.72	158.64	22.34			
88.10.07	90-1	3.03	1.18	4.18	11.16			
88.11.04	61-1	2.64	1.05	161.90	11.42	18.48	.06	
88.11.05	61-0	2.20	.74	166.24	9.62	18.42	.07	
88.11.12	61-0	3.21	1.24	153.95	11.04			
88.11.14	61-0	≤ 3.00				18.45	.08	
89.03.05	61-0	4.61	1.26	172.87	7.81			
89.03.09	61-0	≤ 3.90				18.71	.09	
89.10.23	90-0	3.40	.74	2.13	6.26			
89.10.27	61-0	≤ 5.00				18.41	.06	
88.01.23	90-1	≤ 1.40						Star A, VISP

Table III: MS 0257.9+3429

UT Date (1)	Tel-Apt (2)	Filter (3)	Comp Star (4)	Δm (5)	σ (6)	m (7)	σ (8)
88.09.18	61-1	V	STAR A	2.846	.042	18.61	.04
88.10.08	90-2	V	STAR A	2.808	.036	18.57	.04
88.11.04	61-1	V	STAR A	2.720	.064	18.48	.06
88.11.05	61-2	V	STAR A	2.658	.074	18.42	.07
88.11.14	61-2	V	STAR A	2.693	.082	18.45	.08
89.03.09	61-1	V	STAR A	2.950	.087	18.71	.09
89.10.27	61-1	V	STAR A	2.646	.058	18.41	.06

Table I: MS 0317.0+1834

UT Date (1)	Tel-Apt (2)	P (%) (3)	σ_p (4)	θ (5)	σ_θ (6)	m_v (7)	σ (8)	Comment (9)
87.09.27	60-0	3.53	1.12	134.03	9.08			UC 60
87.11.13	60-0	3.17	1.04	118.56	9.39			UC 60
88.01.23	90-1	2.88	.81	157.40	8.08			
88.01.24	90-0	4.54	.70	163.87	4.41			
88.09.18	61-0	≤ 2.80						
88.10.01	61-0	≤ 3.60						
88.10.07	90-1	5.21	.82	9.38	4.49			
88.10.08	90-0	5.20	.67	12.41	3.67			
88.11.01	61-0	2.80	1.03	7.45	10.52			
88.11.04	61-0	3.25	1.01	9.41	8.91			
88.11.12	61-0	≤ 3.30						
89.02.04	61-0	≤ 3.70						
89.03.06	61-0	3.99	1.19	154.66	8.54	18.13	.06	
89.10.29	61-0	3.81	.84	27.12	6.33			
89.11.28	61-4	5.19	1.27	169.96	7.03			Octopol
90.02.18	61-0	3.76	1.05	172.09	8.00			
88.01.23	90-1	.50	0.12	133.40	7.00			Star A, VISP

Table III: MS 0317.0+1834

UT Date (1)	Tel-Apt (2)	Filter (3)	Comp Star (4)	Δm (5)	σ (6)	m (7)	σ (8)
89.03.06	61-1	V	STAR A	6.271	.062	18.13	.06

Table I: H 0323+022

UT Date (1)	Tel-Apt (2)	P (%) (3)	σ_p (4)	θ (5)	σ_θ (6)	m_v (7)	σ (8)	Comment (9)
87.09.27	60-0	2.00	.39	169.05	5.63			UC 60
87.09.28	60-0	$\leq .86$				16.41	.03	UC 60
87.09.29	60-1	1.47	.24	116.02	4.62	16.40	.03	UC 60
87.11.10	60-1	2.68	.53	154.71	5.72			UC 60
87.11.11	60-0	3.00	.47	178.28	4.45	16.59	.04	UC 60
87.11.12	60-0	3.10	.45	11.24	4.13			UC 60
87.11.13	60-0	3.42	.42	6.99	3.55			UC 60
87.11.29	90-5	5.38	.41	24.00	2.20			Octopol
87.12.11	60-0	4.11	.65	10.42	4.53			UC 60
88.01.23	90-1	3.25	.40	1.67	3.52	16.66	.01	
88.01.24	90-1	4.71	.32	6.48	1.96	16.69	.01	
88.09.18	61-0	7.13	1.15	172.48	4.62	16.67	.02	
88.10.01	61-0	5.44	.59	.04	3.11	16.69	.04	
88.10.07	90-0	10.37	1.03	9.69	2.84			
88.10.08	90-1	5.94	.39	1.03	1.87	16.75	.01	
88.10.31	61-0	6.20	.74	176.90	3.40	16.71	.04	
88.11.02	61-0	6.34	.85	178.61	3.83			
88.11.04	61-0	5.07	.52	165.04	2.94	16.69	.03	
88.11.12	61-0	4.58	.64	3.96	4.02			
88.11.13	61-0	4.54	.49	178.41	3.12	16.67	.04	
89.01.08	90-0	5.29	.47	175.30	2.53			
89.01.09	90-1	4.19	.35	168.27	2.40	16.73	.01	
89.02.03	61-0	4.49	.86	169.10	5.47	17.03	.02	
89.02.04	61-0	4.89	.87	173.07	5.09	16.72	.04	
89.03.06	61-0	4.07	.64	172.50	4.51	16.72	.06	
89.03.08	61-0	4.05	.63	169.53	4.43	16.80	.03	
89.03.10	61-0	3.94	.79	159.00	5.73	16.77	.02	
89.09.05	61-0	8.27	.71	171.27	2.45	16.42	.04	
89.10.27	61-0	6.46	.42	172.30	1.88	16.54	.05	
89.10.29	61-0	6.57	.66	166.78	2.87	16.61	.02	
89.11.02	61-0	4.55	.48	165.67	3.04			
89.11.23	61-4	7.98	.96	169.80	3.43			Octopol
89.11.28	61-5	9.38	.75	167.86	2.30			Octopol
90.02.21	61-0	10.01	.63	164.29	1.80	16.23	.03	
88.01.24	90-2	≤ 0.25						Star A, VISP

Table II: H 0323+022

UT Date (1)	Tel-Apt (2)	Fil (3)	P (%) (4)	σ_p (5)	θ (6)	σ_θ (7)	m (8)	σ (9)	Comment (10)
87.09.14	60-0	B	8.23	1.41	2.10	4.93			UC 60
	60-0	R	4.99	.77	11.03	4.39			UC 60
87.09.15	60-0	B	4.19	1.20	16.27	8.23	16.90	.09	UC 60
	60-0	V	5.38	.89	16.31	4.72	16.31	.06	UC 60
	60-0	R	4.50	.71	10.58	4.49	15.91	.05	UC 60
	60-0	I	3.22	.75	7.53	6.68	15.26	.05	UC 60
87.09.16	60-0	B	3.44	1.03	21.37	8.61			UC 60
88.01.24	90-1	B	4.64	.75	15.15	4.60			
	90-1	V	5.96	.69	3.10	3.30	16.69	.01	
	90-1	R	4.08	.56	.68	3.96			
	90-1	I	3.71	.78	1.01	6.05			
88.10.07	90-1	U	10.48	4.42	.33	12.09			
	90-1	B	10.45	1.04	8.23	2.85			
	90-1	V	8.51	.87	4.94	2.91			
	90-1	R	8.49	.90	7.40	3.04			
	90-1	I	7.06	.91	12.54	3.70			
88.10.31	61-0	B	4.93	1.12	177.04	6.52			
	61-0	I	5.79	.89	3.91	4.40			
88.11.14	61-0	V	5.01	1.25	6.09	7.15			
89.10.29	61-0	B	6.55	1.26	169.73	5.53			
	61-0	I	4.99	.93	163.12	5.37			
89.11.28	61-5	B	10.03	.92	168.49	2.61			Octopol
90.02.21	61-0	B	9.73	1.10	162.00	3.24			
	61-0	V	13.15	.98	158.44	2.14	16.23	.03	
	61-0	R	10.78	.83	164.38	2.22			
	61-0	I	9.98	1.06	168.68	3.04			

Table III: H 0323+022

UT Date (1)	Tel-Apt (2)	Filter (3)	Comp Star (4)	Δ m (5)	σ (6)	m (7)	σ (8)
87.09.15	60-2	U	STAR A	2.142	.135	16.54	.13
	60-2	B	STAR A	3.096	.093	16.90	.09
	60-2	V	STAR A	3.465	.060	16.31	.06
	60-2	R	STAR A	3.592	.051	15.91	.05
	60-2	I	STAR A	3.426	.052	15.26	.05
87.09.28	60-2	U	STAR A	1.989	.047	16.39	.05
	60-2	B	STAR A	3.173	.027	16.97	.03
	60-2	V	STAR A	3.567	.028	16.41	.03
	60-2	R	STAR A	3.615	.024	15.93	.02
	60-2	I	STAR A	3.592	.024	15.42	.02
	60-2	U	STAR B	1.384	.049	16.32	.05
	60-2	B	STAR B	1.982	.028	16.95	.03
	60-2	V	STAR B	1.984	.029	16.38	.03
	60-2	R	STAR B	1.910	.025	15.93	.03
	60-2	I	STAR B	1.791	.026	15.40	.03
	60-2	U	STAR C	2.525	.046		
	60-2	B	STAR C	3.185	.027		
	60-2	V	STAR C	3.227	.028		
	60-2	R	STAR C	3.152	.024		
	60-2	I	STAR C	2.977	.024		
87.09.29	60-2	U	STAR A	1.994	.049	16.39	.05
	60-2	B	STAR A	3.136	.027	16.94	.03
	60-2	V	STAR A	3.574	.027	16.41	.03
	60-2	R	STAR A	3.615	.023	15.93	.02
	60-2	I	STAR A	3.617	.027	15.45	.03
	60-2	U	STAR B	1.434	.052	16.37	.05
	60-2	B	STAR B	1.920	.029	16.89	.03
	60-2	V	STAR B	2.004	.029	16.40	.03
	60-2	R	STAR B	1.921	.025	15.94	.03
	60-2	I	STAR B	1.832	.029	15.44	.03
	60-2	U	STAR C	2.535	.049		
	60-2	B	STAR C	3.130	.028		
	60-2	V	STAR C	3.232	.027		
	60-2	R	STAR C	3.142	.023		
	60-2	I	STAR C	3.047	.027		

Table III continued: H 0323+022

UT Date (1)	Tel-Apt (2)	Filter (3)	Comp Star (4)	Δ m (5)	σ (6)	m (7)	σ (8)
87.11.11	60-2	U	STAR A	2.374	.077	16.77	.08
	60-2	B	STAR A	3.537	.055	17.34	.06
	60-2	V	STAR A	3.786	.034	16.63	.03
	60-2	R	STAR A	3.871	.028	16.19	.03
	60-2	I	STAR A	3.773	.029	15.60	.03
	60-2	U	STAR B	1.800	.079	16.74	.08
	60-2	B	STAR B	2.321	.056	17.29	.06
	60-2	V	STAR B	2.193	.036	16.59	.04
	60-2	R	STAR B	2.143	.029	16.16	.03
	60-2	I	STAR B	1.961	.030	15.57	.03
88.01.23	90-2	V	STAR A	3.825	.012	16.66	.01
88.01.24	90-2	V	STAR A	3.848	.014	16.69	.01
88.09.18	61-1	V	STAR A	3.834	.017	16.67	.02
88.10.01	61-2	V	STAR A	3.854	.035	16.69	.04
88.10.08	90-2	V	STAR A	3.911	.013	16.75	.01
88.10.31	61-2	V	STAR A	3.871	.037	16.71	.04
88.11.04	61-2	V	STAR A	3.855	.030	16.69	.03
88.11.13	61-1	V	STAR A	3.833	.040	16.67	.04
89.01.09	90-2	V	STAR A	3.887	.012	16.73	.01
89.02.03	61-1	V	STAR A	4.190	.022	17.03	.02
89.02.04	61-2	V	STAR A	3.880	.037	16.72	.04
89.03.06	61-2	V	STAR A	3.883	.056	16.72	.06
89.03.08	61-1	V	STAR A	3.962	.028	16.80	.03
89.03.10	61-1	V	STAR A	3.932	.024	16.77	.02
89.09.05	61-2	V	STAR A	3.629	.042	16.47	.04
89.09.05	61-2	V	STAR B	2.018	.043	16.42	.04
89.10.27	61-2	V	STAR A	3.696	.049	16.54	.05
89.10.29	61-1	V	STAR A	3.769	.019	16.61	.02
90.02.21	61-2	V	STAR A	3.293	.019	16.13	.02
	61-2	V	STAR A	3.392	.028	16.23	.03

Table I: MS 0419.3+1943

UT Date (1)	Tel-Apt (2)	P (%) (3)	σ_p (4)	θ (5)	σ_θ (6)	m_v (7)	σ (8)	Comment (9)
88.10.06	90-1	3.66	1.19	63.00	9.37			
88.10.06	90-1	2.90	.08	69.48	.79			Star A, ISP

Table I: 1E 0514+064

UT Date (1)	Tel-Apt (2)	P (%) (3)	σ_p (4)	θ (5)	σ_θ (6)	m_v (7)	σ (8)	Comment (9)
88.01.23	90-1	≤ 2.50				18.35	.06	
88.01.24	90-0	≤ 3.46						
	90-0	≤ 2.10						Avr1.23,1.24
88.09.18	61-0	≤ 5.00				19.03	.11	
88.10.06	90-1	≤ 3.80						
88.10.08	90-1	≤ 3.50				19.00	.06	
88.11.04	61-0	6.91	2.16	165.48	8.95	19.01	.09	
88.11.05	61-1	4.82	2.77	139.87	16.42	19.25	.09	
	61-1	5.80	1.70	157.61	8.40	19.25	.09	Avr11.04,.05
88.11.11	61-0	≤ 5.60						
89.03.08	61-0	≤ 4.26				18.98	.06	
89.03.10	61-0	≤ 5.00						
	61-0	≤ 2.70						Avr3.08,3.10
89.04.01	61-0	5.96	2.87	91.38	13.80			
89.10.23	90-0	≤ 4.36						
89.11.02	61-0	4.54	2.22	153.19	14.04			twilight
89.11.03	61-0	≤ 7.70						
88.01.23	90-1	≤ 0.50						Star A,VISP

Table III: 1E 0514+064

UT Date (1)	Tel-Apt (2)	Filter (3)	Comp Star (4)	Δ m (5)	σ (6)	m (7)	σ (8)
88.01.23	90-2	V	STAR A	5.114	.061	18.35	.06
88.09.18	61-1	V	STAR A	5.789	.114	19.03	.11
88.10.08	90-2	V	STAR A	5.756	.058	19.00	.06
88.11.04	61-1	V	STAR A	5.768	.086	19.01	.09
88.11.05	61-1	V	STAR A	6.012	.089	19.25	.09
89.03.08	61-1	V	STAR A	5.743	.064	18.98	.06

Table I: H 0548-322

UT Date (1)	Tel-Apt (2)	P (%) (3)	σ_p (4)	θ (5)	σ_θ (6)	m_v (7)	σ (8)	Comment (9)
87.11.11	60-1	1.78	.39	177.44	6.26	15.57	.01	UC 60
87.11.12	60-1	1.52	.36	15.07	6.76			UC 60
87.11.13	60-1	2.33	.42	5.03	5.19			UC 60
87.11.28	90-5	2.34	.30	31.90	3.70			Octopol
87.12.10	60-0	≤ 4.00						UC 60
88.01.23	90-1	2.24	.32	34.44	4.04	15.79	.01	
88.01.24	90-1	2.97	.40	35.98	3.91			
88.10.01	61-0	2.53	.50	1.66	5.64			
88.10.07	90-1	2.02	.41	6.64	5.75			
88.10.31	61-0	3.21	.70	4.29	6.20	15.54	.02	
88.11.11	61-0	1.47	.45	167.95	8.69			
89.01.09	90-1	1.41	.33	9.35	6.73	15.48	.01	
89.03.07	61-0	1.58	.39	8.12	7.02	15.57	.02	
89.03.09	61-0	≤ 3.50						
89.04.03	61-0	≤ 4.22						
89.10.28	61-0	1.41	.33	14.18	6.62	16.13	.01	
89.11.28	61-5	1.72	.44	23.71	7.27			Octopol
87.11.12	60-1	≤ 0.54						Star A, ISP
88.01.23	90-1	≤ 0.90						Star A, VISP
88.10.31	61-1	≤ 0.34						Star B, ISP

Table II: H 0548-322

UT Date (1)	Tel-Apt (2)	Fil (3)	P (%) (4)	σ_p (5)	θ (6)	σ_θ (7)	m (8)	σ (9)	Comment (10)
88.01.24	90-1	B	3.32	.82	32.08	7.08			
	90-1	V	2.62	.51	29.86	5.56			
	90-1	R	3.48	.46	22.34	3.82			
	90-1	I	2.16	.46	16.43	6.11			
88.10.07	90-1	B	≤ 5.68						
	90-1	I	≤ 3.67						

Table III: H 0548-322

UT Date (1)	Tel-Apt (2)	Filter (3)	Comp Star (4)	Δ m (5)	σ (6)	m (7)	σ (8)
87.11.11	60-2	V	STAR A	2.208	.014	15.57	.01
88.01.23	90-2	V	STAR A	2.435	.007	15.79	.01
88.10.31	61-2	V	STAR A	2.178	.019	15.54	.02
89.01.09	90-3	V	STAR A	2.122	.010	15.48	.01
89.03.07	61-2	V	STAR A	2.211	.022	15.57	.02
89.10.28	61-1	V	STAR A	2.770	.010	16.13	.01

Table I: MS 0607.9+7108

UT Date (1)	Tel-Apt (2)	P (%) (3)	σ_p (4)	θ (5)	σ_θ (6)	m_v (7)	σ (8)	Comment (9)
88.10.07	90-0	≤ 1.53						
88.10.08	90-1	≤ 1.46						
89.01.08	90-0	≤ 5.40						
89.10.23	90-0	4.82	.67	179.03	4.00			
89.10.23	90-0	0.88	.20	124.53	6.62			Star A, ISP

Table I: MS 0737.9+7441

UT Date (1)	Tel-Apt (2)	P (%) (3)	σ_p (4)	θ (5)	σ_θ (6)	m_v (7)	σ (8)	Comment (9)
88.10.07	90-1	2.35	.50	174.81	6.04			
88.10.08	90-1	1.78	.47	172.85	7.50			
89.01.09	90-1	2.70	.29	148.21	3.12	17.06	.02	
89.10.23	90-0	2.74	.50	160.81	5.24			
88.10.07	90-1	$\leq .20$						Star A, ISP
88.10.07	90-1	$\leq .50$						Star B, ISP
89.10.23	90-0	$\leq .47$						Star C, ISP

Table III: MS 0737.9+7441

UT Date (1)	Tel-Apt (2)	Filter (3)	Comp Star (4)	Δm (5)	σ (6)	m (7)	σ (8)
89.01.09	90-3	V	STAR B	2.834	.022	17.06	.02

Table I: MS 0922.9+7459

UT Date (1)	Tel-Apt (2)	P (%) (3)	σ_p (4)	θ (5)	σ_θ (6)	m_v (7)	σ (8)	Comment (9)
88.01.23	90-1	≤ 6.00				20.02	.11	
88.01.24	90-1	≤ 5.30						
	90-1	≤ 3.90						Avr 1.23, 1.24
88.01.23	90-1	≤ 0.13						Star A, VISP

Table III: MS 0922.9+7459

UT Date (1)	Tel-Apt (2)	Filter (3)	Comp Star (4)	Δ m (5)	σ (6)	m (7)	σ (8)
88.01.23	90-2	V	STAR A	7.326	.108	20.02	.11

Table I: MS 0950.9+4929

UT Date (1)	Tel-Apt (2)	P (%) (3)	σ_p (4)	θ (5)	σ_θ (6)	m_v (7)	σ (8)	Comment (9)
88.03.22	61-0	≤ 5.08						
89.01.09	90-1	4.27	.56	73.90	3.76	18.45	.04	
89.02.04	61-0	≤ 5.50						
89.03.08	61-0	3.07	.79	71.06	7.42	18.71	.04	
89.04.01	61-0	5.19	1.03	118.31	5.69	18.82	.07	
89.04.07	61-0	4.83	1.03	130.37	6.11	18.85	.07	
90.02.18	61-0	≤ 4.70						
88.01.23	90-1	≤ 0.40						Star A, VISP

Table III: MS 0950.9+4929

UT Date (1)	Tel-Apt (2)	Filter (3)	Comp Star (4)	Δ m (5)	σ (6)	m (7)	σ (8)
89.01.09	90-3	V	STAR A	5.401	.042	18.45	.04
89.03.08	61-1	V	STAR A	5.663	.038	18.71	.04
89.04.01	61-1	V	STAR A	5.775	.065	18.82	.07
89.04.07	61-1	V	STAR A	5.801	.069	18.85	.07

Table I: H 1101-232

UT Date (1)	Tel-Apt (2)	P (%) (3)	σ_p (4)	θ (5)	σ_θ (6)	m_v (7)	σ (8)	Comment (9)
89.04.08	61-0	1.33	.42	57.78	8.94	18.35	.02	
90.03.17	60-1	≤ 2.70						
89.04.08	61-1	≤ 0.71						Star A, VISP

Table III: H 1101-232

UT Date (1)	Tel-Apt (2)	Filter (3)	Comp Star (4)	Δm (5)	σ (6)	m (7)	σ (8)
89.04.08	61-1	V	STAR A	4.263	.021	18.35	.02

Table I: MS 1207.9+3945

UT Date (1)	Tel-Apt (2)	P (%) (3)	σ_p (4)	θ (5)	σ_θ (6)	m_v (7)	σ (8)	Comment (9)
88.06.07	90-1	≤ 4.00						

Table I: H 1219+305

UT Date (1)	Tel-Apt (2)	P (%) (3)	σ_p (4)	θ (5)	σ_θ (6)	m_v (7)	σ (8)	Comment (9)
87.11.11	60-0	5.73	.32	4.17	1.60			UC 60
87.11.12	60-1	5.02	.35	7.21	2.00	15.90	.02	UC 60
88.01.23	90-1	3.55	.23	29.92	1.82	15.98	.01	
88.01.24	90-1	3.03	.27	31.42	2.59			
88.03.22	61-0	2.24	.13	25.52	1.66			
88.03.23	61-0	3.49	.26	21.40	2.15	15.66	.02	
88.03.24	61-0	3.30	.24	22.96	2.12	15.70	.02	
88.03.25	61-0	3.53	.20	22.74	1.61			
88.03.27	61-0	4.02	.30	30.28	2.12			
88.03.28	61-0	5.23	.39	37.90	2.14			
88.05.17	90-4	2.69	.23	46.60	2.40			Octopol
88.06.06	90-1	1.27	.18	133.12	4.15			
88.06.07	90-1	≤ 0.92						
89.01.09	90-1	2.65	.29	95.43	3.17	16.22	.02	
89.02.03	61-0	≤ 1.80				16.48	.01	
89.02.04	61-0	2.14	.41	40.47	5.48	16.19	.02	
89.03.05	61-0	1.97	.30	152.91	4.38			
89.03.07	61-1	1.77	.37	133.89	6.05	16.19	.03	
89.03.09	61-0	2.53	.29	148.81	3.24	16.30	.02	
89.03.10	61-0	2.34	.29	143.54	3.59	16.34	.01	
89.04.01	61-0	1.91	.46	93.22	6.88	16.43	.03	
89.04.03	61-0	≤ 1.30						
89.04.07	61-0	≤ 0.99				16.46	.02	
89.04.09	61-0	≤ 2.88						
89.06.04	61-0	≤ 1.35				16.29	.02	
89.06.22	61-0	≤ 1.40						
89.07.04	61-0	1.72	.54	17.13	9.00			
89.11.28	61-5	1.53	.40	166.61	7.46			Octopol
90.02.18	61-0	4.33	.61	118.85	4.03	16.46	.02	
90.02.21	61-0	6.83	.70	120.87	2.94			
90.03.16	60-1	4.92	.43	132.20	2.48	15.30	.01	
89.01.08	90-1	≤ 0.20						Star A, ISP

Table II: H 1219+305

UT Date (1)	Tel-Apt (2)	Fil (3)	P (%) (4)	σ_p (5)	θ (6)	σ_θ (7)	m (8)	σ (9)	Comment (10)
88.01.23	90-1	U	4.23	.66	32.36	4.49			
	90-1	B	4.61	.52	30.42	3.26			
	90-1	V	4.22	.46	24.35	3.14	15.98	.01	
	90-1	R	3.95	.37	27.12	2.66			
	90-1	I	3.09	.47	28.18	4.38			
88.01.24	90-1	B	4.09	.44	35.30	3.07			
	90-1	I	3.62	.38	28.93	2.97			
88.03.22	61-0	B	3.55	.42	27.04	3.42			
	61-0	I	3.59	.66	13.51	5.26			
88.03.23	61-0	R	2.71	.47	22.22	4.98			
88.03.24	61-0	U	3.73	.50	25.36	3.86			
	61-0	I	3.11	.46	18.38	4.20			
88.06.06	90-1	B	≤ 1.89						
	90-1	V	2.06	.52	133.94	7.23			
	90-0	R	1.32	.51	135.90	11.11			
	90-1	I	0.56	.41	140.92	20.89			

Table III: H 1219+305

UT Date (1)	Tel-Apt (2)	Filter (3)	Comp Star (4)	Δ m (5)	σ (6)	m (7)	σ (8)
87.11.12	60-2	V	STAR A	3.426	.024	15.90	.02
88.01.23	90-2	V	STAR A	3.512	.008	15.98	.01
88.03.23	61-2	V	STAR A	3.193	.018	15.66	.02
88.03.24	61-2	V	STAR A	3.233	.016	15.70	.02
88.03.26	61-2	U	STAR A	2.150	.030	15.31	.03
88.03.26	61-2	B	STAR A	2.870	.030	16.00	.03
88.03.26	61-2	V	STAR A	3.180	.020	15.65	.02
88.03.26	61-2	R	STAR A	3.160	.020	15.27	.02
88.03.26	61-2	I	STAR A	3.080	.030	14.85	.03
89.01.09	90-3	V	STAR A	3.750	.015	16.22	.02
89.02.03	61-1	V	STAR A	4.014	.010	16.48	.01
89.02.04	61-2	V	STAR A	3.721	.020	16.19	.02
89.03.07	61-2	V	STAR A	3.717	.026	16.19	.03
89.03.09	61-1	V	STAR A	3.827	.024	16.30	.02
89.03.10	61-1	V	STAR A	3.865	.011	16.34	.01
89.04.01	61-2	V	STAR A	3.955	.033	16.43	.03
89.04.07	61-1	V	STAR A	3.986	.017	16.46	.02
89.06.04	61-1	V	STAR A	3.818	.017	16.29	.02
90.02.18	61-2	V	STAR A	3.989	.023	16.46	.02
90.03.16	60-2	V	STAR A	2.735	.009	15.20	.01
90.03.16	60-2	V	STAR B	1.293	.011	15.30	.01

Table I: MS 1221.8+2452

UT Date (1)	Tel-Apt (2)	P (%) (3)	σ_p (4)	θ (5)	σ_θ (6)	m_v (7)	σ (8)	Comment (9)
88.01.23	90-1	2.08	.28	80.71	3.85	17.33	.02	
88.01.24	90-1	1.69	.37	86.53	6.24			
88.03.22	61-0	8.09	.80	65.87	2.82			
88.03.23	61-0	7.13	.56	60.02	2.25	17.38	.06	
88.03.24	61-0	8.18	.50	57.88	1.76	17.44	.05	
88.03.25	61-0	7.14	.42	64.81	1.67	17.45	.06	
88.03.28	61-0	10.44	1.03	65.53	2.84			
88.06.07	90-1	3.93	.57	43.74	4.12	17.61	.02	
89.02.03	61-0	4.66	.73	9.75	4.52	17.46	.02	
89.02.04	61-0	3.73	.81	.09	6.24	17.25	.04	
89.03.05	61-0	12.30	.97	43.01	2.25			
89.03.06	61-0	10.05	.57	44.91	1.63	17.55	.02	
89.03.07	61-0	10.30	.47	43.13	1.29	17.49	.05	
89.03.09	61-0	11.42	.88	39.86	2.20	17.47	.03	
89.03.10	61-0	9.22	.94	38.56	2.93	17.76	.02	
89.04.01	61-0	11.86	.61	47.53	1.46	17.34	.05	
89.04.03	61-0	10.59	.68	48.23	1.83			
89.04.09	61-0	10.81	.87	47.18	2.31	17.62	.03	
90.02.19	61-0	5.57	1.09	37.26	5.60			
90.02.21	61-0	7.58	1.79	30.44	6.77			
90.03.16	60-1	5.47	1.17	59.24	6.12	18.17	.09	
88.01.23	90-1	≤ 0.6						Star A, VISP

Table II: MS 1221.8+2452

UT Date (1)	Tel-Apt (2)	Fil (3)	P (%) (4)	σ_p (5)	θ (6)	σ_θ (7)	m (8)	σ (9)	Comment (10)
88.03.22	61-0	B	9.17	1.19	61.39	3.73			
	61-0	I	7.56	1.45	67.72	5.49			
89.03.06	61-0	B	12.16	1.83	57.86	4.32			
	61-0	V	14.79	1.66	45.09	3.22	17.55	.02	
	61-0	R	12.16	1.46	44.65	3.45			
	61-0	I	8.11	1.33	46.73	4.71			
89.03.09	61-0	B	12.04	1.48	38.61	3.52			
	61-0	I	7.90	1.44	30.47	5.20			
89.04.01	61-0	B	14.26	1.13	45.13	2.26			
	61-0	I	10.06	1.07	47.06	3.05			

Table III: MS 1221.8+2452

UT Date (1)	Tel-Apt (2)	Filter (3)	Comp Star (4)	Δ m (5)	σ (6)	m (7)	σ (8)
88.01.23	90-2	V	STAR A	3.957	.016	17.33	.02
88.03.23	61-2	V	STAR A	4.010	.055	17.38	.06
88.03.24	61-2	V	STAR A	4.075	.046	17.44	.05
88.03.25	61-2	V	STAR A	4.082	.057	17.45	.06
88.03.26	61-2	U	STAR A	3.210	.090	17.26	.09
	61-2	B	STAR A	3.950	.120	17.93	.12
	61-2	V	STAR A	4.000	.080	17.37	.08
	61-2	R	STAR A	4.140	.080	17.16	.08
	61-2	I	STAR A	3.810	.080	16.48	.08
88.06.07	90-2	V	STAR A	4.241	.022	17.61	.02
89.02.03	61-1	V	STAR A	4.093	.023	17.46	.02
89.02.04	61-2	V	STAR A	3.876	.035	17.25	.04
89.03.06	61-1	V	STAR A	4.190	.020	17.56	.02
	61-1	V	STAR B	3.036	.021	17.55	.02
89.03.07	61-2	U	STAR A	3.376	.071	17.43	.07
	61-2	B	STAR A	3.951	.038	17.93	.04
	61-2	V	STAR A	4.121	.045	17.49	.05
	61-2	R	STAR A	4.044	.040	17.06	.04
	61-2	I	STAR A	3.865	.051	16.53	.05
89.03.09	61-1	V	STAR B	2.956	.026	17.47	.03
89.03.10	61-1	V	STAR A	4.387	.020	17.76	.02
89.04.01	61-2	V	STAR A	3.967	.047	17.34	.05
89.04.09	61-1	V	STAR A	4.245	.030	17.62	.03
90.03.16	60-2	V	STAR A	4.796	.084	18.17	.08
	60-2	V	STAR B	3.657	.086	18.17	.09

Table I: MS 1229.2+6430

UT Date (1)	Tel-Apt (2)	P (%) (3)	σ_p (4)	θ (5)	σ_θ (6)	m_v (7)	σ (8)	Comment (9)
88.01.23	90-1	≤ 1.04				17.47	.02	
88.01.24	90-1	≤ 1.40						
88.06.08	90-1	≤ 1.84				17.41	.02	
89.01.08	90-1	2.28	.35	30.79	4.41			
89.07.02	90-1	≤ 1.76						
90.02.16	90-0	≤ 1.20						
89.01.08	90-1	≤ 0.20						Star A, ISP
89.01.08	90-1	≤ 0.49						GAL X, ISP

Table III: MS 1229.2+6430

UT Date (1)	Tel-Apt (2)	Filter (3)	Comp Star (4)	Δm (5)	σ (6)	m (7)	σ (8)
88.01.23	90-2	V	STAR A	3.111	.013	17.47	.02
88.06.08	90-2	V	STAR A	3.052	.014	17.41	.02

Table I: MS 1235.4+6315

UT Date (1)	Tel-Apt (2)	P (%) (3)	σ_p (4)	θ (5)	σ_θ (6)	m_v (7)	σ (8)	Comment (9)
88.01.23	90-1	≤ 2.60						
88.01.24	90-1	≤ 2.80						
88.06.08	90-1	2.62	.98	134.28	10.73	18.83	.05	
89.01.09	90-1	≤ 4.00				18.53	.05	
89.07.02	90-1	≤ 3.02						
88.01.24	90-1	.17	.08	94.53	13.71			Star A, ISP

Table III: MS 1235.4+6315

UT Date (1)	Tel-Apt (2)	Filter (3)	Comp Star (4)	Δ m (5)	σ (6)	m (7)	σ (8)
88.06.08	90-2	V	STAR A	5.667	.051	18.83	.05
89.01.09	90-3	V	STAR A	5.367	.045	18.53	.05

Table I: MS 1402.3+0416

UT Date (1)	Tel-Apt (2)	P (%) (3)	σ_p (4)	θ (5)	σ_θ (6)	m_v (7)	σ (8)	Comment (9)
88.01.23	90-1	5.79	.50	35.39	2.45	16.84	.02	
88.01.24	90-1	2.72	.33	53.22	3.50			
88.03.22	61-0	3.16	.48	94.46	4.39			
88.03.23	61-0	3.30	.51	120.42	4.42	16.81	.02	
88.03.24	61-0	5.55	.33	102.08	1.69	16.74	.03	
88.03.25	61-0	3.07	.41	96.11	3.86	16.85	.04	
88.03.28	61-0	4.57	.71	81.72	4.42			
88.06.08	90-1	9.52	.44	79.44	1.31	17.14	.02	
89.02.03	61-0	2.04	.61	130.47	8.54	17.30	.02	
89.02.04	61-0	3.89	.73	115.36	5.40	16.93	.03	
89.03.05	61-0	2.85	.38	96.74	3.80			
89.03.08	61-0	5.13	.45	106.88	2.49	16.61	.03	
89.03.10	61-0	6.78	.32	88.88	1.36	16.46	.02	
89.04.01	61-0	6.96	.38	99.97	1.58	16.75	.04	
89.04.03	61-0	8.50	.64	90.21	2.15			
89.04.09	61-0	1.84	.41	117.62	6.38	16.84	.02	
89.06.04	61-0	7.44	.79	100.07	3.05	16.79	.02	
89.07.04	61-0	7.09	.84	90.98	3.38			
90.02.18	61-0	8.55	.82	144.83	2.75	17.07	.05	
88.01.23	90-1	≤ 0.90						Star A, ISP

Table II: MS 1402.3+0416

UT Date (1)	Tel-Apt (2)	Fil (3)	P (%) (4)	σ_p (5)	θ (6)	σ_θ (7)	m (8)	σ (9)	Comment (10)
88.03.23	61-0	B	4.09	.77	119.73	5.40			
88.06.08	90-1	B	11.40	1.10	79.68	2.76			
	90-1	V	7.84	2.11	82.94	7.73	17.14	.02	
	90-1	I	7.92	.60	78.96	2.16			
89.03.08	61-0	B	5.06	.78	98.25	4.39	16.93	.03	
	61-0	R	5.02	.73	103.48	4.14	16.24	.03	
89.03.10	61-0	U	8.33	1.05	90.85	3.60			
	61-0	B	7.29	.60	89.96	2.35			
	61-0	V	7.49	1.07	93.55	4.07	16.46	.02	
	61-0	R	6.53	.59	84.44	2.57			
	61-0	I	6.51	.60	89.13	2.65			
89.04.03	61-0	B	9.20	.99	94.31	3.09			
	61-0	R	9.43	.82	93.08	2.50			
89.07.04	61-0	B	5.56	1.42	96.36	7.31			
	61-0	I	4.46	1.31	88.83	8.39			

Table III: MS 1402.3+0416

UT Date (1)	Tel-Apt (2)	Filter (3)	Comp Star (4)	Δ m (5)	σ (6)	m (7)	σ (8)
88.01.23	90-2	V	STAR A	1.936	.013	16.84	.02
88.03.23	61-2	V	STAR A	1.913	.024	16.81	.02
88.03.24	61-2	V	STAR A	1.838	.028	16.74	.03
88.03.25	61-2	V	STAR A	1.947	.035	16.85	.04
88.06.08	90-2	V	STAR A	2.242	.016	17.14	.02
89.02.03	61-1	V	STAR A	2.401	.024	17.30	.02
89.02.04	61-2	V	STAR A	2.029	.032	16.93	.03
89.03.08	61-2	U	STAR A	.803	.038	16.22	.04
	61-2	B	STAR A	1.470	.028	16.93	.03
	61-2	V	STAR A	1.713	.029	16.61	.03
	61-2	R	STAR A	1.647	.032	16.24	.03
	61-2	I	STAR A	1.551	.035	15.77	.04
89.03.10	61-1	V	STAR A	1.557	.011	16.46	.02
89.04.01	61-2	V	STAR A	1.851	.036	16.75	.04
89.04.09	61-1	V	STAR A	1.936	.019	16.84	.02
89.06.04	61-1	V	STAR A	1.893	.020	16.79	.02
90.02.18	61-2	V	STAR A	2.168	.053	17.07	.05

Table I: MS 1407.9+5954

UT Date (1)	Tel-Apt (2)	P (%) (3)	σ_p (4)	θ (5)	σ_θ (6)	m_v (7)	σ (8)	Comment (9)
88.01.24	90-1	≤ 6.50						
88.06.08	90-1	8.64	1.80	83.28	5.98	19.36	.09	
89.03.07	61-0	≤ 6.40						
89.04.01	61-0	≤ 5.47				19.34	.11	
89.07.02	90-1	4.54	1.69	80.42	10.68			

Table III: MS 1407.9+5954

UT Date (1)	Tel-Apt (2)	Filter (3)	Comp Star (4)	Δm (5)	σ (6)	m (7)	σ (8)
88.06.08	90-2	V	STAR A	4.664	.092	19.36	.09
89.04.01	61-1	V	STAR A	4.644	.108	19.34	.11

Table I: 1E 1415.6+2557

UT Date (1)	Tel-Apt (2)	P (%) (3)	σ_p (4)	θ (5)	σ_θ (6)	m_v (7)	σ (8)	Comment (9)
88.01.23	90-1	5.73	.46	10.47	2.29	16.69	.02	
88.01.24	90-1	5.43	.43	8.35	2.27			
88.03.22	61-0	5.74	.59	22.52	2.96			
88.03.23	61-0	4.81	.44	23.45	2.60	16.84	.03	
88.03.24	61-0	5.68	.43	16.54	2.15	16.80	.03	
88.03.28	61-0	4.45	1.14	4.64	7.31			
88.05.17	90-4	3.42	.54	28.70	4.60			Octopol
88.06.07	90-1	5.48	.33	32.59	1.70	16.78	.01	
89.02.04	61-0	6.84	.76	6.10	3.20	16.71	.02	
89.03.07	61-0	7.26	.65	20.76	2.57	16.79	.03	
89.03.10	61-0	5.89	.66	23.55	3.20	16.82	.03	
89.04.03	61-0	6.74	.81	19.11	3.43			
89.04.09	61-0	7.53	.74	14.31	2.82	17.08	.02	
89.06.04	61-0	5.98	.83	22.74	3.97	16.95	.02	
89.07.05	61-0	5.85	.91	21.01	4.48	16.97	.02	
90.02.16	90-0	4.89	.78	22.65	4.54			
90.02.21	61-0	3.94	.64	24.73	4.64			
88.01.23	90-1	≤ 0.80						Star A, ISP

Table II: 1E 1415.6+2557

UT Date (1)	Tel-Apt (2)	Fil (3)	P (%) (4)	σ_p (5)	θ (6)	σ_θ (7)	m (8)	σ (9)	Comment (10)
88.01.24	90-1	B	8.57	.93	4.34	3.11			
	90-1	I	4.23	.86	8.51	5.83			
88.06.07	90-1	B	7.67	.64	26.90	2.37			
	90-1	R	5.36	.54	31.01	2.86			
	90-1	I	3.85	.59	26.34	4.43			

Table III: 1E 1415.6+2557

UT Date (1)	Tel-Apt (2)	Filter (3)	Comp Star (4)	Δ m (5)	σ (6)	m (7)	σ (8)
88.01.23	90-2	V	STAR A	2.350	.017	16.69	.02
88.03.23	61-2	V	STAR A	2.501	.028	16.84	.03
88.03.24	61-2	V	STAR A	2.465	.026	16.80	.03
88.06.07	90-3	V	STAR A	2.442	.014	16.78	.01
89.02.04	61-2	V	STAR A	2.369	.024	16.71	.02
89.03.07	61-2	V	STAR A	2.447	.028	16.79	.03
89.03.10	61-2	V	STAR A	2.483	.033	16.82	.03
89.04.09	61-1	V	STAR A	2.744	.024	17.08	.02
89.06.04	61-1	V	STAR A	2.613	.023	16.95	.02
89.07.05	61-1	V	STAR A	2.634	.022	16.97	.02

Table I: H 1426+428

UT Date (1)	Tel-Apt (2)	P (%) (3)	σ_p (4)	θ (5)	σ_θ (6)	m _v (7)	σ (8)	Comment (9)
89.04.07	61-0	2.35	.31	174.37	3.76	16.51	.02	
89.07.08	61-0	2.48	.55	17.83	6.39			
89.07.08	61-0	≤ 1.20						Star A, ISP

Table III: H 1426+428

UT Date (1)	Tel-Apt (2)	Filter (3)	Comp Star (4)	Δ m (5)	σ (6)	m (7)	σ (8)
89.04.07	61-1	V	STAR A	2.408	.015	16.57	.02
89.04.07	61-1	V	STAR C	3.050	.015	16.51	.02

Table I: MS 1458.8+2249

UT Date (1)	Tel-Apt (2)	P (%) (3)	σ_p (4)	θ (5)	σ_θ (6)	m_v (7)	σ (8)	Comment (9)
88.01.23	90-1	1.72	.32	78.11	5.29	17.03	.02	
88.03.22	61-0	3.10	.35	77.45	3.21			
88.03.23	61-0	2.59	.36	86.61	3.95	16.80	.03	
88.03.25	61-0	4.24	.36	78.69	2.40	16.79	.03	
88.03.28	61-0	5.00	.65	67.02	3.73			
88.06.08	90-1	7.03	.42	4.22	1.72	16.67	.02	
89.02.03	61-0	5.15	.58	39.50	3.24			
89.03.05	61-0	4.17	.43	14.62	2.96			
89.03.07	61-0	3.89	.55	16.56	4.04	16.58	.04	
89.04.01	61-0	1.98	.52	171.67	7.47	16.60	.02	
89.04.09	61-0	1.63	.45	172.72	7.91	16.57	.02	
89.06.04	61-0	2.37	.50	147.52	5.98	16.46	.02	
89.06.22	61-0	1.56	.62	38.87	11.46			
89.07.05	61-0	3.59	.68	82.27	5.39			
90.02.18	61-0	2.75	.42	157.81	4.39	16.28	.03	
88.01.23	90-1	≤ 1.00						Star A, VISP

Table II: MS 1458.8+2249

UT Date (1)	Tel-Apt (2)	Fil (3)	P (%) (4)	σ_p (5)	θ (6)	σ_θ (7)	m (8)	σ (9)	Comment (10)
88.03.28	61-0	B	5.11	1.97	84.64	11.02			
88.06.08	90-1	B	7.59	.59	5.18	2.24			
	90-1	I	6.79	.80	8.21	3.39			

Table III: MS 1458.8+2249

UT Date (1)	Tel-Apt (2)	Filter (3)	Comp Star (4)	Δ m (5)	σ (6)	m (7)	σ (8)
88.01.23	90-2	V	STAR A	1.451	.015	17.03	.02
88.03.23	61-2	V	STAR A	1.221	.030	16.80	.03
88.03.25	61-2	V	STAR A	1.208	.034	16.79	.03
88.06.08	90-2	V	STAR A	1.088	.016	16.67	.02
89.03.07	61-2	V	STAR A	.997	.039	16.58	.04
89.04.01	61-1	V	STAR A	1.016	.019	16.60	.02
89.04.09	61-1	V	STAR A	.992	.020	16.57	.02
89.06.04	61-1	V	STAR A	.877	.018	16.46	.02
90.02.18	61-2	V	STAR A	.701	.033	16.28	.03

Table I: MS 1534.2+0148

UT Date (1)	Tel-Apt (2)	P (%) (3)	σ_p (4)	θ (5)	σ_θ (6)	m_v (7)	σ (8)	Comment (9)
88.03.23	61-0	8.23	2.79	21.89	9.72			
88.03.24	61-0	3.73	1.20	16.19	9.20			
	61-0	4.51	1.10	17.84	7.00			Avr 3.23, 3.24
88.06.08	90-1	3.54	1.48	1.47	11.98	18.79	.06	
89.02.04	61-0	≤ 4.10						
89.03.06	61-0	4.49	2.16	152.00	13.78			
89.03.07	61-0	3.55	1.30	170.65	10.48	18.73	.11	
	61-0	3.78	1.11	163.14	8.44	18.73	.11	Avr 3.06, 3.07
89.04.07	61-0	≤ 6.00						
89.04.09	61-0	≤ 7.00				18.80	.06	
	61-0	≤ 5.30				18.80	.06	Avr 4.07, 4.09
89.06.04	61-0	≤ 6.00						

Table III: MS 1534.2+0148

UT Date (1)	Tel-Apt (2)	Filter (3)	Comp Star (4)	Δm (5)	σ (6)	m (7)	σ (8)
88.06.08	90-2	V	STAR B	6.076	.061	18.79	.06
89.03.07	61-2	V	STAR B	6.025	.113	18.73	.11
89.04.09	61-1	V	STAR A	7.998	.063	18.80	.06

Table I: MS 1552.1+2020

UT Date (1)	Tel-Apt (2)	P (%) (3)	σ_p (4)	θ (5)	σ_θ (6)	m_v (7)	σ (8)	Comment (9)
88.03.22	61-0	4.80	.58	50.97	3.45			
88.03.25	61-0	4.25	.59	51.08	3.95			
88.03.28	61-0	4.49	1.04	54.85	6.62			
88.06.08	90-1	5.75	.62	46.68	3.08	17.56	.03	
88.09.17	61-0	4.38	1.06	46.53	6.94	17.75	.03	
88.09.18	61-0	≤ 7.00				17.90	.04	
88.10.01	61-0	4.98	1.10	56.45	6.33			
89.02.04	61-0	5.95	1.14	44.07	5.49	17.32	.03	
89.03.07	61-0	≤ 3.20				17.45	.03	
89.04.03	61-0	5.20	1.05	56.87	5.79			
89.04.09	61-0	5.11	1.31	73.60	7.32	17.83	.02	
89.06.04	61-0	4.31	.98	52.48	6.50	17.72	.04	
89.07.04	61-0	≤ 6.00						
90.02.21	61-0	2.77	.80	49.00	8.31			

Table III: MS 1552.1+2020

UT Date (1)	Tel-Apt (2)	Filter (3)	Comp Star (4)	Δm (5)	σ (6)	m (7)	σ (8)
88.06.08	90-2	V	STAR A	3.835	.028	17.56	.03
88.09.17	61-1	V	STAR A	4.034	.034	17.75	.03
88.09.18	61-1	V	STAR A	4.184	.041	17.90	.04
89.02.04	61-2	V	STAR A	3.634	.034	17.35	.03
89.02.04	61-2	V	STAR B	7.494	.034	17.32	.03
89.03.07	61-2	V	STAR A	3.754	.034	17.47	.03
89.03.07	61-2	V	STAR B	7.621	.034	17.45	.03
89.04.09	61-1	V	STAR A	4.111	.024	17.83	.02
89.06.04	61-1	V	STAR A	4.000	.042	17.72	.04

Table I: H 1652+398

UT Date (1)	Tel-Apt (2)	P (%) (3)	σ_p (4)	θ (5)	σ_θ (6)	m_v (7)	σ (8)	Comment (9)
87.09.15	60-0	2.82	.14	125.04	1.39			UC 60
87.09.27	60-0	2.48	.07	123.13	.84			UC 60
87.09.29	60-0	2.61	.11	126.23	1.15			UC 60
87.11.10	60-0	3.16	.14	135.30	1.23			UC 60
87.11.11	60-1	3.63	.26	108.14	2.06			UC 60
87.11.12	60-0	3.30	.18	109.60	1.60			UC 60
87.11.13	60-0	3.41	.18	108.15	1.55			UC 60
87.11.17	60-0	2.87	.22	107.64	2.21			UC 60
88.03.27	61-0	3.34	.21	130.27	1.84			
88.03.28	61-0	2.58	.15	128.22	1.61			
88.05.17	90-6	2.97	.09	127.60	.90			Octopol
88.06.06	90-1	3.88	.11	130.00	.80			
88.09.16	61-0	3.16	.19	124.16	1.77	13.61	.01	
88.10.07	90-0	3.40	.25	123.55	2.07			
88.10.08	90-1	2.77	.16	124.55	1.61	13.85	.01	
88.10.31	61-0	3.02	.27	121.43	2.54	12.90	.01	
88.11.01	61-0	3.55	.25	123.74	2.05			
88.11.02	61-0	3.23	.21	120.86	1.82			
88.11.03	61-0	3.35	.23	120.47	1.94			
88.11.05	61-0	3.17	.23	118.09	2.04	13.64	.01	
88.11.13	61-0	3.00	.25	116.15	2.42			
89.02.04	61-0	3.49	.29	114.91	2.36			
89.03.05	61-0	2.72	.16	105.04	1.67			
89.03.06	61-0	2.97	.21	108.13	2.05			
89.03.09	61-0	2.95	.21	108.25	2.02	13.60	.01	
89.04.03	61-0	4.18	.15	100.97	1.01			
89.04.09	61-0	3.61	.15	106.17	1.20	13.60	.01	
89.06.03	61-0	2.98	.18	91.91	1.71			
89.06.22	61-0	3.24	.53	101.16	4.69			
89.07.04	61-0	3.31	.18	107.37	1.59			
89.07.05	61-0	3.43	.13	109.67	1.05	13.59	.01	
89.07.08	61-0	3.61	.25	108.35	2.01			
89.07.09	61-0	3.47	.21	107.51	1.77			

Table I continued: H 1652+398

UT Date (1)	Tel-Apt (2)	P (%) (3)	σ_p (4)	θ (5)	σ_θ (6)	m_v (7)	σ (8)	Comment (9)
89.09.05	61-0	2.83	.15	109.31	1.49	13.62	.01	
89.09.08	61-0	2.51	.21	104.55	2.34			
89.11.03	61-0	2.49	.21	111.27	2.48			
90.02.16	90-1	2.71	.15	123.70	1.55			
90.02.21	61-0	2.42	.18	124.25	2.12			
87.09.17	60-1	≤ 0.11						Star A, RISP

Table II: H 1652+398

UT Date (1)	Tel-Apt (2)	Fil (3)	P (%) (4)	σ_p (5)	θ (6)	σ_θ (7)	m (8)	σ (9)	Comment (10)
87.09.15	60-0	B	4.25	.52	122.74	3.48			UC 60
	60-0	V	3.49	.34	123.34	2.82			UC 60
	60-0	R	2.73	.27	126.23	2.78			UC 60
	60-0	I	1.77	.29	127.41	4.68			UC 60
87.09.16	60-0	U	4.44	.40	123.92	2.58			UC 60
	60-0	B	3.53	.36	124.55	2.95			UC 60
	60-0	V	2.14	.32	120.42	4.32			UC 60
	60-0	R	2.51	.23	121.54	2.66	13.42	.01	UC 60
88.03.28	60-0	I	1.84	.30	125.15	4.62			UC 60
	61-0	U	4.49	.51	132.82	3.29			
	61-0	B	3.71	.36	128.00	2.77			
	61-0	V	2.29	.21	132.10	2.62			
88.06.06	61-0	R	2.55	.22	127.96	2.47			
	61-0	I	2.04	.20	126.67	2.86			
	90-1	U	7.19	.53	124.35	2.10			
	90-1	B	5.70	.31	125.34	1.56			
	90-1	V	3.84	.30	126.33	2.27			
	90-1	R	3.45	.18	126.59	1.46			
	90-1	I	2.92	.28	128.53	2.71			

Table II continued: H 1652+398

UT Date (1)	Tel-Apt (2)	Fil (3)	P (%) (4)	σ_p (5)	θ (6)	σ_θ (7)	m (8)	σ (9)	Comment (10)
88.09.17	61-0	U	6.27	.64	126.03	2.92			
	61-0	B	3.28	.38	117.61	3.34			
	61-0	V	3.99	.51	125.77	3.65	13.63	.01	
	61-0	R	2.65	.38	118.84	4.09			
	61-0	I	1.94	.34	128.20	4.99			
	61-0	V	2.75	.44	117.04	4.59	13.63	.01	
88.09.18	61-0	U	7.73	.94	125.18	3.48			
	61-0	B	4.17	.58	121.96	3.96			
	61-0	V	4.02	.52	120.95	3.71	13.67	.01	
	61-0	R	3.13	.38	117.83	3.47			
	61-0	I	2.43	.45	122.78	5.25			
88.10.01	61-0	U	5.02	.77	118.56	4.41			
	61-0	B	3.85	.51	125.08	3.82			
	61-0	V	2.69	.33	121.44	3.49	13.63	.01	
	61-0	R	2.41	.27	118.23	3.17			
	61-0	I	2.12	.32	113.85	4.34			
88.10.08	90-1	B	4.10	.36	123.39	2.53			
	90-1	I	1.52	.33	128.56	6.22			
89.02.04	61-0	V	2.52	.44	107.52	5.01			
89.04.04	61-0	U	7.77	.85	106.22	3.15			
	61-0	I	2.75	.34	99.09	3.57			
89.04.05	61-0	U	6.04	1.08	99.86	5.11			
89.04.07	61-0	U	7.03	.62	102.72	2.53			
	61-0	I	3.04	.32	109.95	2.99			
	61-0	U	7.18	.76	104.72	3.02			
89.04.09	61-0	V	2.71	.72	112.82	7.57	13.60	.01	
	61-0	I	2.88	.32	107.05	3.20			
	61-0	B	4.78	.76	93.57	4.53			
89.06.03	61-0	I	2.69	.39	98.72	4.10			
	61-0	B	3.71	.48	108.65	3.73			
89.07.04	61-0	V	2.70	.34	114.13	3.60			
	61-0	R	3.09	.34	110.80	3.19			
	61-0	I	2.81	.39	106.39	3.95			

Table III: H 1652+398

UT Date (1)	Tel-Apt (2)	Filter (3)	Comp Star (4)	Δ m (5)	σ (6)	m (7)	σ (8)
87.09.16	60-1	R	STAR A	1.315	.002	13.42	.01
88.09.16	61-2	U	STAR A	.024	.020	14.25	.02
	61-2	B	STAR A	.843	.010	14.39	.01
	61-2	V	STAR A	1.004	.006	13.61	.01
	61-2	R	STAR A	.967	.005	13.08	.01
	61-2	I	STAR A	.846	.006	12.48	.01
88.09.17	61-2	V	STAR A	1.022	.007	13.63	.01
88.09.18	61-2	V	STAR A	1.060	.006	13.67	.01
88.10.01	61-2	V	STAR A	1.019	.006	13.63	.01
88.10.08	90-2	V	STAR A	1.242	.004	13.85	.01
88.10.31	61-1	V	STAR A	.288	.005	12.90	.01
88.11.05	61-2	V	STAR A	1.030	.005	13.64	.01
89.03.09	61-2	V	STAR A	.995	.006	13.60	.01
89.04.07	61-2	V	STAR A	1.013	.008	13.62	.01
89.04.09	61-2	V	STAR A	.992	.006	13.60	.01
89.07.05	61-1	V	STAR A	1.321	.007	13.93	.01
	61-2	V	STAR A	.982	.007	13.59	.01
89.09.05	61-2	V	STAR A	1.015	.007	13.62	.01

Table I: MS 1704.9+6046

UT Date (1)	Tel-Apt (2)	P (%) (3)	σ_p (4)	θ (5)	σ_θ (6)	m_v (7)	σ (8)	Comment (9)
88.01.24	90-1	\leq 7.48						
88.06.07	90-0	\leq 4.07						
88.10.07	90-0	\leq 3.60				19.86	.05	
89.03.08	61-0	\leq 6.50						
89.03.09	61-0	\leq 4.40				19.21	.06	
	61-0	\leq 3.10				19.21	.06	Avr 3.08, 3.09
89.07.02	90-1	\leq 13.00						
89.10.23	90-0	\leq 5.50						

Table III: MS 1704.9+6046

UT Date (1)	Tel-Apt (2)	Filter (3)	Comp Star (4)	Δm (5)	σ (6)	m (7)	σ (8)
88.10.07	90-1	V	STAR A	5.373	.049	19.86	.05
89.03.09	61-1	V	STAR A	4.717	.061	19.21	.06

Table I: H 1722+119

UT Date (1)	Tel-Apt (2)	P (%) (3)	σ_p (4)	θ (5)	σ_θ (6)	m_v (7)	σ (8)	Comment (9)
89.03.05	61-1	7.27	.37	96.65	1.47			
89.03.08	61-0	4.94	.26	101.84	1.48	15.30	.01	
89.04.01	61-0	8.51	.52	99.56	1.75			
89.04.08	61-0	15.54	.35	90.64	.64	15.47	.02	
89.04.09	61-0	13.55	.38	92.57	.79	15.57	.01	
89.06.03	61-0	5.45	.58	109.09	3.06			
89.07.04	61-0	6.05	.42	105.26	1.98			
89.07.07	61-0	8.84	.34	108.91	1.11			
89.07.08	61-0	7.98	.33	112.26	1.19			
89.07.09	61-0	8.53	.42	109.42	1.40			
89.09.05	61-0	4.33	.45	107.48	2.99	15.24	.03	
89.09.08	61-0	6.24	.44	116.39	2.00			
90.02.21	61-0	3.61	.35	102.52	2.77			

Table II: H 1722+119

UT Date (1)	Tel-Apt (2)	Fil (3)	P (%) (4)	σ_p (5)	θ (6)	σ_θ (7)	m (8)	σ (9)	Comment (10)
89.03.08	61-0	B	5.35	.79	100.51	4.25			
	61-0	R	5.03	.47	104.27	2.68			
89.04.08	61-0	U	18.04	1.40	89.57	2.23			
	61-0	B	16.91	.79	91.55	1.35			
	61-0	V	15.37	.58	90.66	1.09	15.47	.02	
	61-0	R	15.59	.48	90.89	.88			
	61-0	I	14.94	.61	92.88	1.17			
89.04.09	61-0	U	16.36	1.63	91.59	2.86			
	61-0	B	15.28	1.11	91.31	2.08			
	61-1	V	15.57	.92	91.58	1.69	15.57	.01	
	61-0	R	14.16	.70	92.04	1.42			
	61-0	I	13.81	.92	93.52	1.91			
89.06.03	61-0	B	4.44	1.46	108.27	9.44			
89.07.04	61-0	B	7.84	1.51	103.64	5.53			
	61-0	I	6.02	.83	108.25	3.96			
89.07.08	61-0	U	7.85	1.12	110.14	4.08			
	61-0	B	6.76	.96	111.63	4.09			
	61-0	V	9.60	.95	112.05	2.85			
	61-0	I	6.29	.80	108.69	3.64			
89.07.14	90-S	B	14.80	2.50	95.00	10.00			
89.09.05	61-0	U	4.62	.91	111.92	5.64			
	61-0	I	4.15	.54	110.23	3.71			
90.02.18	61-0	V	4.71	.63	85.75	3.82	15.34	.02	
90.03.16	60-1	B	2.63	.67	131.72	7.24	15.83	.02	
	60-1	V	3.51	.67	127.93	5.46	15.28	.02	
	60-1	R	2.25	.27	120.32	3.45	14.88	.02	
	60-1	I	3.07	.38	134.32	3.54	14.29	.02	
90.03.17	60-1	V	1.16	.26	143.64	6.32	15.22	.02	

Table III: H 1722+119

UT Date (1)	Tel-Apt (2)	Filter (3)	Comp Star (4)	Δ m (5)	σ (6)	m (7)	σ (8)
89.03.08	61-1	V	STAR A	2.351	.011	15.30	.01
89.04.08	61-1	V	STAR A	2.523	.015	15.47	.02
89.04.09	61-1	V	STAR A	2.619	.007	15.57	.01
89.09.05	61-2	V	STAR A	2.470	.024	15.42	.02
89.09.05	61-2	V	STAR B	1.534	.025	15.24	.03
90.02.18	61-2	V	STAR A	2.385	.015	15.34	.02
90.03.16	60-2	U	STAR A	.940	.036	15.31	.04
90.03.16	60-2	B	STAR A	1.987	.023	15.85	.02
90.03.16	60-2	V	STAR A	2.321	.016	15.27	.02
90.03.16	60-2	R	STAR A	2.434	.016	14.88	.02
90.03.16	60-2	I	STAR A	2.300	.015	14.29	.02
90.03.16	60-2	U	STAR B	.734	.038	15.31	.04
90.03.16	60-2	B	STAR B	1.391	.024	15.83	.02
90.03.16	60-2	V	STAR B	1.571	.017	15.28	.02
90.03.16	60-2	R	STAR B	1.556	.017	14.88	.02
90.03.16	60-2	I	STAR B	1.398	.017	14.29	.02
90.03.17	60-2	V	STAR A	2.247	.016	15.20	.02
90.03.17	60-2	V	STAR B	1.510	.017	15.22	.02

Table I: MS 1757.7+7034

UT Date (1)	Tel-Apt (2)	P (%) (3)	σ_P (4)	θ (5)	σ_θ (6)	m_v (7)	σ (8)	Comment (9)
88.10.07	90-0	2.36	1.18	130.22	14.31			
89.07.02	90-1	3.70	.85	170.46	6.56			
89.10.23	90-0	3.21	.96	138.97	8.55			
88.10.07	90-1	≤ 1.24						Star A, ISP
88.10.07	90-1	≤ 0.24						Star B, ISP

Table I: MS 2143.4+0704

UT Date (1)	Tel-Apt (2)	P (%) (3)	σ_p (4)	θ (5)	σ_θ (6)	m_v (7)	σ (8)	Comment (9)
87.11.13	60-0	9.98	1.03	19.45	2.96			UC 60 Octopol
87.11.29	90-5	10.03	1.02	48.80	2.90			
88.06.07	90-0	10.10	1.10	48.35	3.13	17.96	.03	
88.06.08	90-1	7.96	.83	45.83	2.99	18.05	.04	
88.09.16	61-0	9.21	1.04	35.88	3.25	18.01	.07	
88.09.17	61-0	10.83	1.01	53.38	2.67	18.05	.03	
88.09.18	61-0	10.53	1.01	41.54	2.75	18.06	.03	
88.10.01	61-0	8.66	.99	47.50	3.26	17.97	.04	
88.10.06	90-1	8.38	.95	52.61	3.25			
88.10.08	90-0	10.27	.91	54.77	2.55	18.01	.02	
88.10.31	61-0	7.61	.89	56.01	3.35	18.26	.04	
88.11.01	61-0	6.70	.88	55.72	3.76	17.86	.05	
88.11.04	61-0	7.28	.87	54.26	3.42	18.07	.04	
88.11.05	61-0	7.90	.93	47.76	3.36	18.00	.07	
88.11.12	61-0	7.82	.95	52.94	3.47			
88.11.13	61-0	8.32	.79	47.12	2.72	18.03	.04	
88.11.14	61-0	8.39	1.13	41.64	3.86	17.80	.05	
89.06.04	61-0	5.45	1.60	45.73	8.40	17.74	.04	
89.07.02	90-1	5.57	.95	49.40	4.88			
89.07.05	61-0	8.08	1.21	44.20	4.31			
89.07.07	61-0	5.68	.97	37.86	4.87			
89.07.08	61-0	6.24	1.21	46.43	5.56			
89.07.09	61-0	6.42	1.50	33.32	6.71			
89.09.05	61-0	7.07	1.16	48.37	4.71			
89.09.07	61-0	7.01	1.77	40.26	7.22			
89.09.08	61-0	6.39	1.27	45.15	5.68			
89.11.03	61-0	≤ 1.10						Star A,ISP
89.11.03	61-0	0.46	0.17	77.50	10.38			Star B,ISP

Table II: MS 2143.4+0704

UT Date (1)	Tel-Apt (2)	Fil (3)	P (%) (4)	σ_p (5)	θ (6)	σ_θ (7)	m (8)	σ (9)	Comment (10)
88.06.07	90-1	B	9.06	1.96	47.25	6.19			
	90-1	I	9.40	1.72	44.79	5.25			
88.10.08	90-1	B	11.62	2.03	48.46	5.00			
	90-0	I	7.83	1.86	53.37	6.80			

Table III: MS 2143.4+0704

UT Date (1)	Tel-Apt (2)	Filter (3)	Comp Star (4)	Δ m (5)	σ (6)	m (7)	σ (8)
88.06.07	90-2	V	STAR A	4.030	.031	17.96	.03
88.06.08	90-2	V	STAR A	4.117	.035	18.05	.04
88.09.16	61-2	V	STAR A	4.080	.067	18.01	.07
88.09.17	61-1	V	STAR A	4.120	.031	18.05	.03
88.09.18	61-1	V	STAR A	4.131	.033	18.06	.03
88.10.01	61-1	V	STAR A	4.041	.036	17.97	.04
88.10.08	90-2	V	STAR A	4.079	.022	18.01	.02
88.10.31	61-1	V	STAR A	4.331	.043	18.26	.04
88.11.01	61-2	V	STAR A	3.935	.052	17.86	.05
88.11.04	61-1	V	STAR A	4.145	.042	18.07	.04
88.11.05	61-2	V	STAR A	4.072	.068	18.00	.07
88.11.13	61-1	V	STAR A	4.096	.037	18.03	.04
88.11.14	61-2	V	STAR A	3.867	.053	17.80	.05
89.06.04	61-1	V	STAR A	3.810	.042	17.74	.04

Table I: H 2154-304

UT Date (1)	Tel-Apt (2)	P (%) (3)	σ_p (4)	θ (5)	σ_θ (6)	m_v (7)	σ (8)	Comment (9)
87.09.27	60-0	2.10	.09	167.01	1.17			UC 60
87.09.28	60-1	6.89	.06	1.27	.26			UC 60
87.09.29	60-1	9.39	.07	170.67	.23	13.12	.01	UC 60
87.11.10	60-0	7.36	.13	143.40	.49			UC 60
87.11.11	60-1	4.04	.12	121.23	.84			UC 60
87.11.12	60-1	6.12	.09	148.35	.42			UC 60
87.11.13	60-1	5.93	.09	160.71	.45			UC 60
87.11.17	60-1	5.54	.12	133.42	.61			UC 60
87.12.10	60-0	8.33	.12	135.90	.40			UC 60
88.06.07	90-1	10.80	.12	134.20	.33	13.07	.01	
88.06.08	90-1	10.33	.12	131.62	.34	13.05	.01	
88.10.01	61-0	5.46	.14	129.45	.73			
88.11.05	61-0	4.75	.07	113.05	.45	13.27	.01	
88.11.12	61-1	4.83	.13	110.81	.75			
89.07.02	90-1	6.73	.15	151.74	.64			
89.07.04	61-0	7.56	.14	144.89	.53			
89.07.05	61-0	7.01	.15	151.86	.60			
89.07.09	61-0	7.34	.25	135.75	.96			
89.09.08	61-0	3.43	.19	117.65	1.58			
89.10.29	61-1	2.27	.22	124.66	2.82	13.38	.01	
89.11.03	61-0	5.79	.23	148.14	1.16			

Table II: H 2154-304

UT Date (1)	Tel-Apt (2)	Fil (3)	P (%) (4)	σ_p (5)	θ (6)	σ_θ (7)	m (8)	σ (9)	Comment (10)
87.09.27	60-1	U	2.39	.35	165.70	4.21			UC 60
	60-1	V	2.05	.20	173.05	2.80			UC 60
	60-1	I	2.11	.19	165.11	2.62			UC 60
87.09.28	60-1	U	7.94	.34	.28	1.23			UC 60
	60-1	B	7.84	.23	2.04	.86			UC 60
	60-1	V	7.29	.20	.58	.78			UC 60
	60-1	R	6.43	.16	.21	.72			UC 60
87.09.29	60-1	I	6.46	.19	179.87	.85			UC 60
	60-1	U	10.92	.36	171.98	.95	12.70	.03	UC 60
	60-1	B	10.03	.28	170.40	.79	13.44	.02	UC 60
	60-1	V	9.99	.19	171.00	.55	13.12	.01	UC 60
	60-1	R	9.40	.19	170.19	.58	12.78	.02	UC 60
87.11.11	60-1	I	9.06	.21	169.85	.68	12.41	.02	UC 60
	60-1	U	4.32	.50	120.78	3.29			UC 60
	60-1	B	4.03	.44	123.99	3.13			UC 60
	60-1	V	4.00	.31	121.32	2.25			UC 60
	60-1	R	4.20	.21	124.35	1.45			UC 60
87.11.12	60-1	I	3.95	.35	122.97	2.51			UC 60
	60-1	U	7.11	.36	150.32	1.43			UC 60
	60-1	B	6.73	.25	150.49	1.06			UC 60
	60-1	V	6.33	.20	148.75	.90			UC 60
	60-1	R	6.34	.18	145.75	.83			UC 60
87.12.10	60-1	I	5.95	.16	147.06	.79			UC 60
	60-0	B	8.35	.38	135.70	1.29			UC 60
	60-0	V	9.28	.37	138.90	1.14			UC 60
	60-0	R	8.48	.36	136.60	1.20			UC 60
	60-0	I	8.14	.38	136.80	1.33			UC 60
88.06.07	90-1	U	10.72	1.17	132.99	3.13			
	90-1	B	11.27	.41	135.26	1.05			
	90-1	V	10.81	.28	134.71	.75	13.07	.01	
	90-1	R	10.91	.23	133.93	.60			
	90-1	I	10.54	.29	133.56	.78			

Table II continued: H 2154-304

UT Date (1)	Tel-Apt (2)	Fil (3)	P (%) (4)	σ_p (5)	θ (6)	σ_θ (7)	m (8)	σ (9)	Comment (10)
88.06.08	90-1	U	10.35	1.04	132.07	2.88			
	90-1	B	10.11	.42	132.97	1.19			
	90-1	V	10.52	.28	131.38	.75	13.05	.01	
	90-1	R	9.91	.22	131.02	.63			
	90-1	I	10.28	.28	132.07	.78			
88.09.17	61-0	U	6.80	.63	155.11	2.65			
	61-0	B	6.69	.40	153.99	1.73			
	61-0	V	7.03	.32	153.97	1.29	13.62	.01	
	61-0	R	7.52	.31	155.22	1.17			
	61-0	I	6.33	.37	153.99	1.67			
88.09.18	61-0	U	9.26	.55	142.07	1.71			
	61-0	V	7.47	.32	140.79	1.24	13.69	.01	
	61-0	I	7.20	.32	140.68	1.28			
88.10.01	61-0	B	6.00	.35	127.99	1.66			
	61-0	I	5.70	.28	130.35	1.39			
88.10.31	61-1	B	7.31	.32	138.68	1.25			
	61-1	R	7.12	.27	137.10	1.08			
88.11.04	61-0	U	6.60	.52	110.57	2.26			
	61-0	B	6.06	.47	110.43	2.23			
	61-0	V	6.34	.39	113.70	1.78	13.19	.01	
	61-0	R	6.79	.29	111.35	1.21			
	61-0	I	6.32	.39	110.77	1.78			
88.11.12	61-0	B	5.03	.30	108.29	1.74			
	61-0	R	4.25	.30	111.24	2.01			
	61-0	I	5.14	.39	111.37	2.18			
89.07.09	61-0	B	6.65	.60	133.55	2.58			
	61-0	I	6.23	.60	136.70	2.76			
89.10.29	61-0	B	2.37	.29	124.68	3.53	13.67	.01	
	61-0	V	2.12	.19	118.81	2.61	13.38	.01	
	61-0	R	2.65	.26	139.82	2.77	13.05	.01	

Table III: H 2154-304

UT Date (1)	Tel-Apt (2)	Filter (3)	Comp Star (4)	Δ m (5)	σ (6)	m (7)	σ (8)
87.09.29	60-2	U	STAR A	-.199	.012	12.72	.02
	60-2	B	STAR A	.681	.007	13.39	.01
	60-2	V	STAR A	1.077	.006	13.11	.01
	60-2	R	STAR A	1.134	.005	12.75	.01
	60-2	I	STAR A	1.143	.007	12.40	.01
	60-2	U	STAR B	-1.767	.034	12.77	.03
	60-2	B	STAR B	-.419	.011	13.46	.01
	60-2	V	STAR B	.184	.008	13.14	.01
	60-2	R	STAR B	.359	.006	12.82	.02
	60-2	I	STAR B	.457	.008	12.45	.01
	60-2	U	STAR C	-.471	.013	12.70	.03
	60-2	B	STAR C	.283	.008	13.44	.02
	60-2	V	STAR C	.543	.007	13.12	.01
	60-2	R	STAR C	.562	.006	12.78	.02
	60-2	I	STAR C	.539	.008	12.41	.02
88.06.07	90-2	V	STAR A	1.040	.003	13.07	.01
88.06.08	90-2	V	STAR A	1.020	.002	13.05	.01
88.09.17	61-2	V	STAR A	1.589	.007	13.62	.01
88.09.18	61-2	V	STAR A	1.656	.006	13.69	.01
88.10.31	61-2	V	STAR A	1.465	.006	13.49	.01
88.11.04	61-2	V	STAR A	1.162	.005	13.19	.01
88.11.05	61-2	V	STAR A	1.242	.005	13.27	.01
89.10.29	61-2	U	STAR A	.080	.016	13.00	.02
	61-2	B	STAR A	.960	.007	13.67	.01
	61-2	V	STAR A	1.354	.006	13.38	.01
	61-2	R	STAR A	1.433	.006	13.05	.01
	61-2	I	STAR A	1.418	.007	12.68	.01

Table I: MS 2336.5+0517

UT Date (1)	Tel-Apt (2)	P (%) (3)	σ_p (4)	θ (5)	σ_θ (6)	m_v (7)	σ (8)	Comment (9)
88.09.16	61-0	≤ 8.70						
88.09.17	61-0	≤ 4.20				19.50	.12	
	61-0	≤ 3.90				19.50	.12	Avr 9.16,9.17
88.10.01	61-0	4.54	2.76	102.35	17.41			
88.10.07	90-0	≤ 2.80				19.57	.06	
88.11.13	61-0	5.13	1.69	155.58	9.46	19.53	.11	
89.10.23	90-0	≤ 3.63						
89.11.03	61-1	≤ 2.00						Star A,ISP
89.11.03	61-1	≤ 1.20						Star B,ISP

Table III: MS 2336.5+0517

UT Date (1)	Tel-Apt (2)	Filter (3)	Comp Star (4)	Δm (5)	σ (6)	m (7)	σ (8)
88.09.17	61-1	V	STAR A	4.819	.117	19.50	.12
88.10.07	90-1	V	STAR A	4.895	.056	19.57	.06
88.11.13	61-1	V	STAR A	4.852	.110	19.53	.11

Table I: MS 2342.7-1531

UT Date (1)	Tel-Apt (2)	P (%) (3)	σ_p (4)	θ (5)	σ_θ (6)	m_v (7)	σ (8)	Comment (9)
88.10.07	90-0	5.33	1.60	177.23	8.57	19.81	.07	
88.10.08	90-0	7.87	1.99	166.28	7.23			
	90-0	6.33	1.24	171.92	5.63			Avr10.07,10.08
88.11.05	61-0	7.37	2.85	116.83	11.08			
89.10.29	61-0	≤ 9.00						

Table III: MS 2342.7-1531

UT Date (1)	Tel-Apt (2)	Filter (3)	Comp Star (4)	Δ m (5)	σ (6)	m (7)	σ (8)
88.10.07	90-1	V	STAR A	4.110	.072	19.81	.07

Table I: MS 2347.4+1924

UT Date (1)	Tel-Apt (2)	P (%) (3)	σ_p (4)	θ (5)	σ_θ (6)	m_v (7)	σ (8)	Comment (9)
88.10.06	90-1	≤ 3.50						
88.10.08	90-0	3.09	.92	159.82	8.56			
89.01.09	90-0	≤ 3.10				19.93	.12	
89.07.02	90-1	≤ 5.63						
89.11.03	61-0	0.63	.28	80.12	12.26			Star A,ISP
89.11.03	61-0	0.38	.18	75.46	12.35			Star B,ISP

Table III: MS 2347.4+1924

UT Date (1)	Tel-Apt (2)	Filter (3)	Comp Star (4)	Δ m (5)	σ (6)	m (7)	σ (8)
89.01.09	90-2	V	STAR A	6.728	.121	19.93	.12

Table IV: Limits From CCD Polarimetry

Object (1)	UT Date (2)	P_B (%) (3)	Analzser (4)
1E 0514+064	90.02.25	< 7.0	Savart Plate
MS 0737.9+7441	90.02.25	< 30.0	Savart Plate
MS 0922.9+7459	90.02.25	< 30.0	Savart Plate
MS 1133.7+1618	90.02.24	< 15.0	Polaroid Filter
MS 1258.4+6401	90.02.24	< 20.0	Polaroid Filter
MS 1258.4+6401	90.02.25	< 20.0	Savart Plate
MS 1229.2+6430	90.02.25	< 7.5	Savart Plate

APPENDIX II

NOTES ON INDIVIDUAL OBJECTS

Notes on Appendix II

In this appendix we present brief notes on our observations of the individual objects included in our study of XSBLs and more plots of some of our data. In figures II.1 through II.4 we plot the frequency dependence of the polarization of four objects for selected epochs. In figures II.5 through II.20 we present Q vs. U plots for the well studied objects in our observing program (see Chapter 5).

This section is not intended as a bibliography of all past observations of these objects. Such a bibliography is being compiled and will be included when this work is published in refereed journals.

Redshifts for most of these objects were not available when we began our research. Simon Morris, John Stocke, and their collaborators were kind enough to provide the redshifts prior to publication and we have used them in our analysis of the properties of XSBLs. We only present redshifts that have already been published. The updated and additional redshifts for the EMSS objects will be published by Morris *et al.* (1991). When a redshift published by Maccacaro *et al.* (1989) is now known to be improved by the Morris *et al.* (1991) data, we have chosen not to list the older and erroneous redshift.

The positions of many of these objects were also made available to us before publication and we thank the EMSS team for providing us with the list of objects. All of the positions for the EMSS objects will be published in 1991

by John Stocke and his collaborators. The x-ray positions for the EMSS are presented by Gioia *et al.* (1990). A catalogue of the *HEAO*-1 sources including the BL Lacs observed by *HEAO*-1 will be published in 1991 (Remillard 1990).

MS 0122.1+0903

This object has a redshift of 0.339 (Maccacaro *et al.* 1989). It is very faint and has proved difficult to monitor. We have not detected polarized emission from this object.

MS 0158.5+0019

We confirm that this object is a BL Lac. There is no redshift available, but it is resolved in a *R* band CCD frame (Maccacaro *et al.* 1989).

MS 0205.5+3509

We are not able to confirm the identification of this object as a BL Lac. The polarization we have detected could be interstellar in origin since we have detected ISP for stars in the field. We do not have enough accurate photometry of this object to confirm the variability reported by Schild *et al.* 1990. Our measurement of a *V* magnitude of 18.38 is questionable since it is possible that the wrong comparison star was observed on that night. On a later observing run we will calibrate additional nearby stars to help remove this uncertainty.

MS 0257.9+3429

While this object was observed to be highly polarized on one occasion and significantly polarized on five separate epochs, we note that the measurement of the interstellar polarization along this line of sight needs to be improved. If there is significant interstellar polarization it might have affected our determination of this object as having a preferred position angle for its polarization. This object is in a field that has an object with (or potentially has) extended x-ray emission (see §3.1). It has a tentative redshift of 0.245 (Maccacaro *et al.* 1989).

MS 0317.0+1834

This object is a confirmed BL Lac with a redshift of 0.190 (Maccacaro *et al.* 1989). Star A in this field has detectable interstellar polarization at a position angle coincident with some of our measurements of the polarization of MS 0317.0+1834. The variability of the position angle of the polarization from the XSBL confirms that it is intrinsically polarized. It has a redshift of 0.190 (Maccacaro *et al.* 1989).

H 0323+022

This BL Lac was found as part of the HEAO 1 all-sky survey. It was first identified as a BL Lac object by Margon and Jacoby (1984). It has also been noted that this BL Lac had periods of rapid variability and significant polarization (2-7%) (Feigelson *et al.* 1986). We note that when this object was observed in 1983 October and December (Feigelson *et al.* 1986) it had polarization

position angles consistent with the range observed during our monitoring program. We also note that this object exhibited two different aspects of wavelength dependence of its polarization. On October 7, 1988 (UT) this object was more highly polarized at U than I , consistent with the idea that the synchrotron emission from this object was being diluted by the stellar light of the host galaxy. On February 21, 1990 (UT) this object showed comparable percent polarization (9 to 12%) but of contrasting wavelength dependence. In this later case there was no significant wavelength dependence detected. Unfortunately we were not able to obtain photometry on October 7, 1988 and we are unable to examine the correlation of this dependence with the total flux output of the source. This object is also the only BL Lac in our program and the first XSBL observed to exhibit a rotation of its polarization position angle with frequency (on 24 January 1988 UT). This object has a redshift of 0.147 (Schwartz *et al.* 1989).

MS 0419.3+1943

We can not confirm this objects identification as a BL Lac. It is very faint and was therefore difficult for us to monitor. There is ISP in the field.

1E 0514+064

We confirm that this object is a BL Lac.

H 0548–322

This is a confirmed BL Lac which has a redshift of 0.069 (Schwartz 1989) and preferred polarization position angle.

MS 0607.9+7108

We confirm this objects identification as a BL Lac.

MS 0737.9+7441

We confirm this objects identification as a BL Lac. It has a stable polarization position angle.

MS 0922.9+7459

We are unable to confirm this objects classification as a BL Lac. This object is in a field that contains an object with (or potentially has) extended x-ray emission (See §3.1).

MS 0950.9+4929

We confirm this objects classification as a BL Lac.

H 1101–232

We confirm that this object has intrinsic polarized emission and should be classified as a BL Lac. We note, however, that the maximum observed percent polarization for this object is only 2.7% (Schwartz *et al.* 1989). This object has a redshift of 0.180.

MS 1207.9+3945

We are unable to confirm the classification of this object. There is only one reported detection of polarization from this object (Stocke *et al.* 1985) and it was a marginal detection of 4.1 % polarization. This object has a redshift of 0.61 (Maccacaro *et al.* 1989).

H 1219+305

We note that Wills *et al.* (1980) published two distinct epochs of polarimetry of this object. They observed it in January and June of 1980. On both occasions the polarization position angle they measured was between 45 and 50 degrees.

MS 1221.8+2452

We confirm this objects classification as a BL Lac. It has preferred polarization position angle.

MS 1229.2+6430

This object is in a field that contains an object with (or potentially has) extended x-ray emission (see §3.1).

MS 1235.4+6315

We are unable to confirm this objects classification as a BL Lac. We were not able to obtain a three sigma detection of polarized emission from this object. It has a redshift of 0.297 (Maccacaro *et al.* 1989).

MS 1258.4+6401

We have not been able to place a good limit on the polarization of this faint object.

MS 1402.3+0416

We confirm this objects classification as a BL Lac. It has a preferred polarization position angle.

MS 1407.9+5954

We are able to confirm this objects classification as a BL Lac. This object has a redshift of 0.452 (Maccacaro *et al.* 1989).

1E 1415.6+2557

This might be the only known example of a BL Lac object in a host galaxy that is not an elliptical galaxy (see Chapter 1 and Ulrich 1989). This object has a redshift of 0.237.

H 1426+428

We confirm this objects classification as a BL Lac, but note that we did not observe it to have a polarization greater than 2.48%. This object has a redshift of 0.130.

MS 1534.2+0148

We are able to confirm this objects classification as a BL Lac.

MS 1552.1+2020

We confirm this objects classification as a BL Lac. It has a preferred polarization position angle and a redshift of 0.222.

H 1652+398

This well known BL Lac (also named Mrk 501) is one of the most observed objects in our sample. Polarimetry has been published by various authors including those presented in Angel and Stockman 1980. The narrow range of variability of the polarization position angle had already been noted at that time. Rusk (1988) gives a mean polarization position angle of 136° and notes that the VLBI observations give a position angle of $128^\circ \pm 5$ for the small scale radio emission. During our monitoring the mean θ was 115° . This object has a redshift of .033.

MS 1704.9+6046

We are unable to confirm this objects classification as a BL Lac. It has a redshift of 0.280.

H 1722+119

This object is also known as 4U 1722+119. Of all XSBLs, it has reached the highest levels of percent polarization. The first polarimetry of this object was presented by Brissenden *et al.* 1990.

MS 1757.7+7034

We confirm this objects classification as a BL Lac, but note that the maximum observed polarization for this object was only 3.70 %.

MS 2143.4+0704

We confirm this objects classification as a BL Lac. This highly polarized object has a preferred polarization position angle. This object is in a field that contains an object with (or potentially has) extended x-ray emission (see §3.1). This objects relatively bright magnitude would make it an excellent choice for more detailed study as a representative of the XSBLs with preferred position angles.

H 2154–304

This well known BL Lac is unusually well studied. It is well known for its short timescales of variability at optical to x-ray wavelengths. We have a large data set of polarimetry on this object which can be merged with other existing data sets to provide a large set of constraints for detailed models like those made by Königl (1989). This object is one of the most variable in our sample. This object has a redshift of 0.117.

MS 2336.5+0517

We have a marginal detection of polarized emission from this object. We do not have any data to check for variability. This object is probably a BL Lac, but we can not confirm the classification at this time.

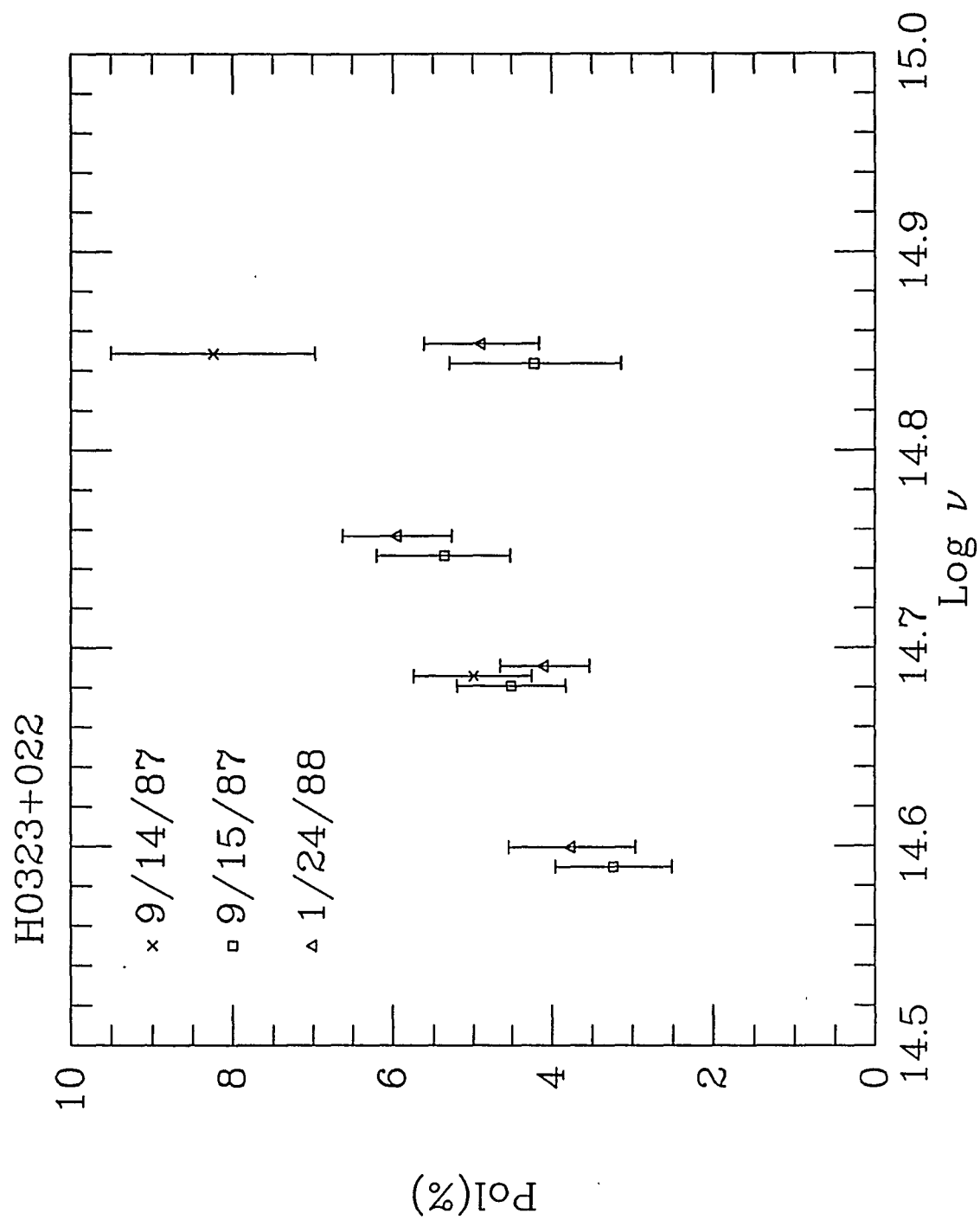
MS 2342.7-1531

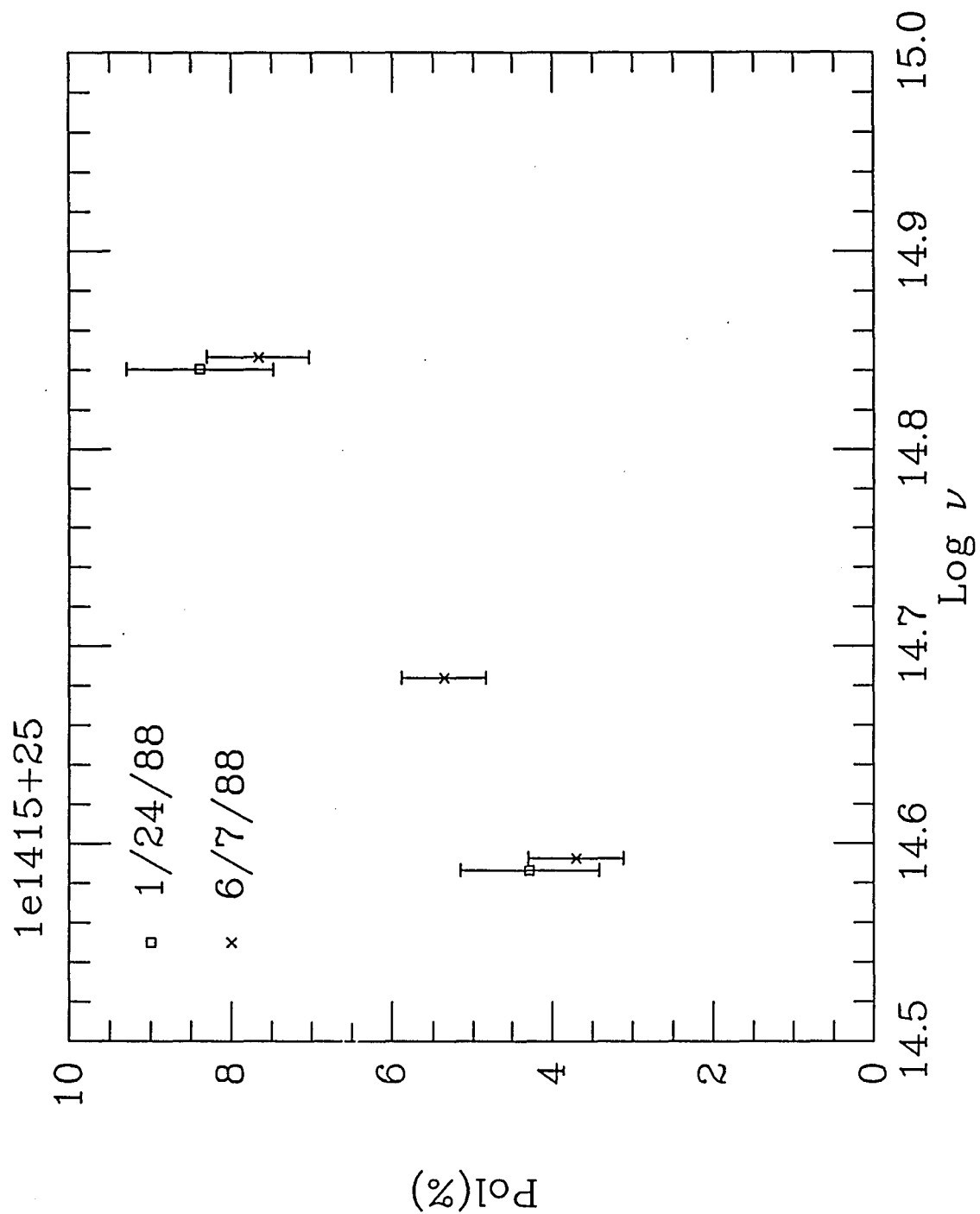
We confirm this objects classification as a BL Lac.

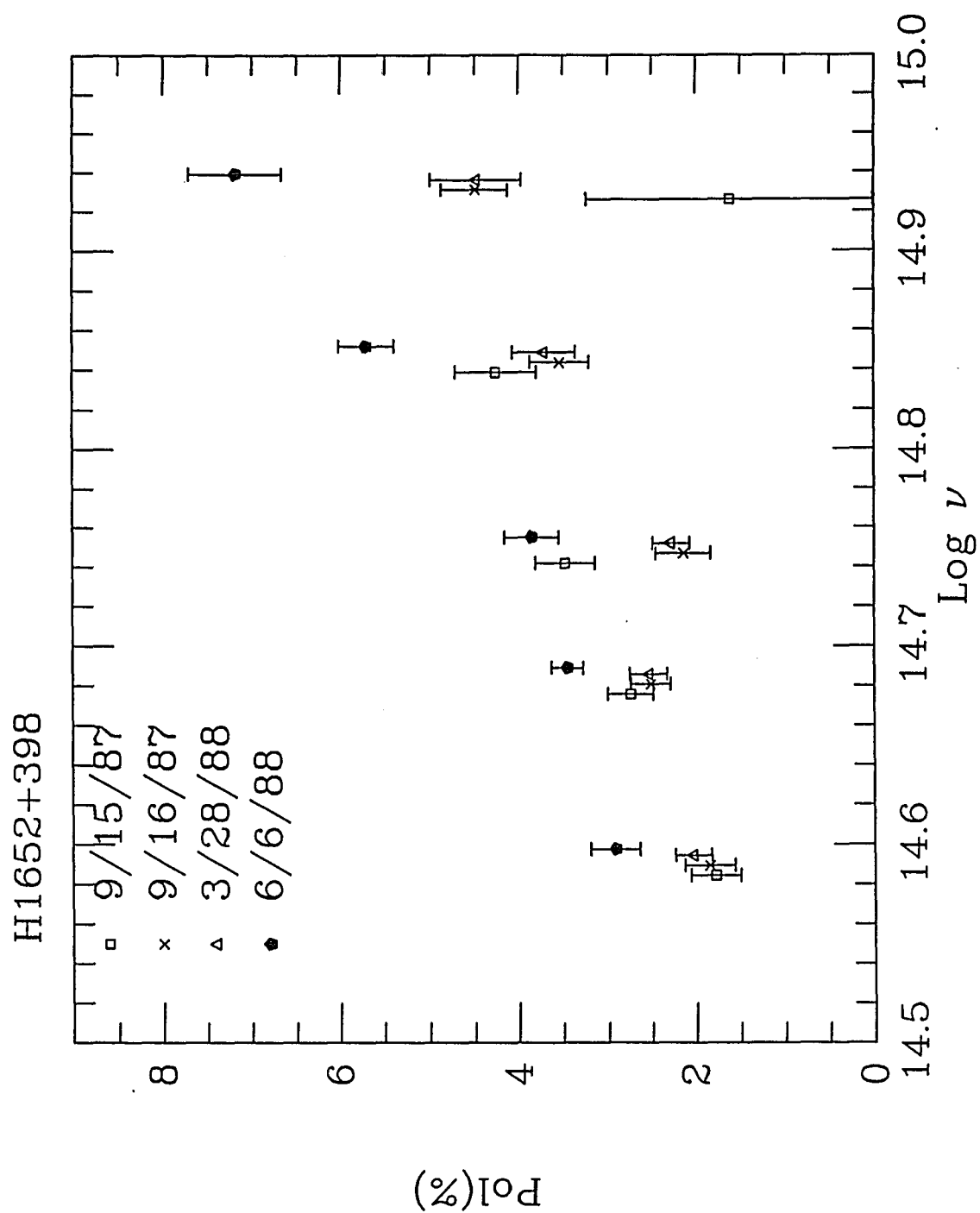
MS 2347.4+1924

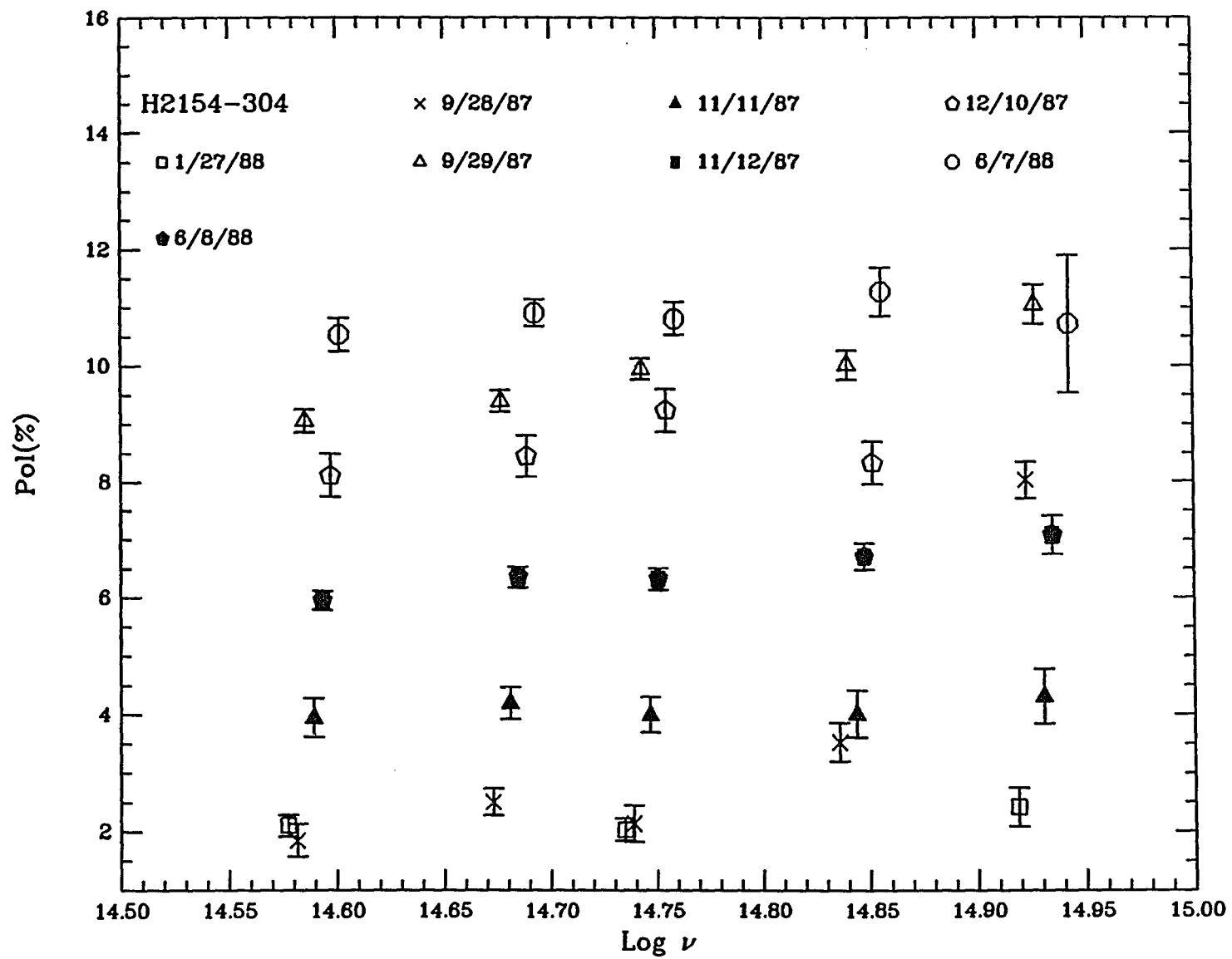
We have detected polarized emission from this object, but can not yet confirm its classification as a BL Lac. We need to confirm our detection of polarization.

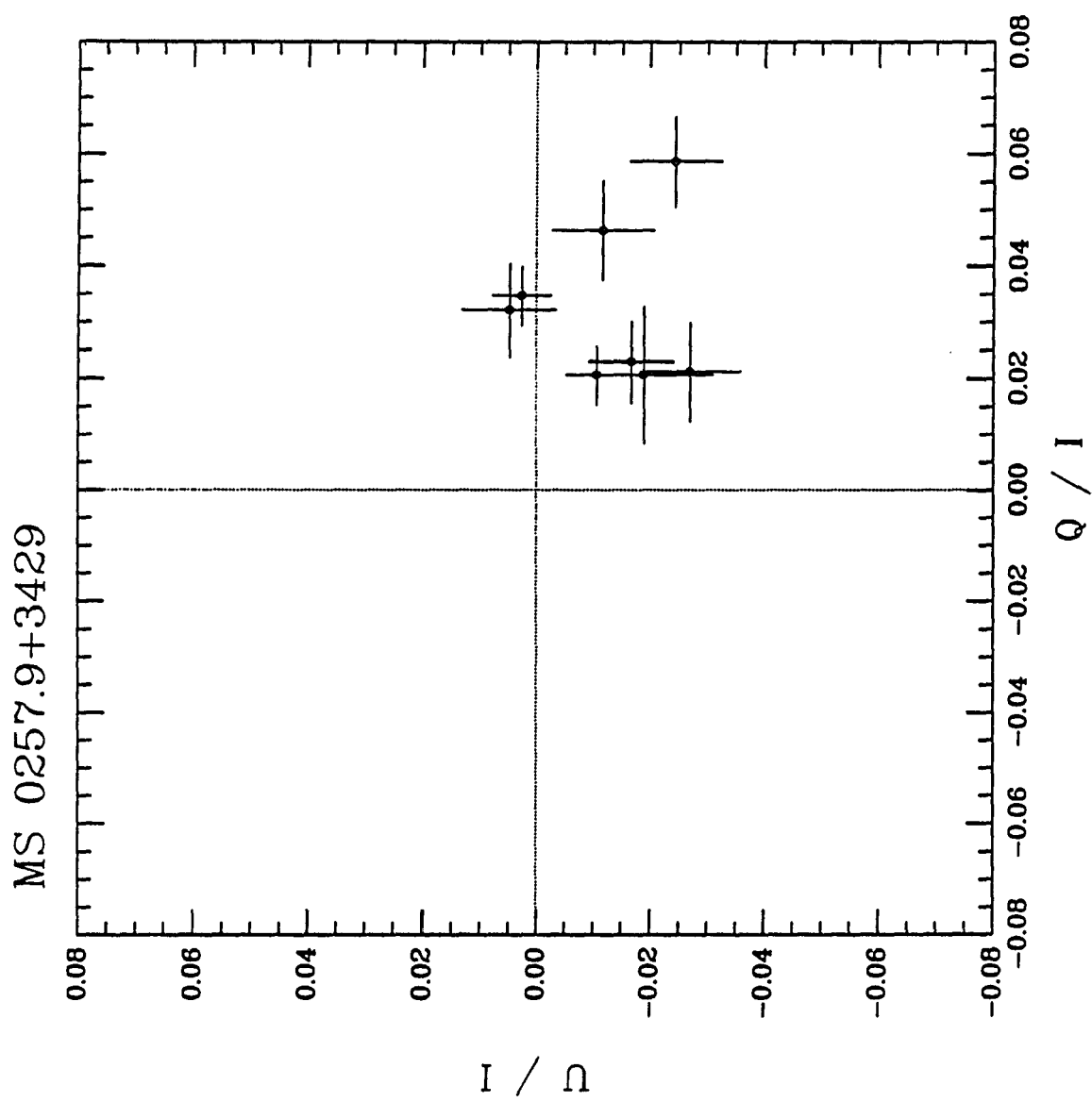
Figures II.1 through II.20 follow.

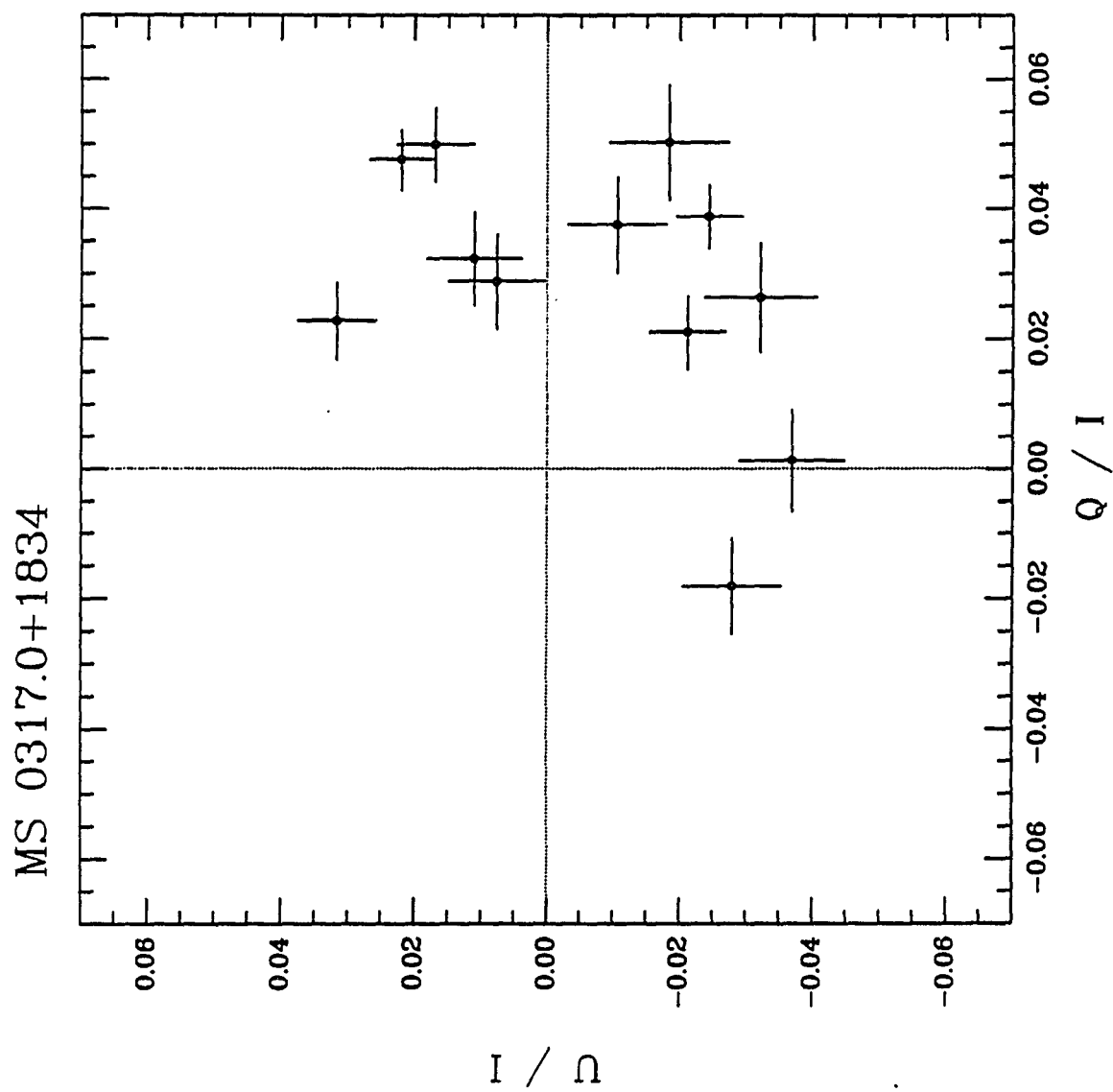


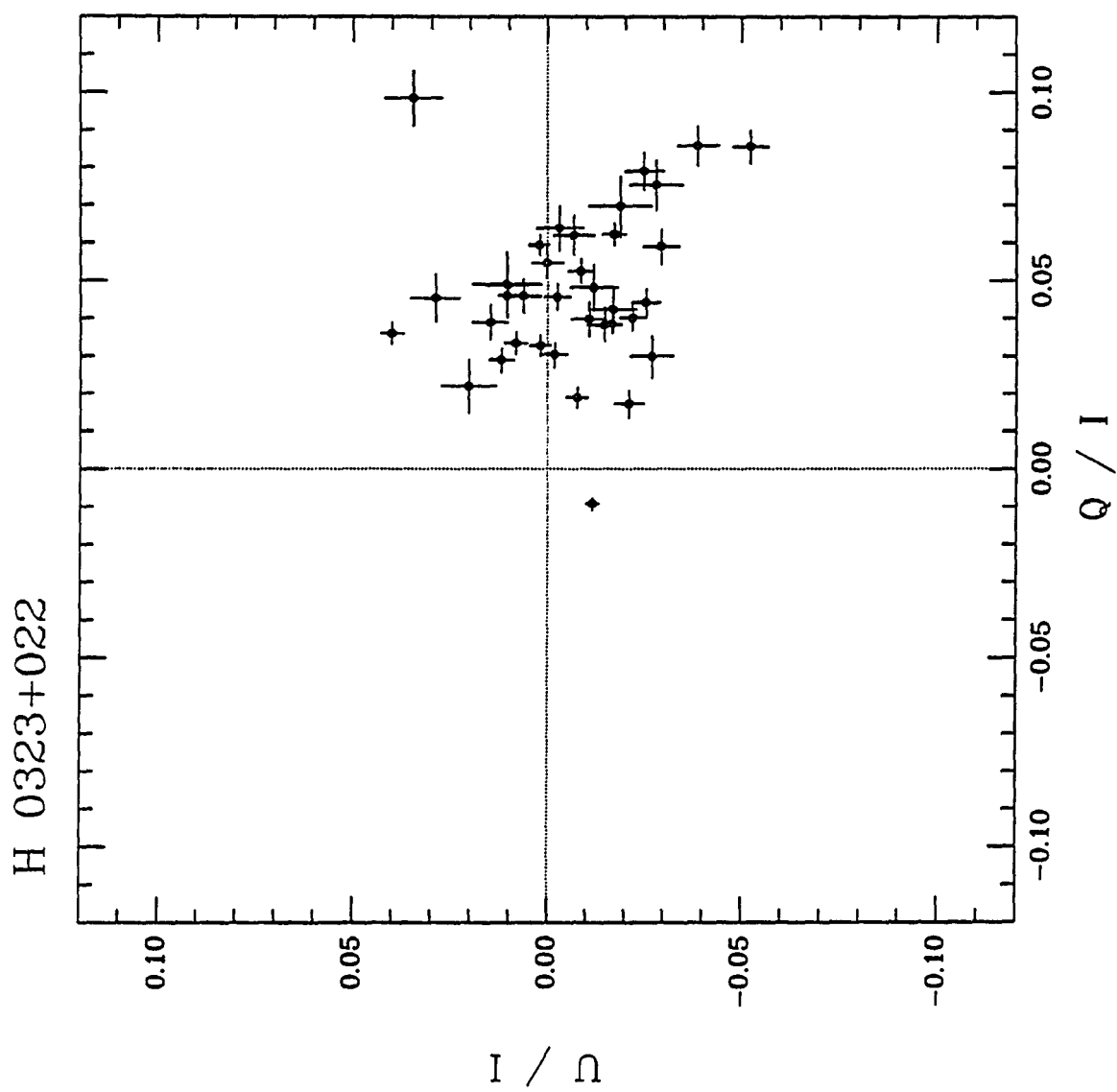


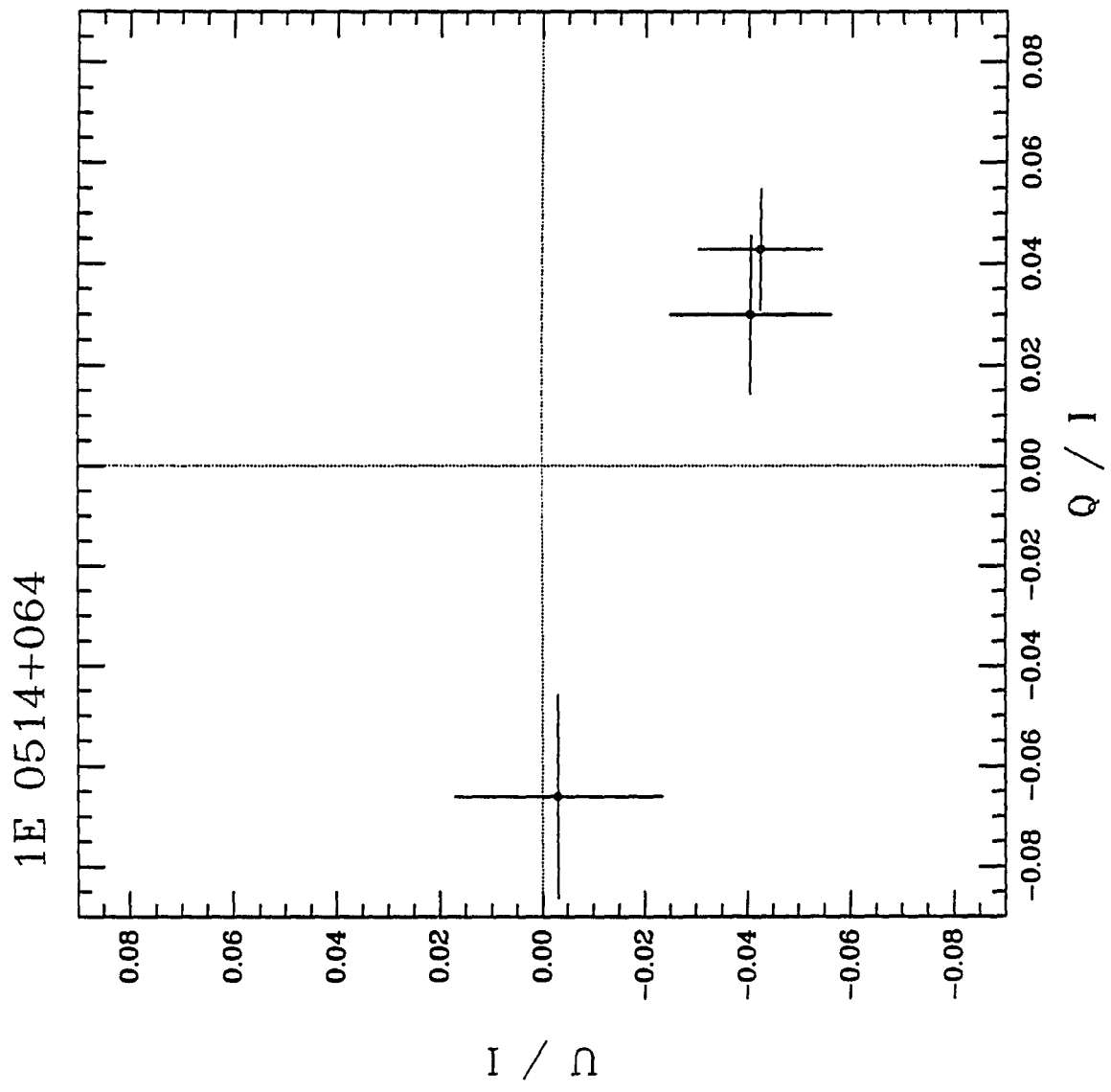


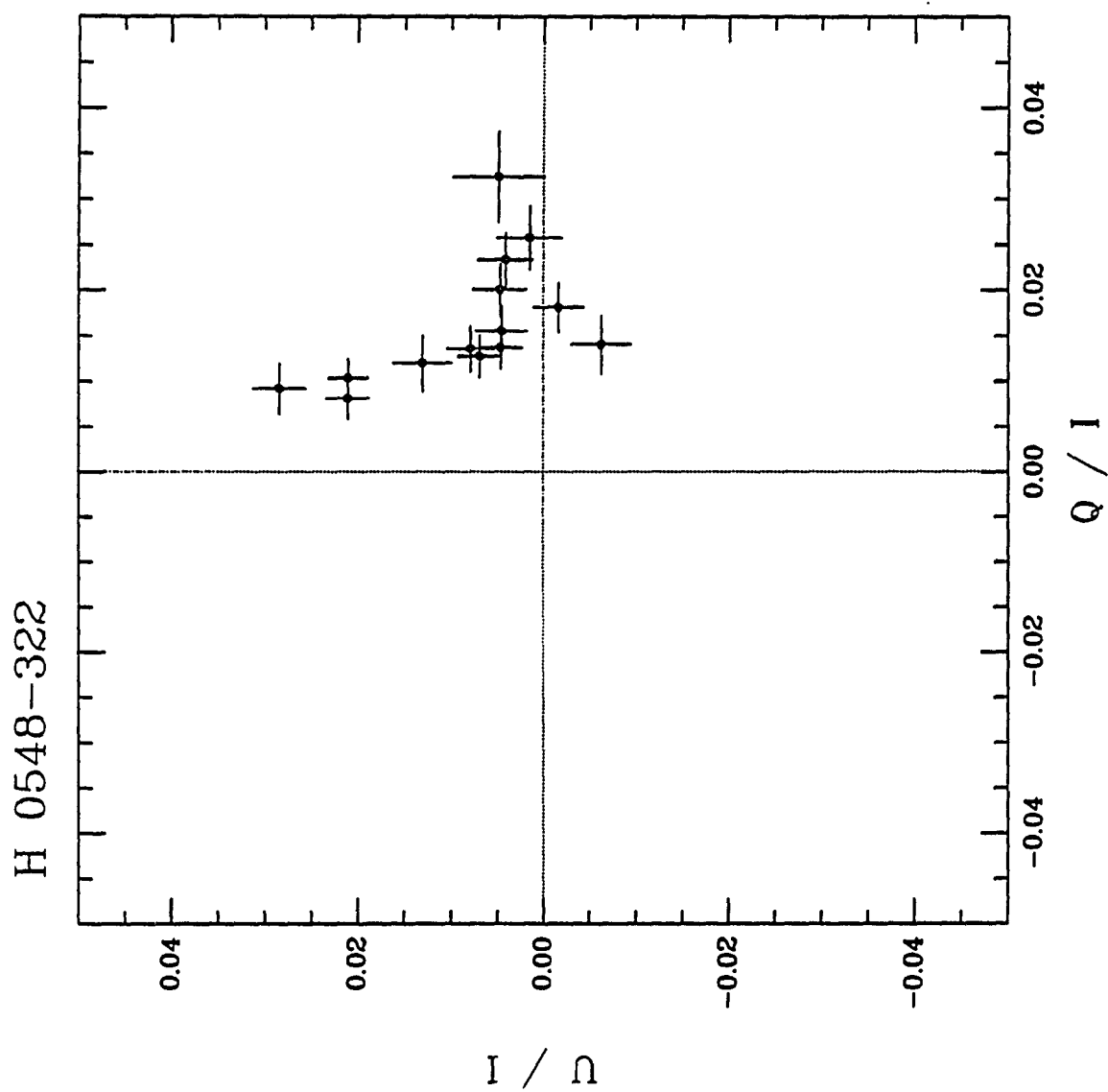


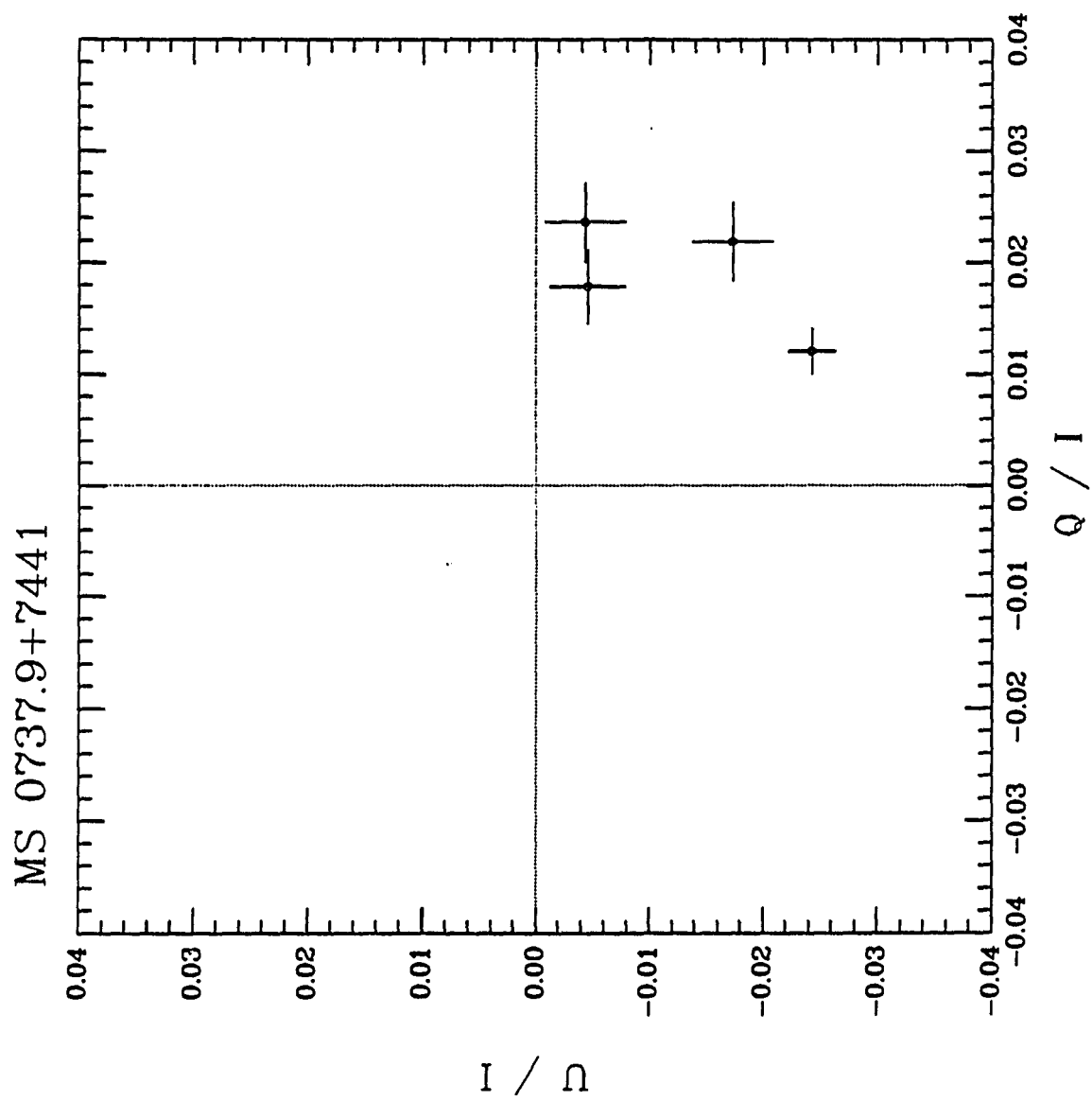


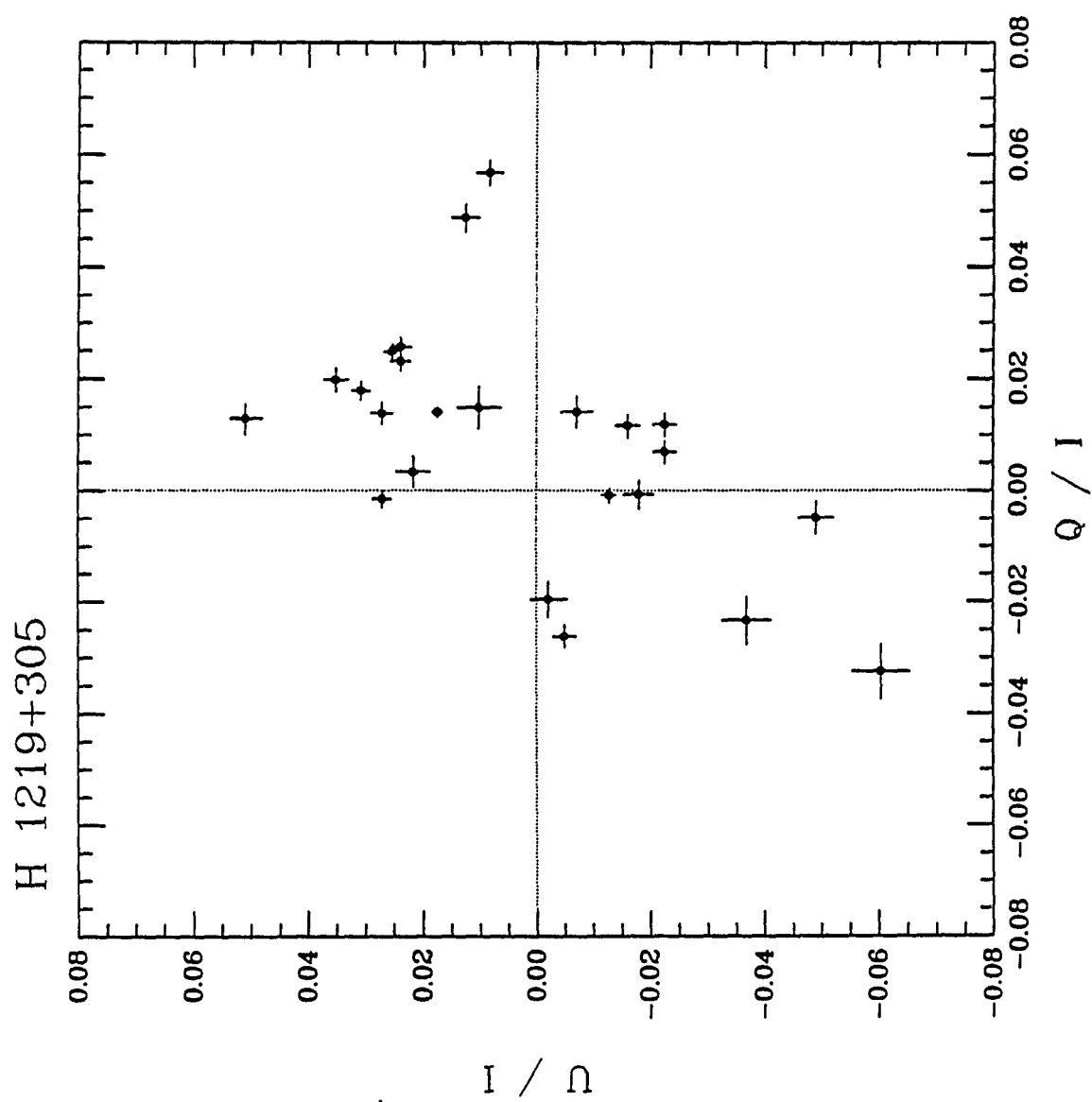


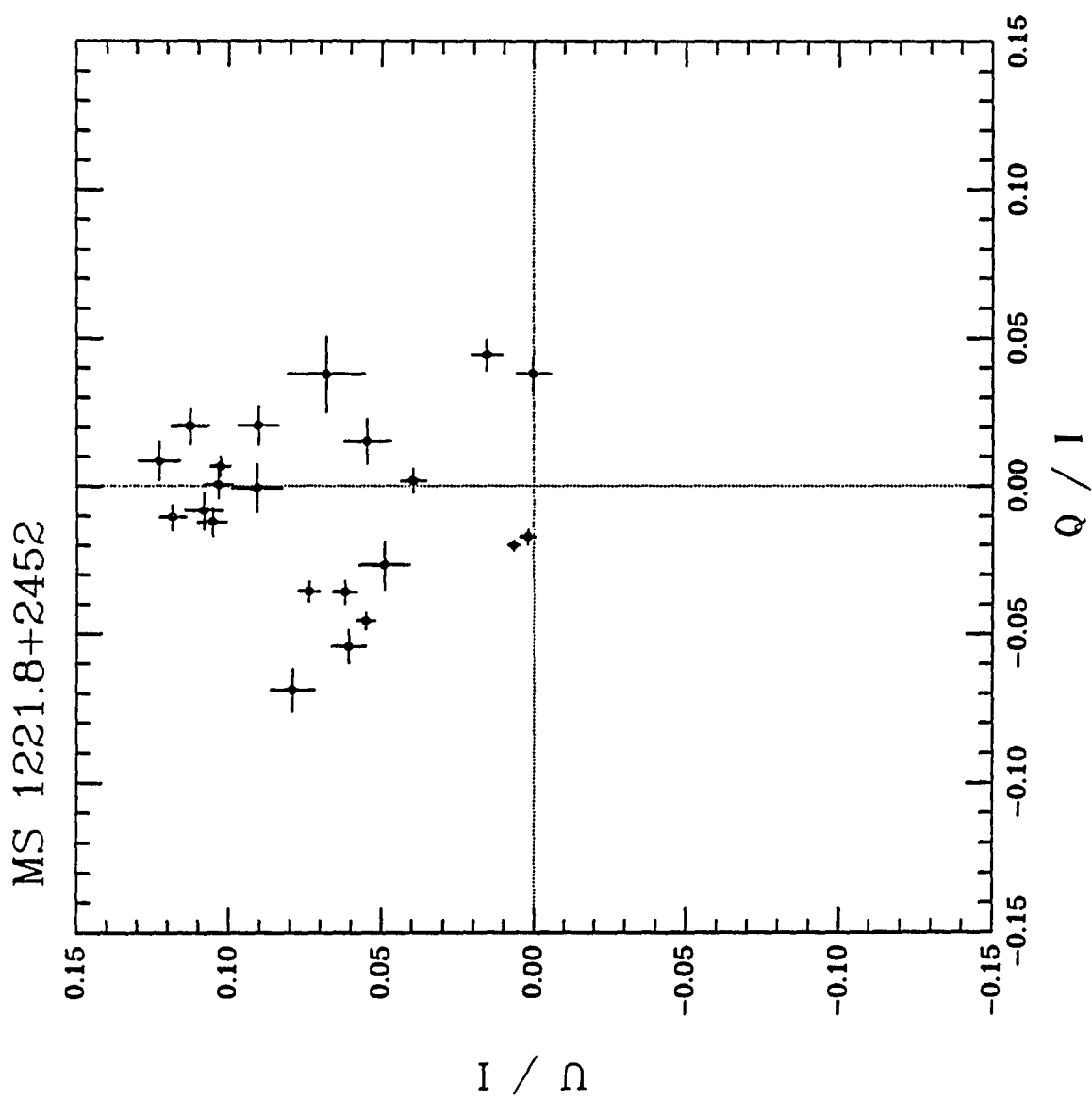


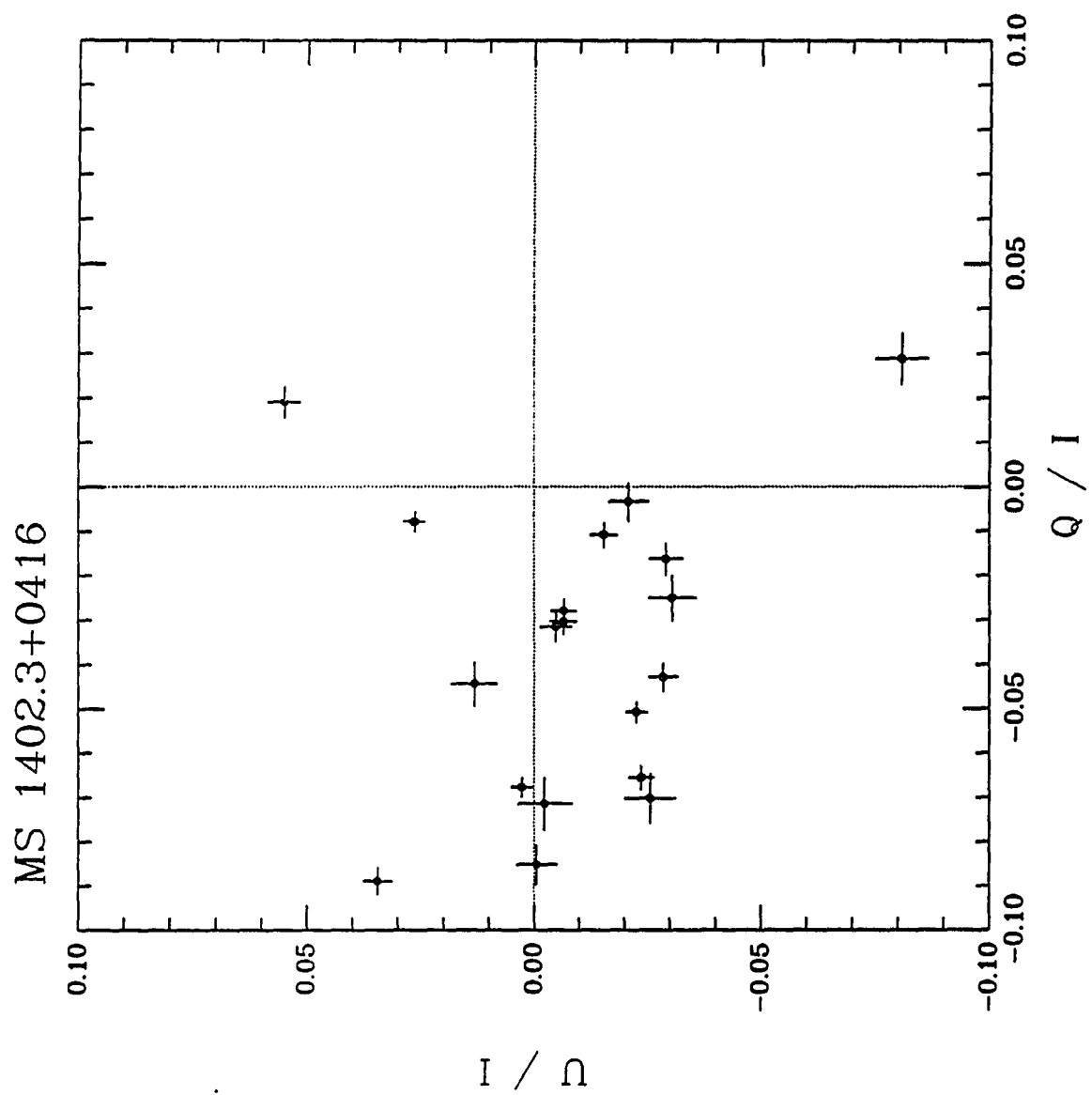


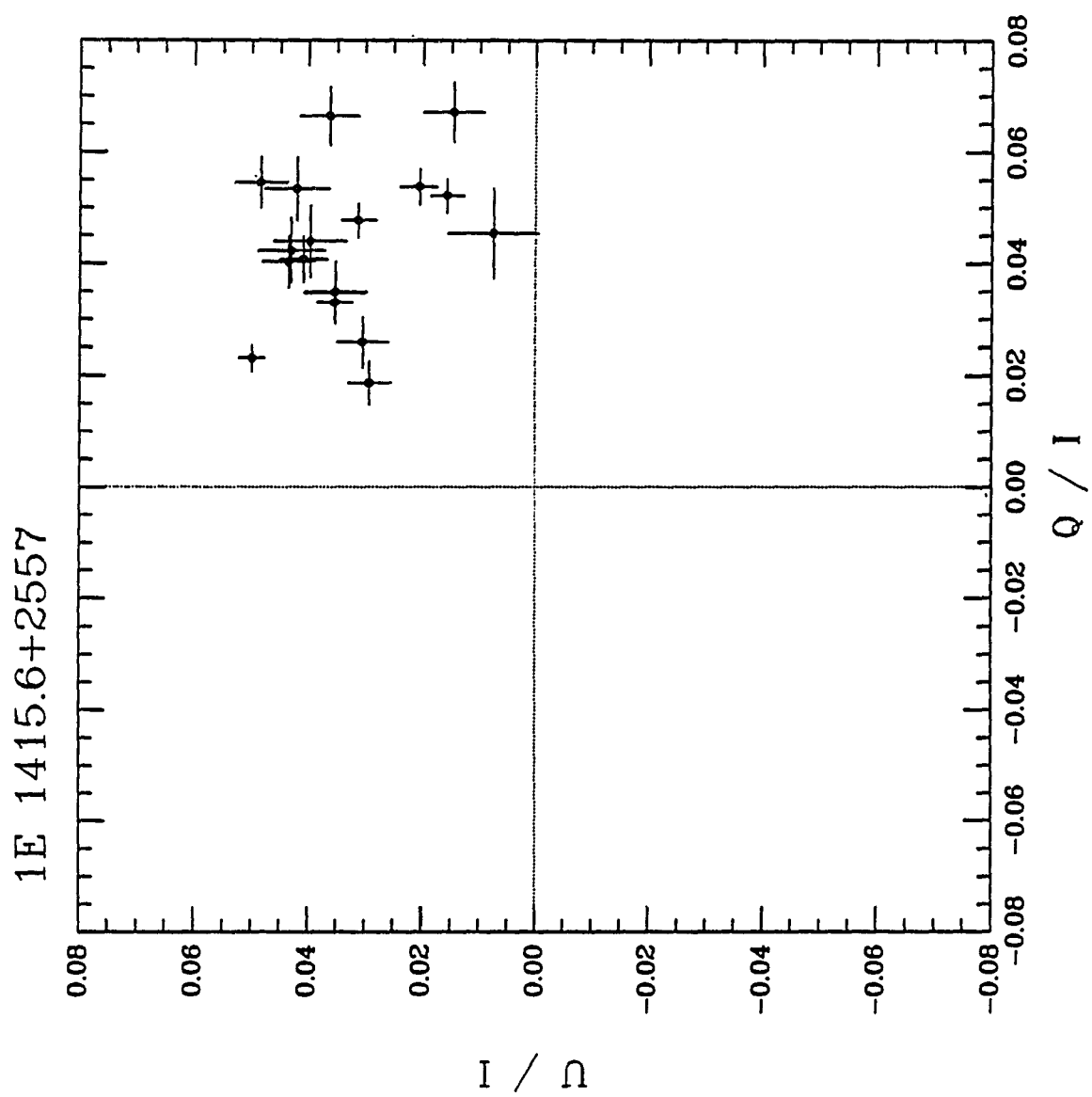


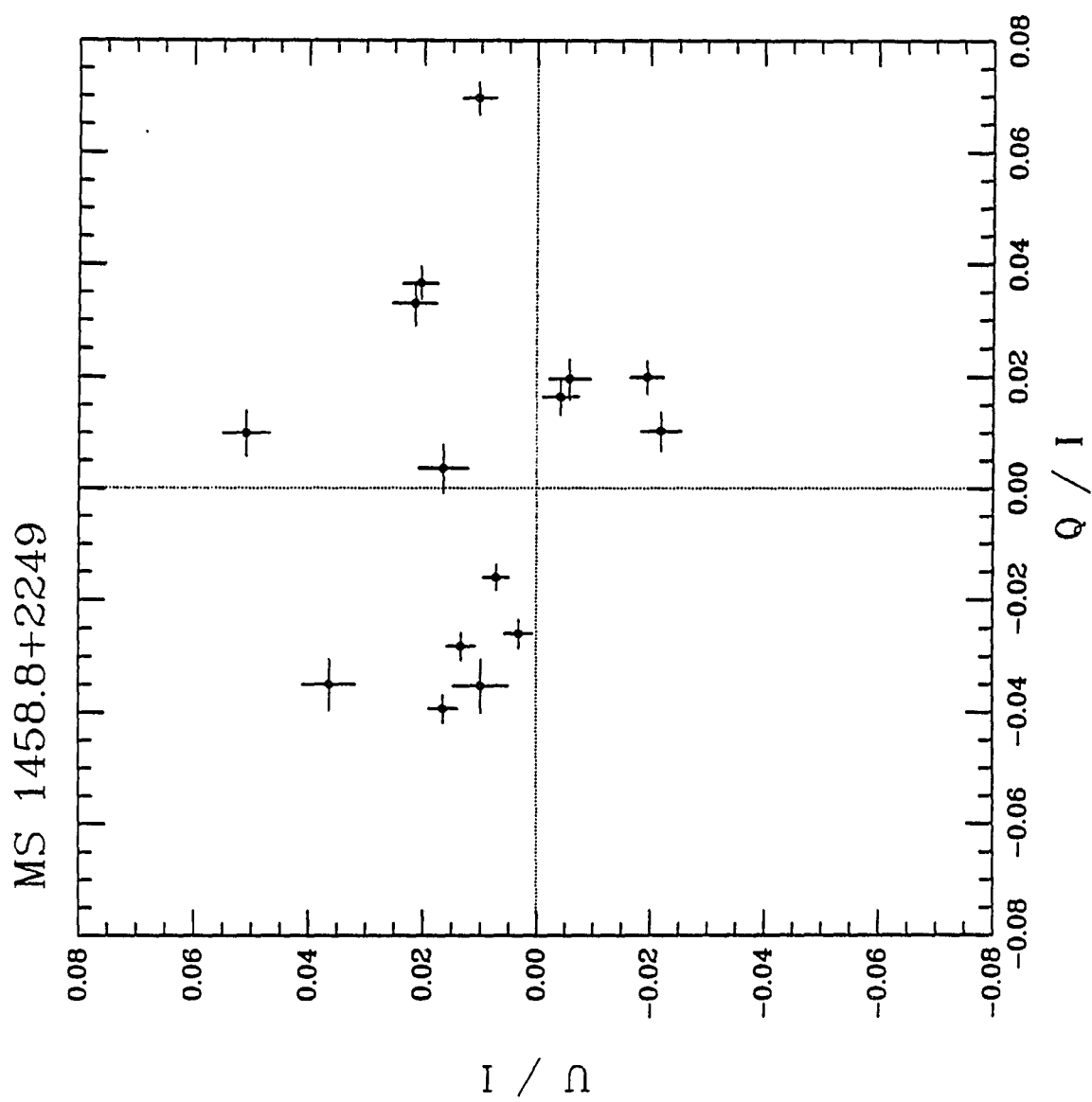


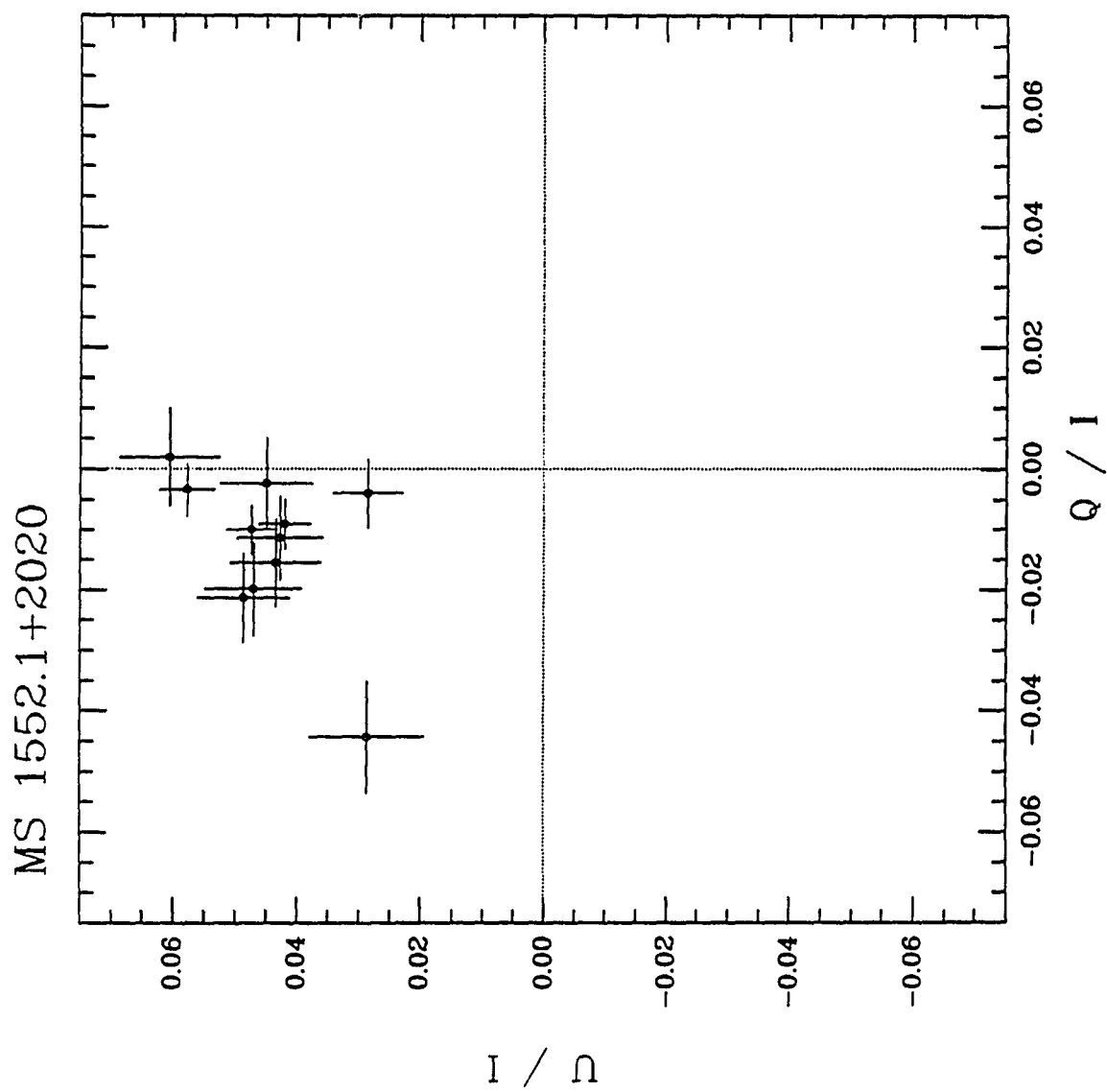


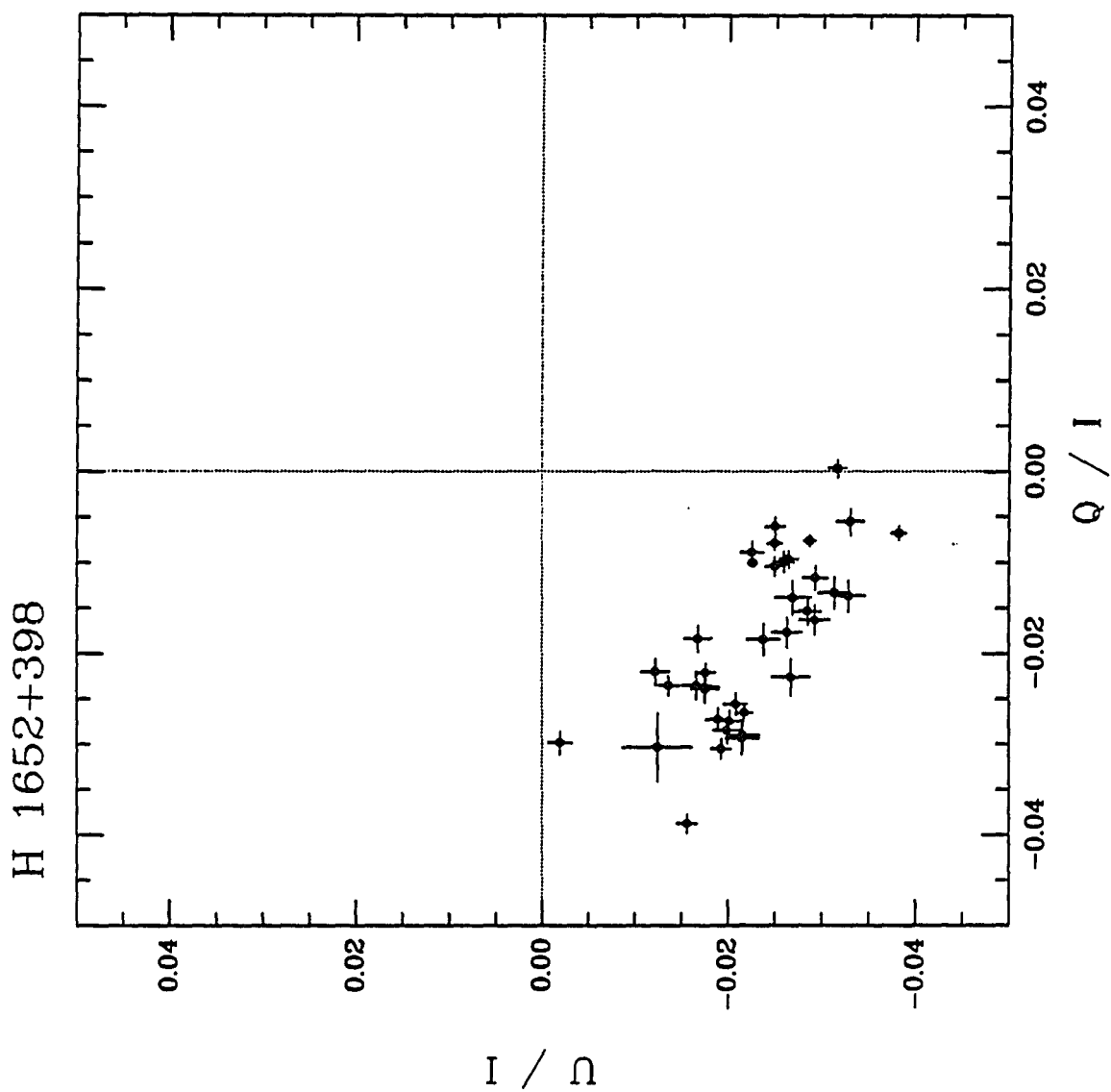




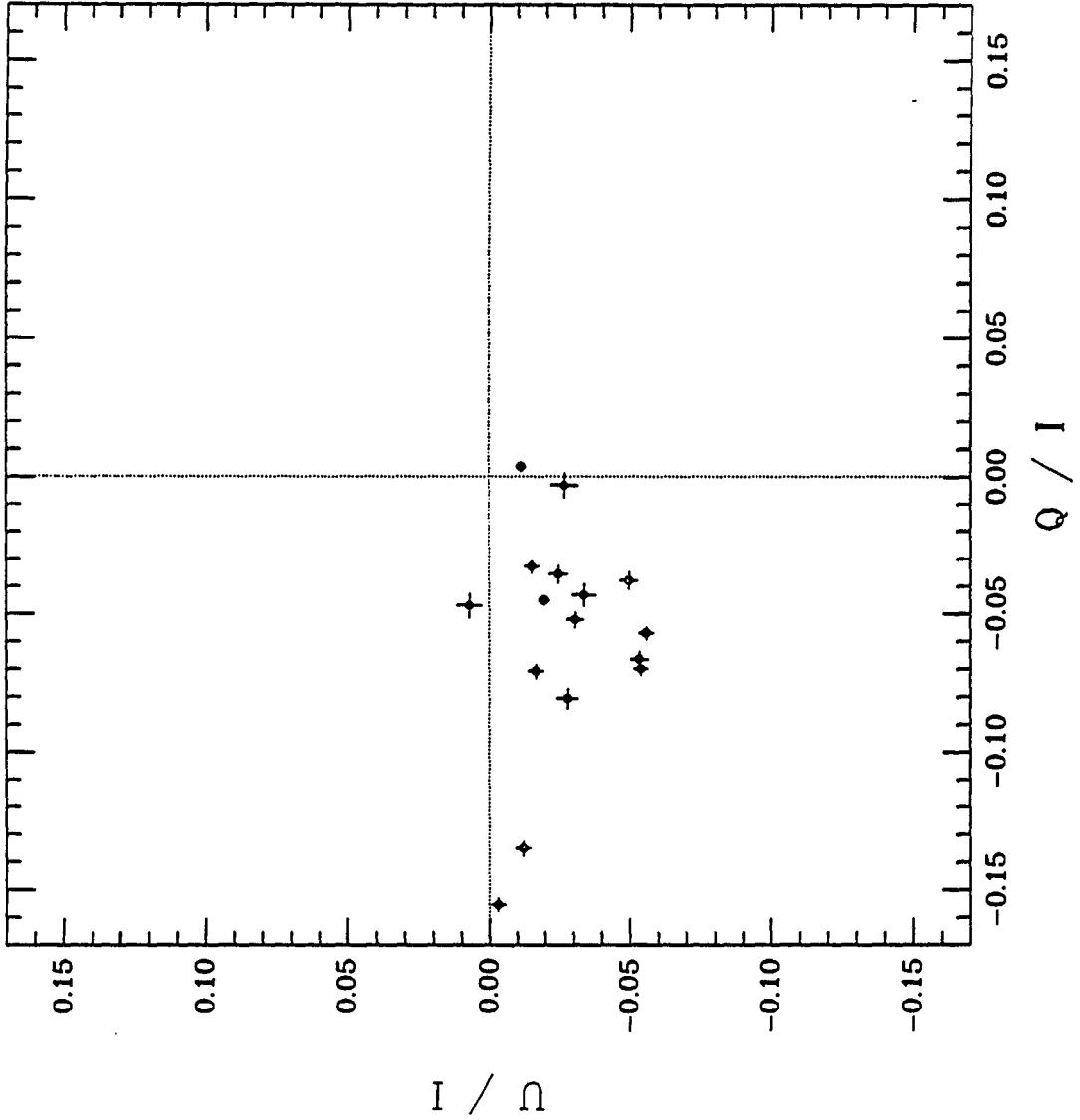




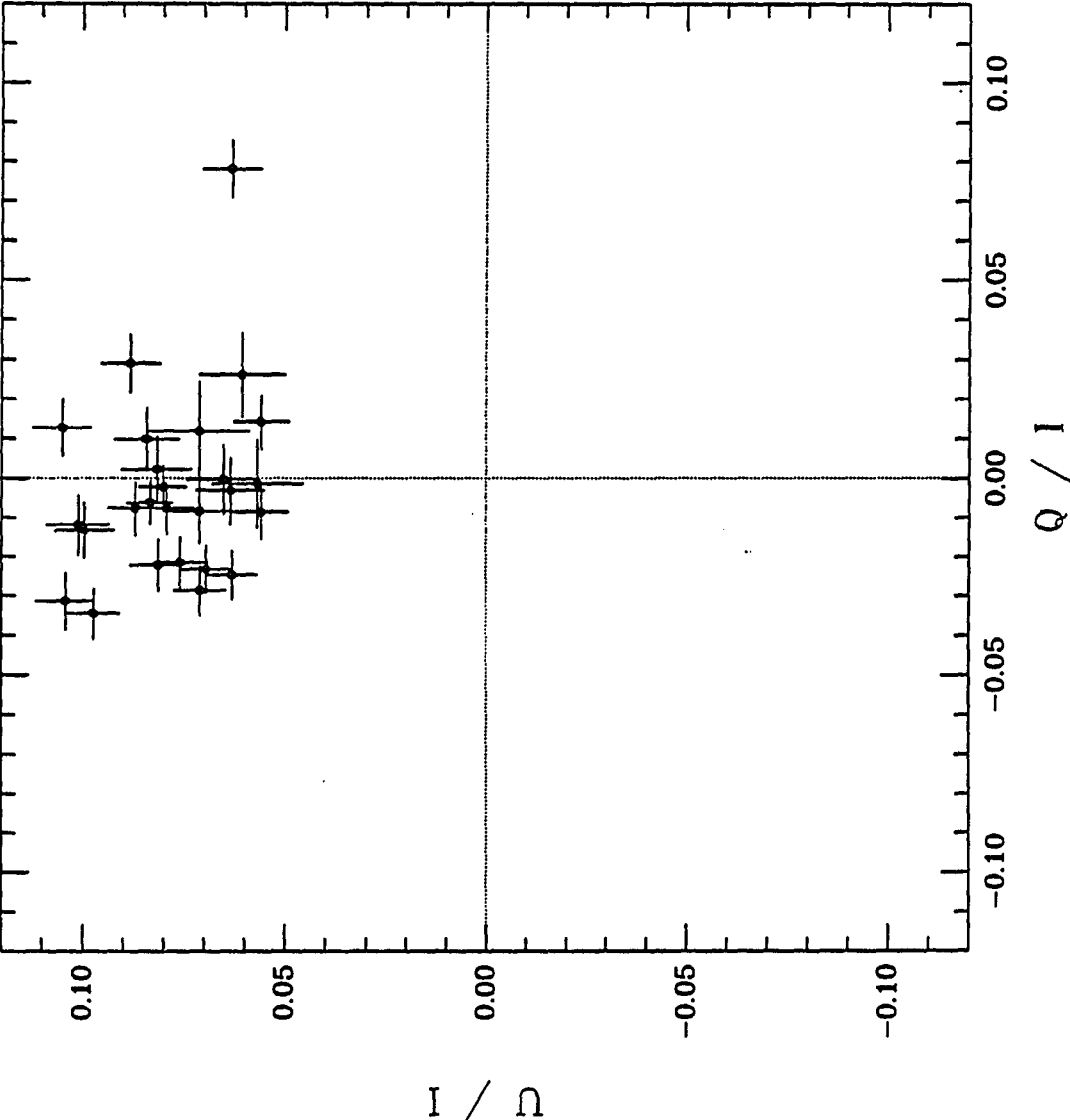




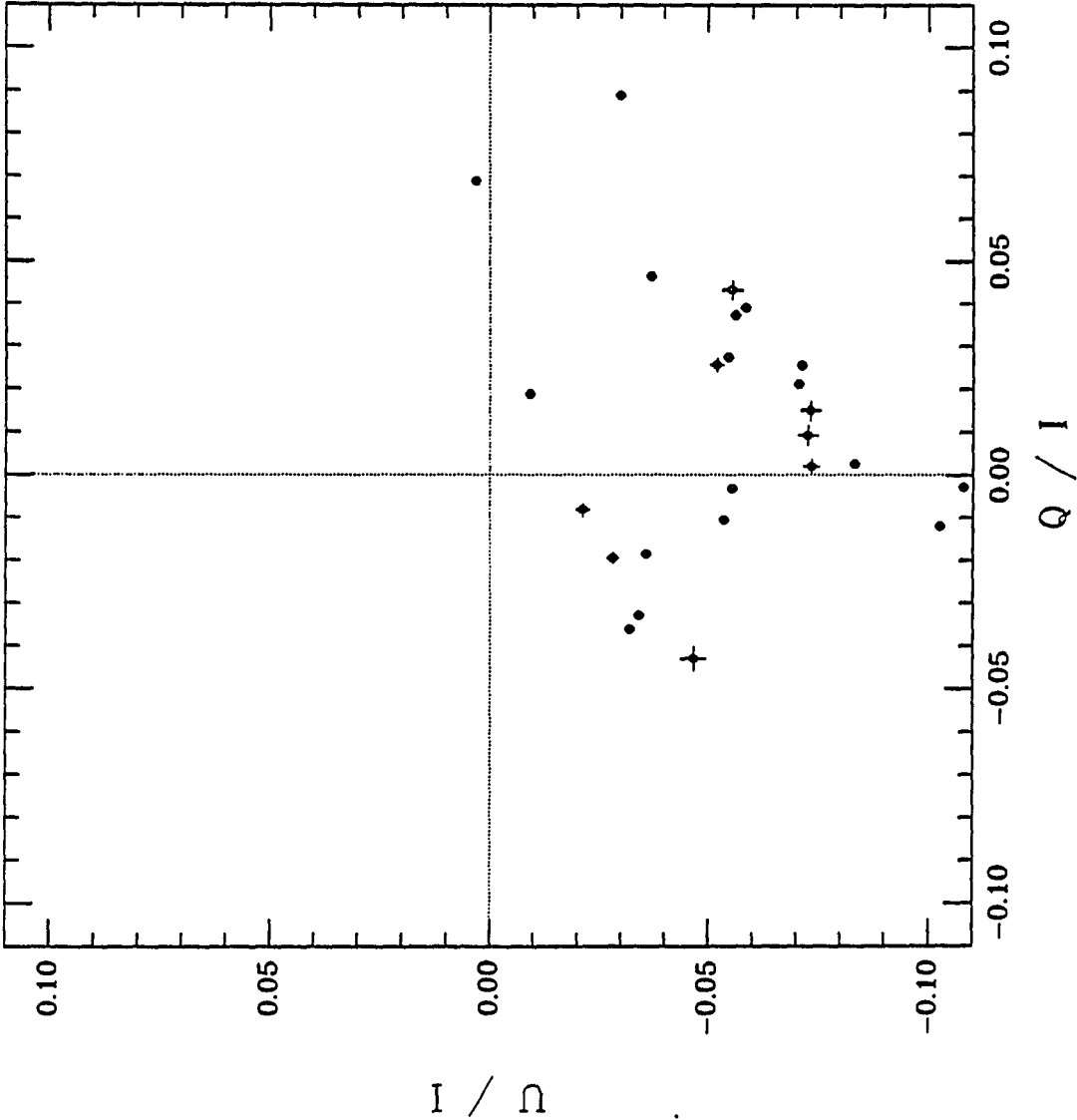
H 1722+119



MS 2143.4+0704



H 2154-304



APPENDIX III

POLARIMETRY OF RADIO LOUD X-RAY SELECTED ACTIVE GALACTIC NUCLEI

Notes For Appendix III

In this appendix we present our polarimetry and photometry of x-ray selected AGN from the *Einstein* Extended Medium Sensitivity Survey. The individual columns contain the following information: (1) Object Name, (2) UT Date of the observation, (3) the code indicating the telescope and instrument aperture (of "Two-Holer") used for the polarimetry (not for the photometry) observation (see Table 4.1 for explanation of the code), (4) the two sigma limit on the white light percent polarization, (5) the *V* band apparent magnitude of the object on the night the polarimetry observation was made, and (6) the one sigma error in the *V* magnitude.

Table III.1: Polarimetry of Radio Loud X-ray Selected AGN

Object Name (1)	UT Date (2)	Tel-Apt (3)	P (%) (4)	m_v (5)	σ (6)
MS 0038.7+3251	88.10.31	61-0	≤ 4.10		
MS 0038.7+3251	89.07.08	61-0	≤ 5.62		
MS 0038.7+3251	89.07.09	61-0	≤ 4.50		
MS 0038.7+3251	89.10.28	61-0	≤ 3.70		
MS 0038.8-0159	88.10.31	61-0	≤ 3.00		
MS 0012.5-0024	88.11.04	61-0	≤ 3.50		
MS 0136.3+0606	88.11.04	61-0	≤ 4.00		
MS 0226.8-1041	88.11.01	61-0	≤ 2.97		
MS 0232.5-0414	88.11.04	61-0	≤ 1.18		
MS 0311.8-0801	88.11.01	61-0	≤ 5.45		
MS 0311.8-0801	89.10.23	90-0	≤ 3.36		
MS 0449.4-1823	88.11.01	61-0	≤ 5.35		
MS 0449.4-1823	89.10.23	61-0	≤ 2.10		
MS 0521.7+7918	89.10.23	90-0	≤ 2.30		
MS 0815.7+5233	88.01.23	90-0	≤ 2.20	19.40	.07
MS 0815.7+5233	88.01.24	90-1	≤ 3.10		
MS 0815.7+5233	88.03.22	61-0	≤ 4.30		
MS 0815.7+5233	89.03.05	61-0	≤ 7.00		
MS 0815.7+5233	89.03.06	61-0	≤ 4.00	19.64	.13
MS 0815.7+5233	89.03.09	61-0	≤ 5.60		
MS 0815.7+5233	90.02.18	61-0	≤ 2.53	19.87	.20
MS 0822.0+0309	89.02.04	61-0	≤ 3.40		
MS 0822.0+0309	89.04.08	61-0	≤ 2.60		
MS 0822.0+0309	89.03.10	61-0	≤ 3.90		
MS 0833.3+6523	89.10.23	90-0	≤ 2.30		
MS 0850.2+2825	88.11.11	61-0	≤ 7.60		
MS 0850.2+2825	88.11.12	61-0	≤ 6.31		
MS 0850.2+2825	89.03.07	61-0	≤ 3.70		
MS 0850.2+2825	89.03.10	61-0	≤ 3.10		
MS 0850.2+2825	89.04.07	61-0	≤ 2.81		

Table III.1 continued

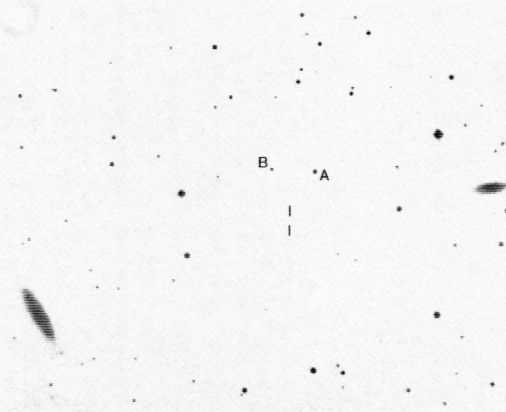
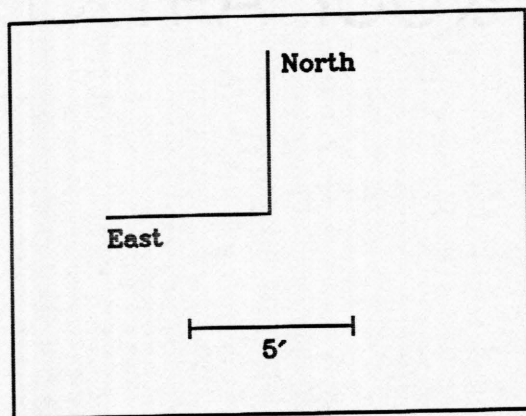
Object Name (1)	UT Date (2)	Tel-Apt (3)	P (%) (4)	m _v (5)	σ (6)
MS 0952.3+4412	89.02.03	61-0	≤ 2.60		
MS 1003.6+1300		61-0	≤ 2.90		
MS 1138.6+6553	89.07.02	90-1	≤ 3.52		
MS 1234.9+6651		90-1	≤ 3.23		
MS 1326.6+2546	89.07.04	61-0	≤ 3.40		
MS 1340.7+2859		61-0	≤ 2.97		
MS 1442.8+6344		90-1	≤ 1.83		
MS 1623.4+2712		61-0	≤ 2.34		
MS 1640.0+3940		61-0	≤ 5.00		
MS 1640.0+3940		61-0	≤ 3.89		
MS 2134.0+0028	89.10.29	61-0	≤ 1.30		
MS 2134.0+0028	88.10.31	61-0	≤ 2.61		
MS 2141.2+1730	88.11.02	61-0	≤ 1.12		
MS 2141.2+1730		61-1	≤ 2.10		

APPENDIX IV

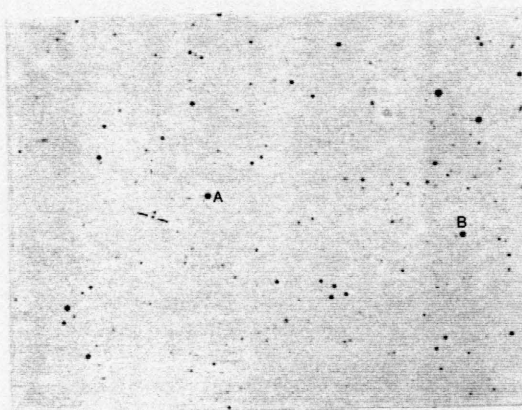
FINDING CHARTS

Notes on Appendix IV

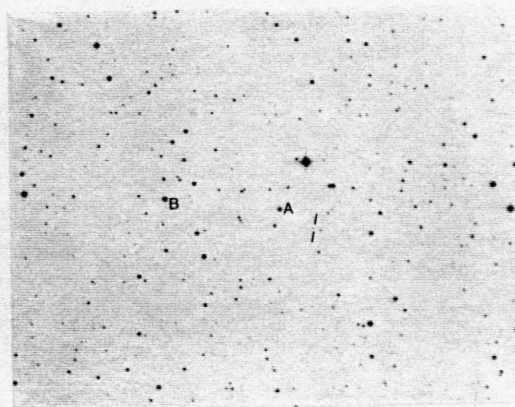
In this appendix we provide Finding Charts for the x-ray selected BL Lacs in our monitoring program and for two of the optical polarization survey candidate objects. The x-ray positions for the EMSS XSBLs are given by Gioia *et al.* 1990. The offsets to the optical identifications will be given by Stocke *et al.* 1991. The comparison stars that we have calibrated to be *UBVRI* photometric standards are labeled with letters in each field. The objects are indicated by two lines pointed at the object. The data for these stars is presented in Table 4.4 (Chapter 3). An improved finder of MS 0607.9+7108 (a CCD image) will be provided (along with all of the XSBL finders and positions) in Smith, Jannuzi, and Elston 1991. The two optical polarization survey candidates are presented at the end of this appendix. Their coordinates are presented in Chapter 7.



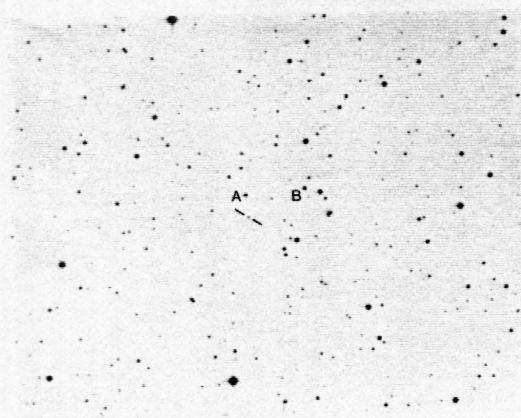
MS 0122.1+0903



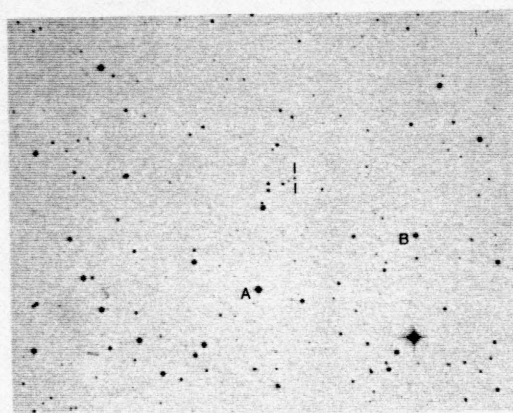
MS 0158.5+0019



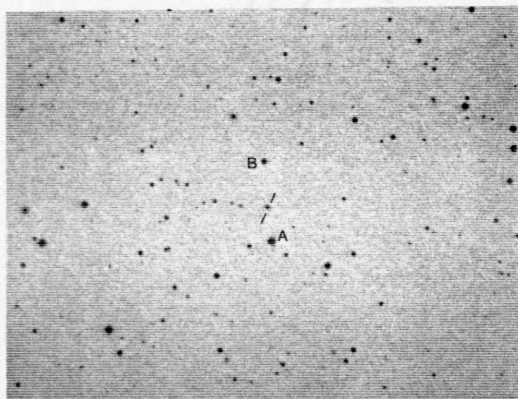
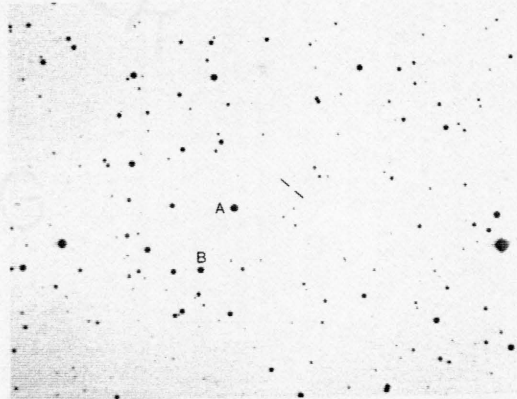
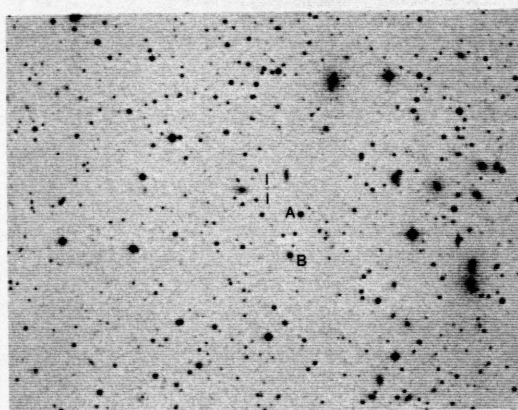
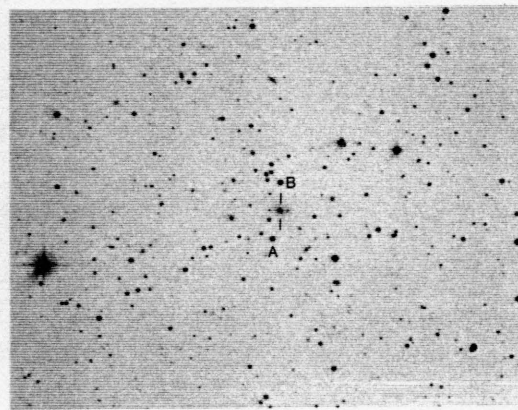
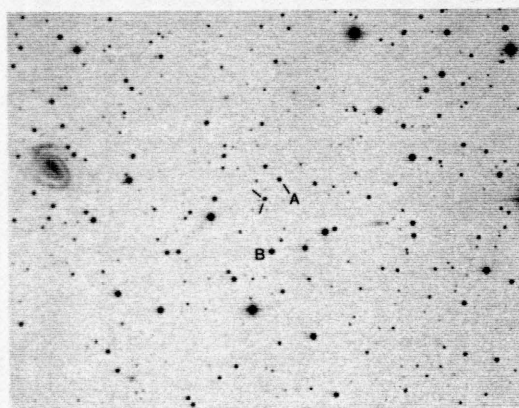
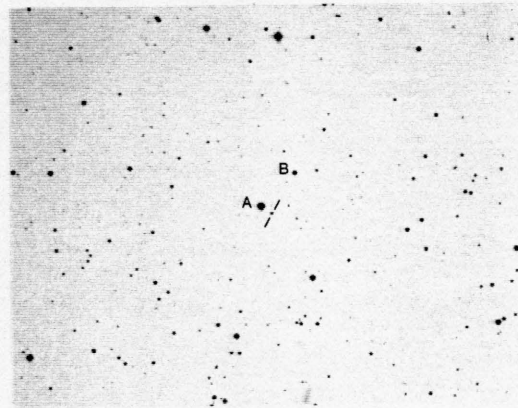
MS 0205.7+3509

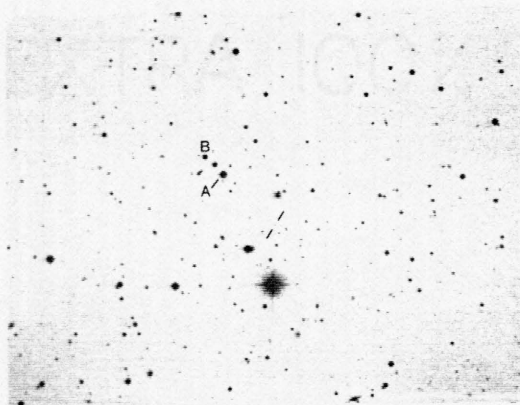


MS 0257.9+3429

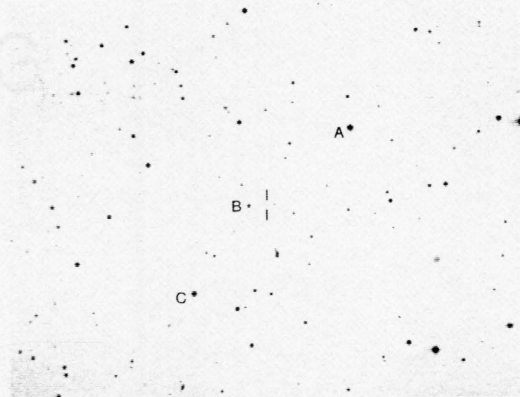


MS 0317.0+1834

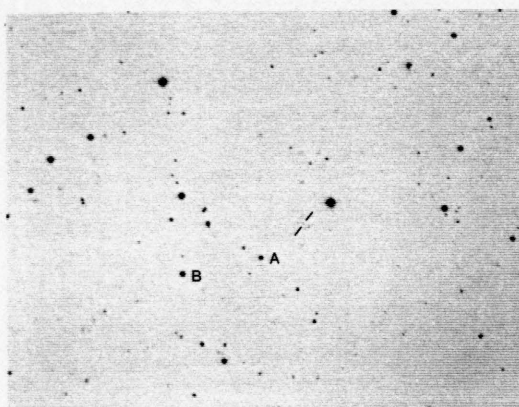
**H 0323+022****MS 0419.3+1943****1E 0514+064****H 0548-322****MS 0607.9+7108****MS 0737.9+7441**



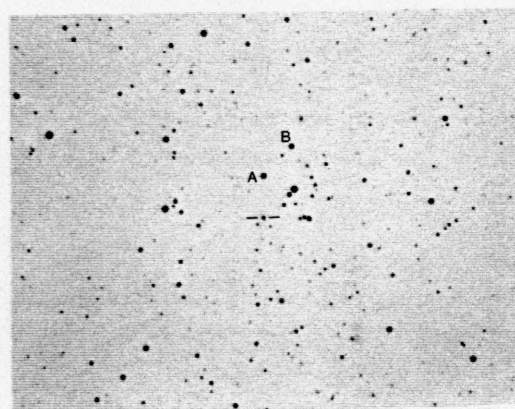
MS 0922.9+7459



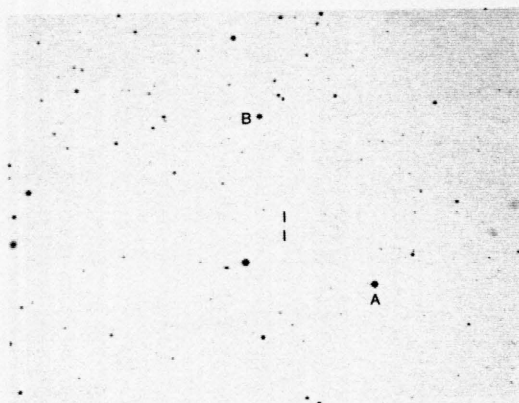
MS 0950.9+4929



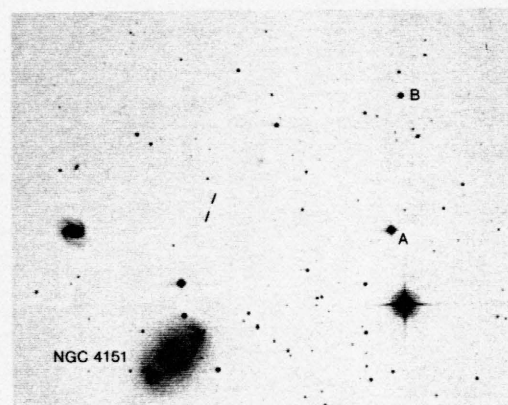
MS 0958.9+2102



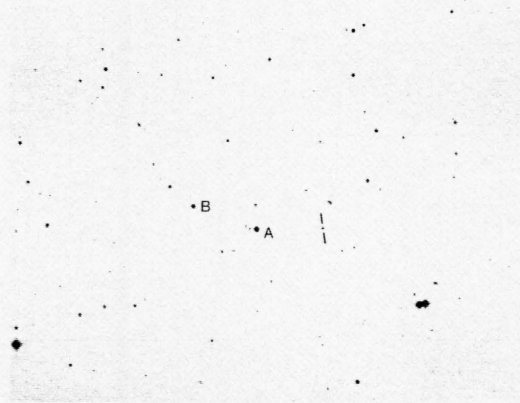
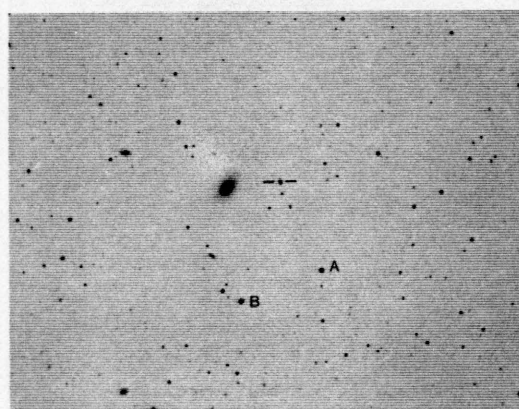
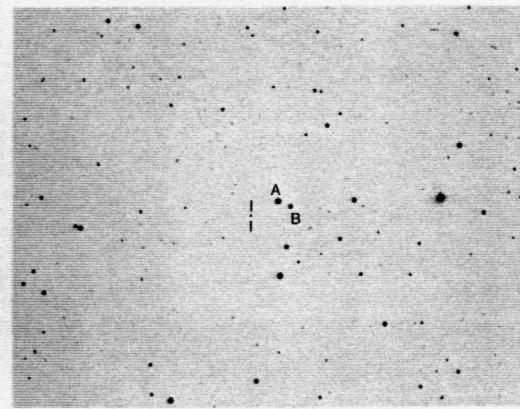
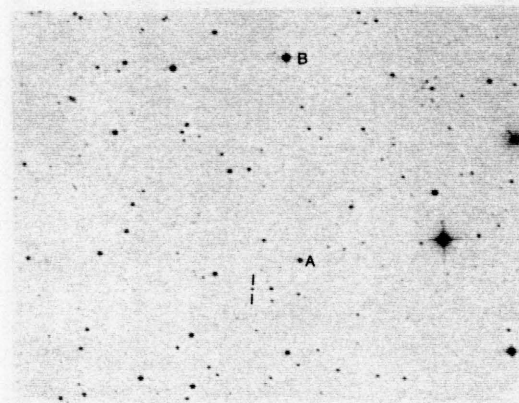
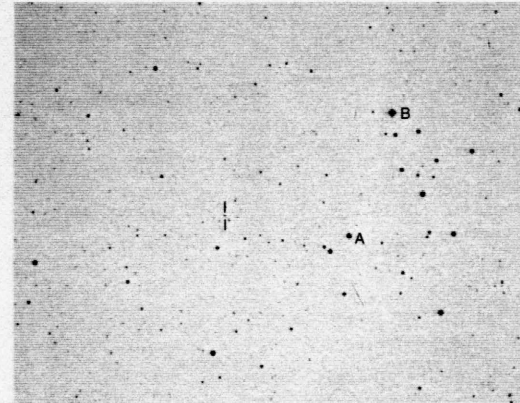
H 1101-232

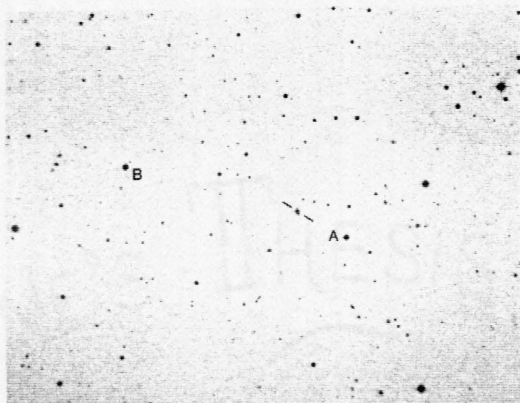
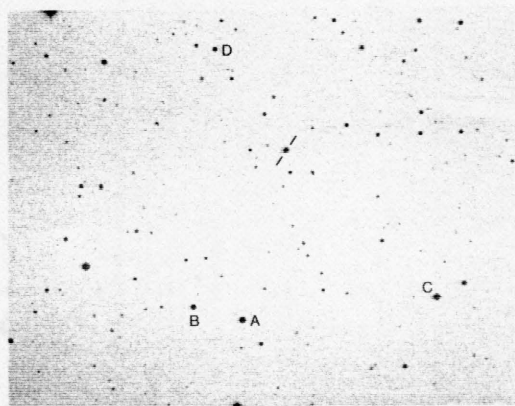
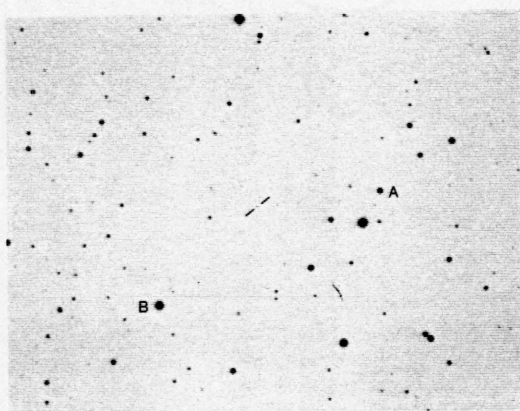
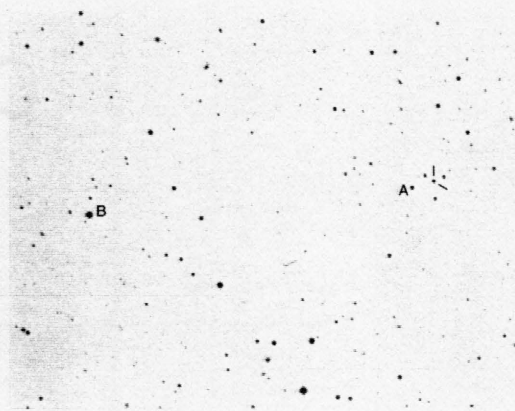
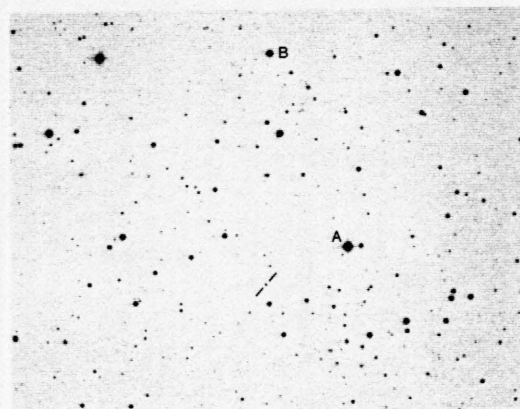
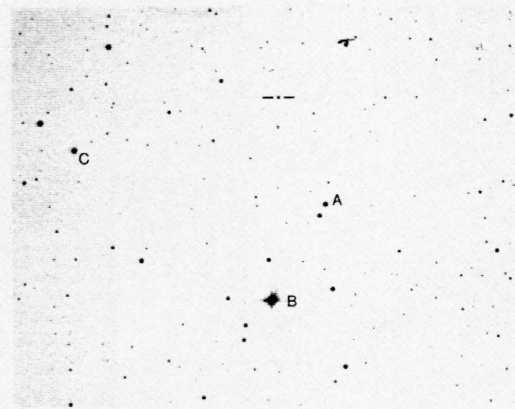


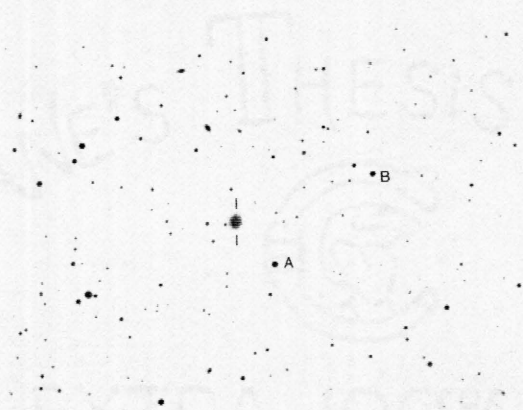
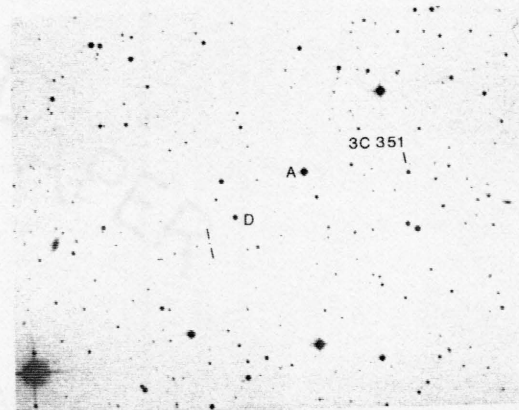
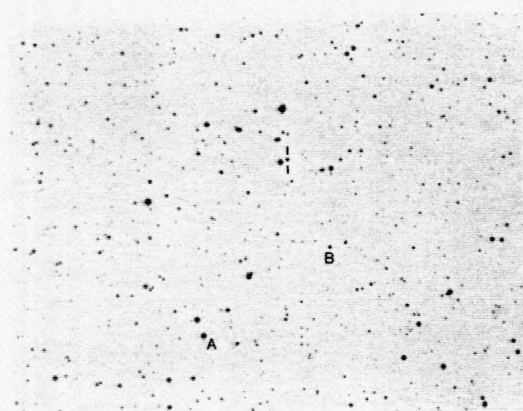
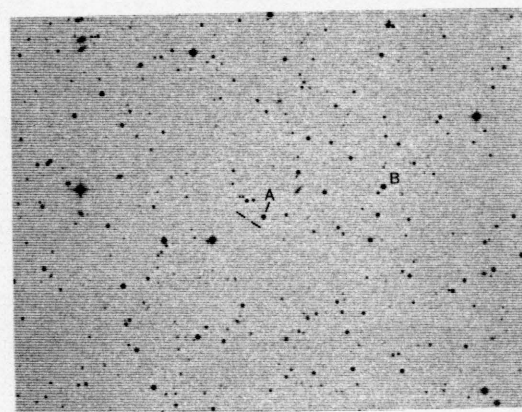
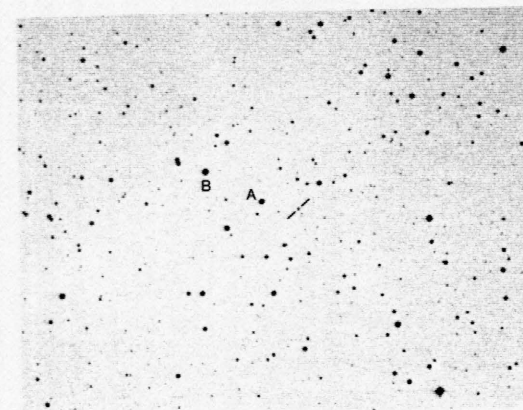
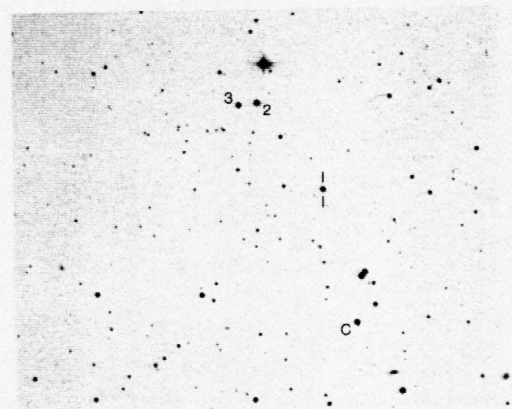
MS 1133.7+1618

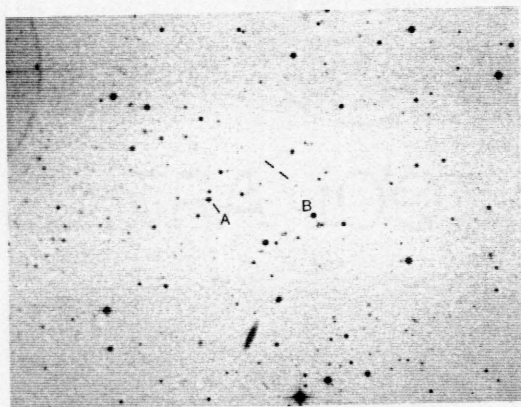


MS 1207.9+3945

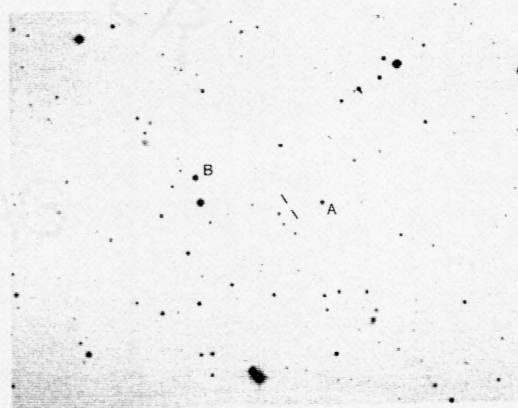
**H 1219+305****MS 1221.8+2452****MS 1229.2+6430****MS 1235.4+6315****MS 1402.3+0416****MS 1407.9+5954**

**1E 1415.6+2557****H 1426+428****MS 1443.5+6349****MS 1458.8+2249****MS 1534.2+0148****MS 1552.1+2020**

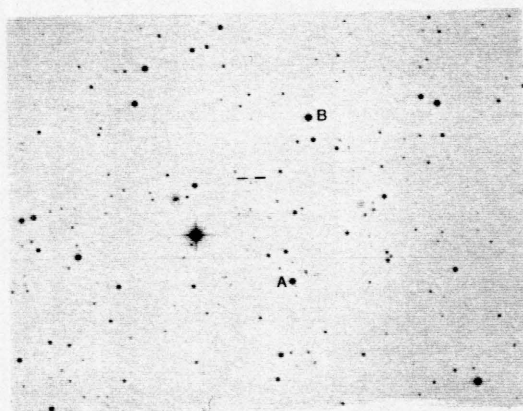
**H 1652+398****MS 1704.9+6046****H 1722+119****MS 1757.7+7034****MS 2143.4+0704****H 2154-304**



MS 2336.5+0517



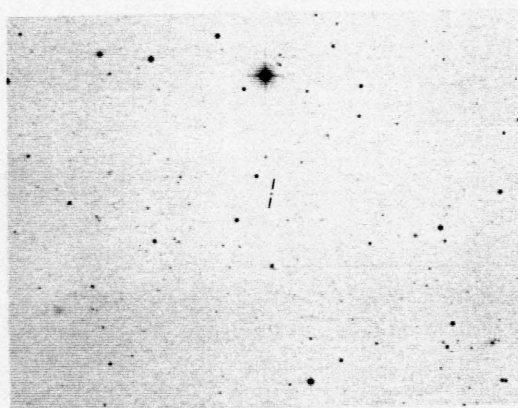
MS 2342.7-1531



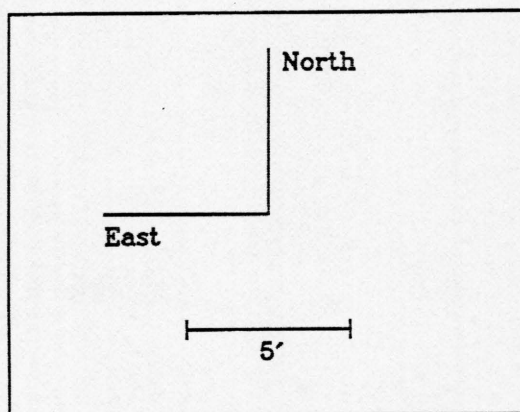
MS 2347.4+1924



OP 0229.0+0629



OP 1106.7+3654



LIST OF REFERENCES

- Angel, J. R. P., and Stockman, H. S. 1980, *Ann. Rev. Astr. Ap.*, **8**, 321.
- Angel, J. R. P. 1974, " Mechanisms That Produce Linear and Circular Polarization" in *Planets, Stars and Nebulae Studied with Photopolarimetry*, ed. T. Gehrels, (Tucson: University of Arizona Press), p. 54.
- Antonucci, R. R. J. 1984, *Ap. J.*, **278**, 499.
- Antonucci, R. R. J., and Ulvestad, J. 1985, *Ap. J.*, **294**, 158.
- Bahcall, J. N., and Soneira, R. M. 1980, *Ap. J. Suppl.*, **44**, 73.
- Ballard, K. R., Mead, A. R. G., Brand, P. W. J. L., and Hough, J. H. 1990, *M. N. R. A. S.*, **243**, 640.
- Barthel, P. 1989, *Ap. J.*, **336**, 606.
- Bartusiak, M. 1986. *Thursday's Universe*, (New York: Random House).
- Berriman, G. 1989, *Ap. J.*, **345**, 713.
- Berriman, G., Schmidt, G. D., West, S. C., and Stockman, H. S. 1990, *Ap. J. Suppl.*, in press.
- Bessel, M. S. 1976, *Pub. A. S. P.*, **88**, 557.
- Blandford, R. D., and Königl, A. 1979, *Ap. J.*, **232**, 34.
- Blandford, R. D., and Rees, M. J. 1978, *Pittsburgh Conference on BL Lac Objects*, ed. A. M. Wolfe, (Pittsburgh: University of Pittsburgh) p. 328.
-

- Björnsson, C.-I. 1982, *Ap. J.*, **260**, 855.
- Borra, E. F. and Corriveau, G. 1984, *Ap. J.*, **276**, 449.
- Borra, E. F., Edwards, G. E., and Petrucci, F. 1985, *A. J.*, **90**, 1529.
- Brissenden, R. J. V., Remillard, R. A., Tuohy, I. R., Schwartz, D. A., and Hertz, P. L. 1990, *Ap. J.*, **350**, 578.
- Brindle, C., Hough, J. H., Bailey, J. A., Axon, D. J., and Hyland, A. R. 1986, *M.N.R.A.S.* **221**, 739.
- Browne, I. W. A. 1989, in *BL Lac Objects*, ed. L. Maraschi, T. Maccacaro, and M.-H. Ulrich, (Berlin: Springer-Verlag), p. 401.
- Burbidge, G. and Hewitt, A. 1987, *A. J.*, **92**, 1.
- Burbidge, G., and Hewitt, A. 1989, in *BL Lac Objects*, ed. L. Maraschi, T. Maccacaro, and M.-H. Ulrich, (Berlin: Springer-Verlag), p. 413.
- Carswell, R. F., Strittmatter, P. A., Williams, R. E., Kinman, T. D., and Serkowski, K. 1974, *Ap. J. (Letters)*, **190**, L101.
- Chanan, G. A., Margon, B., Helfand, D. J., Downes, R. A., and Chance, D. 1982, *Ap. J. (Letters)*, **261**, L31.
- Clarke, D. and Stewart, B. G. 1986, *Vistas in Astronomy* **29**, Part 1, 27.
- di Serego Alighieri, S., Fosbury, R. A. E., Tadhunter, C. N., and Quinn, P. J. 1990, *Nature*, **341**, 307.
- Fanaroff, B. L., and Riley, J. M. 1974, *M.N.R.A.S.*, **167**, 31P.
- Fugmann, W. 1988, *Astr. Ap.*, **205**, 86.
- Fugmann, W., and Meisenheimer, K. 1988, *Astr. Ap. Suppl.*, **76**, 211.
-

- Gabuzda, D. C., Cawthorne, T. V., Roberts, D. H., and Wardle, J. F. C. 1989, in *BL Lac Objects*, ed. L. Maraschi, T. Maccacaro, and M.-H. Ulrich, (Berlin: Springer-Verlag), p. 22.
- Gehrels, N. 1986, *Ap. J.*, **303**, 336.
- Ghisellini, G. and Maraschi, L. 1989, *Ap. J.*, **340**, 181.
- Ghisellini, G., Maraschi, L., Tanzi, E. G., and Treves, A. 1986, *Ap. J.*, **310**, 317.
- Gioia, I. M., Maccacaro, T., Schild, R. E., Stocke, J. T., Liebert, J. W., Danziger, I. J., Kunth, D., and Lub, J. 1984, *Ap. J.*, **283**, 495.
- Gioia, I. M., *et al.* 1990, *Ap. J. Suppl.*, **72**, 567.
- Giommi, P., *et al.* 1989, in *BL Lac Objects*, ed. L. Maraschi, T. Maccacaro, and M.-H. Ulrich, (Berlin: Springer-Verlag), p. 231.
- Giommi, P., Barr, P., Garilli, B., Maccagui, D., and Pollock, A. M. T. 1990, *Ap. J.*, **356**, 432.
- Green, R. F., Schmidt, M., and Liebert, J. 1986, *Ap. J. Suppl.*, **61**, 305.
- Guilbert, P. W., Fabian, A. C., and McCray, R. 1983, *Ap. J.*, **266**, 466.
- Feigelson, E. D., *et al.* 1986, *Ap. J.*, **302**, 337.
- Halpern, J. P., Impey, C. D., Bothan, G. D., Tapia, S., Skillman, E. D., Wilson, A. S., and Meurs, E. J. A. 1986, *Ap. J.*, **302**, 711.
- Hearn, D. R., Marshall, F. J., and Jernigan, J. G. 1979, *Ap. J. (Letters)*, **227**, L63.
- Impey, C. D. and Brand, P. W. J. L. 1982, *M. N. R. A. S.*, **201**, 849.
- Impey, C. D., Brand, P. W. J. L., and Tapia, S. 1981, *M. N. R. A. S.*, **198**, 1.
-

- Impey, C. D., Malkan, M. A., and Tapia, S. 1989, *Ap. J.*, **347**, 96.
- Impey, C. D., and Tapia, S. 1990, *Ap. J.*, **354**, 124.
- Jackson, J. D. 1975, *Classical Electrodynamics, Second Edition*, (New York: John Wiley and Sons).
- Jannuzi, B. T., and Elston, R. 1991, *Ap. J. (Letters)*, in press.
- Jannuzi, B. T., and Green, R. F. 1989, in *BL Lac Objects*, ed. L. Maraschi, T. Maccacaro, and M.-H. Ulrich, (Berlin: Springer-Verlag), p. 135.
- Jarvis, J. F., and Tyson, J. A. 1981, *A. J.*, **86**, 476.
- Kristian, J., Sandage, A., and Westphal, J. A. 1978, *Ap. J.*, **221**, 383.
- Knacke, R. F., Capps, R. W., and Johns, M. 1976, *Ap. J. (Letters)*, **210**, L69.
- Königl, A. 1989, in *BL Lac Objects*, ed. L. Maraschi, T. Maccacaro, and M.-H. Ulrich, (Berlin: Springer-Verlag), p. 321.
- Krzeminski, W., and Serkowski, K. 1967, *Ap. J.*, **147**, 988.
- Kühr, H., Pauling-Toth, I. I. K., Witzel, A., and Schmidt, J. 1981, *A. J.*, **86**, 854.
- Kühr, H., and Schmidt G. D. 1990, *A. J.*, **99**, 1.
- Landolt, A. U. 1983, *A. J.*, **88**, 439.
- Lasker, B. M., Sturch, C. R., *et al.* 1988, *Ap. J. Suppl.*, **68**, 1.
- Loeb, A., McKee, C. F., and Lahav, O. 1990, *Ap. J.*, submitted.
- Ledden, J. E., and O'Dell, S. L. 1985, *Ap. J.*, **298**, 630.
- Maccacaro, T., Feigelson, E. D., Fener, M., Giacconi, R., Gioia, I. M., Griffiths, R. E., Murray, S. S., and Zamorani, G. 1982, *Ap. J.*, **253**, 504.

- Maccacaro, T., Gioia, I. M., Maccagni, D., and Stocke, J. T. 1984, *Ap. J. (Letters)*, **284**, L23.
- Maccacaro, T., Gioia, I. M., Schild, R. E., Wolter, A., Morris, S. L., and Stocke, J. T. 1989, in *BL Lac Objects*, ed. L. Maraschi, T. Maccacaro, and M.-H. Ulrich, (Berlin: Springer-Verlag), p. 222.
- Madejski, G. M., and Schwartz, D. A. 1989, in *BL Lac Objects*, ed. L. Maraschi, T. Maccacaro, and M.-H. Ulrich, (Berlin: Springer-Verlag), p. 267.
- Maraschi, L., Ghisellini, G., Tanzi. E. G., and Treves, A. 1986, *Ap. J.*, **310**, 325.
- Maraschi, L., Maccacaro, T., Ulrich, M.-H. 1989, preface in *BL Lac Objects*, ed. L. Maraschi, T. Maccacaro, and M.-H. Ulrich, (Berlin: Springer-Verlag), p. i.
- Margon, B., Boroson, T. A., Chanan, G. A., Thompson, I. B., and Schneider, D. P. 1986, *Pub. A. S. P.*, **98**, 1129.
- Margon, B., and Jacoby, G. H. 1984, *Ap. J. (Letters)*, **286**, L31.
- Mathewson, D. S., and Ford, V. L. 1970, *Mem. R. astr. Soc.*, **74**, 139.
- Miller, J. S. 1989, in *BL Lac Objects*, ed. L. Maraschi, T. Maccacaro, and M.-H. Ulrich, (Berlin: Springer-Verlag), p. 395.
- Miller, J. S., and Antonucci, R. R. J. 1983, *Ap. J. (Letters)*, **271**, L7.
- Monet, D. G. and Green, R. F. 1989, "User's Guide to the PDS/IIS Measuring Engine", available at Kitt Peak National Observatory, Tucson, Arizona.
- Moore, R. L., and Stockman, H. S. 1981, *Ap. J.*, **243**, 60.
-

- Moore, R. L., and Stockman, H. S. 1984, *Ap. J.*, **279**, 465.
- Morris, S. L., *et al.* 1990a, preprint.
- Morris, S. L., Stocke, J. T., Maccacaro, T., Wolter, A., Gioia, I. M., and Schild, R. E. 1990b, preprint.
- Mushotzky, R. F., *et al.* 1978, *Ap. J. (Letters)*, **226**, L65.
- Olsen, E. T. 1969, *Nature*, **224**, 1008.
- Orr, M. J. L., and Browne, I. W. A. 1982, *M. N. R. A. S.*, **200**, 1067.
- Ostriker, J. P., and Vietri, M. 1983, *Ap. J.*, **267**, 488.
- Ostriker, J. P., and Vietri, M. 1985, *Nature*, **318**, 446.
- Ostriker, J. P., and Vietri, M. 1990, preprint.
- Ostriker, J. P. 1989, in *BL Lac Objects*, ed. L. Maraschi, T. Maccacaro, and M.-H. Ulrich, (Berlin: Springer-Verlag), p. 420.
- Padovani, P., and Urry, C. M. 1990, preprint.
- Pacholczyk, A. G. 1970, *Radio Astrophysics*, (San Francisco: W. H. Freeman).
- Pacholczyk, A. G. 1977, *Radio Galaxies*, (New York: Pergamon).
- Pica, A. J., Smith, A. G., Webb, J. R., Leacock, S. C., and Gombola, P. P. 1988, *A. J.*, **96**, 1215.
- Piccinotti, G., Mushotzky, R. F., Boldt, E. A., Holt, S. S., Marshall, F. E., Serlemitsos, P. J., and Sharer, R. A. 1982, *Ap. J.*, **253**, 485.
- Press, W. H., Flannery, B. P., Teukolsky, S. A., and Vetterling, W. T. 1986, *Numerical Recipes, The Art of Scientific Computing*, (New York: Cambridge University Press).

- Remillard, R. A. 1990, personal communication.
- Remillard, R. A., Bradt, H. V., Buckley, D. A. H., Roberts, W., Schwartz, D. A., Tuohy, I. R., and Wood, K. 1986, *Ap. J.*, **301**, 742.
- Remillard, R. A., Tuohy, I. R., Bissenden, R. J. V., Buckley, D. A. H., Schwartz, D. A., Feigelson, E. D., and Tapia, S. 1989, *Ap. J.*, **345**, 140.
- Rudy, R. J., Schmidt, G. D., Stockman, H. S., and Moore, R. L. 1983, *Ap. J.*, **271**, 59.
- Sandage, A. 1972, *Ap. J.*, **173**, 485.
- Saikia, D. J., and Salter, C. J. 1988. *Ann. Rev. Astr. Ap.*, **26**, 93.
- Scheuer, P. A. G., and Readhead, A. C. S. 1979, *Nature*, **277**, 182.
- Schmidt, G. D. 1982, Two-holer Polarimeter/Photometer Manual.
- Schmidt, G. D., and Stockman, H. S. 1991, *Ap. J.*, in press.
- Schmitt, J. L. 1968, *Nature*, **218**, 663.
- Schwartz, D. A., *et al.* 1989, in *BL Lac Objects*, ed. L. Maraschi, T. Maccacaro, and M.-H. Ulrich, (Berlin: Springer-Verlag), p. 209.
- Schwartz, D. A., *et al.* 1978, *Ap. J. (Letters)*, **224**, L103.
- Serkowski, K. 1974, in *Planets, Stars, and Nebulae studied with Photopolarimetry*, edited by T. Gehrels, (Tucson: The University of Arizona Press) p. 135.
- Sitko, M. L., Schmidt, G. D., and Stein, W. A. 1985, *Ap. J. Suppl.*, **59**, 323.
- Smith, P. S. 1986, Ph. D. Dissertation, University of New Mexico.
- Smith, P. S. 1990, personal communication.

- Smith, P. S., Balonek, T. J., Elston, R., and Heckert, P. A. 1987, *Ap. J. Suppl.*, **64**, 459.
- Smith, P. S., Balonek, T. J., Heckert, P. A., and Elston, R. 1986, *Ap. J.*, **305**, 484.
- Smith, P. S., Jannuzi, B. T., and Elston, R. 1991, *A. J.*, submitted.
- Stein, W. A., O'Dell, S. L., and Strittmatter, P. A. 1976, *Ann. Rev. Astr. Ap.*, **4**, 173.
- Stickel, M., Fried, J. W., and Kühr, H. 1989a, in *BL Lac Objects*, ed. L. Maraschi, T. Maccacaro, and M.-H. Ulrich, (Berlin: Springer-Verlag), p. 64.
- Stickel, M., Fried, J. W., and Kühr, H. 1989b, *Astr. Ap. Suppl.*, **80**, 103.
- Stickel, M., Padovani, P., Urry, C. M., Fried, J. W., and Kühr, H. 1990a, preprint.
- Stickel, M., Fried, J. W., and Kühr, H. 1990b, in preparation.
- Stickel, M. 1990, personal communication.
- Stocke, J. T., Liebert, J., Schmidt, G., Gioia, I. M. Maccacaro, T., Schild, R. E., Maccagni, D., and Arp, H. C. 1985, *Ap. J.*, **298**, 619.
- Stocke, J. T., Morris, S. L., Gioia, I. M., Maccacaro, T., Schild, R. E., and Woter, A. 1989, in *BL Lac Objects*, ed. L. Maraschi, T. Maccacaro, and M.-H. Ulrich, (Berlin: Springer-Verlag), p. 242.
- Stocke, J. T., Morris, S. L., Gioia, I. M., and Maccacaro, T. 1990, *Ap. J.*, **348**, 141.
- Stocke, J. T., *et al.* 1991, in preparation.
- Stockman, H. S., Moore, R. L., and Angel, J. R. P. 1984, *Ap. J.*, **279**, 485.

- Strittmatter, P. A., Serkowski, K., Carswell, R. F., Stein, W. A., Merrill, K. M., and Burbidge, E. M. 1972, *Ap. J. (Letters)*, **175**, L7.
- Turnshek, D. A., Bohlin, R. C., Williamson II, R. L., Lupie, O. L., Koornneef, J., and Morgan, D. H. 1990, *A. J.*, **99**, 1243.
- Ulrich, M.-H. 1989, in *BL Lac Objects*, ed. L. Maraschi, T. Maccacaro, and M.-H. Ulrich, (Berlin: Springer-Verlag), p. 45.
- Usher, P. D. 1978, *Ap. J.*, **222**, 40.
- Visvanathan, N. 1969, *Ap. J. (Letters)*, **155**, L133.
- Worrall, D. M. 1989, in *BL Lac Objects*, ed. L. Maraschi, T. Maccacaro, and M.-H. Ulrich, (Berlin: Springer-Verlag), p. 305.
- Wills, B. J. 1989, in *BL Lac Objects*, ed. L. Maraschi, T. Maccacaro, and M.-H. Ulrich, (Berlin: Springer-Verlag), p. 109.
- Wills, D., Wills, B. J., Breger, M., Hsu, J.-C. 1980, *A. J.*, **85**, 1555.
- Wolfe, A. M. 1978, preface to *Pittsburgh Conference on BL Lac Objects*, ed. A. M. Wolfe, (Pittsburgh: University of Pittsburgh).
- Wood, K. S., *et al.* 1984, *Ap. J. Suppl.*, **56**, 507.
- Zensus, J. A., and Pearson, T. J. 1987, editors *Superluminal Radio Sources*, (New York: Cambridge University Press).